UNIVERSIDADE DE LISBOA
FACULDADE DE MEDICINA DE LISBOA


# Regulatory interactions between the metabolic sensors SIRT1 and AMPK in modulating PPARα linked functions, in obesity-dependent type 2 diabetes mellitus

**Marta Silvestre**

Orientada por: Dr. Paul Caton
Co-orientada por: Profa. Maria Carlota Saldanha e Profa. Maria Helena Cortez Pinto

Biomedical Sciences
Functional Sciences

A impressão desta dissertação foi aprovada pelo Conselho Científico da Faculdade de Medicina de Lisboa da Universidade de Lisboa em reunião de 22 de Abril de 2014.

(…)

Enfim duma escolha faz-se um desafio

Enfrenta-se a vida de fio a pavio

Navega-se sem mar, sem vela ou navio

Bebe-se a coragem até dum copo vazio

E vem-nos à memória uma frase batida

Hoje é o primeiro dia do resto da tua vida

E entretanto o tempo fez cinza da brasa

E outra maré cheia virá da maré vaza

Nasce um novo dia e no braço outra asa

Brinda-se aos amores com o vinho da casa

E vem-nos à memória uma frase batida

Hoje é o primeiro dia do resto da tua vida."

O PRIMEIRO DIA - Sérgio Godinho

# Acknowledgements

I would like to thank, my supervisor Dr. Paul Caton for his supervision and guidance through out my PhD and for having accepted to supervise me after Professor Mary Sugden get retired.

I would like to thank, my previous supervisor Professor Mary Sugden for giving me opportunity to work with her at the Blizard Institute, Queen Mary University of London, for her supervision and guidance during my PhD and for keeping guiding me on an informal basis, after getting retired.

I would also like to thank, my supervisors Professor Maria Carlota Saldanha and Professor Helena Cortez Pinto for their help and guidance throughout my PhD and for allowing me to work at Instituto de Medicina Molecular.

Additionally, I would like to thank, Professor Isabel do Carmo for giving me the opportunity to study at Faculdade de Medicina da Universidade de Lisboa and for her incredible support for the last 4 years.

I would like to thank everyone who has helped me throughout the past 4 years, in particular Dr. Mark Holness, Mr. Sharif Hegazy, Ms. Gertrud Kourtman, Dr. Tania Maffucci, Professor Benoit Viollet, Mrs. Irene Smith and Mrs. Susanne Bell.

I would also like to thank Bruno, my husband, for leaving his life in Portugal to join me in London UK and for his constant support over the last years.

Finally, thank you to Fundação para a Ciência e Tecnologia for funding throughout my PhD and thank you Queen Mary University of London for being my host university and allow me to work on your laboratories.

**Resumo**

A diabetes mellitus tipo 2 (T2DM) é uma doença metabólica de etiologia variada que continua a afectar pessoas em todo o mundo. Caracteriza-se essencialmente por alterações da ação da insulina e/ou da sua secreção, que resultam numa hiperglicémia crónica. O excesso de peso/obesidade e a inactividade física são as principais causas da T2DM em indivíduos geneticamente predispostos. A carência proteica durante a gravidez (restrição proteica na gravidez; MLP), resulta em recém-nascidos de baixo peso (LBW) que, numa fase mais tardia da vida desenvolvem insulinorresistência e um fenótipo de diabetes. A SIRT1 e a proteína cinase ativada-AMP (AMPK) constituem importantes enzimas responsáveis pela longevidade e pela homeostasia energética e, consequentemente, desempenham um papel importante no desenvolvimento de doenças metabólicas tais como a T2DM. Através de mecanismos de desacetilação, a SIRT1 regula a atividade do receptor nuclear - proliferador de peroxissoma α (PPARα) -, controlando assim a expressão de genes envolvidos no metabolismo da glucose e dos lípidos. Os factores que regulam o interferão 3 e 4 (IRF3 e IRF4), por serem repressores chave no processo de adipogénese, também merecem especial atenção no que respeita ao desenvolvimento de doenças metabólicas. O trabalho aqui proposto tem como objetivo investigar a potencial existência de um circuito positivo entre as proteínas AMPK e SIRT1 e tentar caracterizar o papel deste circuito, na indução da expressão genética regulada pelo PPARα. Ratinhos *C57Bl/6* submetidos a jejum ou a uma dieta hiperlipídica (HF) e ratos MLP foram usados neste estudo. Os modelos descritos foram usados para avaliar o impacto da disponibilidade calórica e proteica no desenvolvimento de insulinorresistência e, consequentemente, da T2DM no fígado e tecido adiposo (WAT), respectivamente; ratinhos em que o gene AMPK α1/2 foi especificamente eliminado no fígado e músculo ($AMPK^{-/-}$) foram usados para identificar o papel da ativação da AMPK e da SIRT1 nas funções ligadas ao PPARα; ratinhos PPARα *knockout* foram usados para investigar a deficiência de PPARα na lipogénese e beta-oxidação do tecido adiposo visceral; células hepáticas H4IIEC3 cultivadas e tratadas com um SIRT1 siRNA, serviram para caracterizar o circuito positivo entre SIRT1 e AMPK; mioblastos L6 foram cultivados e tratados com um agonista da AMPK (adiponectina) e com insulina; adipócitos 3T3-L1 foram cultivados e tratados com um

agonista do PPARα (WY14683) para identificar o papel do PPARα no IRF3 e no IRF4.

Através da utilização de tecido hepático AMPK$^{-/-}$ e de células H4IIEC3 silenciadas para a SIRT1 verificou-se que, no fígado, a AMPK e SIRT1 regularam-se reciprocamente num processo que impede a acumulação de triacilgliceróis. O estudo de ratinhos alimentados com uma dieta HF, tratados com mononucleótido de nicotinamida (NMN), permitiu estabelecer uma ligação entre o circuito AMPK/SIRT1 e a fosforilação do substrato do receptor de insulina (IRS-1), sugerindo uma relação entre o circuito SIRT1/AMPK e a via da sinalização de insulina. No músculo-esquelético, a deficiência da AMPK altera os efeitos benéficos da restrição calórica na tolerância à glucose, o que prova que este benefício é dependente da AMPK. A diminuição da expressão da SIRT1 aliada à deficiência da AMPK, altera a via da sinalização de insulina, o que resulta numa diminuição da entrada de glucose para as células. No tecido adiposo visceral, a inibição do IRF3 e do IRF4 reduz o processo de β-oxidação e aumenta o processo de lipogénese em ratos MLP. Os estudos realizados no tecido adiposo levaram à conclusão de que o IRF3 é potencialmente ativado pela AMPK, e o IRF4 é ativado pelo PPARα, num processo que envolve adiponectina.

Os resultados obtidos sugerem que o eixo AMPK-SIRT1-PGC-1α-SIRT3 durante o jejum/CR é importante na prevenção de distúrbios metabólicos. Regular a atividade da AMPK e da sua interação com as sirtuinas na funções ligadas ao PPARα, pode ser potencialmente importante para o tratamento de distúrbios como a T2DM e outros associados ao envelhecimento. A adiponectina e o NMN são potenciais alvos terapêuticos para o tratamento de doenças metabólicas.

# Abstract

Both genetic and environmental influences determine the risk of developing type 2 diabetes mellitus (T2DM). Epidemiological studies indicate that factors influencing the prevalence of T2DM include lifestyle (e.g. inactivity and dietary macronutrient composition), obesity and age. Interestingly maternal protein restriction (Maternal Low Protein; MLP) generates low birth weight (LBW) offspring, who develop insulin resistant and diabetic phenotype in later life. Interferon regulatory factors 3 and 4 (IRF3 and IRF4) are key repressors of adipogenesis. SIRT1, a histone/protein deacetylase, and AMP-activated protein kinase (AMPK) are key enzymes responsible for longevity and energy homeostasis. Through deacetylation and activation of peroxisome proliferator-activated receptor-γ coactivator 1 α (PGC-1α), a transcriptional regulator of fatty acid (FA) oxidation, SIRT1 mediates activation of peroxisome-proliferator-activated receptor α (PPARα), which is a nuclear receptor that controls the expression of genes involved in glucose and lipid homoeostasis. The proposed study aims to investigate whether a positive feed back loop exists in response to AMPK/SIRT1 activation and try to characterize the role of this pathway in the regulatory circuit through which PPARα induces gene expression. *C57Bl/6* mice fasted or fed a high fat diet (HF) and rat MLP-offspring were used to understand the importance of nutrient availability in the development of insulin-resistance and T2DM in liver and visceral white adipose tissue (WAT) respectively; specific liver and muscle AMPK α1/2 double null ($AMPK^{-/-}$) mice were used to understand the role of AMPK on SIRT1 activation and PPARα linked functions; PPARα deficient mice were used to investigate the influence of PPARα deficiency on lipogenesis and β oxidation in mice visceral WAT; H4IIEC3 liver cell line was cultured and treated with a SIRT1 siRNA to better understand the feedback loop between SIRT1 and AMPK; L6 myoblasts were cultured and treated with AMPK agonist adiponectin and with insulin, and 3T3-L1 adipocytes were cultured and treated with PPARα agonists (WY14683) to understand the role of PPARα in IRF3 and IRF4.

Using $AMPK^{-/-}$ liver and SIRT1 knockdown H4IIEC3 cells we found that, in the liver, AMPK and SIRT1 regulate each other to prevent lipid accumulation. Studies on HF fed mice, treated with nicotinamide mononucleotide (NMN), linked this

AMPK/SIRT1 pathway to phosphorylation of the insulin receptor substrate (IRS-1) at tyrosine residues, suggesting an involvement of the SIRT1/AMPK axis in the insulin-signalling pathway. In skeletal muscle AMPK deficiency impairs the beneficial effects of CR on glucose tolerance. This is linked to decreased SIRT1 gene expression, which could impair insulin signalling pathway, culminating in reduced glucose uptake. Using MLP-offspring visceral WAT, we found that suppression of interferon regulatory factors 3 and 4 (IRF3 and IRF4, respectively) represses fatty oxidation and enhances lipogenesis in MLP-offspring. IRF3 is possibly activated by AMPK, where IRF4 is activated by PPARα.

Taken together, our results suggest that AMPK-SIRT1-PGC-1α-SIRT3 axis during fasting/CR is important to prevent metabolic disorders. Regulation of AMPK and PPARα linked functions together with deacetylation catalyzed by the sirtuins may prove to be important for the treatment of T2DM and other disorders associated with aging. Adiponectin (which activates AMPK and PPARα) and NMN (which increases SIRT1 activity) are potential therapeutic targets for the treatment of metabolic disorders.

# List of Abbreviations

| | |
|---|---|
| **ACC** | acetyl CoA carboxylase |
| **ACoA** | acetyl CoA |
| **ADP** | adenosine diphosphate |
| **AICAR** | 5-aminoimidazole-4-carboxamide 1-β-D-ribofuranoside |
| **AL** | *ad libitum* fed |
| **AMP** | adenosine monophosphate |
| **AMPK** | AMP-activated protein kinase |
| **ANOVA** | analysis of variance |
| **APS** | ammonium persulfate |
| **ATP** | adenosine triphosphate |
| **BSA** | bovine serum albumin |
| **$CaCl_2$** | calcium chloride |
| **CaMKKβ** | $Ca^{2+}$/calmodulin dependent protein kinase beta |
| **cAMP** | cyclic adenosine monophosphate |
| **CBS** | cystathionine β-synthase |
| **$CO_2$** | carbone dioxide |
| **CPT-1** | carnitine palmitoyltransferase 1 |
| **CR** | caloric restriction |
| **CREB** | cAMP response element binding protein |
| **DAG** | diacyl-glycerol |
| **DMEM** | Dulbecco's modified eagle medium |
| **DMSO** | dimethyl sufoxide |
| **dNTP** | deoxyribonucleic acid triphosphate |
| **DPP-IV** | dipeptidyl peptidase IV |
| **DTT** | dithiothreitol |
| **ECACC** | European Collection of Animal Cell cultures |
| **EDTA** | ethylenediaminetetracetic acid |
| **ELISA** | enzyme-linked immunosorbent assay |
| **ER** | endoplasmatic reticulum |
| **FAS** | fatty acid synthase |
| **FCS** | foetal calf serum |
| **FFA** | free fatty acid |
| **FOXA2** | forkhead box protein A2 |
| **FOXO** | forkhead box protein O |
| **FOXO1** | forkhead box protein O1 |
| **FPG** | fasting plasma glucose |
| **FR** | high fructose diet |
| **F2,6$P_2$** | fructose 2,6-biphosphate |
| **FXR** | farnesoid X receptor |
| **GDM** | gestational diabetes mellitus |
| **GLP-1** | glucagon-like peptide-1 |
| **GLUT** | glucose transporter |
| **GLUT4** | glucose transporter 4 |
| **G6P** | glucose-6-phosphate |
| **G6Pase** | glucose -6-phosphatase |
| **GS** | glycogen synthase |
| **GSK3** | glycogen synthase kinase-3 |

| | |
|---|---|
| **GTT** | glucose tolerance test |
| **HDAC** | histone deacetylase |
| **HF** | high fat diet |
| **HMGCR** | 3-hydroxy-3-methylglutaryl coenzyme A reductase |
| **HST** | homologues of SIR2 |
| **IDDM1** | insulin-dependent diabetes mellitus |
| **IKKbeta** | IkappaB kinase beta |
| **IL-1β** | interleukin-1β |
| **IL-6** | interleukin-6 |
| **IMCL** | intramyocellular lipid |
| **iNOS** | inducible nitric oxide synthase |
| **INSIGs** | insulin induced genes |
| **IR** | insulin receptor tyrosine kinase |
| **IRF3** | interferon regulatory factor 3 |
| **IRF4** | interferon regulatory factor 4 |
| **IRS** | insulin receptor substrate |
| **IRS1** | insulin receptor substrate 1 |
| **IRS2** | insulin receptor substrate 2 |
| **JNK-1** | c- jun N-terminal kinase-1 |
| **KCl** | potassium chloride |
| **KG** | α –keto-glutarate |
| **$KHCO_3$** | potassium hydrogen carbonate |
| **$KH_2PO_4$** | potassium dihydrogen orthophosphate |
| **IMCL** | intramyocelular lipids |
| **LBW** | low birth weight |
| **LCCoA** | long chain acetyl-Coenzyme A |
| **LCFA** | long chain fatty acids |
| **LDH** | lactate dehydrogenase |
| **LDL** | low density lipoprotein |
| **LKB1** | liver kinase B1 |
| **LXR** | liver X receptor |
| **LXRα** | liver X receptor alpha |
| **MAR1** | mating-type regulator 1 |
| **MAT1** | ménage-a-trois protein 1 |
| **MEF** | mouse embryonic fibroblasts |
| **$MgCL_2$** | magnesium chloride |
| **$MgSO_4$** | magnesium sulphate |
| **MLP** | maternity low protein diet |
| **mmHg** | milimeteres of mercury |
| **MO25** | mouse protein 25 |
| **mTOR** | *mammalian target of rapamycin* |
| **MTT** | 3-(4,5-dimethylthiazol-2-yl)-2,5-dipheyltetrazolium bromide |
| **MW** | molecular weight |
| **Na-azide** | sodium azide |
| **NaCl** | sodium chloride |
| **NAD** | nicotinamide adenine dinucleotide |
| **NADH** | nicotinamide adenine dinucleotide (reduced form) |
| **NAFLD** | non-alcoholic fatty liver disease |
| **$NaHCO_3$** | sodium carbonate |
| **$NaH_2PO_4$** | sodium dihydrogen orthophosphate |

| | |
|---|---|
| **NAMPT** | nicotinamide phosphoribosyltransferase |
| **NaOH** | sodium hydroxide |
| **NCoR** | nuclear receptor co-repressor |
| **NEFA** | non esterified fatty acids |
| **NHP** | non-human primates |
| **NIDDM** | non insulin dependent diabetes mellitus |
| **NMN** | nicotinamide mononucleotide |
| **NMNAT** | NMN adenylyltransferase |
| **NR** | Nuclear Receptor |
| **nPKCs** | novel protein kinase C |
| **OAA** | oxaloacetate |
| **P** | phosphate |
| **PBS** | phosphate buffered saline |
| **PCA** | perchloric acid |
| **PDC** | pyruvate dehydrogenase complex |
| **PDH** | pyruvate dehydrogenase |
| **PDHK4** | pyruvate dehydrogenase kinase 4 (protein) |
| **PDK4** | pyruvate dehydrogenase kinase 4 (gene) |
| **PEPCK** | phosphoenolpyruvate carboxykinase |
| **PFK1** | 6-phosphofructo-1-kinase |
| **PFK2** | 6-phosphofructo-2-kinase |
| **PGC-1α** | peroxisome proliferator-activated receptor gamma co-activator 1alpha |
| **PGC-1β** | peroxisome proliferator-activated receptor gamma co-activator 1beta |
| **PH** | pleskstrin homology |
| **PI** | proinsulin |
| **PI3K** | phosphatidylinositol 3-kinase |
| **PIP2** | 3′-phosphoinositides [phosphatidyl-inositol-3,4-bisphosphate |
| **PIP3** | phosphatidyl-inositol-3,4,5-trisphosphate |
| **PKB** | protein kinase B (also known as Akt) |
| **PKC** | protein kinase C |
| **PKC-ε** | protein kinase C-ε |
| **PPARα** | peroxisome proliferator-activated receptor alpha |
| **PPARγ** | peroxisome proliferator-activated receptor gamma |
| **PPI** | preproinsulin |
| **PP2C** | protein phosphate 2 C |
| **PRPP** | nicotinamide and 5-phosphoribosyl-pyrophosphate |
| **PTB** | phophotyrosine binding domanin |
| **PTK** | protein tyrosine kinase |
| **RCT** | reverse cholesterol transport |
| **RER** | rough endoplasmatic reticulum |
| **RNA** | ribonucleic acid |
| **ROS** | reactive oxygen species |
| **RSK** | ribossomal S6 Kinase |
| **RXR** | retinoid X receptor |
| **SCAP** | SREBP cleavage-activating protein |
| **SCD-1** | sterol CoA desaturase-1 |
| **SDS-PAGE** | sodium dodecyl sulphate-polyacrylamide gel electrophoresis |
| **SH2** | src homology domain |
| **shRNAi** | short hairpin RNA interference |
| **siRNA** | small interfering RNA |

| | |
|---|---|
| **SIR** | silent information regulator |
| **SIRT** | silent information regulator two orthologue |
| **SIRT1** | silent information regulator two orthologue 1 |
| **SIRT3** | silent information regulator two orthologue 3 |
| **SIRT6** | silent information regulator two orthologue 6 |
| **SMRT** | silencing mediator of retinoid and thyroid hormone receptors |
| **SREBP** | sterol regulatory element binding |
| **SREBP-1c** | sterol regulatory element binding 1c |
| **SREBP -1α** | sterol regulatory element binding 1alpha |
| **SREBP2** | sterol regulatory element binding 2 |
| **STRAD** | Ste 20-related adapted protein |
| **S6K** | p70 ribossomal protein S6 kinase |
| **TAG** | triacylglycerol |
| **TAK1** | transforming growth factor β-activated kinase |
| **TBC1D4** | TBC1 domain family member 4 |
| **TG** | triglycerides |
| **TNF- α** | tumour necrosis factor α |
| **TORC2** | transducer of regulated CREB activity 2 |
| **TSC** | tuberous sclerosis complex |
| **TZDs** | thiazolidinediones |
| **T2DM** | type 2 diabetes mellitus |
| **VLDL** | very low density lipoprotein |
| **WAT** | white adipose tissue |
| **WNPRC** | Wisconsin National Primate Research Center |
| **XBP1** | X-box binding protein 1 |
| **ZMP** | AICAR monophosphatase |
| **4E-BP** | eucaryotic initiating factor 4E (elF4E) biding protein |

**Chapter:**

*1. General Introduction*

## 1.1 Insulin

Insulin is a naturally-occurring peptide hormone synthesized and secreted by pancreatic β cells. The release of insulin from secretory granules is dependent on the ability of each granule to translocate to the cell surface and fuse with the plasma membrane [1].

### 1.1.1 Insulin Signalling Cascade

Glucose is an essential nutrient, supplying fuel for many different organs of the body, for which it is the sole source of energy. These include the brain and neurons in particular, as well as other organs and tissues, particularly those that lack (e.g. red blood cells) or have low oxidative capacity. Since glucose enters cells via facilitated diffusion, it is vital that blood glucose levels are maintained within a very narrow range, approximately 3.9 – 6.6 mM, depending on prandial state [2].

Insulin is the major hormone controlling critical energy functions such as glucose and lipid metabolism. Insulin activates the insulin receptor tyrosine kinase (IR), which phosphorylates and recruits different substrate adaptors such as the insulin receptor substrate (IRS) family of proteins (Fig. 1.1) [3]. The IR is a heterotetramer consisting of two α subunits and two β subunits that are linked by disulphide bonds. Insulin binds to the α subunit of the insulin receptor and activates the tyrosine kinase in the β subunit (Fig. 1.1). Once the tyrosine kinase of insulin receptor is activated, it promotes autophosphorylation of the β subunit, where phosphorylation of three tyrosine residues ($Tyr^{1158}$, $Tyr^{1162}$, and $Tyr^{1163}$) is required for amplification of the kinase activity [4]. Receptor activation leads to the phosphorylation of key tyrosine residues on IRS proteins, which interact with phosphatidylinositol (PI) 3-kinase (also known as PI3K, a lipid kinase). PI3K consists of a p110 catalytic subunit and a p85 regulatory subunit that possesses two Src homology 2 (SH2) domains that recognise the tyrosine-phosphorylated residues in IRS proteins [5] (Fig. 1.1). The activated PI3K phosphorylates 3′-phosphoinositides [phosphatidyl-inositol-3,4-bisphosphate (PIP2) generating phosphatidyl-inositol-3,4,5-trisphosphate (PIP3) [6], which bind to the phosphoinositidedependent kinase 1 (PDK1). Known substrates of the PDKs are Akt, also known as protein kinase B (PKB), and also atypical forms of the protein kinase C (PKC) [7]. Once active, Akt enters the cytoplasm where it functions to regulate a range of cellular metabolic functions in tissues such as the liver, skeletal

muscle and white adipose tissue, which serve to regulate glucose and lipid homeostasis [8].

#### 1.1.1.1 Insulin-mediated glycogen regulation

With respect to glycogen metabolism in liver and skeletal muscle, Akt induces the phosphorylation and inactivation of glycogen synthase kinase 3 (GSK3) (Figure 1.1). A major substrate of GSK3 is glycogen synthase, an enzyme that catalyses the final step in glycogen synthesis. Phosphorylation of glycogen synthase by GSK3 inhibits glycogen synthesis; therefore insulin-mediate inactivation of GSK3 by Akt promotes glucose storage as glycogen [9].

#### 1.1.1.2 Insulin-mediated regulation hepatic glucose production

In addition to promoting glucose storage, insulin inhibits the production and release of glucose by the liver by blocking gluconeogenesis and glycogenolysis [5]. Insulin directly controls the activities of a set of gluconeogenic enzymes by phosphorylation and dephosphorylation events leading to regulated expression of hepatic gluconeogenesis genes. Forkhead box protein O1 (FOXO1) stimulates expression of gluconeogenic genes (e.g. PEPCK and suppresses genes involved in glycolysis and lipogenesis, including glucokinase and the transcription factor steroid regulatory element-binding protein (SREBP)-1c, respectively [5]. Insulin induces phosphorylation of FOXO1, in an Akt-dependent manner, resulting in nuclear exclusion of FOXO1 and repression of gluconeogenic gene expression.

#### 1.1.1.3 Insulin-mediated glucose uptake

Insulin also promotes glucose uptake in skeletal muscle, adipose tissue and liver, in a process mediated by glucose transporters from the GLUT family. GLUT4 is distinguished from the other glucose transporters as a high-affinity, insulin-responsive glucose transporter protein that is highly expressed in muscle and adipose tissue [10]. Insulin activates GLUT4, in a process mediated by Akt signalling, which results in GLUT4 translocation to the cell surface to transport glucose into the cell [11].

#### 1.1.1.4 Insulin action in adipose tissue

Insulin is considered the major anti-lipolytic [12] and prolipogenic regulator [13] in

white adipose tissue (WAT). It is well known that insulin stimulates the redistribution of GLUT4 from intracellular compartment to plasma membrane in adipocytes [14]. As a result, increased postprandial blood glucose was transported into adipose tissue through GLUT4. In addition, insulin increases the activity of lipoprotein lipase on adipose cell surface, leading to the lipolysis of serum lipoprotein and subsequent uptake of free fatty acids (FFA) into adipose tissue. Insulin-induced increase of glucose and FFA uptake is important as substrate supply in efficient triglyceride synthesis in adipocytes [15].

Data from Akt knockout mouse models offer a clearer answer to the question of whether Akt is required for normal glucose homeostasis. While disruption of Akt1 isoform in mice did not cause any significant perturbations in metabolism, mice with a knockout of the Akt2 isoform show insulin resistance, ending up with a phenotype closely resembling type 2 diabetes in humans [16, 17]. Consistently, recent studies of inherited insulin post-receptor mutations in humans detected a missense mutation in the kinase domain Akt2 in a family of severely insulin resistant patients. The mutant kinase was unable to phosphorylate downstream targets and to mediate inhibition of phosphoenolpyruvate carboxykinase (PEPCK), a gluconeogenic key enzyme [18]. Taken together, studies of transgenic mice and rare human genetic syndromes suggest that the impairment of insulin activity leading to insulin resistance is linked to insulin signalling defects, and specifically, impaired Akt signalling.

Figure 1.1

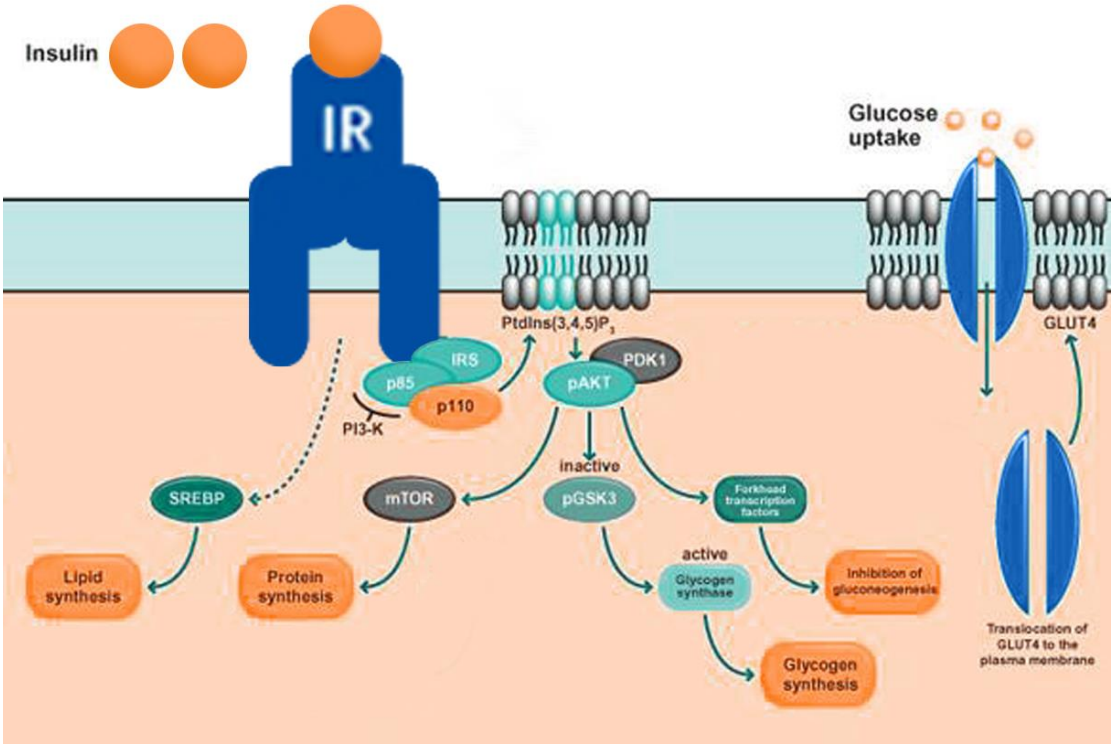


Figure 1.1: Insulin signaling pathway. SREBP: sterol regulatory element-binding protein; IRS: insulin receptor substrate, PI3-K: phosphoinositide 3 kinase (composed of a heterodimer between a p110 subunit and a p85 subunit); PDK1: phosphoinositide-dependent kinase 1; pAkt: phosphorylated protein kinase B (also known as PKB); pGSK3: phosphorylated glycogen synthase kinase 3; mTOR: mammalian target of rapamycin. These molecules act in a coordinated manner to regulate glucose, lipid and protein metabolism.

In summary, insulin plays a central role in the regulation of blood glucose levels and acts in a coordinated fashion to stimulate protein and lipid metabolism by modifying the activity of various enzymes and/or transport proteins [3]. Insulin stimulates glucose uptake and the anabolic pathways of glycogenesis (synthesis of glycogen), lipogenesis [synthesis of long chain fatty acids (LCFA) and their subsequent esterification as triacylglycerol (TAG)] and cholesterol synthesis. Concurrently, insulin suppresses glycogenolysis (hydrolysis of glycogen) and lipolysis (hydrolysis of TAG). Other metabolic effects include suppression of hepatic gluconeogenesis (*de novo* glucose synthesis), hepatic very-low-density-lipoprotein (VLDL) secretion, suppression of mitochondrial LCFA oxidation, enhancement of tissue uptake of

amino acids, and stimulation of protein synthesis. The overall role of insulin, therefore, is to promote anabolism [19].

## 1.2 Type 2 Diabetes Mellitus

### 1.2.1 Prevalence of T2DM

Type 2 diabetes mellitus (T2DM) has become a leading health problem throughout the world, accounting for almost 90% of all cases of diabetes in adults worldwide [20]. Once thought of as a disease of the Western world, the prevalence of T2DM is increasing at alarming rates in developing countries [21]. The emerging pandemic is driven by the combined effects of population ageing, rising levels of obesity and inactivity, and greater longevity among patients with T2DM that is attributable to improved management [22]. According to a study by Sardinha et al. in 2012 of a representative sample of 9447 individuals, overweight and obesity now affects 66.6% of Portuguese males and 57.9% of Portuguese females [23]. Since obesity is unequivocally linked to T2DM [24], its prevalence is also expected to increase significantly in coming years. As a result of this epidemic increase in T2DM prevalence, a progressive change is predicted in the epidemiological view of various pathologies, including coronary artery disease, stroke, diabetic retinopathy and neuropathy, and chronic renal failure [24]. Worldwide, it is projected that by 2025 there will be 380 million people with T2DM and 418 million people with impaired glucose tolerance, impacting significantly in economic terms as well as resulting in increased morbidity and mortality [20, 22].

### 1.2.2 Characterization of T2DM

T2DM is defined by a fasting plasma glucose (FPG) equal or higher than 126 mg/dl or 7 mmol/l [25]. T2DM, associated with ageing and obesity, is characterized by altered lipid and glucose metabolism (fasting or postprandial hyperglycaemia, dyslipidemia) as a consequence of combined insulin resistance in skeletal muscle, liver and adipose tissue and relative defects of insulin secretion by β cells that may arise due to an imbalance between energy intake and expenditure [5]. A degree of hyperglycaemia sufficient to cause pathological and functional changes in various

target tissues, but without clinical symptoms, may be present for a long period of time before T2DM is detected. During this asymptomatic period, it is possible to demonstrate an abnormality in carbohydrate metabolism by measurement of plasma glucose in the fasting state or after a challenge with an oral glucose load [25]. In the natural history of T2DM, pancreatic β cells initially compensate for insulin resistance by increasing insulin secretion, but with time, progressive β cell failure leads to insulin deficiency, and hyperglycaemia ensues [26]. The chronic hyperglycaemia of T2DM is associated with long-term damage, dysfunction, and failure of different organs, especially the eyes, kidneys, nerves, heart, and blood vessels [25, 27]. The aetiology of the disease remains unclear, but T2DM can now be described as complex polygenic disease with a strong genetic component, as indicated by the high prevalence in certain ethnic groups and by studies of identical twins [28-31]. Nevertheless, the rapid increase in the prevalence of obesity-associated disease conditions, (including T2DM) in worldwide populations, suggests the contribution of environmental factors. A widely accepted explanation implicates the frequent consumption of processed foods with a high-calorie content and the reduction in physical exercise due to sedentary lifestyle in modern urban environment, as a major cause of obesity and subsequent insulin resistance and T2DM [32, 33]. Indeed, it is well known that obesity itself causes some degree of insulin resistance [34]. Lifestyle changes, consisting of diet and exercise is often an effective measure to improve glucose tolerance in the early stages of T2DM, often complemented with anti-diabetic drugs or insulin therapy [35, 36].

### 1.2.3 Hepatic glucose and lipid regulation in T2DM

The liver plays a major role in maintenance of glucose homeostasis through control of glucose production and uptake. This is achieved through regulation of glucose uptake and utilisation through glycolysis and glycogenesis and glucose production via glycogenolysis and gluconeogenesis. These processes are particularly important considering raised blood glucose levels are a characteristic of T2DM and the metabolic syndrome [37].

In healthy individuals, in the fed state, dietary carbohydrate increases plasma glucose levels and promotes insulin secretion from the pancreatic β cells. In the liver, insulin

promotes glycogen synthesis and *de novo* lipogenesis while also inhibiting gluconeogenesis and glycogenolisis. In the fasted state, insulin secretion is decreased as a result of lower blood glucose concentrations. The drop in insulin (as well as the increased action of other hormones, including glucagon) leads to increased hepatic gluconeogenesis and glycogenolysis and resultant elevated hepatic glucose production. This regulatory system is impaired in T2DM, leading to abnormally increased hepatic glucose production, which contributes significantly to hyperglycaemia.

Hepatic lipid production diminishes while adipose lipolysis increases. In T2DM, ectopic lipid accumulation impairs insulin signalling. With accumulation of intramyocellular lipid (IMCL), insulin-mediated skeletal muscle glucose uptake is impaired. In the liver, increased lipid accumulation also impairs the ability of insulin to regulate gluconeogenesis and activate glycogen synthesis. In contrast, lipogenesis remains unaffected and, together with the increase delivery of dietary glucose, leads to increased lipogenesis and worsening non-alcoholic fatty liver disease (NAFLD), very common in obesity-associated T2DM [37].

### 1.2.4 Skeletal muscle glucose regulation in T2DM

Under hyperglycemic, hyperinsulinemic conditions, muscle glycogen synthesis is the major pathway for glucose metabolism in both normal and diabetic individuals, and defective muscle glucose uptake and glycogen synthesis play a major role in causing insulin resistance in patients with T2DM [38]. Defects in the ability of insulin to activate enzymes in glycogen synthase, hexokinase II, and enzymes in glucose transport have all been implicated in the loss of skeletal-muscle glycogen synthesis in type 2 diabetics, making each of the corresponding biochemical events a potential target for antidiabetic therapy [38].

Insulin-mediated translocation of GLUT4 to the muscle sarcolemmal membrane is impaired in patients with T2DM [39, 40]. Thus, a defect in skeletal-muscle glucose transport was implicated as the cause of reduced insulin-mediated glucose metabolism in patients with T2DM in two independent studies [39, 40]. Moreover, the results of

these studies suggested that ectopic accumulation of lipid within the muscle cell might be the cause of insulin resistance.

In healthy fed individuals, in the skeletal muscle, insulin increases glucose transport through GLUT4, facilitating glucose entry and glycogen synthesis. On the other hand, in fasting conditions, glycogen synthesis stops and glycogenolysis takes place, generating glucose-1-phosphate, which is converted to glucose-6-phosphate, which is subsequently converted in glucose (plus a phosphate group), by the enzyme glucose -6-phosphatase. At the same time, gluconeogenesis takes place in the liver. Both processes are important to produce enough glucose to feed the muscle under these conditions. In T2DM, ectopic lipid accumulation impairs insulin signalling as mentioned above. With accumulation of intramyocellular lipid (IMCL), insulin-mediated skeletal muscle glucose uptake is impaired. Glycogenolysis occours and glucose transport as well as glycogen synthase are inhibited [37].

### 1.2.5 T2DM in white adipose tissue

In white adipose tissue (WAT), insulin suppresses lipolysis and promotes lipogenesis during the fed state. During fasting, adipose TAG lipolysis increases while hepatic lipid production diminishes. Impaired insulin action in adipose tissue allows for increased lipolysis, which will promote inappropriate direction of lipids to other tissues (such as liver) and further exacerbates insulin resistance. Coupled with a decline in pancreatic β cells, hyperglycemia develops [37].

### 1.2.6 Insulin resistance as a primary factor of T2DM

Although the primary factors causing T2DM are unknown, it is clear that insulin resistance, which can be defined as a state of reduced responsiveness to normal circulating levels of insulin, plays a major role in its development. Evidence for this comes from: a) cross-sectional studies demonstrating the consistent presence of insulin resistance in patients with T2DM [41]; b) the presence of insulin resistance in non-diabetic offspring of patients with T2DM [42]; c) prospective studies demonstrating the usefulness of insulin resistance as a predictive marker of the future

development of T2DM [41, 42]; d) prevention of diabetes by insulin-sensitizing agents [43, 44].

### 1.2.7 Obesity-induced insulin resistance and T2DM

Insulin resistance is defined as a subnormal biologic response to a given concentration of insulin. Virtually all patients with T2DM have some degree of insulin resistance [45].

Lipid accumulation in skeletal muscle and liver may be a result of increased delivery/synthesis of FA to/in these tissues in states in which energy intake exceeds adipose tissue storage capacity (as seen in obesity and lipodystrophy), or a consequence of either acquired or inherited mitochondrial dysfunction. In 1963, Randle et al. [46] suggested that elevated non esterified fatty acids (NEFA) concentrations were associated with "several abnormalities of carbohydrate metabolism, common to many endocrine and nutritional disorders." The first of these abnormalities described was impaired sensitivity to insulin. Insulin resistance associated with longer-term lipid overload is now considered to involve accumulation of lipids in insulin-responsive tissues other than adipose tissue, so- called ectopic fat deposition [47]. The detrimental effects on insulin sensitivity and other cellular processes are known as lipotoxicity [48]. It should be noted that is not only pure plasma NEFA elevation that is responsible for insulin resistance—plasma TAG concentrations are also increased [38].

In skeletal muscle, insulin resistance manifests primarily as a reduction in insulin-stimulated glycogen synthesis, which is in turn a consequence of reduced glucose transport into the myocyte. The coordinated intracellular response to insulin requires a complex signaling pathway. In muscle, insulin binds to its receptor, activating the receptor tyrosine kinase activity, with subsequent phosphorylation and activation of insulin-receptor substrate 1 (IRS1). When phosphorylated, IRS1 activates PI3K. This enzyme, through signaling intermediates, activates Akt2, which phosphorylates and inactivates AS160, a protein that prevents translocation of GLUT4 through its interaction with Rab proteins. Thus, insulin promotes the docking and fusion of GLUT4-containing vesicles to the plasma membrane [49] (Fig. 1.2).

Figure 1.2

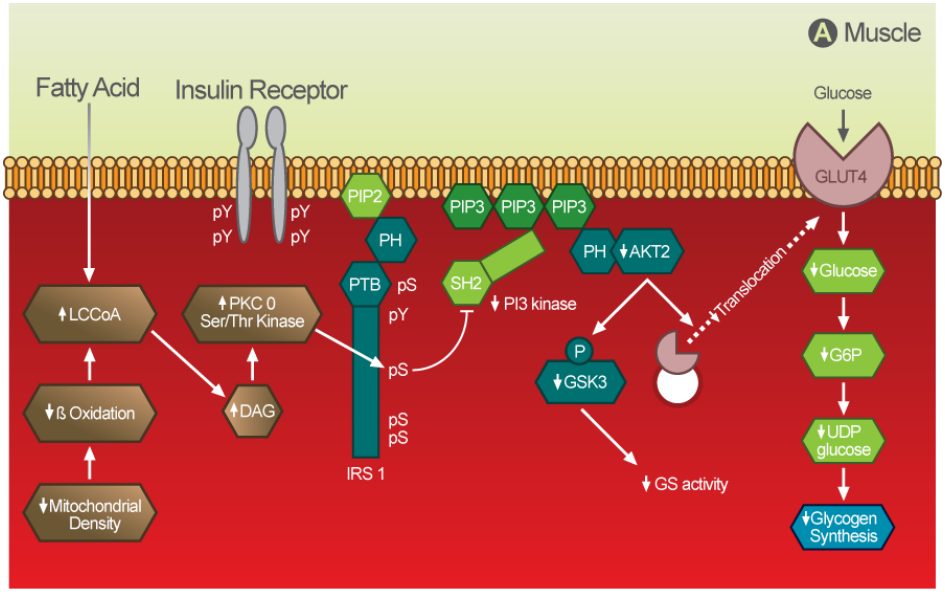


Figure 1.2: Muscle insulin-resistance. DAG: diacylglycerol; GLUT4: glucose transporter: 4 G6P, glucose 6-phosphate: GSK3: glycogen synthase kinase- 3; IRS: insulin receptor substrate; IKK-β: IkB kinase-β; JNK-1: Jun kinase-1; LCCoA: long-chain acylcoenzyme A; nPKCs: novel protein kinase Cs; PI 3-kinase: phosphoinositol 3-kinase; PIP2: phosphatidylinositol 4,5-bisphosphate; PIP3: phosphatidylinositol (3,4,5)-trisphosphate; PTB: phosphotyrosine binding domain; PH: pleckstrin homology domain; SH2: src homology domain, UDP-glucose: uridindiphosphat-glucose. Adapted from Savage, Petersen and Shulman 2007.

Peterson and his collaborators discovered that an impaired mitochondrial function with a lower rate of conversion of diacyl-glycerol (DAG) to triglycerides (TGs) (due to a genetic predisposition) would lead to intracellular DAG accumulation, which impairs insulin-signalling pathways [50].

In the liver, insulin resistance is associated with a reduced ability of insulin signalling to inhibit glucose production, whereas somewhat paradoxically insulin-stimulated lipogenesis seems to be enhanced [51]. Increases in intracellular DAG, due to increased lipogenesis and/or decreased mitochondrial FA oxidation, activate PKC-ε (protein kinase C-ε), which binds to and inactivates the insulin receptor kinase resulting in reduced insulin-stimulated IRS-1 and IRS-2 tyrosine phosphorylation. This in turn results in reduced insulin activation of PI3K and Akt2. Reduced Akt2

activation results in lower GSK3 phosphorylation and lower FOXO phosphorylation, which in turn results in lower insulin-stimulated liver glycogen synthesis and decreased suppression of hepatic gluconeogenesis, respectively [51] (Fig. 1.3).

Figure 1.3

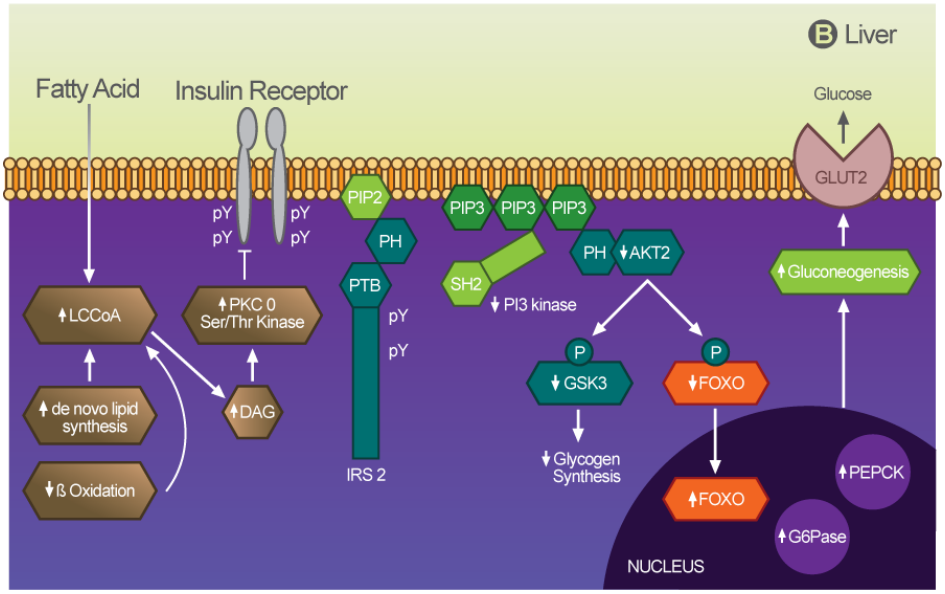


Figure 1.3: Liver insulin-resistance. DAG, diacylglycerol; FOXO, forkhead box protein O; GLUT2, glucose transporter2; G6P, glucose 6-phosphate; GSK3, glycogen synthase kinase- 3; IRS, insulin receptor substrate; IKK-β, IkB kinase-β; JNK-1, Jun kinase-1; LCCoA, long-chain acylcoenzyme A; nPKCs, novel protein kinase Cs; PEPCK, phosphoenolpyruvate carboxykinase; PIP2: phosphatidylinositol 4,5-bisphosphate; PIP3: phosphatidylinositol (3,4,5)-trisphosphate PI 3-kinase, phosphoinositol 3-kinase; PTB, phosphotyrosine binding domain; PH, pleckstrin homology domain; SH2, src homology domain. Adapted from Savage, Petersen and Shulman 2007.

The tyrosine phosphorylation of IRS1 and associated activation of PI3K are impaired in rodent models of insulin resistance in liver, muscle tissue and adipose tissue [3, 52-54]. Similarly, IRS1-associated PI3K activity is greatly reduced in muscles of individuals being given a five-hour intra-lipid infusions (1.5ml/min), indicating that the lipid-induced reduction in insulin-stimulated glucose transport was attributable to a defect in insulin signaling [55].

As well as reinforcing the importance of life-style interventions in the management of T2DM, dietary restriction to limit the stress on energy stores, and exercise to increase mitochondrial number and function, these ideas about the molecular pathogenesis of insulin resistance have provided several new therapeutic targets for the treatment and possible prevention of T2DM [51]. Savage, Petersen and Shulman [51] suggest that insulin resistance in skeletal muscle is the earliest event in the pathogenesis of T2DM in most patients. Muscle insulin resistance is, in turn, associated with peripheral and portal vein hyperinsulinemia, which promotes hepatic steatosis, at least in part by inducing SREBP-1c-mediated de novo lipogenesis and inhibiting fatty acid oxidation. Research conducted by Wolfram et al. [56] suggests that hyperinsulinemia induces nuclear exclusion and inhibition of forkhead box protein A2 (FOXA2), a regulator of fatty acid oxidation. In time, this leads to lipid accumulation in the liver, hepatic insulin resistance, and ultimately T2DM. Adipocyte dysfunction due to either obesity or lipodystrophy is associated with excessive and untimely delivery of fatty acids to the liver and skeletal muscle and probably contributes to insulin resistance in both organs, by altering the balance between fatty acid uptake/synthesis and disposal leading to increases in intracellular lipid content [38] (Fig. 1.4).

Figure 1.4

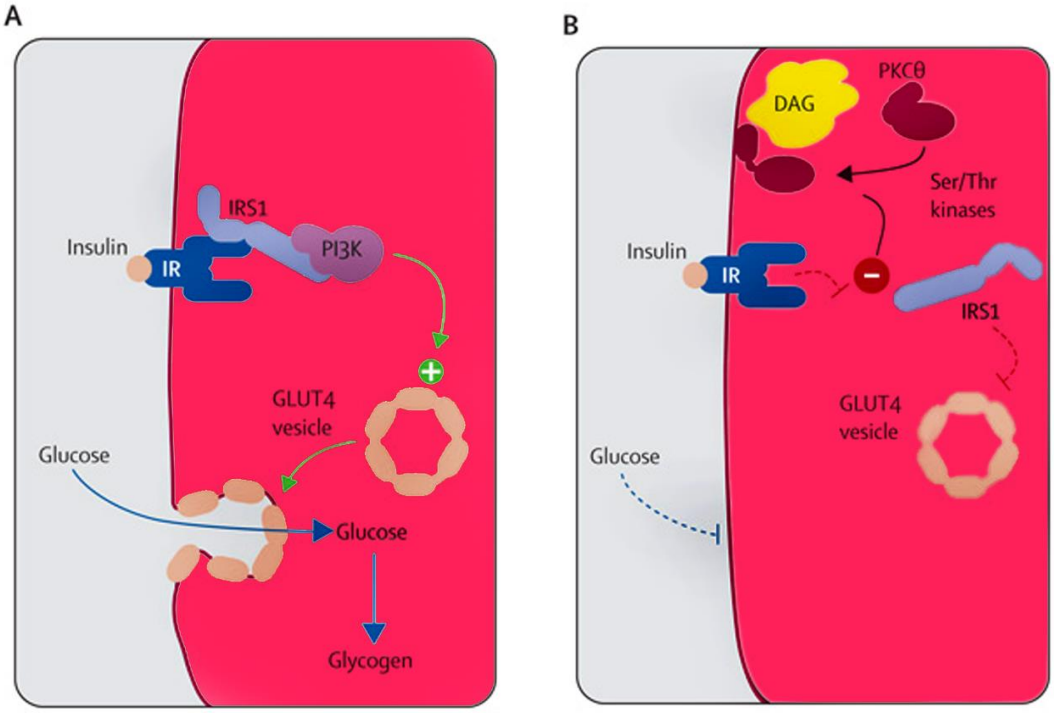

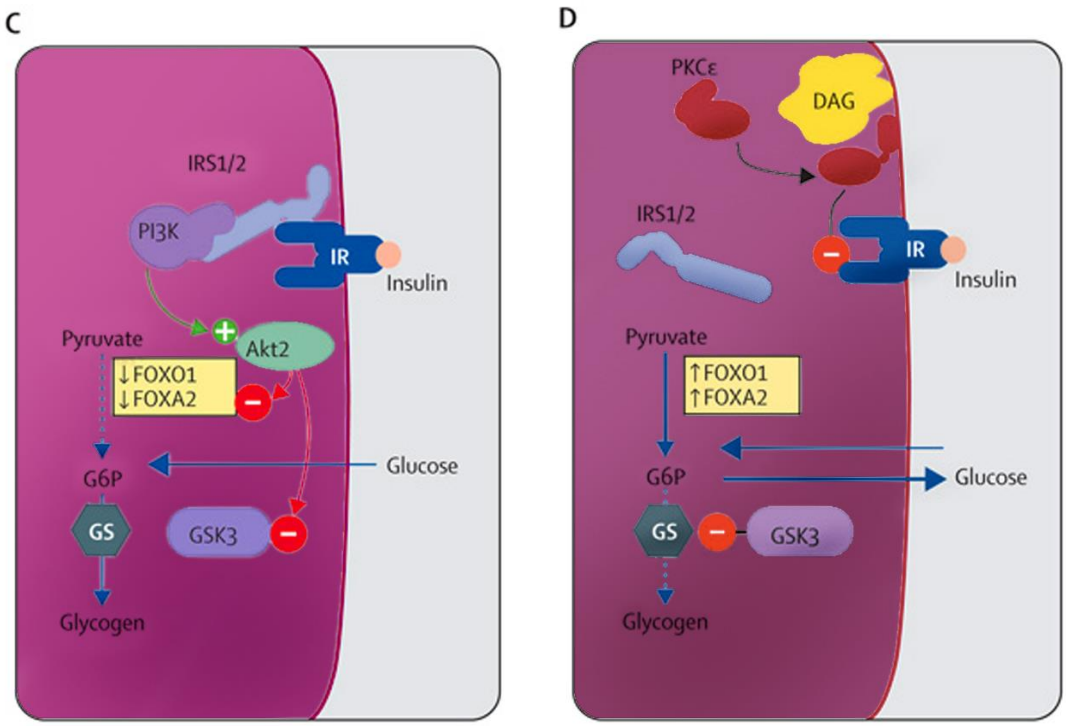


Figure 1.4: Obesity induced insulin resistance (A) Insulin-sensitive muscle. (B) Insulin-resistant muscle. (C) Insulin-sensitive liver. (D) Insulin-resistant liver. IRS=insulin-receptor substrate. IR=insulin receptor. PI3K=1-phosphatidylinositol 3-kinase. GLUT4=glucose transporter 4. DAG=diacylglycerol. PKC=protein kinase C. Ser=serine. Thr=threonine. FOX01=forkhead box O1. FOXA2=forkhead box A2. G6P=glucose-6-phosphate. GS=glycogen synthase. GSK=glycogen synthase kinase. Green circle with plus sign represents activation. Red circle with minus sign represents inactivation. Solid line with arrowhead represents increase or accumulation of substrate. Dotted line indicates inhibition of pathway. Adapted from Samuel et al. 2010.

### 1.2.8 Treatment of T2DM

Non-pharmacological approaches including diet modification, weight control, regular exercise and patient education are used as first-line therapy for the management of T2DM and remain important for optimization of metabolic control. When lifestyle modification fails to achieve or sustain adequate glycemic control, insulin or oral anti-diabetic agents are typically used to manage the disease [36].

#### 1.2.8.1 Oral agents

Treatment options with oral agents are quite diverse, including metformin (insulin sensitising, primarily via inhibition of hepatic glucose production), thiazolidinediones (TZDs) (insulin sensitising PPARγ ligands/activators), α-glucosidase inhibitors (inhibition of gut glucose absorption) and sulphonylureas (β cell insulin secretagogues) [36]. Several new drugs with glucose-lowering efficacy offering certain advantages have recently become available, such as injectable glucagon-like peptide-1 (GLP-1) agonists and oral dipeptidyl peptidase-IV (DPP-IV) inhibitors. These drugs exacerbate the effects of the incretin pathway, leading to elevated glucose-stimulated insulin secretion, reduced gastric emptying and direct action on the hypothalamus to suppress appetite and ultimately, normalised fasting and postprandial glycaemia [57].

Metformin is typically prescribed as the first-line therapy following life-style changes, followed by co-prescription of other therapies if adequate glycaemic control is not maintained. The choice of therapy usually depends on a number of factors, including age of patient and presence of contraindications [58].

## 1.3 AMPK

### 1.3.1 AMPK as a pharmacological target

Several studies have reported that AMP-activated protein kinase (AMPK), a phylogenetically conserved serine/threonine protein kinase, is one of the probable targets of major anti-diabetic drugs in particular metformin, and of insulin sensitizing adipokines (e.g., adiponectin), which are in turn target of TZD's [58-60]. Evidence accumulated over the past few years indicates that AMPK acts as an integrator of regulatory signals monitoring systemic and cellular energy status, thus providing powerful validation of the concept of targeting the AMPK pathway for the treatment of T2DM [36].

### 1.3.2 Functions of AMPK

ATP hydrolysis provides the energy required for cellular functions. Thus, cells require strategies to ensure that adequate regeneration of ATP (from ADP and $P_i$) is maintained. ATP regeneration must be matched to cellular ATP demand, which varies with cellular functions, such as muscle cell contraction, hepatic synthesis of glucose, adipocyte-dependent synthesis of TAG, cellular synthesis of proteins or pancreatic β cell insulin secretion. In addition, many metabolic stressors including glucose deprivation, poisoning and hypoxia, lower ATP availability and therefore require adjustments to conserve ATP expenditure, in order to allow the cell survive. AMPK responds to a requirement to increase cellular ATP production and/or conserve available ATP. AMPK is activated by a decline in intracellular ATP concentrations, which, through the adenylate kinase reaction, concomitantly elevates intracellular ADP and AMP concentrations. As a consequence, AMPK activation occurs in response to a rise in AMP associated with metabolic stresses that interfere with ATP production (e.g., hypoxia or glucose deprivation) or accelerated ATP consumption (e.g., muscle contraction), so as to preserve or maintain tissue function [19]. More recently, not only AMP but also ADP, has been shown to activate mammalian and yeast AMPK and thus, a rise in intracellular ADP may equally be important for AMPK activation [61].

AMPK achieves its capacity to control cellular energy balance by switching on ATP generating catabolic pathways and switching off ATP consuming anabolic pathways. Thus, for activating catabolism and production of ATP, AMPK increases the following processes; long-chain fatty acid (LCFA) uptake into skeletal muscle and its mitochondrial oxidation; glucose uptake and glucose and glycogen breakdown. Conversely, in order to preserve cellular ATP, AMPK supresses anabolic pathways, such as glycogen, lipid and protein synthesis and gluconeogenesis [19].

The acute metabolic actions of AMPK are particularly important in insulin-responsive tissues, such as liver, cardiac and skeletal muscle, adipose tissue and the pancreatic β cell. Through phosphorylation of key downstream targets, AMPK can regulate essential metabolic fluxes, such as glycemic control, insulin action, insulin secretion and metabolic substrate selection. In poorly controlled T2DM, AMPK plays an

essential role in opposing hyperglycemia, through its glucose-lowering effect, follow activation by metformin. It is also important in preventing lipid-induced insulin resistance, because of its capacity to inhibit adipocyte lipolysis and to promote LCFA uptake, suppressing circulating lipid levels. Furthermore, by stimulating mitochondrial LCFA oxidation, AMPK can attenuate ectopic lipid accumulation in skeletal muscle and liver [19, 62]. Taken together the physiological functions of AMPK and the suspected role of AMPK in metabolic disorders, activation of AMPK pathway appears as a promising tool to prevent and/or to treat metabolic disorders, in particular, obesity, insulin-resistance and T2DM.

### 1.3.3 AMPK structure, activation & post-translational modification

AMPK is a heterotrimer of three subunits: α, β and γ subunits, appearing in several isoforms with different action properties [19, 62, 63] (Fig.1.5). The α-subunit ($\alpha_1$ and $\alpha_2$ in mammals) contains the catalytic site whereas regulatory β- ($\beta_1$ and $\beta_2$) and γ- ($\gamma_1$, $\gamma_2$ and $\gamma_3$) subunits are important to maintain the stability of the heterotrimeric complex. The β subunit contains a central region that allows AMPK complex to bind glycogen. The γ subunit contains four tandem repeats known as cystathionine β-synthase (CBS) motifs and each one of them bind one molecule of an adenine nucleotide in a mutually exclusive manner (Fig. 1.5). Charge occupations depend on the relative intracellular concentrations of AMP, ADP and ATP, which means, depend on the 'energy state' of the cell (Fig. 1.5) [19, 62, 63]. ADP, like AMP, stimulates AMPKα ($Thr^{172}$) phosphorylation but, unlike AMP, ADP does not directly activate phosphorylated AMPK [61].

Figure 1.5

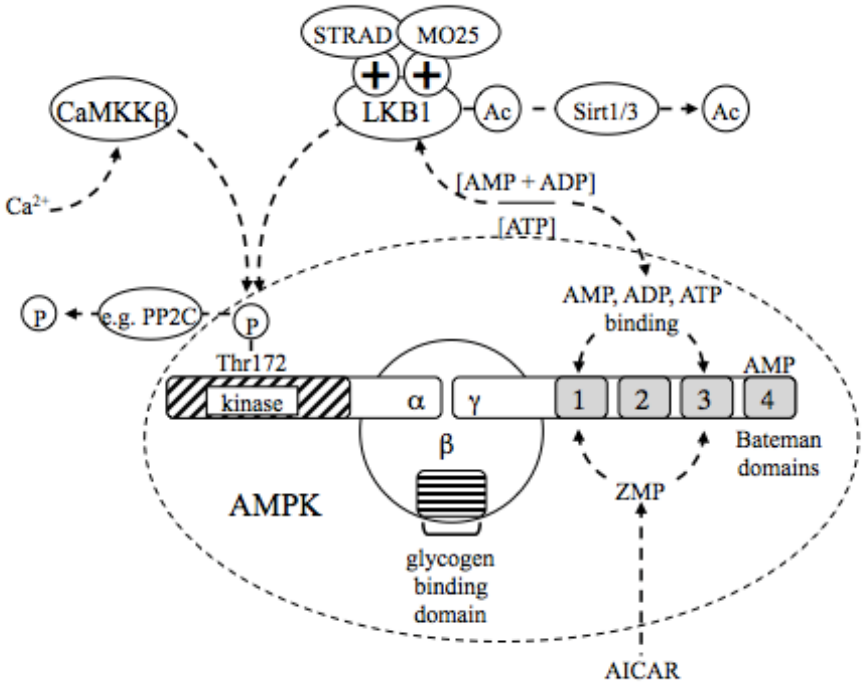


Figure 1.5: Mechanisms regulating AMP-activated protein kinase activity. AMPK is composed of three subunits (α, β and γ) shown within the oval area delimited by the dashed membrane. Arrow-headeddashed lines indicate mechanisms of regulation. AICAR: 5-aminoimidazone-4-carboxmide-1- β-D-ribofuranoside; AMPK: AMP-activated protein kinase; CAMKKβ: $Ca^{2+}$-calmoduline dependent protein kinase kinase β; MO25: Mouse protein 25; P: Phosphate, PP2C: Protein phosphate 2 C; SIRT1: Sirtuin 2 orthologue; STRAD: Ste 20-related adaptor protein; ZMP: AICAR monophosphatase.

### 1.3.4 Upstream regulators of AMPK

AMPK upstream kinases include liver kinase B1 (LKB1), which also activates additional kinases of the AMPK family [64], and the $Ca^{2+}$-calmodulin-dependent protein kinase kinase β (CaMKKβ) [61, 63] (Fig. 1.5). LKB1, originally identified as a tumor suppressor, exists as a complex with two accessory subunits, STRAD and MO25. Studies have suggested that constitutive activity of the LKB1 complex is required to promote activation by the AMP-dependent pathway [65]. However, recent studies indicate that cytosolic localization and activity of LKB1 can be governed by LKB1 acetylation status in the liver (Fig. 1.5) [66]. The phosphorylation status of AMPKα ($Thr^{172}$) is also determined by the rate of phosphor-AMPKα ($Thr^{172}$) dephosphorylation, catalyzed by AMPK phosphatases (Fig 1.5). Dephosphorylation is slower when either AMP or ADP is bound to the γ subunit, such that net AMPKα

(Thr$^{172}$) is increased and AMPK activity is sustained. AMPK phosphatases include members of the protein phosphatase 2C (PP2C or PPM1) family [19] (fig. 1.5).

### 1.3.5 AMPK activation and improved lipid-induced insulin resistance in T2DM

As described in section 1.1, in insulin-responsive tissues, insulin signalling is initiated following the binding of insulin to the cell surface insulin receptor, a member of the receptor protein tyrosine kinase superfamily. Insulin binds to the leucine-rich C-terminal domains in two extracellular α chains. This results in conformational change that brings the two transmembrane/intracellular β chains (which each contain a PTK domain) into closer association, stimulating auto- and trans- phosphorylation of tyrosine residues on the β chains. In turn, this initiates an intracellular signalling cascade, which phosphorylates tyrosine residues on downstream target proteins, including the insulin receptor substrate (IRS) proteins. Most insulin responses are initiated through IRS1 and IRS2; both of them are expressed in the main insulin target tissues (skeletal muscle, heart, adipocyte and liver) as well as in the pancreatic β cell. Defects in phosphorylation of tyrosine residues on the insulin receptor β chains and on the IRS proteins represent a central feature of the impaired insulin-stimulated uptake of glucose into striated muscle seen in lipid-induced insulin-resistance. Impaired insulin signalling related to reduced IRS tyrosine phosphorylation is associated with excessive intracellular lipid accumulation [38]. Activation of AMPK promotes acute oxidation of LCFA, an opposite action to that of insulin. Increased LCFA oxidation (induced by AMPK activation) can suppress glucose breakdown through substrate competition (the glucose/FA cycle) and, therefore, can lower ectopic lipid accumulation, improving insulin signaling. LCFA oxidation directly inhibits glucose transport and phosphorylation and high rates of LCFA exert an acute and sustained inhibitory effect in glucose oxidation [19].

### 1.3.6 AMPK activation combats obesity by suppression of adipogenesis and adipocyte glucose uptake

Obesity can arise either from the recruitment of adipocyte progenitor cells (preadipocytes) that differentiate into additional mature adipocytes or from excessive

TAG accumulation in mature adipocytes resulting in adipocyte hypertrophy. Although insulin and AMPK have opposite effects on adipogenesis and adipocyte glucose uptake, effects of AMPK activation to suppress adipogenesis and adipocyte glucose uptake are beneficial in metabolic diseases (such as T2DM) associated with obesity since they attenuate expansion of the adipose tissue mass and the development of obesity. Increases in AMPK activity caused by administering AICAR in vivo are associated with anti-obesity and insulin-sensitising effects [67]. Importantly, AICAR-induced AMPK activation evokes a reduction in fat mass without any evidence of ectopic lipid deposition, even though it does not increase ATP demand [68].

The PPAR subtypes (α, β/δ and γ) are transcription factors of the nuclear hormone receptor superfamily. PPARs are activated by lipid-derived ligands and thereby act as sensors of "lipid status", translating nutritional signals into metabolic responses. PPAR activation is potentially important for the correction of dyslipidemia and the associated hyperglycemia in T2DM: PPARγ activation augments white-adipocyte glucose uptake and lipid storage, whereas activation of PPARs α and β/δ promote lipid clearance via oxidation in liver and striated muscle. PPARγ activation is necessary and sufficient for differentiation of pre-adipocytes into adipocytes (increasing the storage capacity for TAG), and is essential for the survival of the differentiated adipocyte [69]. The AMPK activator AICAR inhibits adipogenesis in 3T3-L1 or F442A preadipocytes [70, 71], and suppresses PPARγ mRNA expression in cultured adipocytes [72].

### 1.3.7 AMPK opposes insulin's anabolic actions mediated via mTORC1

The mammalian target of rapamycin (mTOR) is a Ser-/Thr- protein kinase that operates as a catalytic subunit in two multimeric signalling complexes, mTORC1and mTORC2 [73-75]. mTORC1 activation promotes anabolism, including protein and lipid/sterol synthesis [76], ketogenesis [77] and inhibition of autophagy [78]. The mTORC2 complex has emerged as a strong candidate kinase for hydrophobic domain phosphorylation of the insulin-signalling kinase Akt [79]. In mTORC2, mTOR is complexed with mLST8 (also known as GβL, G protein β-like), mSin and RICTOR (Rapamycin-Insensitive Companion of mTOR, a positive regulator of mTORC2). Tissue-specific knock-out of RICTOR in adipose tissue decreases insulin-stimulated

glucose uptake and GLUT4 translocation [80].

A widely-accepted pathway of mTORC1 activation involves activation of PI3K and Akt. Akt on mTOR has now been identified as mTOR($Ser^{1261}$), and phosphorylation of this site may initially regulate mTOR activity in mTORC1 [81]. In contrast to phosphorylation of $Ser^{2448}$, $Ser^{248}1$ and $Ser^{1261}$, phosphorylation of mTOR ($Ser^{2446}$) by AMPK inhibits mTOR protein kinase activity, and this phosphorylation is increased by nutrient deprivation but suppressed by insulin [82].

Thus, to summarise, whereas insulin stimulates mTORC1 activity, AMPK inhibits it, thereby opposing insulin's anabolic actions mediated via mTORC1. Nonetheless, AMPK activation can oppose the development of insulin resistance in skeletal muscle induced by nutrient excess (exposure to high glucose or high glucose plus branched chain amino acids), which has been proposed to be secondary to mTOR hyperactivation [83]. These authors suggested that down-regulation of AMPK activity in skeletal muscle in response to nutrient excess precedes mTOR activation and, moreover, that AMPK activation by AICAR diminishes mTOR signalling and insulin resistance in concert.

The livers of insulin-resistant, diabetic mice manifest selective insulin resistance, suggesting a bifurcation in the insulin-signaling pathway: Insulin loses its ability to block glucose production (i.e., it fails to suppress PEPCK and other genes of gluconeogenesis), yet it retains its ability to stimulate fatty acid synthesis (i.e., continued enhancement of genes of lipogenesis). Enhanced lipogenesis is accompanied by an insulin-stimulated increase in the mRNA encoding SREBP-1c [84]. Li et al. have shown that exposure of rat hepatocytes to insulin produced a sugnificnt increase in SREBP-1c mRNA and a significant decrease in PEPCK mRNA. Insulin-mediated changes in both mRNAs are blocked by inhibitors of PI3K and Akt, indicating that these kinases are required for both pathways. In contrast, subnanomolar concentrations of rapamycin, an inhibitor of the mTORC1 kinase, blocked insulin induction of SREBP-1c, but had no effect on insulin suppression of PEPCK. A similar selective effect of rapamycin was observed in livers of rats and mice that experienced an insulin surge in response to a fasting-refeeding protocol. These results establish mTORC1 as an essential component in the insulin-regulated

pathway for hepatic lipogenesis but not gluconeogenesis, and may help to resolve the paradox of selective insulin resistance in livers of diabetic rodents.

### 1.4 PPARα

Peroxisome proliferator activated receptor-alpha (PPARα), along with PPARδ and PPARγ, is a member of the nuclear hormone receptor superfamily. At binding of their ligand, PPARs form heterodimers with 9-*cis* retinoid X receptors (RXRs) and bind to DNA response elements in target gene promoter regions. Forming a heterodimer with RXRα, PPARα binds to a DNA response element, namely the nuclear receptor response element (NRRE). At binding of the NRRE within the promoter of PPAR target genes, gene transcription is activated. Induction of PPARα gene targets requires the interaction of PPARα with PGC-1, often in complex with other enzymes and co-activators. Formation of these complexes is required for full transcriptional induction of PPARα targets in a variety of tissues. [85-87]. The main physiological function of PPARα appears to involve control of critical genes in lipid and lipoprotein metabolism. Thus, PPARα regulates lipid uptake and oxidation, in contrast with that of PPARγ, which promotes uptake but subsequent storage of lipid as TAG in adipose tissue [85, 88]. PPARα expression is relatively high in hepatocytes, enterocytes, vascular and immune cell types such as monocytes/macrophages, endothelial cells, smooth muscle cells, skeletal muscle, lymphocytes, non-neuronal cells like microglia and astroglia [89]. PPARα target genes include carnitine palmitoyltransferase I (CPT I), mitochondrial 3-hydroxy-3-methylglutaryl-CoA synthase (the rate limiting enzyme of ketogenesis), peroxisomal acyl-CoA oxidase (peroxisomal β-oxidation), and microsomal cytochrome P450 (CYP) FA ω-hydroxylases. Thus, PPARα plays a critical role in maintenance of lipid homeostasis (oxidation and production) [86]. In the fasting state, PPARα is activated by adipose-derived FAs, thereby enhancing the generation of ketone bodies through FA oxidation in liver and peripheral blood mononuclear cells [90]. Despite suppression of insulin levels and increases in FA supply, PPARα-deficient mice exhibit an impaired ability to adequately up-regulate hepatic FA oxidation in response to fasting [91]. PPARα deficiency leads to accumulation of hepatic TAG and elicits dysregulation of hepatic lipid and carbohydrate metabolism in mice [92]. Insulin resistance induced by excess of non-

esterified FA and circulating TAG can be corrected by the administration of PPARα activators by actions to promote removal of intracellular lipid through tissue FA oxidation [93]. In light of these findings, PPARα is potentially a powerful molecular target for the treatment of obesity and metabolic disorders.

In WAT, the role of PPARα is not yet established because of the low expression of the nuclear receptor in that tissue [85]. PPARγ is highly expressed and active in WAT, suggesting that in this tissue adipocyte differentiation and TG storage are dominant and lipid catabolism occurs in a very low rate [85]. One study showed that PPARα activation in WAT prevents inflammation, and dual activation of PPARα and -γ enhances the action of adiponectin by increasing both adiponectin and adiponectin receptors (AdipoRs), which can result in the amelioration of obesity-induced insulin resistance [94].

### 1.5 PGC-1α

In addition to ligand-mediated activation, PPARs also are co-activated by transcriptional co-activators and co-repressors. Transcriptional co-activators interact indirectly with the PPARs and other nuclear receptors to establish a platform for recruitment of other proteins important to chromatin remodeling and recruitment of the RNA polymerase II complex. One of the most well studied PPARα co-activators is PGC-1 [95] The PGC-1 co-activators [PGC-1α, PGC-1β, and PGC-related co-activator (PRC)] have been well described as important regulators of mitochondrial metabolism [95]. These co-activators have an impact on cellular biologic responses, enabling the cell to meet changing energy demands associated with various physiologic stimuli. These responses include augmenting mitochondrial biogenesis, respiratory rates, and uptake and metabolism of substrate. The first member of the PGC-1 family to be identified was PGC-1α. It was discovered as a result of its interactions with the nuclear receptor, PPAR-γ, in brown adipose tissue, a mitochondria-rich tissue specialized for thermogenesis. Expression of PGC-1α, also is increased in association with physiologic and pathologic stimuli such as exercise and starvation [95].

PGC-1α is highly expressed in tissues that rely on aerobic metabolism for ATP

production (e. g. skeletal muscle) and relatively low expressed in the liver [95]. However, hepatic PGC-1α gene expression is robustly induced in response to fasting (Yoon et al. 2001). PGC-1α activates expression of PPARα target genes involved in hepatic FA oxidation [96]. Rates of FA oxidation are also diminished in hepatocytes isolated from PGC-1α–deficient mice [97]. The reduction in FA oxidative capacity likely contributes to the fasting-induced hepatic steatotic phenotype observed in one of the mutant lines. Surprisingly, the expression of PPARα target genes involved in β-oxidation is not reduced in generalized PGC-1α$^{-/-}$ mice [97]. However, hepatocytes isolated from PGC-1α–deficient mice exhibit diminished mitochondrial respiration rates[97], providing one mechanistic explanation for the reduced capacity for hepatic fatty acid oxidation. During periods of fasting, the liver catabolises fatty acids to produce 3-carbon substrates for use in gluconeogenesis, the most important source of *de novo* glucose production in higher organisms. PGC-1α gene expression is activated in liver by fasting and glucocorticoids, and it is now recognized that it regulates hepatic gluconeogenesis [95].

### 1.6 Calorie Restriction

Calorie restriction (CR; also called dietary, food, or energy restriction), a reduction of intake of a nutritious diet (at least, 30% reduction), is often reported as the most robust non-genetic mechanism to extend healthspan and lifespan of yeast, worms, flies, and rodents [98, 99]. Studies in the lower-order organisms have sparked interest in the possibility that CR or a CR mimetic can have similar effects on health and lifespan in larger, more complex, and longer-lived species and, potentially, in humans. To explore this possibility, studies of the effects of CR on aging in nonhuman primates (NHP) formally began nearly 25 years ago. In 2009, a study [100] which began in 1989 at the Wisconsin National Primate Research Center (WNPRC) in Madison, concluded that CR did extend life in rhesus monkeys. The investigators found that only 13% of the dieting group died from age-related causes, compared with 37% of the control group. The investigation started when the animals were aged 7-14 (adults) and the maximal lifespan of these animals in captivity is nearly 40 years. Nevertheless, another 25-year study in rhesus monkeys, fed 30% less than control animals, more recently published in *Nature* [98], represents a setback for the notion that a simple, diet-triggered switch can slow ageing. Instead, the findings, suggest that

genetics and dietary composition matter more for longevity than a simple calorie count. Meanwhile, there is a dearth of evidence that caloric restriction slows ageing in humans. Observational studies have found that people of average weight tend to live longest [101]. To date, CR has not been conclusively proved to slow ageing and related diseases in human and non-human primates but, however, fasting and CR have been shown to result in increased insulin sensitivity and lower blood glucose as well as reduced body weight and fat in rhesus monkeys.

It is has been proposed that the response to CR may have evolved as an adaptive trait to postpone reproduction during food scarcity to times of greater food availability. This may have led animals to take advantage of the fact that storage of fat was a sign of food availability and in turn that leanness was a sign of food scarcity. Thus when food was plentiful, the most advantageous strategy was to reproduce. On the other hand when food was scarce the opposite strategy would be most advantageous. In modern times, particularly in the Western society, calorie-rich foods are freely available but food behavior and metabolic processes did not evolve for an environment permitting continual over consumption [102].

### 1.6.1 Sirtuins

There is growing evidence that the metabolic network is an integral regulator of cellular physiology. Dynamic changes in metabolite concentrations, metabolic flux, or network topology act as reporters of biological or environmental signals, and are required for the cell to trigger an appropriate biological reaction. Changes in the metabolic network are recognized by specific sensory macromolecules and translated into a transcriptional or translational response. The protein family of sirtuins, discovered more than 30 years ago as regulators of silent chromatin, potentially fulfills the role of a metabolic sensor during aging and conditions of caloric restriction [103].

The *SIR* (silent information regulator) mutants and genes were first discovered in 1979 in *saccharomyces cerevisiae* [104]. In mammals, the sirtuin family of proteins is a seven-member group (SIRT1–7) of highly conserved, NAD-dependent protein deacetylases that function in the regulation of various biological processes. Each

member of the family is characterised by a conserved 275 amino acid catalytic core domain and a unique N-terminal and/or C-terminal domain of variable length [105]. The mammalian sirtuins occupy different sub-cellular compartments. SIRT1, SIRT6 and SIRT7 are nuclear based. SIRT2 (and under certain conditions, SIRT1) is present in the cytoplasm, whilst SIRTs3 - SIRT5 are found in the mitochondria. The activity within the cell of each sirtuin also differs. SIRT1 and SIRT5 are histone deacetylases, but SIRT5 can also exert demalonylase and desuccinylase activity [106]. SIRT 4 and SIRT6 have ADP-ribosyl transferase activity [105]. However several studies have shown that SIRT6 has also deacetylase activity [107]. SIRT2 and SIRT3 demonstrate both deacetylase and ADP-ribosyl transferase activity. SIRT7 enhances rDNA transcription in the nucleous [108].

#### 1.6.1.1 Regulation of sirtuins in calorie restriction

CR decreases the activity of pro-aging pathways such as insulin and growth hormone signaling and oxidative stress. On the other hand, CR stimulates the activity of cellular stress-resistance pathways including DNA repair and autophagy promoting cell survival in response to environmental stress [109]. It has been shown that in yeast, CR reduces cellular NADH concentrations, thereby increasing the $NAD^+$/NADH ratio and promoting *SIR2* activity [110]. In a number of lower model organisms, sirtuins are required for the lifespan extension provided by CR [109]. Studies have shown that in mice, SIRT1 protein levels are elevated during CR in the brain, WAT, muscles, liver, and kidney [111, 112].

CR induces the expression of SIRT3, particularly in brown adipose tissue (BAT) [113]. However, during CR in mice, cellular $NAD^+$ levels and the $NAD^+$/NADH ratio fluctuate significantly depending on tissue type, suggesting that sirtuins have tissue-specific responses to CR. Nevertheless, it appears that SIRT1 regulates energy metabolism and physical responses to CR, while SIRT3 is able to mediate CR-associated reduction of oxidative damage, preventing age-associated hearing loss [109]. These evidences clarify the importance of sirtuins in CR-mediated prevention of age-associated functional decline, suggesting that sirtuins may be important therapeutic targets for a number of age-related diseases.

In summary, over-expression of sirtuins has been reported to increase lifespan in model organisms [114, 115]. CR is known to increase lifespam in yeast, worms, flies, and rodents [98, 99], and studies suggested that CR increases lifespan by activating sirtuins in yeast, *C. elegans* and *Drosophila* [115-117]. However, several aspects of the role of sirtuins in ageing have proved controversial. Subsequent studies have suggested that sirtuins do not mediate CR effects on ageing, at least in budding yeast and *C. elegans* [118, 119]. Burnett et al. have found that CR increased fly lifespan independently of *SIR2* [120]. These recent findings do not rule out a role for sirtuins in determination of metazoan lifespan, but they do cast doubt on the robustness of the previously reported effects on lifespan inmodel organisms.

#### 1.6.1.2 SIRT1

Mammalian SIRT1 shares the closest similarity to *SIR2*, a protein that was first shown to play an essential role in the control of yeast replicative life span. In mammals, SIRT1 appears to play an important role in controlling glucose metabolism, insulin action, fat storage, and nutrient sensing [102, 121].

Although there is no consistent evidence that SIRT1 content and/or activity declines with ageing, activating this pathway might still be beneficial in preventing some manifestations of aging. Resveratrol is a plant-derived polyphenol that may activate SIRT1 [122] and is reported to exert antioxidant, anti-inflammatory, and anti-tumorigenic properties. It has been suggested that through activation of SIRT1, resveratrol may function as a CR mimetic. Resveratrol treatment has been shown to increase life span in several organisms, including, most notably, high-fat–fed mice, which had improved insulin sensitivity, mitochondrial function, and survival [123]. More recently, treatment of obese mice with SRT1720, a synthetic activator of SIRT1, resulted in similar improvements in survival as were observed in resveratrol-treated mice [124]. These studies make a case that both natural and synthetic SIRT1 activators can improve health and survival, though the belief that these effects are SIRT1-dependent remains controversial, particularly with respect to the actions of resveratrol. In addition, the concept that CR uniformly increases SIRT1 has also been challenged, as one study reported that CR decreased SIRT1 activity in liver [125] and another study has reported that CR has no effect on SIRT1 protein expression in

skeletal muscle and adipose tissue, while increases SIRT3 expression in the same tissues [126]. This suggests that targeting SIRT1 to delay age related diseases (such as T2DM) might be more complex than had been originally anticipated.

#### 1.6.1.3 SIRT1 in hepatic glucose and lipid metabolism

SIRT1 is an important regulator of hepatic glucose and lipid metabolism. Contrasting effects of SIRT1 are reported with respect to hepatic gluconeogenesis. For instance, SIRT1 has been shown to repress gluconeogenic gene expression through inhibition of HNF4α [127] and, during short-term fasting (6 to 8 hours), SIRT1 inhibits cAMP response element binding protein (CREB)-regulated transcriptional coactivator 2 (CRTC2; also known as TORC2), a key mediator of early phase gluconeogenesis [128]. In contrast, prolonged fasting (24 to 48 hours) increases SIRT1-mediated deacetylation (and activation) of PGC-1α leading to elevated gluconeogenesis [128, 129]. Furthermore, several studies support the notion that elevated SIRT1-mediated gluconeogenesis plays a key role in mediated abnormal elevation of hepatic glucose production in T2DM [130-132].

SIRT1-has also been reported to play a critical role in regulation of hepatic FA oxidation and regulation of lipid homeostasis [109]. Hepatic deletion of SIRT1 leads to impaired PPARα signaling, while overexpression of SIRT1 activates PPARα, increasing expression of PPARα gene targets, and increased fatty acid oxidation. SIRT1 induces PPARα signaling through deacetylation of PGC-1α [133]. Interestingly, SIRT1 does not affect the formation of the PPARα–PGC-1α complex, since in SIRT1 knockdown hepatocytes PGC-1α is still recruited to the PPAR response element (PPRE) of FA oxidation genes. However, PGC-1α remains acetylated when SIRT1 is not present so it is unable to induce transcription of PPARα gene targets.

SIRT1 also regulates hepatic cholesterol and bile acid homeostasis through direct modulation of the liver X receptor (LXR), farnesoid X receptor (FXR), and SREBP family of transcription factors [109]. Li and collaborators have previously shown that SIRT1 can directly deacetylate LXRs, resulting in increased LXR turnover and target

gene expression [134]. Systemic deletion of SIRT1 in mice results in decreased serum HDL levels [125, 134].

Consistent with the notion of an important role for SIRT1 in regulating hepatic fatty acid oxidation, a deletion of hepatic SIRT1 by floxing exons 5 and 6 leads to the development of liver steatosis even under normal chow diet [135], whilst hepatic overexpression of SIRT1 mediated by adenovirus attenuates hepatic steatosis and ER stress, and restores glucose homeostasis in mice [136], confirming the essential role of SIRT1 in maintaining hepatic metabolic homeostasis.

GCN5 counters the effect of SIRT1 by acetylating PGC-1α, inhibiting its transcriptional activity [137-139]. Hence, the balance between relative levels and activity of SIRT1 and GCN5 could provide regulatory convergence point for induction of PPARα gene targets and potentially other SIRT1 targets.

In summary, these findings imply that hepatic SIRT1 plays a critical role in metabolic regulation, and activation of SIRT1 in the liver may prove beneficial in treating obesity-associated diseases, such as T2DM. However, contrasting effects of SIRT1 are reported with respect to hepatic gluconeogenesis. Further studies need to be done in order to understand the role of SIRT1 in the development of T2DM, concerning the gluconeogenic pathway.

#### 1.6.1.4 SIRT1 regulates skeletal muscle glucose and lipid metabolism

In skeletal muscle, SIRT1 regulates glucose and lipid metabolism in part through deacetylation of PGC-1α. PGC-1α is responsible for switching mitochondrial metabolism from glucose to fatty acid oxidation under conditions of starvation [138]. In muscle (and also in liver), GCN5 acetylates PGC-1α with a repressive effect on its activity [137], whereas SIRT1, induced by fasting, deacetylates PGC-1α *in vitro* [138, 140].

Additionally, SIRT1 improves insulin sensitivity in skeletal muscle. A study from Schenk et al. has shown an improvement in insulin sensitivity, secondary to increased

insulin-stimulated PI3K activity, in mice submitted to 20 days of CR although, in mice lacking SIRT1 (through deletion of the exon 4 that encodes for the deacetylase activity of SIRT1 gene), this improvement in insulin sensitivity was completely abrogated [141]. In this study Schenk has found that SIRT1 is required for the deacetylation and inactivation of the transcription factor Stat3 during CR, which resulted in decreased gene and protein expression of the p55α/p50α subunits of PI3K, thereby promoting more efficient PI3K signaling during insulin stimulation.

#### 1.6.1.5 SIRT1 in white adipose tissue

White adipose tissue (WAT) is the major fat storage organ in the body. SIRT1 is up regulated in WAT in response to food withdrawal, where has been shown to repress PPARγ, by docking with its cofactors NCoR (nuclear receptor co-repressor) and SMRT (silencing mediator of retinoid and thyroid hormone receptors) [111]. Moreover, in differentiated adipose cells, up regulation of SIRT1 leads to decreased fat storage and increased lipolysis [87].

WAT also functions as an endocrine organ, secreting a number of bioactive peptides, known as adipokines, such as leptin and adiponectin, which control energy balance, glucose regulation, and FA catabolism. In addition, adipose tissue macrophages (ATMs) are prone to secrete high levels of inflammatory mediators, such as tumor necrosis factor alpha (TNFα), interleukin-6 (IL-6), and inducible nitric oxide synthase (iNOS), resulting in a heightened inflammatory status particularly under obesity conditions [142]. In obesity, insulin resistance has been linked to leptin resistance and decreased plasma adiponectin [143, 144]. SIRT1 increases adiponectin transcription in adipocytes through deacetylation and activation of FOXO1, which enhances the interaction between FOXO1 and C/EBPalpha, resulting in increased adiponectin production [145]. Effects of SIRT1 in leptin levels are not well established yet.

#### 1.6.1.6 SIRT1 and AMPK: A regulatory feedback loop?

##### *1.6.1.6.1 AMPK regulation by SIRT1*

Downregulation of AMPK in response to high glucose, with a parallel decrease in SIRT1 activity was observed in cultured HepG2 cells [146, 147]. In both studies there was an increase in the release of lactate, suggesting a decrease in the $NAD^+$/NADH ratio, which could have contributed to the decrease in SIRT1 activity. Lan et al demonstrated that overexpression of SIRT1 in human embryonic kidney-293T cells diminished lysine acetylation of LKB1 and caused its movement from the nucleus to the cytoplasm, where LKB1 became active and activated AMPK. In contrast, transfection with short hairpin (sh)RNAi for SIRT1 had opposite effects on these parameters and also decreased the phosphorylation of another LKB1 target, the AMPK-related kinase MARK1 [66]. Hou et al found later that the ability of resveratrol to activate AMPK *in vitro* (HepG2 cultured cells) and *in vivo* (mouse liver) required the presence of both: LKB1 and SIRT1 [148]. These findings together with the demonstration that SIRT1 and AMPK share common activators, actions and target molecules [149], led us to believe that AMPK activity is regulated by SIRT1 in an LKB1-dependent manner.

##### *1.6.1.6.2 SIRT1 regulation by AMPK*

Fulco et al observed that glucose restriction impaired the differentiation of skeletal muscle myoblasts, an effect preceded by a much earlier decrease in cellular ATP and an increase in the activity of AMPK. They also found that incubation with 5-aminoimidazole-4-carboxamide-1-β-d-ribofuranoside (AICAR), a more direct AMPK activator, produced a similar sequence of events. In both situations, the inhibition of myoblast differentiation was accompanied by an increased transcription of the $NAD^+$ biosynthetic enzyme NAMPT, which in turn increased the $NAD^+$/NADH ratio. Conversely, both myoblasts derived from $SIRT1^{+/-}$ mice and cells transduced with shRNAi for SIRT1 were resistant to the effect of AMPK activation on muscle differentiation, strongly suggesting that it was SIRT1 mediated [150]. In a subsequent study, Canto and Auwerx [151] demonstrated that AMPK activation by AICAR increased PGC-1α-mediated gene expression in a SIRT1-dependent manner in $C_2C_{12}$

myocytes and mouse embryonic fibroblasts. They have also shown that various AMPK activators (AICAR, metformin and the mitochondrial uncoupler dinitrophenol), but not direct SIRT1 activators, increased $NAD^+$ levels and the $NAD^+$/NADH ratio and that this resulted in SIRT1 activation, as evidenced by the deacetylation and activation of PGC-1α. The two groups differ in that Fulco et al. [150] proposed that the key linkage between increased AMPK and SIRT1 activities was the upregulation of NAMPT, whereas Canto et al. [151] found that AMPK could alter the $NAD^+$/NADH ratio and activate SIRT1 apparently independently of NAMPT. Iwabu et al. have provided evidence that adiponectin induces extracellular $Ca(2^+)$ influx by adiponectin receptor 1 (AdipoR1), which was necessary for subsequent activation of CaMKKβ (AMPK upstream kinase), AMPK and SIRT1, increased expression and decreased acetylation of PGC-1α, and increased mitochondria in myocytes [152]. Moreover, muscle-specific disruption of AdipoR1 suppresses the adiponectin-mediated increase in intracellular $Ca(2^+)$ concentration, and decreased the activation of CaMKKβ, AMPK and SIRT1 by adiponectin. Suppression of AdipoR1 also resulted in decreased PGC-1α expression and deacetylation, decreased mitochondrial content and enzymes, decreased oxidative type I myofibres, and decreased oxidative stress-detoxifying enzymes in skeletal muscle, which are associated with insulin resistance [152]. These studies, together with the studies that show that AMPK is regulated by SIRT1, suggest a possible feedback loop between both proteins, which might be an interesting target for the treatment of T2DM.

#### 1.6.1.7 SIRT3

SIRT3, the most well characterised mitochondrial sirtuin, is highly expressed in metabolically active tissues such as brown adipose, muscle, liver, kidney, heart, and brain [109]. SIRT3 deficient mice exhibited striking mitochondrial protein hyperacetylation [153]. These hyperacetylated proteins include subunits of oxidative phosphorylation complexes and metabolic enzymes such as: a) acetyl-CoA synthetase 2 (AceCS2), an enzyme that catalyzes the production of acetyl-CoA from acetate; b) glutamate dehydrogenase (GDH), which interconverts glutamate and α-ketoglutarate (KG) and is a pivotal enzyme in regulating amino acid entry into the TCA cycle; c) long-chain acyl CoA dehydrogenase (LCAD), a central enzyme in the fatty acid β-

oxidation pathway; and d) 3-hydroxy-3-methylglutaryl CoA synthase 2 (HMG-CoAS2), the rate-limiting step in β-hydroxybutyrate synthesis, as well as oxidative stress reducing enzymes, in particular, isocitrate dehydrogenase 2 (ICDH2), superoxide dismutase 2 (SOD2), and MnSOD [109, 154]. ICDH2 catalyzes the irreversible oxidative decarboxylation of isocitrate to KG and $CO_2$ [154]. The increased production of KG mediated by NADP-dependent isocitrate dehydrogenase (NADP-ICDH) and its decreased utilization via the TCA cycle confer a unique strategy to modulate the cellular redox environment. KG is a key participant in the detoxification of reactive oxygen species (ROS) in live organisms [155]. The capacity of SIRT3 to deacetylate and activate ICDH2 is then important to protect cells from ROS production and age-related oxidative damage [154]. SIRT3 also protects *in vitro* fertilized mouse pre-implantation embryos against oxidative stress [156]. Furthermore, two studies showed that SIRT3 deficient mice failed to suppress oxidative stress in response to CR, where in cultured cells overexpression of SIRT3 and/or ICDH2 increases NADPH levels and protects from oxidative stress-induced cell death [157, 158]. These observations demonstrate that SIRT3 can delay the onset of a number of oxidative stress-associated pathologies in multiple tissues and suggest that SIRT3 may be a novel target for these age-associated diseases as well as aging itself.

A number of recent studies have reported that hyperacetylation of mitochondrial proteins in SIRT3 deficient mice results in a variety of metabolic abnormalities including reduced ATP production, decreased rates of fatty acid oxidation, and fatty liver [159-162]. However, since SIRT3 null mice display minimal phenotypes under normal feeding conditions, particularly when they are young [153], much work still needs to be done to determine whether the effects of SIRT3 deletion on these processes are physiologically relevant, and whether they are direct consequences of particular hyperacetylated mitochondrial proteins. Furthermore, it remains to be answered whether SIRT3 is required for CR-mediated extension of lifespan or it is only a part of CR- elicited anti-aging circuits [153].

## 1.7 The interacting metabolic roles of AMPK, the lipo-oxidative PPARs and SIRTs

Whereas PPARγ activation augments white-adipocyte glucose uptake and lipid storage in the fed state, activation of the lipo-oxidative PPARs α and β/δ promote lipid clearance via oxidation in liver and striated muscle and assume an important role in lipid management during periods of carbohydrate scarcity (e.g., fasting). By promoting metabolic adaptations that enhance the oxidation of lipid, which might otherwise be stored (adipose tissue) or accumulated ectopically (liver, skeletal muscle), PPARα and PPARδ/β shift energy production away from carbohydrate oxidation and are insulin sensitising and, in this regard, have metabolic actions that complement the more acute actions of AMPK.

There is an associated loss of co-repressors and recruitment of coactivators (e.g. PPARγ co-activator-1α, PGC-1α). PGC-1α induces mitochondrial biogenesis and triggers mitochondrial proliferation. In oxidative muscle and liver, PGC-1α cooperates with PPARα to increase the expression of genes encoding mitochondrial FA oxidation enzymes, thereby increasing the capacity for FA oxidation and intracellular lipid clearance [163]. AMPK activation by AICAR increases expression of PPARα target genes and PGC-1α in cultured muscle cells and mouse skeletal muscle, whereas inhibition of PPARα and PGC- α by siRNAs prevents AICAR-stimulated increases in LCFA oxidation [164].

PGC-1α and -β are also substrates for the sirtuin class of $NAD^+$- dependent protein deacetylases. In general, AMPK and SIRT1 have similar metabolic effects: they mutually regulate one other and share common metabolic targets [149]. As noted previously, SIRT1 (and possibly SIRT3) deacetylate and activate the AMPK kinase LKB1. Both SIRT1 and SIRT3, similarly to AMPK and the lipo-oxidative PPARs, promote LCFA oxidation. SIRT1 protein expression increases in response to prolonged caloric restriction. This is associated with increased mitochondrial biogenesis mediated by activated PGC-1α [112], which is post-translationally deacetylated and activated by SIRT1 [129, 140]. AMPK could be a key sensor and effector in mediating the beneficial effect of caloric restriction on health and lifespan, as discussed in detail elsewhere [165]. Deficient AMPK activity compromises

SIRT1-dependent responses of skeletal muscle to both fasting and exercise, resulting in impaired PGC-1α deacetylation, which in turn suppresses induction of mitochondrial biogenesis and mitochondrial gene expression [166].

In liver, SIRT3 regulates the acetylation status of several metabolic enzymes in the mitochondrial matrix, including LCAD. LCAD is deacetylated and activated in wild-type mice on fasting, promoting β-oxidation [167]. Like PPARα$^{-/-}$ mice, SIRT3$^{-/-}$ mice appear phenotypically normal in the fed state (although they show marked hyperacetylation of several mitochondrial proteins) but, during fasting, their livers exhibit lower rates of LCFA oxidation, together with higher levels of FA-oxidation intermediates and TAG accumulation [168]. Increased SIRT3 preserves ATP biosynthetic capacity and protects myocytes from oxidative stress-mediated cell death [159]. Conversely, SIRT3 deficiency decreases $O_2$ consumption and causes the development of oxidative stress, leading to impaired insulin signaling via increased Ser-phosphorylation and decreased Tyr-phosphorylation of IRS-1. This effect is mimicked by knockdown of SIRT3 in cultured myoblasts, which exhibit reduced mitochondrial oxidation, increased ROS, and increased Ser- phosphorylation in combination with decreased Tyr-phosphorylation of IRS-1 [169]. Steady-state ATP levels are reduced in SIRT3$^{-/-}$ mouse embryonic fibroblasts, which may result from a defect in deacetylation of electron transport chain components [159]. AMPK regulates the expression of oestrogen-related receptor α (ERRα), which binds to the SIRT3 promoter [170].

## 1.8 Aim of the thesis

AMPK and SIRT1 both regulate each other and share many common target molecules. Furthermore, both AMPK and SIRT1 can interact with and regulate PGC-1α and PPARα and this is an essential requirement for full transcriptional induction of PPARα gene targets as well as interaction with other nuclear receptors. Given this, my research sought to establish and characterise the links between SIRT1 and AMPK and induction of PPARα gene targets in modulating insulin-responsive tissues, with the view of establishing the potential for use of dual SIRT1 and AMPK activators as an effective treatment in T2DM.

Specific aims:

1. To delineate further the potential regulatory importance of deacetylation of PGC-1α by the $NAD^+$ regulated protein deacetylase SIRT1 and its regulation by AMPK in modulating the function of PPARα gene expression in the liver, in response to alteration in nutritional status;

2. To understand the impact of nutrient availability (starvation, high fat, and maternity low protein diet) in lipogenesis in insulin sensitive tissues;

3. To investigate whether a feedback loop exists to regulate AMPK and SIRT1 activation in liver and muscle, *in vivo* and *in vitro*, whereby AMPK activates SIRT1 through NAMPT or β-oxidation and, in turn, SIRT1 causes further activation of AMPK;

4. To investigate whether AMPK deficiency modulates SIRT1 activity and to understand the role of AMPK-SIRT1 pathway in the context of insulin response, in skeletal muscle and liver *in vivo* and *in vitro*;

5. To examine the role of IRF3 and IRF4 in the maternal low-protein model of fetal programming, to better understand the mechanisms responsible for onset of obesity following exposure to an adverse intra-uterine environment.

I have used disease models (muscle and liver specific AMPK $\alpha 1/2^{-/-}$ mice, PPARα knockout mice) as well as specific diet administration (CR, high fat, high fructose and maternity low protein diet) to achieve the objectives.

**Chapter:**

*2. Materials and Methods*

## 2.1 Materials

Reagents of analytical grade and deionized water (obtained from ***Triple Red Laboratory Technology Ltd., Buckinghamshire, UK***) were used.

Nuclease-free water, RNase-free 50 ml and 15 ml falcon tubes, 1.5 ml microfuge tubes, 0.2 ml qPCR tubes and the scrambled sequence siRNA (negative control) were purchased by ***Ambion (Cambridgeshire, UK)***. Full range rainbow recombinant protein molecular weight marker (range 10,000 – 250,000), hybond ECL nitrocellulose membranes and hyperfilm ECL were obtained from ***Amersham***, ***GE Healthcare (Uppsala, Sweden)***. Acrylamide (40%), Ammonium Persulfate (APS), DC Protein Assay and Western Blotting system were purchased from ***Bio-rad laboratories (Hertfordshire, UK)***. Triglyceride assay kit was purchased from ***Cayman Chemicals (Ann Arbor, US)***. Antibodies were purchased from ***Cell Signaling Biomanufacturing and Life Science Research (New England Biolabs, Hertforshire, UK)***. Optimem Medium® was purchased from ***Gibco, Life Technologies Ltd*** **(Paisley, Strathclyde, UK)**. Polyclonal goat-anti-rabbit secondary antibody, Lipofectamine® RNAiMAX (transfection reagent) was purchased from ***Invitrogen***, ***Life Technologies Ltd*** **(Paisley, Strathclyde, UK)**. Insulin ELISA kit was purchased from ***Mercodia (Uppsala, Sweden)***. Catch and Release v2.0 immunoprecipitation reversible kit, monoclonal mouse anti-SIRT1 and monoclonal rabbit anti-SIRT6 antibodies were obtained from ***Millipore (Millipore UK Limited, Watford, UK)***. Proteinase K®, RNase – Free DNase® set, RNeasy® mini, midi and maxi RNA extraction kits for total RNA isolation and were obtained from ***Qiagen Sample and Assay technologies (West Sussex, UK)***. Polyclonal goat anti-PGC1-α, polyclonal mouse anti-IRS-1 antibodies were obtained from ***Santa Cruz Biotechnology (Santa Cruz, CA, USA)***. Ammonium persulfate ($NH_4S_2O_8$), Antibiotics (100 U/ml penincillin and 0.1g/l streptomycin), bovine serum albumin (BSA) lyophilized powder, bromophenol blue, 2-deoxy-D-glucoseethanol, dimethyl sulphoxide (DMSO), Dulbelcco's Modified Eagle Medium (DMEM), Dulbecco's phosphate – buffered saline (DPBS), ethylene diaminetetraacetic acid (EDTA), Foetal Calf Serum (FCS), glycerol, Hank's Balanced Salt Solution (HBSS) + $Ca^{2+}$ and $Mg^{2+}$, hydrochloride acid (HCL), insulin solution from bovine pancreas 10 mg/ml in 25 mM HEPES pH 8.2, l-glutamine 200 mM (100x stock), 2-β-mercaptonethanol, magnesium sulphate ($MgSO_4.7H_2O$), methanol,

N,N,N,N tetramethylethylenediamine (TEMED), penicillin 5000 U/ml – streptomycin 5 mg/ml (50x stock), phosphate-buffered saline (PBS) tablets, polyclonal rabbit anti-mouse secondary antibody, potassium chloride (KCL), protease inhibitor cocktail, radio-immunoprecipitation assay (RIPA) buffer, sodium carbonate ($Na_2CO_3$), sodium chloride (NaCl), sodium dodecyl sulphate (SDS), tris(hydroxymethyl)aminomethane [$NH_2C(CH_2OH)_3$ ] (TRIS-base), tris(hydroxymethyl)aminomethanehydrochloride ($C_4H_{11}NO_3 \cdot HCl$ ) (TRIS-HCL), Trypsin/EDTA solution and Tween® 20 viscous liquid were purchased from ***SIGMA – Aldrich (Guillingham, UK)***. Pipettes, tips, serological pipettes, 96 well plates (for protein essay and qPCR) and disposable gloves were purchased from ***Starlab (Blakelands, UK)***. Glucose assay kit was purchased from ***Thermo Electron (Melbourbe, Australia)***. Absolute qPCR Mix, One target plus siRNA rat SIRT1 predicted (CAGAACCACCAAAGCGGAA) and Supersignal West Pico Cheminoluminescent Substrate were purchased from ***Thermo Fisher Scientific (ABgene, Epsom, UK)***. Primers were purchased from ***Eurogentec (Hampshire UK)***. Ultrasensitive mouse Insulin ELISA kit was purchased from ***Mercodia (Uppsala, Sweden)***. Reverse transcription kit was purchased from ***Promega UK (Southampton, UK)***. 6-Chloro-2,3,4,9-tetrahydro-1H-carbazole-1-carboxamide (Ex527) was purchased from ***Tocris Bioscience (Bristol, UK)***. Non-esterified fatty acids (NEFA) assay kit was purchased from ***Wako Pure Chemical Industries (Osaka, Japan)***.

## 2.2 Methods

### 2.2.1 Cell Cultures

All cell lines were cryopreserved at the Blizard Institute of Cell and Molecular Science, Barts and the London School of Medicine and Dentistry, Queen Mary University of London, in 1.5 ml vials (Sterilin Ltd, Houslow, UK) containing freezing media with a final concentration of 10% (v/v) DMSO, 10% (v/v) tissue culture medium [DMEM (25mM glucose)] and 80% (v/v) foetal bovine serum. Prior to culture, cells were removed from liquid nitrogen and thawed in a water bath maintained at 37 ° C. The contents of the vials were suspended in 10 ml of warmed tissue culture medium and centrifuged for 5 min at 1200 x g. Centrifugation resulted in a cell pellet that was re-suspended in fresh culture medium to give a cell

suspension. The cell suspension was transferred to a tissue culture flask (Falcon, Becton Dickinson, NJ, USA) and stored in an incubator at 37 ° C and at an atmosphere of 5% $CO_2$ and 95% $O_2$, until the cells had reached the required confluency for passage.

#### 2.2.1.1 H4IIEC3 hepatocyte cell line

H4IIEC3 cells (rat hepatocyte cell line) obtained from the European Collection of Animal Cell Cultures (ECACC; ECACC no. 85061112) were used. The cell line was initially derived from the Reuber H-35 hepatoma, which was induced in AXC rat by the carcinogen N-2 fluoroenyldiacetamide [171]. Cells were cultured in DMEM containing 25mM of glucose (Appendix I.), non-essential amino acids and supplemented with 10% (v/v) foetal calf serum (FCS) (Appendix II.), 2 mM glutamate, 500 IU/ml penicillin and 100 µM streptomycin, in 95% $O_2$ and 5% $CO_2$, and incubated at 37° C. Cells were routinely passaged (when they were approximately 90% confluent) as follows. Briefly, cells were washed with phosphate buffered saline (PBS) (Appendix III.) following aspiration of DMEM culture medium from the cells. Cellular detachment from tissue culture flasks was achieved using 5 ml of 0.05% trypsin (diluted in PBS), containing 0.02% ethylenediaminetetraacetic acid (EDTA). Cells were then re-suspended in a small amount of tissue culture medium (usually 5 ml), transferred to a polypropylene tube (Ambion, Cambridgeshire, UK) and pelleted by centrifugation at 1200 x g for 5 min. The supernatant was discarded and 10 ml of fresh culture medium was added to the cells to create a cell suspension for experimental use. For experiments, cells were seeded at a density of $1.2 \times 10^6$ cells into 6-well flat-bottomed plates (9.5 $cm^2$ growth area) (Falcon, Becton Dickinson, NJ, USA), creating a cell monolayer. Cells were then returned to culture and allowed to attach overnight as monolayers.

Transient knockdown of target proteins was achieved using siRNA duplex technology. SIRT1 siRNA (target sequence: CAGAACCACCAAGCGGAA) and the scrambled siRNA sequence (negative control) were purchased from Dharmacon, USA. Transfection of H4IIEC3 was performed using Oligofectamine® (Invitrogen, USA) following the manufacturer's instruction for transfection of adherent cells

seeded in 6-well plates. 1.2 x $10^6$ cells/well were seeded in complete growth media (DMEM, 25 mM glucose) and incubated at 37°C in 95% $O_2$ and 5% $CO_2$. When cells were grown 25-30% confluent, a mix (A) of 7.5 µl siRNA duplexes (stock solution of 20 µM) and 177.5 µl of serum-free, penincilin-streptomycin-free Optimem® (Invitrogen, UK) was prepared. In parallel, a mix (B) of 7.5 µl of Oligofectamine® and 7.5 µl of serum-free, penincilin-streptomycin-free Optimem® (Invitrogen, UK) was prepared. The two mixes were incubated for 10 min, at room temperature. Subsequently, the content of the tubes were mixed (total volume of 200 µl) and incubated for 25 min at room temperature. Cells were washed in 1X PBS solution and 800 µl of Optimem® plus 200 µl of the transfection mix were added to each well and incubated for 4h at 37°C in 95% $O_2$ and 5% $CO_2$. Subsequently, 1ml of DMEM 25mM glucose supplemented with 30% FCS was added to each well. The plates were incubated at 37°C in 95% $O_2$ and 5% $CO_2$ for 72h. Then, cells were washed in ice-cold PBS, lysed in RLT buffer® (from RNeasy kit, Quiagen) containing β-mercaptoethanol, and collected for RNA extraction, or lysed in RIPA buffer® (ready to use solution containing 150 mM NaCl, 1.0% IGEPAL® CA-630, 0.5% sodium deoxycholate, 0.1% SDS, 50 mM Tris, pH 8.0) purchased from Sigma Aldrich (Guillingham, UK) and collected for protein extraction and measurement.

#### 2.2.1.2 L6 rat myoblast cell line

L6 rat myoblasts were kindly provided by Dr. Tania Maffucci, Centre of Diabetes, Blizard Institute, Queen Mary University of London (UK). The L6 myogenic line was isolated originally by Yaffe from primary cultures of rat thigh muscle maintained for the first two passages in the presence of methyl cholanthrene [172]. Cells were cultured in DMEM containing 25mM of glucose, non-essential aminoacids and supplemented with 10% (v/v) foetal calf serum (FCS), 2 mM glutamate, 500 IU/ml penicillin and 100 µM streptomycin, in 95% $O_2$ and 5% $CO_2$, and incubated at 37°C. Cells were routinely passaged (when they were approximately 90% confluent) as follows. Briefly, cells were washed with PBS following the aspiration of DMEM culture medium from the cells. Cellular detachment from tissue culture flasks was achieved using 5 ml of 0.05% trypsin (diluted in PBS), containing 0.02% EDTA. Cells were then re-suspended in a small amount of tissue culture medium (usually 5

ml), transferred to a polypropylene tube (Ambion, Cambridgeshire, UK) and pelleted by centrifugation at 1,200 x g for 5 min. The supernatant was discarded and 10 ml of fresh culture medium was added to the cells to create a single cell suspension for experimental use. For experiments, cells were seeded at a density of 1.2 x $10^6$ cells into 6-well flat-bottomed plates (9.5 $cm^2$ growth area) (Falcon, Becton Dickinson, NJ, USA), creating a cell monolayer. Cells were then returned to culture and allowed to attach overnight as monolayers.

After the experiments, described further in Chapter 4, section 4.2.1, cells were either lysed in RLT® buffer (from RNeasy kit, Quiagen) containing β-mercaptoethanol, and collected for RNA extraction and measurement, or lysed in ice-cold RIPA buffer (ready to use solution containing 150 mM NaCl, 1.0% IGEPAL® CA-630, 0.5% sodium deoxycholate, 0.1% SDS, 50 mM Tris, pH 8.0) purchased from Sigma Aldrich (Gillingham, UK), and collected for protein extraction and measurement.

#### 2.2.1.3 3T3-L1 adipocyte cell culture

Pre-adipocyte differentiation to mature adipocytes was carried out by Dr. Paul Caton, Centre for Diabetes, Blizard Institute, Queen Mary University of London.

3T3-L1 preadipocytes were cultured (37ºC; 5% CO2) in DMEM 25 mM glucose supplemented with 10% BSC until confluent. Two days post-confluency (Differentiation day 0), to induce differentiation media was changed and replaced with DMEM/10% FCS, supplemented with insulin (1 μg/ml), dexamethasone (0.25 mM) and isobutyl-1-methylxanthine IBMX (0.5 mM). After 2 days (differentiation day 2), media was replaced with DMEM/10% FCS supplemented with insulin (1 μg/ml). After 4 days (differentiation day 4) media was replaced with DMEM/10% FCS. All media contained 100 U/ml penicillin and 100 μg/ml streptomycin. Differentiation of pre-adipocytes to adipocytes was confirmed by measurement of PPARγ gene expression (qPCR). Treatments, carried out on differentiation day 8, were as follows; adiponectin (30 μg/ml), WY-14643 (10 μM) for 24 h. All treatments were carried out in DMEM containing 10% FCS.

#### 2.2.1.4 Cell Counting

For each experimental condition, cell viability was assessed using a haemocytometer, a counting chamber that was originally designed for performing blood cells counts. To prepare the counting chamber, the mirror-like polished surface was carefully cleaned with lens paper. The cover-slip was cleaned and then placed over the counting surface, prior to addition of the cell suspension into one of the V-shaped wells. The area under the cover-slip filled by capillary action and the mirrored surface was covered. The charged counting chamber was then placed on the microscope stage and the counting grid was brought into focus at low power. See Fig. 2.1.

Figure 2.1

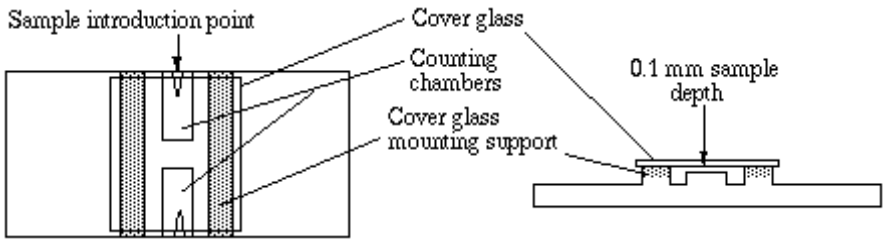


Figure 2.1: Illustration of the counting chamber.

#### 2.2.1.5 Protein extraction from cultured cells

Culture medium was removed and cells were lysed in ice-cold RIPA® buffer (containing 150 mM NaCl, 1.0% IGEPAL® CA-630, 0.5% sodium deoxycholate, 0.1% SDS, 50 mM Tris, pH 8.0), with added protease inhibitor (1:100; containing AEBSF, 104 mM; aprotinin, 80 μM; bestatin, 4 mM; E-64, 1.4 mM; leupeptin, 2 mM; pepstatin A, 1.5 mM). Cells were scraped and transferred to 1.5 ml Eppendorf tube then centrifuged at 8,000 x g for 15 min at 4 °C (Sigma 1-15K). The pellet was discarded, whilst the supernatant was transferred to a new 1.5 ml Eppendorf tube and sonicated at 4 °C for 3 x 10 sec pulses. Sonicated samples were centrifuged at 6,000 x g for 8 min at 4 °C in a refrigerated centrifuge. The resulting supernatant was transferred to a fresh 1.5 ml Eppendorf tube and stored at -20 °C and the pellet was discarded.

#### 2.2.1.6 RNA extraction and quantification

Total RNA was extracted from 3 x $10^6$ monolayer cells, harvested as outlined in section 2.2.1.

RNA was isolated from cultured cells using a QUIAGEN RNeasy Mini Kit® (Quiagen, West Sussex, UK). The kit purifies RNA through the addition of a specialized high salt buffer that promotes the binding of up to 100 µg of RNA (which must be longer than 200 bases) to a silica-based membrane.

Approximately 350 µl of RLT buffer® containing β-mercaptoethanol (β-ME) (10 µl/ ml) were added to 3 x $10^6$ cells per well. The solution was transferred to an RNase free Eppendorf tube and homogenized by vortexing (for 30 sec each sample). 350 µl of ethanol 70% were pipetted to each tube and the solutions were mixed well by pipetting, to provide the suitable binding conditions and to enable re-suspension of any precipitated material. Up to 700 µl of each sample, including any precipitate that might have been formed, were transferred to an RNeasy spin column® placed in a 2 ml collection tube. The samples were centrifuged (centrifuge 1-15 K) at 20 – 25 °C for 15 sec, at 8,000 x g. The flow-through was discarded. 700 µl of RW1 buffer® were added to each RNeasy spin column® for washing of membrane-bound RNA. The samples were centrifuged (centrifuge 1-15 K) at 20 – 25 °C for 15 sec, at 8,000 x g to wash the membrane. The flow-through was discarded. 500 µl of RPE buffer® (diluted 4:1 in 100% ethanol) were added to each RNeasy spin column®, to remove traces of salts, which might remain on the column due to buffers used earlier in the extraction protocol. The samples were centrifuged (centrifuge 1-15 K) at 20 – 25 °C for 15 sec, at 8,000 x g to wash the membrane. The flow-through was discarded. A further 500 µl of RPE buffer® was added to each RNeasy spin column®. The samples were centrifuged (centrifuge 1-15 K) at 20 – 25 °C for 2 min, at 8,000 x g to wash the membrane. The RNeasy spin column® was carefully removed from the collection tube® to avoid contact with flow-through. Otherwise, carryover of ethanol could have occurred. The RNeasy spin column® was placed in a new 2 ml collection tube® and the old collection tube® was discarded with the flow-through. The RNeasy spin column® in a new collection tube was then centrifuged (centrifuge 1-15 K) at 20 – 25

°C for 1 min at 13,300 x g. The spin column was placed in a new 1.5 ml collection tube® and 40 µl of RNase-free water® were added directly in the RNeasy spin column® membrane. To elute the RNA, the tubes were centrifuged (centrifuge 1-15 K) at 20 – 25 °C for 1 min at 8,000 x g. This last elution step was repeated, using the eluate previously obtained instead of fresh RNase-free water®, to have a higher RNA yield. The eluted RNA was retained from the collection tube, and the yield and purity of the RNA was assessed using a NanoDrop® ND-1000 spectrophotometer (*NanoDrop Technologies, Delaware USA*). Samples were diluted in RNase-free water to equalize their concentrations.

### 2.2.2 Animals

#### 2.2.2.1 Skeletal muscle and liver specific AMPK knockout mice

Female skeletal muscle-specific and liver specific AMPKα1/2-knockout ($AMPK^{-/-}$) or wild-type control (WT) mice were maintained at Institute Cochin INSERM, Paris, France. Only female mice were used, because of the established sexual dimorphisms known to exist with respect to the responses to dietary changes [173].

To obtain skeletal muscle specific AMPK-deficient mice ($AMPK\alpha1^{-/-}\alpha2^{fl/fl}$ HSA-$Cre^{+}$ mice), $AMPK\alpha1^{-/-}\alpha2^{fl/fl}$ mice were interbred with transgenic mice expressing the Cre recombinase under the control of the human skeletal actin (HSA) promoter, which is specifically expressed in differentiated multinucleated skeletal fibers [174].

To obtain specific deletion of both catalytic subunits in the liver ($AMPK\alpha_1\alpha_{2LS}^{-/-}$), a liver-specific AMPK$\alpha_2$-null mouse ($AMPK\alpha_2^{-/-}$) was generated by crossing floxed AMPK$\alpha_2$ mice [175] with AlfpCre transgenic mice, which express Cre recombinase under control of the albumin and α-fetoprotein regulatory elements. Subsequently, a liver-specific AMPK$\alpha_2$ deletion was produced on an $AMPK\alpha1^{-/-}$ background, by crossing liver-specific $AMPK\alpha_2^{-/-}$ mice with $AMPK\alpha_1^{-/-}$ mice [176]. Mice were genotyped by PCR on DNA extracted from a tail biopsy using specific primers for the Cre transgene and for the floxed AMPK$\alpha_2$, the deleted AMPK$\alpha_1$, and the wild-type AMPK$\alpha_1$ allele.

Genetic background is mixed C57Bl6J and 129Sv for muscle-specific knockout and for liver-specific, the mice have been backcrossed on C57Bl6J more than 5 times.

Animals were maintained on a 12:12-h light-dark cycle (light from 7am to 7pm), with controlled temperature (22° C ± 2° C) and air conditioned environment, and received standard high-carbohydrate rodent chow obtained from SAFE (Scientific Animal Food & Engineering, Augy, France) (diet number A03) for mice and contained 69.2% of cereals, 20.2% vegetal protein, 6% animal protein and 4.6% of a variety of essential vitamins and trace elements. The nutritional composition of the diet was 51.7% of carbohydrates, 21.4% of protein, 5.7% of minerals, 5.1% of lipids and 3.9% of fiber. Water was provided *ad libitum.*

Muscle specific AMPK$^{-/-}$ and WT were sacrificed in the immediately post-absorptive state after 5 hours of fasting. Liver-specific AMPK$^{-/-}$ and WT mice were sacrificed immediately after the re-feeding period. All mice were sacrificed by cervical dislocation. Tissues were extracted and flash frozen in liquid nitrogen. Whole blood was collected to obtain plasma.

AMPK knockout mouse studies were reviewed and approved (agreement no. 75-886) by the Directeur Départemental des Services Vétérinaires of the Préfecture of Police of Paris. All the procedures carried on using these samples were performed in accordance with the principles and guidelines established by the European Convention for the Protection of Laboratory Animals.

#### 2.2.2.2 C57BI/6 mice

Male C57BI/6 were obtained from Charles River (Kent, UK) and maintained on a 12:12-h light-dark cycle (light from 7am to 7pm), with controlled temperature (22° C ± 2° C) and air conditioned environment, and received standard laboratory (Lab Diets, Testdiets UK) or experimental chow. Water was provided *ad libitum.*

Animal experiments were conducted in accordance with the Home Office regulations on the Operation of Animals (Scientific Procedures) Act 1986, published by HMSO, London.

#### 2.2.2.3 PPARα-null mice

From Islam et al. [177], PPARα-null mice (PPARα$^{-/-}$), bred onto a SV/129 genetic background, were kindly provided by Dr. J. Peters and Dr. F.J.Gonzalez [178] (National Institutes of Health, Bethesda, MD). Wild-type SV/129 mice (Charles River, UK) were used as controls. Male mice (14–20 weeks old) were housed (4 per cage) and maintained in a temperature controlled, air conditioned environment, subject to a 12-h light/dark cycle with the dark period beginning at 0300 h'. Mice were fed ad libitum with a standard diet unless specified. WAT was dissected from both wild type and PPARα$^{-/-}$ mice, which required them to be anaesthetized by an intraperitoneal injection of sodium pentobarbital (60 mg/ml in 0.9% NaCl; 1ml/kg of body weight i.p.). Specifically, epididymal fat pads were quickly excised, freeze-clamped and stored in liquid nitrogen.

#### 2.2.2.4 Maternal low protein rat model

Pregnant female Wistar rats (250 – 300 g; Charles River, Kent, UK) were randomly assigned to either control (control; 20% protein) or an isocaloric maternal low protein (MLP; 8%) diets (Hope Farms BV, Woerden, Netherlands) and maintained on the respective diet throughout pregnancy and lactation. Pregnant dams fed the low-protein diet did not exhibit any differences in caloric intake compared to controls. Despite this, MLP offspring weighed significantly less at 3 days of age than control offspring (28%; $P<0.05$). Male offspring were weaned at 24 days and maintained on standard rodent diet thereafter. Pregnant female rats and offspring were housed and maintained in a temperature controlled, air conditioned environment, subject to a 12-h light/dark cycle with the dark period beginning at 0700 h'. Controls and MLP offspring were killed at 8 weeks and visceral WAT depots were snap-frozen for analysis, whilst blood was collected for measurement of glucose and insulin.

#### 2.2.2.5 Experimental animal dietary regimens and treatments

##### *2.2.2.5.1 Calorie restriction*

Female muscle specific AMPK$^{-/-}$ and WT *ad libitum* fed mice (AL) and calorie restricted mice (CR) were used in this experiments (17/group). Caloric restriction was conducted between 2.5 - 4 months of age and lasted for 10 weeks. Body weight changes over the period of CR were measured. Food was adjusted on a daily basis so that CR mice consumed 70% of the calories consumed by free feeding mice (calculated on the average of food intake during the last week before starting the caloric restriction protocol).

##### *2.2.2.5.2 Oral Glucose tolerance test (OGTT)*

To examine whole-body glucose homeostasis, female muscle specific AMPKα1/2 $^{-/-}$ and AMPKα1/2 $^{+/+}$ *ad libitum* fed- and calorie restricted mice were used in this experiments (n=17/group). Mice were fasted overnight, followed by oral gavage of glucose (3 g/kg of body weight). Blood samples for glucose analysis were collected from the tail vein at 0, 20, 40, 60, 80 and 120 min after glucose gavage. Blood glucose concentration was measured in whole blood with an automatic glucose monitor (Glucotrend II; Roche Diagnostics). Serum insulin levels were measured in the blood samples collected during OGTT at time 0 and at time 20 min, using a specific ELISA (Linco, St Charles, MO).

##### *2.2.2.5.3 Insulin administration*

For investigations of insulin action, female muscle specific AMPKα1/2 $^{-/-}$ (n=10) and wild type control (n=10) *ad libitum* fed mice (AL, n=20) and calorie restricted mice (CR, n=20) were used in this experiments. Mice (n=10/group) received an intraperitoneal injection of insulin (1 Unit of insulin/kg of body weight) *in vivo*, 5 minutes before sacrifice.

#### *2.2.2.5.4 Immunihistochemistry*

Soleus and gastrocnemius CR femal specific AMPKα1/2$^{-/-}$ and AMPKα1/2$^{+/+}$ muscles were embedded in cryomatrix and quickly frozen in isopentane cooled with liquid nitrogen. Cryostat sections (10 µm) were washed in PBS, permeabilized with 0.1% Triton X-100 and left for 1 hour in blocking solution (1x PBS, 1.5% goat serum, 0.1% Triton X-100). Rabbit poly-clonal antibodies directed against Laminin (Z0097, Dako) (1/100 dilution), and monoclonal antibodies against MyHCI (NOQ7.5.4D, Sigma) and MyHCIIA (SC-71, Santa Cruz biotechnology) were applied overnight at 4 °C to the treated sections. The next day, after three washes with 1× PBS containing 0.05% Tween-20, cryosections were incubated for 1 h with appropriate fluorescent secondary antibodies (Alexa Fluor 488 goat anti-rabbit IgG 1/1000 dilution, Alexa Fluor 594 goat anti-mouse IgG 1/1000 dilution, Invitrogen). After three washes with 1× PBS containing 0.05% Tween 20, samples were mounted in Vectashield mounting medium.

#### *2.2.2.5.5 Fasting and re-feeding*

To assess the effects of fasting and re-feeding, female liver specific AMPKα1/2$^{-/-}$ (n=4) and AMPKα1/2$^{+/+}$ (n=4) mice were fasted for 24 h with access to water *ad libitum* and then re-fed with a standard diet for a period of 4 h prior to sacrifice. In addition, C57BI/6 mice (n = 6) were either fed *ad libitum* or fasted overnight for 16 hours.

#### *2.2.2.5.6 Feeding and fasting*

To assess the effects of feeding and fasting, C57BI/6 mice (n=6) were fasted overnight for 16 hours (fasted animals) prior to sacrifice while the others (controls; n=6) continued to be fed with a standard laboratory diet until sacrifice. Mice were anaesthetized by an intraperitoneal injection of sodium pentobarbital (60 mg/ml in 0.9% NaCl; 1ml/kg of body weight i.p.) [177]. Livers were quickly excised, freeze-clamped and stored in liquid nitrogen.

#### *2.2.2.5.7 High fat diet*

Diets rich in saturated fat have been linked to obesity and development of T2DM. To examine this concept experimentally, eight-week old; male C57Bl/6 mice (n= 15) were fed with either a standard rodent laboratory chow (control) or an experimental high saturated fat diet (16 weeks; HF; AIN-76A w/11% Fat Energy/ Corn Starch/ Yellow, (diet number 58R0, TestDiet Richmond, IN USA), containing 11% saturated fat (high fat diet, n=15). See Table 2.1. Vitamin, mineral and amino acid content was equivalent in control and HF diet. Mice were sacrificed after 10 (Controls, n= 5 and HF, n=5) or 16 weeks (Controls, n=10 and HF, n=10) of administrated diet, by administration of anaesthetic, containing 100 mg/ml ketamine and 20 mg/ml xylazine, in a 2:1 ratio (2 ketamine: 1 xylazine), administrated at 1.5 ml/kg body weight. Liver tissue samples were quickly frozen in liquid nitrogen for protein and mRNA measurements. Blood was collected and centrifuged to obtain plasma for measurement of plasma glucose and insulin levels.

Table 2.1

**Energy content**

| | |
|---|---|
| **Energy (Kcal/g)[2]** | 4.02 |
| **Protein (%)** | 15.6 |
| **Fat (ether extracts) (%)** | 10.9 |
| **Carbohydrates (%)** | 73.5 |

Table 2.1: Table showing the nutritional composition of the high fat diet.

#### *2.2.2.5.8 Nicotinamide mononucleotide (NMN) administration*

Mice were administered NMN (500 mg/kg/body weight; i.p.) or saline equivalent 16 h before sacrifice, to give four separate groups (n = 5/group); (A) Control + Saline; (B) Control + NMN; (C) HF + Saline; (D) HF + NMN. These experiments were conducted to assess the effects of amplification of the $NAD^+$ biosynthetic salvage pathway. NMN is the reaction product of the enzyme nicotinamide mononucleotide phosphoribosyltransferase (NAMPT) [179]. NMN circulates systemically in mouse

plasma [179], suggesting that administration of NMN could promote $NAD^+$ synthesis and thereby activate NAD-dependent enzymes such as SIRT1 and SIRT3.

#### *2.2.2.5.9 Metformin administration*

Eight-week old male C57Bl/6 mice (Charles River, Kent, UK) maintained on standard rodent diet were administered metformin (250 mg/kg/day; 7 days) or an equal volume of water daily by oral gavage.

### 2.2.2.6 Protein extraction from liver, muscle and white adipose tissue samples

Approximately 60 mg of tissue was homogenised with a tissue tearor/electronic homogeniser (EW-04750-55 Tissue Tearor™ Homogeniser), previously washed with methanol, at moderate speed (speed 4 or 5) in 1 ml of ice cold RIPA® buffer (ready to use solution containing 150 mM NaCl, 1.0% IGEPAL® CA-630, 0.5% sodium deoxycholate, 0.1% SDS, 50 mM Tris, pH 8.0) purchased from Sigma Aldrich (Guillingham, UK), with protease inhibitor (containing AEBSF, 104 mM; aprotinin, 80 μM; bestatin, 4 mM; E-64, 1.4 mM; leupeptin, 2 mM; pepstatin A, 1.5mM) diluted in 1:100, in a conical bottomed Falcon tube. Samples were homogenized for at least 20 seconds or until all tissue was homogenized to create a uniformly homogenised solution. The homogenate was split into 1.5 ml Eppendorf tubes and centrifuged at 5000 x g for 10 min at 4º C in a refrigerated centrifuge. The pellet was discarded and the supernatant transferred to a new 1.5 ml Eppendorf tube (placed on ice). Care was taken to avoid the upper fatty layer present in some samples, and only transfer the supernatant. Supernatatants were then sonicated for 3 x 10 sec pulses. Sonicated samples were centrifuged at 6000 x g for 8 min at 4 °C in a refrigerated centrifuge, producing a new cell lysate supernatant. The supernatant was transferred to a fresh 1.5 ml Eppendorf tube and stored at -20 °C and the pellet was discarded.

#### 2.2.2.7 RNA extraction and quantification

*Liver Tissue*

Cellular RNA was isolated using QUIAGEN RNeasy Midi Kit® (Quiagen, West Sussex, UK). The kit purifies RNA through the addition of a specialized high salt buffer that promotes the binding of up to 1 mg of RNA to a silica-based membrane.

A tissue tearor/electronic homogeniser (EW-04750-55 Tissue Tearor™ Homogeniser) was washed with methanol and rinsed with RNase-free water®. Approximately 250 mg of liver tissue from each sample was disrupted with the clean tissue tearor in 4 ml of RLT buffer®, containing β-mercaptoethanol (β-ME) (10 µl/ ml), in a 50 ml Falcon® tube. The lysates were centrifuged at 5,000 x g for 10 min, at 20 – 25 °C. After centrifugation a small pellet has been formed, accompanied by a fatty upper layer and an intermediary phase (or supernatant). The supernatant of each sample was transferred to a new Falcon® tube by pipetting, avoiding transferring the fatty upper layer or the pellet. Transferring the pellet or the fatty layer might reduce the amount of RNA that binds to the membrane and could cause the spin column to clog. 4 ml (1 volume) of ethanol 70% were pipetted to each tube and the solutions were mixed well by shaking vigorously, to provide the suitable binding conditions and to enable re-suspension of any precipitated material. Up to 4 ml of each sample were transferred to an RNeasy midi column® placed in a 15 ml collection tube. The samples were centrifuged (centrifuge 40K) at 20 – 25 °C for 5 min, at 5,000 x g. The flow-through was discarded. The previous centrifugation step was repeated using the reminding 4 ml of lysate. 4 ml of RW1 buffer® were added to each RNeasy midi column® for washing of membrane-bound RNA. The samples were centrifuged (centrifuge 40K) at 20 – 25 °C for 5 min, at 5,000 x g to wash the membrane. The flow-through was discarded. 2.5 ml of RPE buffer® (diluted 4:1 in 100% ethanol) were added to each RNeasy midi column®, to remove traces of salts, which might remain on the column due to buffers used earlier in the extraction protocol. The samples were centrifuged (centrifuge 40K) at 20 – 25 °C for 2 min, at 5,000 x g to wash the membrane. The flow-through was discarded. A further 500 µl of RPE buffer® was added to each RNeasy spin column®. The samples were centrifuged (centrifuge 40K) at 20 – 25 °C for 5 min, at 5,000 x g to dry the RNeasy silica-gel membrane®. The RNeasy midi

column® was carefully removed from the collection tube® to avoid contact with flow-through. Otherwise, carryover of ethanol could have occurred. The RNeasy midi column® was placed in a new 15 ml collection tube® and the old collection tube® was discarded with the flow-through. To elute, 200 µl of RNase-free water® were pipetted directly in the RNeasy silica-gel membrane®. The columns were incubated at room temperature for 1 min. To elute the RNA, the tubes were centrifuged (centrifuge 40K) at 20 – 25 °C for 3 min at 5,000 x g. This last elution step was repeated, using the eluate previously obtained instead of fresh RNase-free water®, to have a higher RNA yield. The eluted RNA was retained from the collection tube, and the yield and purity of the RNA was assessed using a NanoDrop® ND-1000 spectrophotometer (NanoDrop Technologies, Delaware USA). Samples were diluted in RNase-free water to equalize their concentrations.

*Muscle tissue*

RNA extraction was performed according to the manufacturer (Quiagen, UK) instructions, using an RNeasy mini kit® for fibrous tissue (with proteinase K). A tissue tearor/electronic homogeniser (EW-04750-55 Tissue Tearor™ Homogeniser) was washed with methanol and rinsed with RNase-free water®. Approximately 30 mg of tissue from each sample was homogenised at moderate speed (speed 4 or 5) in 300 µl of RLT buffer®, containing β-mercaptoethanol (10 µl/ ml), in an RNase free Eppendorf round bottomed tube. Tissue was homogenized for, at least 20 seconds or until all tissue was homogenized. The homogenisation process was repeated until solution being uniformly homogenised. 590 µl of RNase-free water® were added to each lysate. Then, 10 µl of proteinase K solution were added to each previous solution and the solution was mixed thoroughly by pipetting. The solutions were incubated for 10 min in a water bath, previously heated at 55 °C. After incubation, the solutions were centrifuged (centrifuge 1-15 K) at 20 – 25 °C for 3 min, at 10,000 x g. Approximately 900 µl of each supernatant were pipetted to a new RNase free 1.5 ml micro-centrifuge tube. 0.5 volumes (450 µl) of ethanol (100%) were added to each cleared lysate, and the solutions were mixed well by pipetting, to provide the suitable binding conditions and to enable re-suspension of any precipitated material. 700 µl of each sample, including any precipitate that might have been formed, were transferred to an RNeasy spin column® placed in a 2 ml collection tube. The samples were

centrifuged (centrifuge 1-15 K) at 20 – 25 °C for 3 min, at 8,000 x g. The flow-through was discarded. The reminder 700 µl of each sample were transferred to the previous RNeasy spin columns® placed in a 2 ml collection tube®. The samples were centrifuged again (centrifuge 1-15 K) at 20 – 25 °C for 3 min, at 8,000 x g. The flow-throw was discarded. 350 µl of RW1 buffer® were added to each RNeasy spin column® for washing of membrane-bound RNA. The samples were centrifuged (centrifuge 1-15 K) at 20 – 25 °C for 15 sec, at 8,000 x g to wash the membrane. The flow-through was discarded. For each column, 10 µl of DNase I stock solution were added to 70 µl of Buffer RDD®. The solution was gently mixed, inverting the tube, and briefly centrifuged to collect residual liquid from the sides of the tube. This DNase I incubation mix (80 µl) was directly added to the RNeasy spin column® membrane and placed on the bench-top (20 – 30 °C) for 15 min. 350 µl of RW1 buffer® were added to each RNeasy spin column®. The samples were centrifuged (centrifuge 1-15 K) at 20 – 25 °C for 15 sec, at 8,000 x g to wash the membrane. The flow-through was discarded. 500 µl of RPE buffer® (diluted 4:1 in 100% ethanol) were added to each RNeasy spin column®, to remove traces of salts, which might remain on the column due to buffers used earlier in the extraction protocol. The samples were centrifuged (centrifuge 1-15 K) at 20 – 25 °C for 15 sec, at 8,000 x g to wash the membrane. The flow-through was discarded. A further 500 µl of RPE buffer® was added to each RNeasy spin column®. The samples were centrifuged (centrifuge 1-15 K) at 20 – 25 °C for 2 min, at 8,000 x g to wash the membrane. The RNeasy spin column® was carefully removed from the collection tube® to avoid contact with flow-through. Otherwise, carryover of ethanol could have occurred. The RNeasy spin column® was placed in a new 2 ml collection tube® and the old collection tube® was discarded with the flow-through. The RNeasy spin column® in a new collection tube was then centrifuged (centrifuge 1-15 K) at 20 – 25 °C for 1 min at 13,300 x g. The spin column was placed in a new 1.5 ml collection tube® and 40 µl of RNase-free water® were added directly in the RNeasy spin column® membrane. To elute the RNA, the tubes were centrifuged (centrifuge 1-15 K) at 20 – 25 °C for 1 min at 8,000 x g. This last elution step was repeated, using the eluate previously obtained instead of fresh RNase-free water®, to have a higher RNA yield. The eluted RNA was retained from the collection tube, and the yield and purity of the RNA was assessed using a NanoDrop® ND-1000 spectrophotometer (NanoDrop Technologies, Delaware USA). Samples were diluted in RNase-free water to equalize their concentrations.

*White adipose tissue*

RNA extraction was performed according to the manufacturer (Quiagen, UK) instructions, using an RNeasy midi kit® for lipid tissue.

A tissue tearor/electronic homogeniser was washed with methanol and rinsed with RNase-free water®. Approximately 300 mg of tissue from each sample was homogenised at moderate speed (speed 4 or 5) in 5 ml of QIAzol lysis reagent®, which immediately inactivates any RNases (to prevent RNA degradation), in an RNase-free Falcon tube. Tissue was homogenized for, at least 20 seconds or until all tissue was homogenized. The homogenisation process was repeated until solution being uniformly homogenised. The tubes were placed at the benchtop, at room temperature (15 - 25 °C) for 5 min. 1 ml of chloroform was added to the lysate and the mixture was vigorously shaken for the subsequent phase of lysate separation. The tubes were placed on the benchtop, at room temperature for 2-3 min. The lysate underwent centrifugation ate 5000 x g for 15 min, at 4 °C. After centrifugation, four layers could be observed: an upper, colourless, aqueous phase containing RNA; a white interphase; a lower, red, organic phase and an additional clear phase. The volume of the aqueous phase should be approximately 3 ml. This clear supernatant was transferred to another RNase-free Falcon tube and the other phases (fatty layer and pellet) were discarded. 1 volume (about 3 ml) of 70% ethanol was added to each cleared lysate. The solutions were immediately mixed by vortexing, to be able to provide the suitable binding conditions and to enable re-suspension of any precipitated material. 4 ml of each sample, including any precipitate that might have been formed, were transferred to an RNeasy Midi column® (which binds DNA and RNA) placed in a 15 ml collection tube. The samples were centrifuged (centrifuge 1-15 K) at 20 – 25 °C for 5 min, at 5,000 x g. The flow-through was discarded from the collection tube. The reminder 2 ml of each sample were transferred to the previous RNeasy Midi columns® placed in 15 ml collection tube®. The samples were centrifuged once more (centrifuge 1-15 K) at 20 – 25 °C for 5 min, at 5,000 x g. The flow-throw was discarded. 4 ml of RW1 buffer® were added to each RNeasy Midi column® for washing of membrane-bound RNA. The samples were centrifuged (centrifuge 1-15 K) at 20 – 25 °C for 5 min, at 5,000 x g to wash the membrane. The flow-through was discarded. 2.5 ml of RPE buffer® (diluted 4:1 in 100% ethanol),

were added to each RNeasy Midi column®, to remove traces of salts, which might remain on the column due to buffers used earlier in the extraction protocol. The samples were centrifuged (centrifuge 1-15 K) at 20 – 25 °C for 2 min, at 5,000 x g to wash the membrane. The flow-through was discarded. A further 2.5 ml of RPE buffer® was added to each RNeasy Midi column®. The samples were centrifuged (centrifuge 1-15 K) at 20 – 25 °C for 5 min, at 5,000 x g to wash the membrane. The RNeasy spin column® was carefully removed from the collection tube® to avoid contact with flow-through. Otherwise, carryover of ethanol could have occurred. The RNeasy Midi column® was placed in a new 15 ml collection tube® and the old collection tube was discarded with the flow-through. The RNeasy Midi column® in a new collection tube was then centrifuged (centrifuge 1-15 K) at 20 – 25 °C for 2 min at 5,000 x g. The column was placed in a new 15 ml collection tube® and 250 µl of RNase-free water® were added directly in the RNeasy Midi column® membrane. The columns were allowed to stand with RNase-free water for 1 min. To elute the RNA, the tubes were centrifuged (centrifuge 1-15 K) at 20 – 25 °C for 3 min at 5,000 x g. The eluted RNA was retained from the collection tube, and the yield and purity of the RNA was assessed using a NanoDrop® ND-1000 spectrophotometer (NanoDrop Technologies, Delaware USA). Samples were diluted in RNase –free water to equalize their concentrations.

#### 2.2.2.8 Plasma analysis

Whole blood samples were collected in microcentrifuge tubes containing heparin as an anticoagulant. After collection, tubes were centrifuged at 1,000 x g for 10 min at 4° C. The top yellow plasma layer was transferred to a new tube and stored at -80° C.

##### *2.2.2.8.1 Glucose assay*

Glucose assay was performed according to the manufacturers instructions (Thermo Electro Corporation, Melbourne, Australia).

The method utilised in this reagent is based on the hydrogen peroxide indicator reaction which couples 4-aminoantipyrine to a phenolic compound as first proposed by Trinder [180]. Glucose standards were prepared by labelling nine clean test tubes

from 0 - 9. 250 µl of ultrapure water were added to tubes 1-8. 500 µl of ultrapure water were added to tube 0. 250 µl of Glucose Standard® (1.441 g/dl) was added to tube 1 and this was mixed thoroughly. 250 µl of the solution in tube 1 was transferred to tube 2 and mixed thoroughly. This process was repeated for tubes 3 to 8. Tube 0 has only ultrapure water and is used as blank. See Fig. 2.3.

Figure 2.3

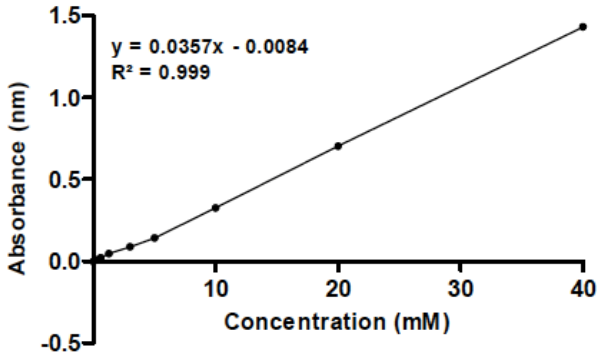


Figure 2.3: Glucose assay curve.

Duplicate glucose standards and plasma samples (2 µl) were added into a clean, dry 96-well micro-plate (Starlab, UK). 300 µl of the reagent (containing >15,000 U/l of glucose oxidase, >100 U/l of peroxidase, 0.5mmol/l of aminoantipyrine, 10 mmol/l of hydroxybenzoic acid and 119 mmol/l of phosphate buffer) were added to each well and mixed thoroughly. The plate was incubated for 30 min at room temperature. Absorbance was measured at 490 nm on an optical plate reader (Anthos Labtee HT3 Version 1.21). Using a linear range of the standard curve from 0.0 mM to 40 mM (Figure 2.3), glucose was calculated and expressed as mM.

#### *2.2.2.8.2 Insulin ELISA*

Plasma insulin levels were assessed by specific insulin ELISA (Mercodia AB, Uppsala, Sweden). The ELISA is a solid two-site enzyme immunoassay with a colourimetric endpoint that is read spectrophotometrically. The assay is based on the direct sandwich technique in which two monoclonal antibodies are directed against

separate antigenic domains in the insulin molecule. All reagents and plasma samples were brought to room temperature before use. Enzyme Conjugate® (peroxidase conjugate mouse monoclonal anti-insulin) 1X, was prepared by mixing 5 µl of Enzyme Conjugate® 11x with 50 µl of Enzyme Conjugate Buffer® (color coded blue) (1:10) for each sample. The Wash Buffer® was prepared by diluting 10 µl of Wash Buffer® 21x in 2000 µl redistilled water (1:20) for each sample. To prepare the calibration curve, duplicated aliquots (10 µl) of calibrator and sample were pipetted into a provided mouse monoclonal anti-insulin 96-well Coated Plate® (coted with anti-mouse insulin). 100 µl of an HRP-conjugated (Horse Radish Peroxidase) - conjugated anti-mouse insulin antibody (Enzyme Conjugate®) was added to the sample before incubating the plate on an orbital shaker (400 rpm) for 2 h, at room temperature. After 2 h, the wells were washed 5 times by adding 350 µl of Wash Buffer® to each well. After each wash, the wells were dried by firmly inverting against absorbent paper. After the final wash, 200 µl of chromogenic TMB® substrate (3,3',5,5'-tetramethylbenzidine), was added to each well, and incubated at room temperature for 15 mins, protected from light. After 15 min, 50 µl of Stop Solution® (0.5 M $H_2SO_4$) was pipetted into each well, to stop the reaction. The plate was gently agitated for approximately 5 seconds to ensure mixing the substrate and Stop Solution®. Absorbance was measured at 450 nm, using an optical plate reader (Anthos Labtee HT3 Version 1.21). The equation obtained from the linear regression of the standard curve was used to calculate the concentration of insulin in ng/ml. See Fig. 2.4.

Figure 2.4

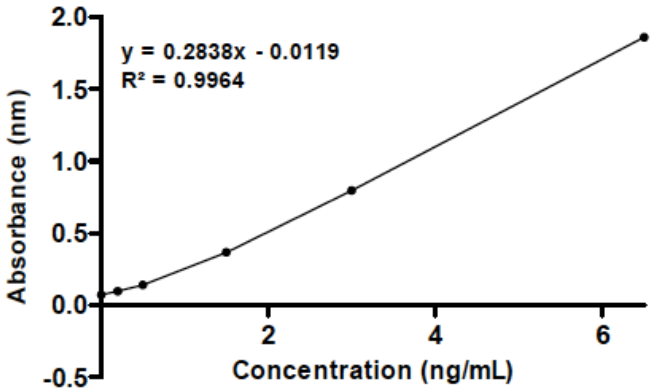

Figure 2.4: Insulin standard curve.

### 2.2.3 Common Methods used for cells and tissue preparation and analysis

#### 2.2.3.1 Protein quantification

Protein Concentrations were measured using the RC DC-BioRad protein assay system (BioRad, UK) – a colorimetric assay based on the method of Lowry [181]. The assay involves the reaction of the protein with an alkaline copper tartrate solution and Folin reagent (mixture of inorganic salts). Proteins (tyrosine and tryptophane residues) react with the Folin reagent promoting its reduction to produce a blue colour. The intensity of the colour is directly proportional to the concentration of the protein within the sample. Dilutions of bovine serum albumin (BSA) ranging from 0,0015625 – 2 mg/ml were prepared in $dH_2O$ and used as standards. Aliquots (5 µl) of standards and protein test samples (thawed on ice) were prepared in duplicate and pipetted into a clean, dry 96-well micro-plate (Starlab, UK). 25 µl of reagent A (prepared previously by adding 20 µl surfactant solution to 1ml alkaline copper tartrate solution) and 200 µl of Folin reagent were added to samples and standards, and the plate was incubated at room temperature for 15 minutes, with gently agitation. Absorbance was then measured at 650 nm on an optical plate reader (Wallac 1420 Victor 2; Perkin-Elmer – company details). Using a linear range of the standard curve from 0.0 mg/ml to 25 mg/ml (Figure 2.7), sample protein was calculated and expressed as µg protein/µl. The protein concentration of each sample was established via extrapolation from the standard curve obtained by plotting the absorbance of the protein standards against their concentration, and protein concentrations of the samples determined from this.

Figure 2.7

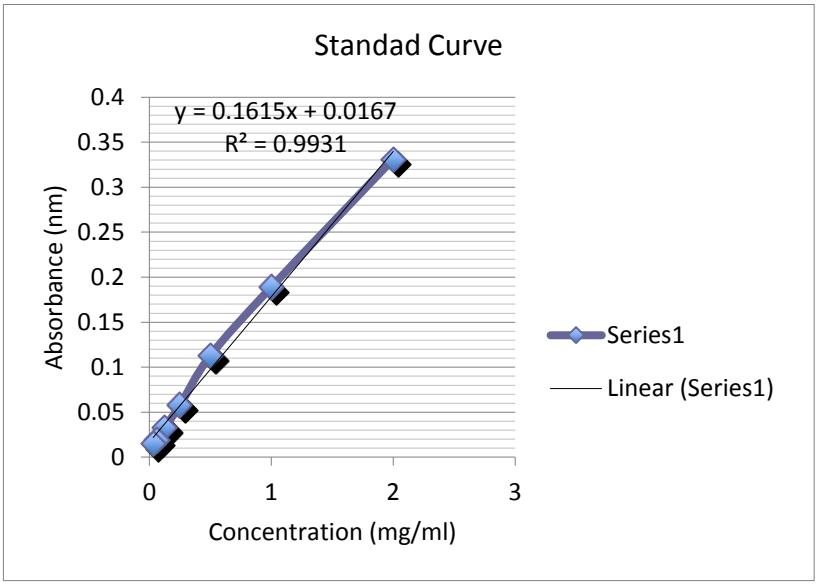


Figure 2.7: Graph illustrates a standard curve for the protein assay.

### 2.2.3.2 Western blotting

Sodium dodecyl sulphate-polyacrylamide gel electrophoresis (SDS-PAGE) was performed as a modification of the method described by Laemmli [182]. Denatured proteins bind SDS and become negatively charged. The amount of SDS bound is usually proportional to the molecular weight of the protein and the polypeptide-SDS complex migrates through the gel according to the size of the polypeptide and not its charge. The separated proteins are transferred to a nitrocellulose membrane and probed with an appropriate antibody.

#### *2.2.3.2.1 SDS-PAGE gel electrophoresis*

After being extracted as detailed above, protein samples were separated by SDS-PAGE on a 5%, 7.5% or 10% lower resolving gel (based on the size of the protein) and an upper 4.5% stacking gel. The gels were made by adding the reagents as listed below (see Table 2.3).

Table 2.3

| | Resolving gel 5% | Resolving gel 7.5% | Resolving gel 10% | Stacking gel 4% |
|---|---|---|---|---|
| **40% (v/v) Acrylamide/bis** | 2.5 ml | 3.75 ml | 5 ml | 1 ml |
| **1.5M Tris-HCl pH 8.8** | 5 ml | 5 ml | 5 ml | |
| **0.5 M Tris-HCL pH 6.8** | | | | 2.5 ml |
| **10% (w/v) SDS** | 200 µl | 200 µl | 200 µl | 100 µl |
| **dH2O** | 12.2 ml | 10.95 ml | 9.7 ml | 6.35 ml |
| **TEMED** | 10 µl | 10 µl | 10 µl | 10 ml |
| **10% (w/v) Amonium persulfate (APS)** | 100 µl | 100 µl | 100 µl | 100 µl |
| **Molecular weight** | 57-212 kDa | 36-94 kDa | 16-68 kDa | |

Table 2.3: Illustrates the required volume of reagents needed to make up the acrylamide gels.

The gel, separated by two layers (the upper stacking gel and the lower resolving/running gel) had 1.5 mm of thickness. Gel apparatus was assembled (Bio-Rad, Hemel Hempstead, UK) and the lower gel poured to 1 cm below the level of the gel comb. A thin layer of butan-2-ol (400 µl) was added to ensure that the gel front was level, to prevent the gel from drying out, and to remove any air bubble that might have been formed while the gel was being poured. The gel was then allowed to set for 1 h. Once the lower gel had set, butan-2-ol was rinsed 3 times with distilled water. Water was removed using filter paper, and the upper stacking gel was poured and the comb was inserted. The gel was allowed to polymerize for 30 min and the comb was then removed.

Protein sample preparation

Protein samples were mixed at a ratio of 1:1 with Laemmelli buffer (62.5 mM Tris-HCl, pH 6.8; 2% (w/v) SDS, 40% (v/v) glycerol, 0.01% (w/v) bromophenol blue and 10% (v/v) β-mercaptoethanol). Samples were vortexed and heated for 3 min at 100 °C to denature the proteins in the SDS sample buffer, containing β-mercaptoethanol as a reducing agent, giving them a uniform negative charge. The SDS binds consistently along the length of the proteins, equalizing the mass/charge ratio. As a result the proteins migrate towards the cathode separated primarily by molecular weight, which is important for later detection of the target protein. Samples were then allowed to cool before loading onto a gel.

SDS-PAGE electrophoresis was performed in a Bio-Rad Mini-Protean® kit (BioRad; California, USA) using 20 – 40 µg protein per lane, depending on the concentration of the protein and the well volume. Gels were electrophoresed in 1X running buffer (0.05 M Tris base, 0.384 M glycine and 0.1% (w/v) SDS) at 100 V for 20 min and then 150 V for 45 min or until the bromophenol blue gel front reached the bottom of the gel. Amersham, full-range rainbow molecular weight markers (12 000 – 225 000 Da; GE Healthcare, UK) were run in parallel with unknown samples.

#### *2.2.3.2.2 Protein Transfer*

Following removal of the gel from the electrophoresis cassette, the upper stacking gel was removed. The top right hand corner of the lower gel was also removed, for orientation later. Proteins were transferred from SDS-PAGE gel to nitrocellulose Hybond membrane (GE Healthcare, UK) as described by Towbin (Towbin et al. 1979), using a Bio-Rad Mini Trans-Blot® Electrophoretic Tranfer Cell (BioRad California, USA). Prior to transfer, SDS gels were equilibrated in transfer buffer (0.25 mM TRIS, 0.19 mM glycine, 15% (v/v) methanol) for 30 min, whilst nitrocellulose membranes were soaked for 15 min in transfer buffer. Following this, each SDS-PAGE gel with nitrocellulose membrane was placed in a transfer cassette between two sheets of 3 mm thick blotting paper, which had been pre-wetted in transfer buffer. The loaded cassettes were prepared in water and any air bubbles removed by rolling with a Pasteur pipette. The cassettes were placed into the transfer tank (Bio-Rad Transblot system; Richmond, CA, USA), containing transfer buffer pre-cooled at 4

ºC, with the nitrocellulose membrane side towards the cathode. The gel was then electro-eluted at 200 mA for 2h. The transfer was performed in the cold room to keep the gels cold as this process generated a lot of heat and the gels could melt if care was not taken.

#### *2.2.3.2.3 Immunodetection*

After transfer, membranes were rinsed in TNT buffer (2mM Tris-HCL, pH 7.6, 15 mM NaCl, 0.01% Tween-20). After washing, non-specific hybridisation to the membrane was blocked by gentle mix for 1 h in 5% (w/v) blocking solution (consisting of 0.5 g of dried skimmed milk or BSA in 10 ml of TBS-Tween solution, per membrane). Membranes were washed 3 x 10 min periods in TBS-Tween buffer, with vigorous mixing. After washing, nitrocellulose membranes were incubated overnight on a shaking platform (gentle mix) at 4° C with primary antibody (1µl/ml) in a solution of 5% (w/v) BSA, dissolved in TBS-Tween buffer solution (see appendix XIV). After overnight incubation, the washing steps were repeated on a shaking platform at room temperature, followed by 1 h incubation with an appropriate secondary antibody. After incubation with the secondary antibody, the washing steps were repeated again with vigorous mixing (see appendix XIV).

#### *2.2.3.2.4 Visualisation*

To detect the protein bands, membranes were incubated for 5 min at room temperature in chemiluminescent reagent (Thermo Scientific Pierce ECL, Thermo Scientific USA) with gentle mixing. The system consists in an enhanced chemiluminescent substrate for detection of horseradish peroxidase (HRP) activity from antibodies and other Western blot probes. The HRP/$H_2O_2$ catalised oxidation of luminol in alkaline conditions takes place in the presence of chemical enhancers such as phenols. To detect the proteins, nitrocellulose Hybond membranes were exposed to blue-light sensitive autoradiography film (Hyperfilm ECL, GE Healthcare UK). The exposure time varied from 15 sec to 12 min depending on antibody and sample. Developement was then carried out using an automated Kodak developing machine. The densitometric readings of the resultant protein bands were analysed using

ImageJ® program (Image Processing and Analysis in Java). At least three independent western-blotting experiments were carried out for each antibody.

#### 2.2.3.3 Immunoprecipitation

Immunoprecipitation (IP) was performed regarding to manufactures Catch and release v2.0 instruction manual.

10X Catch and Release Wash Buffer® was diluted to 1X working concentration with Milli Q® water for incubation and all washes. Spin Columns®, Capture Tubes® and micro-centrifuge tubes were labelled. The snap-off bottom plug was removed from the Spin Columns® and saved for later use. The Spin Columns® were inserted in the Capture Tubes®. The screw-on cap of each Spin Column® was removed and the columns were centrifuged at 2,000 x g for 15-30 seconds to remove the resin slurry buffer. The resins in the Spin Columns® were washed twice with 400 µl of 1X Wash Buffer®. The Capture Tubes® were emptied and the bottom end of each Column was plugged with the snap-off bottom plug saved earlier.

The volume of combined reagents was determined:

a) 500 µg of cell lysate;
b) 4 µg of the specific primary antibody and negative control antibody. 5-10 µl of whole antiserum;
c) 10 µl of Antibody Capture Affinity Ligand®;
d) Sufficient 1X Wash Buffer® to provide a total volume of 500 µl.

With the bottom end of the Spin Column® plugged, the reagents were added in the following order:

1) 1X Wash Buffer®;
2) Cell Lysate;
3) Specific primary antibody or negative control antibody;
4) Antibody Capture Affinity Ligand®

Using the screw-on caps, the top of the Columns were capped and the columns were incubated overnight in a rotator, at 4° C. After incubation, the snap-off bottom plugs

were removed and discarded. The Columns were placed in the Capture Tubes®; the screw-on caps were removed and the Tubes were centrifuged at 2,000 x g for 15-30 seconds to collect the flow-through. The flow-through was transferred to a new micro-centrifuge tube and saved for Western Blot analysis (it could have been useful for trouble-shooting, if necessary).

The Columns were washed 3X with 400 µl of 1X Wash Buffer®, spinning at 2,000 x g for 15-30 seconds, for each wash. The Columns were placed into fresh Capture Tubes®. 70 µl of 1X Denaturing Elution Buffer® containing β-mercaptoethanol were added to each Spin Column®. The Columns were centrifuged at 2,000 x g and saved for Western Blot analysis.

#### 2.2.3.4 Reverse transcription-polymerase chain reaction

##### *2.2.3.4.1 Reverse transcription*

In reverse transcription PCR, RNA strands are reverse transcribed into cDNA, using the enzyme reverse transcriptase extracted from avian myeloblastosis virus, HIV or moloney murine leukemia virus. Reverse transcriptase requires a double stranded primer that allows 5' to 3' cDNA synthesis. Several types of primers are available such as random primers or gene specific primers. We, however, employ random primers as they convert all the mRNA and as a result several genes can be measured on one sample. Since the goal of the RT-PCR is to synthesise certain amount of mRNA into an equal amount of cDNA, the analysis is just one cycle.

Reverse Transcription was carried out according to manufacturer's instructions (Promega, UK). Complementary DNA (cDNA) was generated from RNA templates (500 – 1000 ng). Reverse transcription was carried out in a reaction mix containing 5 mM MgCl2, 10X Reverse transcription buffer (10 mM Tris-HCL, pH 9, 50 mM KCL, 0.1% Triton X-100, 1 mM deoxyribonucleotide triphosphates (dNTP), 1U/ml recombinant RNase inhibitor (RNAsin), 15 U/µg RNA AMV reverse transcriptase and 0.5 µg//µl RNA random primers). Reverse transcription reactions were carried out in 20 µl volumes at 37 ° C for 1 h, 70 ° C for 15 min. See table 2.4

Table 2.4

| Reagent | Quantity/tube in µl |
|---|---|
| **$MgCl_2$** | **4** |
| **Reverse Transcriptase buffer** | **2** |
| **dNTP** | **2** |
| **RNAsin** | **0.5** |
| **Random Primers** | **0.72*** |
| **Reverse Transcriptase** | **1.2*** |
| **Nuclease Free $H_2O$** | **4.4** |
| **Total Amount:** | **15** |

Table 2.4 Illustrates the reagents used for RT-PCR and their quantity.
*The amount of these reagents depends on the RNA concentration in the sample. The numbers given equals to an RNA yield of 144.6ng/µl. There is added 5 µl of RNA to the 15 µl of the mixed solution. To calculate the amount of Random primers and Reverse transcriptase the total amount of RNA to be added (723ng) is divided by 1000 = random primers (0.72µl). 0.72 is then multiplied with 25 and divided with 15 = reverse transcriptase (1.2µl). RNAsin is added to inhibit any RNAse activity.

15 µl of the reagent mix shown in table 2.4 were added to a 200µl thin walled RNAse free Eppendorf tube, and 5µl RNA sample was added. The Eppendorf tube was then placed in a PCR machine and set to the following program: The reverse transcription reaction was at 37°C for 1 hour where the RNA is converted into cDNA. Initially the random primers bind the complementary RNA- strands. Then the reverse transcriptase binds where the primers are annealed and extends the template. Following this, samples were incubated at 75°C for 15 min to denature the reverse transcriptase. Samples were then cooled to 4°C until the PCR machine was switched off. This step is to ensure preservation of the cDNA until the samples were transferred to the -20°C freezer.

#### *2.2.3.4.2 Polymerase chain reaction*

Quantitative reverse transcription polymerase chain reaction (qRT-PCR) was carried out using sequence specific primers (all Eurogentec, UK) using either Sybr green

(Invitrogen, UK) or Taqman methodology (Eurogentec, UK). The sense and anti-sense primers sequence and PCR cycle used are shown in Appendix XV. The reaction mix (16 µl), containing master mix (ThermoScientific, UK), forward and reverse primers, probe (Sybr green or Taqman) and nuclease-free water was prepared as described below and added, along with cDNA sample (4 µl), to a 96 well-plate (MicroAmp® Optical Reaction Plate with Barcode, Applied Biosystems, UK). The plate was mixed and centrifuged briefly to force the solution to the bottom of the wells and to eliminate any air bubbles, prior to running of qPCR reaction.

Table 2.5

| **Reagents** **Final concentration** | Amount/well (µl) SYBR Green | Amount/well (µl) Taqman |
|---|---|---|
| **Absolute QPCR mix (+ ROX) 1x** | 10 | 10 |
| **Forward primer (300 nM)** | 1 | 1* |
| **Reverse Primer (300 nM)** | 1 | 1* |
| **Probe (25/100nM)** | 1 | 1* |
| **Nuclease-free $H_20$** | 3 | 4.7 |
| **Sample DNA (5 ng/µl)** | 4 | 4 |

Table 2.5 Illustrates the reagents used, for qRT-PCR with SYBR Green and Taqman as detectors, and the volume needed. * For 18S gene, use 0.1 µL of probe, forward and reverse primer. Samples were analysed in duplicate in reactions containing 1X QPCR mix, 100 nM of ROX reference Dye, 300 nM forward and reverse primers, 100 nM probe, 20 ng (5ng/µl) cDNA sample and nuclease-free water to a final volume of 20 µl. 18S ribosomal RNA was measured as a control gene, using a commercial Taqman assay (Applied Biosystems, USA).

The RT-PCR reaction was run using a 7500 Real-Time PCR System (Applied Biosystems, US). The RT-PCR thermal cycling program was set up as listed below, in Table 2.6.

Table 2.6

| | Temperature | Time | Number of cycles |
|---|---|---|---|
| | 50°C | 2 min | 1 |
| **Enzyme activation** | 95°C | 15 min | 1 |
| **Denaturation** | 95°C | 15 sec | 40 |
| **Annealing/Extension** | 60°C | 60 sec | |

Table 2.6: RT-PCR thermal cycling programme.

The volume was set 20 µl as this was the amount present in the tubes. A dissociation curve was added at the end of the last PCR cycle, as a control of the amplified product. Then the set-up was saved and the PCR started. An incubation step of 50°C for 2 min was added to the cycling programme before activation of DNA polymerase. During the activation step, DNA polymerase is heat-activated at 95°C for 15 min: hot-start PCR. The hot-start eliminates secondary structures and straightens the DNA, in addition, preventing any DNA amplification prior to the first thermal cycle of the real time PCR. The denaturation step was performed at 95°C for 15 seconds and caused DNA melting of the DNA template by disrupting the hydrogen bonds between complementary bases, yielding single-stranded DNA molecules. The annealing and extension step was performed at 60°C for 1 minute and allowed annealing of the primers to the single-stranded DNA template. The polymerase bound to the primer-template hybrid and begun DNA formation. At this step the DNA polymerase synthesized a new DNA strand complementary to the DNA template strand by adding dNTPs that are complementary to the template in 5' to 3' direction, condensing the 5'-phosphate group of the dNTPs with the 3'-hydroxyl group at the end of the nascent (extending) DNA strand. Exponential amplification of the specific DNA fragment happened. After the PCR is finished, a relative quantification study is opened and the saved data is opened using the programme. This is where the CT values are set and then imported into Microsoft Excel®. The CT value is based on the fact that a large amount of a specific gene within a sample will cause the sample to reach the cut off point in an earlier cycle compared to samples where the gene is less expressed. This principle is used when calculating the gene expression.

A relative quantification is done, where the calculations of the fold increase or decrease in gene expression is based on the calculations from Livak et al. [183]. In short ΔCT= CT Sample - CT reference gene. ΔΔCT= ΔCTsample – ΔCT control (e.g. non-mated mouse). Then use the formula to calculate the gene expression relative to the control.

The dissociation curve is used to control the accumulated DNA. Since SYBR Green is not sequence specific, the product of the PCR has to be verified. The verification consists of dissociation curve, which records the melting temperature of the DNA. The DNA should have the same melting temperature in all the samples, if there is deviation it indicates the presence of primer dimers or accumulation of another gene. This could happen if primers had homology with other genes. And primer dimers occur when there are complementarities between the forward and reverse primer. An example of a dissociation curve is shown in Figure 2.8.

Figure 2.8

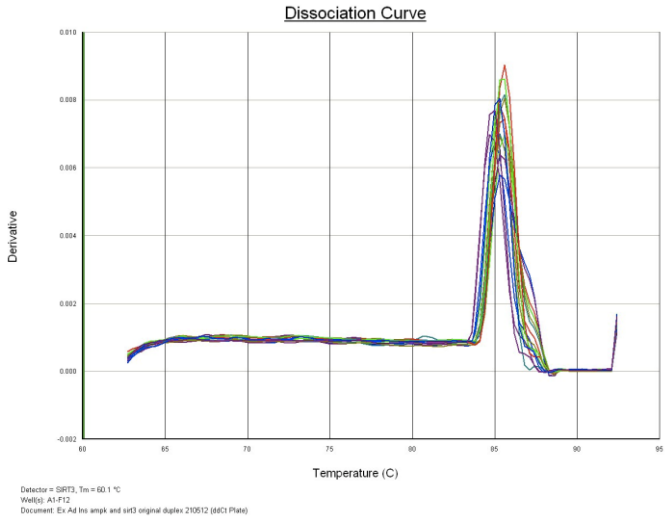


Figure 2.8: Illustration of a dissociation curve. There doesn't seem to be much deviation, indicating no or very little presence of primer dimers and that the same gene has been amplified in all the samples.

#### *2.2.3.4.3 Analysis*

Results were analysed using GeneAmp software (Applied Biosystems, USA). A threshold level was set during the linear, exponential amplification phase of the logarithmic amplification plot. The quantity of cDNA/mRNA present in the unknown samples was then calculated using the standard curve at the point where the threshold crossed the amplification plot.

A housekeeping gene that is expressed at a constant level in most cell types, 18S, was used as an endogenous control to normalize the expression pattern of each gene. The mean sample content of the product of interest was divided by the respective mean level of 18S reference RNA for each sample. The mean average of these values for the control (untreated) sample was then calculated. Each sample was then divided by the mean average of the control sample to produce a value for each sample relative to the control. Results were then expressed as fold-increase in mRNA/cDNA level, relative to the control sample.

### 2.2.3.5 Statistical Analysis

All data are expressed as mean ± SEM. Statistical comparisons were carried out using Graphpad Prism (GraphPad Software) and StatView. Statistical differences were evaluated by unpaired t-test or one-way analysis of variance (ANOVA), followed by a Newman-Keuls, Tuckey post-hoc or Fisher's post-test where appropriate. Statistical differences were accepted as $P<0.05$.

**Chapter:**

***3.*** *Studies on the effect of experimental diets on the regulation of hepatic lipogenesis.*

## 3.1 Introduction

AMPK and SIRT1 play important roles in the maintenance of hepatic lipid homeostasis, via PPARα-mediated regulatory effects on lipogenesis and fatty acid oxidation, as well as regulating hepatic glucose homeostasis via direct effects on insulin signaling and gluconeogenesis [19, 88, 184, 185]. Recent studies have suggested that PPARα – AMPK – SIRT1 interact to form a complex regulatory feedback network controlling glucose and lipid metabolism in the liver [149, 163, 164]. However, this system is not well understood, particularly with respect to potential interactions between AMPK and SIRT1 (Chapter 1, section 1.6.1.7). In addition, the effects of hepatic SIRT1 are also controversial, with various studies reporting contrasting effects of SIRT1 on lipogenesis and gluconeogenesis [128, 130-132, 186].

This chapter aims to characterise the putative AMPK-SIRT-PPARα regulatory network in liver. This will be done by using the following *in vivo* models; (a) alterations in nutritional status viz. starvation (where the hepatic capacity for gluconeogenesis and fat oxidation is increased), (b) re-feeding after starvation (which suppresses hepatic glucose production and fat oxidation), and (c) in the well-fed state, where the glucose supply is ample, insulin levels are high, and incoming FA are predominantly esterified rather than oxidized. In addition, comparisons will be made between *ad libitum* feeding of control rodent diet and a diet enriched with saturated fat, which affect hepatic glucose production and fat metabolism. Finally, to elucidate further the potentially complex interplay between AMPK with the PPARs and SIRTs in regulating hepatic metabolism, we utilized (f) AMPK null mice and (g) SIRT1 knockdown H4IIEC3 cells. Studies described in this chapter were performed in liver (a key tissue for glucose and lipid homeostasis) where SIRT1 has previously been reported to activate AMPK [148].

## 3.2 Materials and methods

To examine the effects of experimental diets and nutritional status on regulation of hepatic lipid homeostasis, the following in vivo models were utilised; C57BI/6 fasted and fed mice, liver specific AMPK$^{-/-}$ fasted and refed mice and high fat fed C57BI/6

mice (these models are described in detail in the general methods chapter; Chapter 2, sections: 2.2.2.1 and 2.2.2.2; animal diets and treatments described on Chapter 2, section 2.2.2.5)

All the procedures carried on using these samples were performed in accordance with the principles and guidelines established by the European Convention for the Protection of Laboratory Animalsof Animals (Scientific Procedures) Act 1986, published by HMSO, London.

Culture, treatment and transfection of the hepatocyte cell line, H4IIEC3 (Chapter 2, section 2.2.1.1), western blotting (Chapter 2, section 2.2.3.2), immunoprecipitation (Chapter 2, section 2.2.3.3), qRT-PCR (Chapter 2, section 2.2.3.4) and plasma analysis (Chapter 2, section 2.2.2.8) were conducted as described in the general methods section.

## 3.3 Results

### 3.3.1 Effects of 24h starvation on hepatic lipid homeostasis

The liver is the central metabolic organ that regulates several key aspects of lipid metabolism including fatty acid β-oxidation, lipogenesis, and lipoprotein uptake and secretion, in response to nutritional and hormonal signals [187]. During the fed state, dietary glucose stimulates insulin secretion from the pancreas, increasing hepatic lipogenesis and lipoprotein secretion. Conversely, upon fasting, hepatic fatty acid oxidation is enhanced [188, 189]. C57BI/6 mice were either starved for 24h or fed a control diet to provide context for the later studies on specific $AMPK^{-/-}$ liver (fasted or refed).

#### 3.3.1.1 Plasma glucose and insulin levels were reduced by fasting

Plasma glucose levels were decreased in fasted compared to fed mice (30%; $P$ <0.001; Fig. 3.1A). Plasma insulin levels were decreased in fasted mice relative to fed mice (40 %; $P$<0.01; Fig. 3.1B).

Figure 3.1

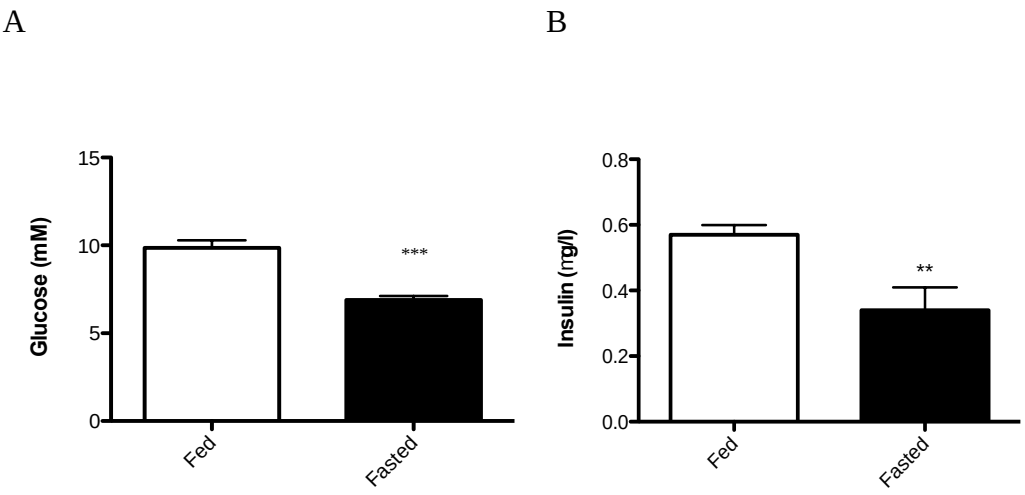


Figure 3.1 Plasma glucose and insulin concentrations in fed or fasted mice. Mice were either killed at the mid-point of the dark phase on day 5 (fed) or starved for 24 h after 5 days of maintenance on the standard diet. Blood samples were collected for measurement of plasma glucose (A) or plasma insulin (B). Results are expressed as means ± SEM. n = 8 mice in each group. Statistically significant effects of fasting are indicated by $^{**}P<0.01$ and $^{***}P<0.001$.

### 3.3.1.2 Lipogenic gene expression is suppressed by fasting.

SREBP1 and stearoyl-CoA desaturase-1 (SCD-1) are key lipogenic genes, whose expression is up regulated in liver under lipogenic conditions, including insulin stimulation and high-carbohydrate feeding. Consistent with this, starvation (24 h) of control mice resulted in a marked decline in both SREBP1 (93%; $P<0.001$) and SCD-1 (71%) gene expression (Fig. 3.2A and 3.2B, respectively). Studies have reported a key role for X-box binding protein 1 (XBP1) in induction of hepatic lipogenic genes, including SCD1 [190]. In liver, starvation-induced decreases in lipogenic gene expression were not associated with a decline in XBP1 mRNA or protein expression (Fig. 3.2B). On the contrary, XBP1 was 2-fold increased ($P<0.001$) relative to fed samples.

Figure 3.2

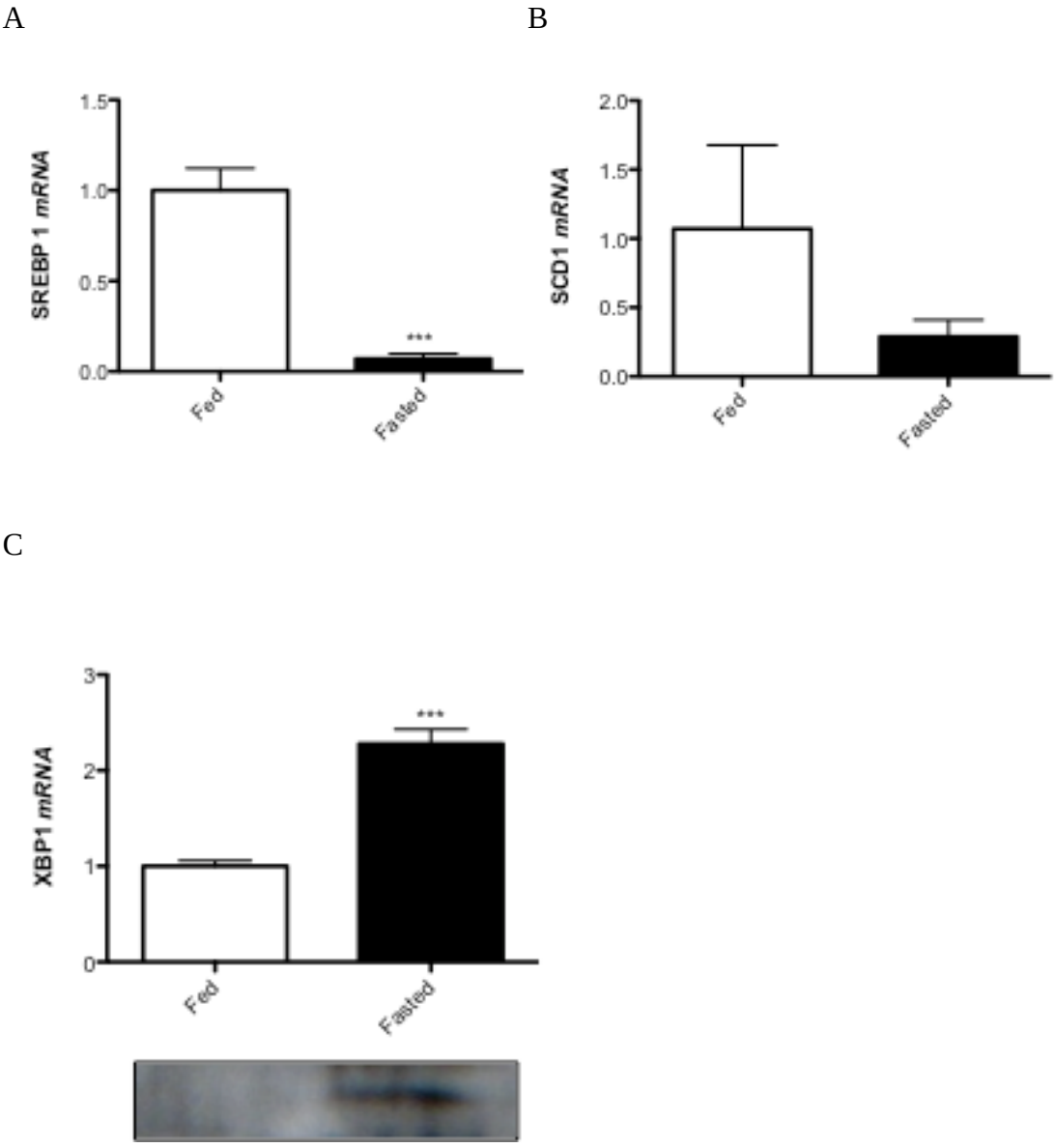


Figure 3.2: Expression of genes regulating hepatic lipogenesis (SREBP1, SCD1) and the mammalian XBP1 in liver of fasted and fed mice. Mice were either killed at the mid-point of the dark phase on day 5 (fed) or starved for 24 h after 5 days of maintenance on the standard diet. Gene expression for SREBP-1 (A), SCD1 (B) and XBP1 (C) were measured in liver by qRT-PCR. Representative Western blots for XBP-1 protein expression in liver (C) of mice sampled in the fed or 24 h-fasted state are also shown. Results are expressed as means ± SEM. Statistically significant effects of fasting are indicated by ***$P$<0.001.

### 3.3.1.3 Effects of fasting on PGC-1α and PDHK4 expression.

PPARα is a key regulator of hepatic FA oxidation [88]. In addition, the nuclear receptor co-activator PGC-1α participates in regulating glucose and lipid metabolism in liver by interacting with PPARα [86]. Hepatic PGC-1α gene expression was significantly increased in WT starved compared with fed mice (Fig. 3.3A), as is consistent with its role in coordinating the response of hepatic nutrient handling to starvation. Protein expression of PGC-1α was also enhanced by fasting.

The gene expression of PDHK4 (encoded by PDK4 gene), a regulatory kinase that inactivates PDC, blocking glucose oxidation and thereby forcing fat oxidation, is PPARα responsive [185]. As expected, fasting also elevated hepatic *PDK4* expression, with a greater (3.2-fold; $P<0.01$) increase in protein expression (Fig. 3.3B) than gene expression.

Figure 3.3

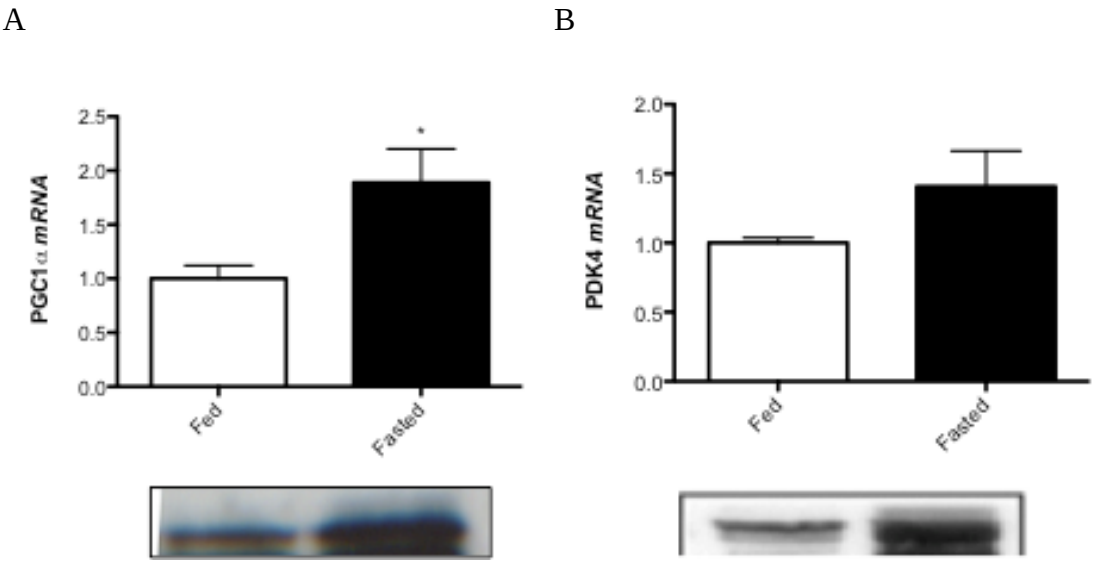


Figure 3.3: Gene and protein expression of key regulators of lipid (PGC-1α) and glucose (PDK4) oxidation in liver of fasted and fed mice. Mice were either killed at the mid-point of the dark phase on day 5 (fed) or starved for 24 h after 5 days of maintenance on the standard diet before being killed. Gene expression for PGC-1α (A) and PDHK4 (B) were measured in liver by qRT-PCR. Representative Western blots for PGC-1α (A) and PDHK4 (B) protein expression in liver sampled in the fed or 24 h-fasted state are also shown. Results are expressed as means ± SEM. Statistically significant effects of fasting are indicated by *$P<0.05$. n = 6-8 mice.

3.3.1.4 Effects of fasting on SIRT1, SIRT3 and GCN5 expression.

Nutrient-mediated control of PGC-1α activity is tightly correlated with its acetylation state [139]. Here we measured SIRT1 and GCN5 to understand how the nutrient regulation of PGC-1α activity previously seen (Fig. 3.3) squares with the regulation of its acetylation state. SIRT1 gene expression was markedly up regulated in response to fasting in livers of WT mice, with a concomitant 15-fold increase in SIRT1 protein expression (***P*<0.01) (Fig. 3.4A). In contrast, hepatic GCN5 gene expression was unaffected by fasting, although there was a 2.6-fold increase (**P*<0.05) in GCN5 protein expression (Fig. 3.4B), suggestive of post-transcriptional control.

Acetylation targets most enzymes in most metabolic pathways including those occurring within mitochondria, such as the Krebs cycle and mitochondrial β oxidation [191]. SIRT3 is localized in the mitochondrial matrix, where it regulates the acetylation levels of metabolic enzymes [109], and its expression is up-regulated in liver in response to starvation, leading to promotion of FA oxidation [130]. Starvation increased hepatic SIRT3 gene expression (~3.2-fold; ***P*<0.01) (Fig. 3.4C).

Figure 3.4

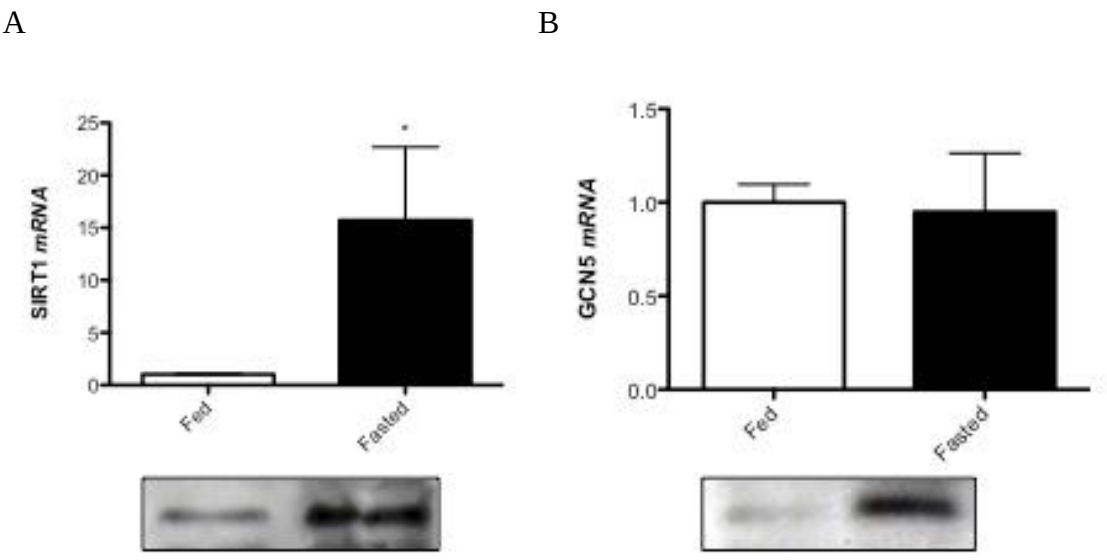

C

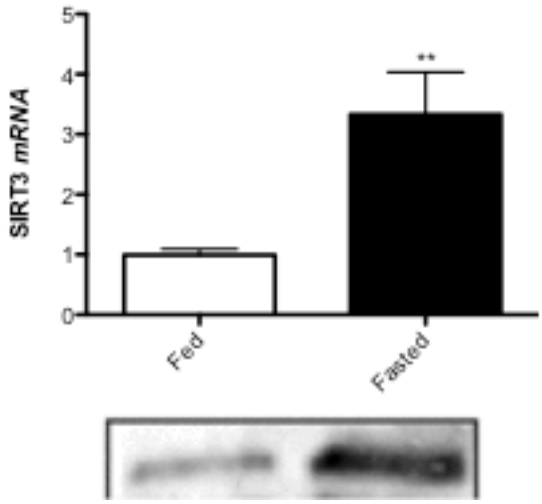


Figure 3.4: Response of gene and protein expression of the deacetylases SIRT1 and SIRT3 and acetylase GCN5 to fed or fasted conditions. Mice were either killed at the mid-point of the dark phase on day 5 (fed) or starved for 24 h after 5 days of maintenance on the standard diet, before being killed. Gene expression for SIRT1 (A), GCN5 (B) and SIRT3 (C) were measured in liver by qRT-PCR. Representative Western blots for SIRT1 (A), GCN5 (B) and SIRT3 (C) in liver of mice sampled in the fed or 24 h-fasted state are also shown. Results are expressed as means ± SEM (n = 6-8 mice). Statistically significant effects of fasting are indicated by $^{**}P<0.01$.

### 3.3.2 Effects of AMPK deletion

According to the previous results described in this chapter, the SIRT1-PGC-1α-SIRT3 lipolytic axis is induced by fasting, whereas lipogenesis is decreased. In the liver, SIRT1 has been reported to activate AMPK [148]. Lee et al. have reported that, in the liver, SIRT1 is directly phosphorylated and inactivated by AMPK [192]. These findings, together with evidence that AMPK and SIRT1 share the common activators (including fasting), actions and target molecules [149], led us to examine the effect of AMPK deficiency in SIRT1 target molecules, during fasting and after refeeding (which suppresses hepatic glucose production and fat oxidation).

#### 3.3.2.1 Loss of AMPKα1 and α2 subunit decreases AMPK protein expression in liver

As expected, Western blot analysis (Fig. 3.5) confirmed reduced hepatic AMPK protein levels in AMPK $^{-/-}$ mice compared to WT, under fed conditions. Western blotting revealed that, consistent with lower total AMPK expression, AMPK

phosphorylation on Thr$^{172}$ is 80% (**$P$<0.01) decreased in livers of AMPK$^{-/-}$ mice compared to WT mice (Fig. 3.5).

Figure 3.5

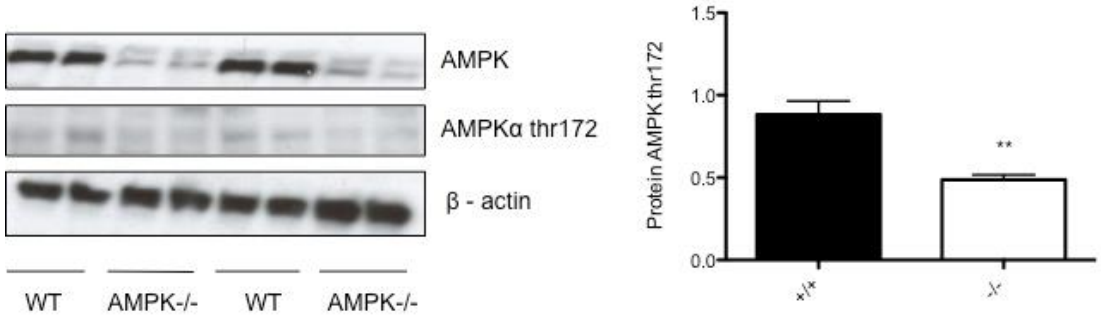


Figure 3.5: Western blot analysis showing decreased phospho-AMPK-thr$^{172}$ protein expression in AMPK knockout fed livers. Values are represented as means ± SEM (n=8). **$P$< 0.01 vs. +/+. -/- = AMPK α1/2 knockout mice. +/+ = WT mice.

### 3.3.2.2 SIRT1 gene expression is decreased in mice after re-feeding

AMPK increases SIRT1 activity by increasing cellular NAD$^+$ levels [151] or by increasing NAMPT activity [150]. Like SIRT1, AMPK is activated by glucose deprivation [19]. A 24h period of fasting in mice promoted an increased expression of SIRT1 mRNA and protein in liver (Fig. 3.4). In mouse embryonic fibroblasts (MEF), Wang and his collaborators have shown that SIRT1 activity is impaired by AMPK inhibition [193]. In the present study SIRT1 gene expression was analyzed in livers of WT and AMPK$^{-/-}$mice, fasted for 24h, or after refeeding. SIRT1 gene expression was about 98% decreased (*$P$<0.05) in refed animals, but there were no significant changes between WT and AMPK$^{-/-}$ livers (Fig. 3.6A).

Enzymatic activity of SIRT3 promotes oxidative phosphorylation. Mitochondrial proteins of SIRT3 knockout mice are hyperacetylated and cellular ATP levels of such animals are reduced in high-energy tissues in, for example, the liver [159]. Loss of SIRT3 appears to decrease mitochondrial substrate oxidation and results in more intensive glycolysis [194]. In line with these observations, SIRT3 knockout attenuates oxygen consumption, while overexpression increases it [113, 195]. The effect of SIRT3 deficiency on ATP production is further aggravated by fasting, underlying its

reliance on $NAD^+$ [167]. In this study, we analysed SIRT3 gene expression in livers of WT and $AMPK^{-/-}$, under 24h fasting conditions or after a 4h-refeeding period. SIRT3 gene expression did not change with AMPK knockout. However there is a marked difference in SIRT3 gene expression between the fasted-refed state (~75% vs. fasted, **P*<0.05, Fig. 3.6B).

Figure 3.6

A B

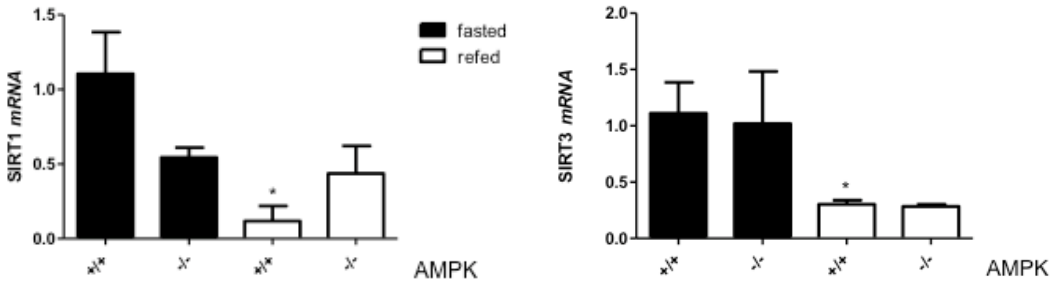


Figure 3.6: Relative gene expression of SIRT1 (A) and SIRT3 (B) vs. 18S gene expression in mice fasted for 24h (fasted) or re-fed with a standard diet for a period of 4h (re-fed). qRT-PCR was performed to measure mRNA expression of SIRT1 and SIRT3 gene. Values are represented as means ± SEM (n=8). **P*< 0.05 vs. fasted +/+. -/- = AMPK α1/2 knockout mice. +/+ = WT mice.

#### 3.3.2.3 Hepatic gene expression of the gluconeogenic enzymes PEPCK and G6Pase were suppressed in livers of re-fed $AMPK^{-/-}$ mice.

SIRT1 deacetylates and activates PGC-1α, resulting in increased gluconeogenesis [129]. According with this, a decreased activity of SIRT1 could impair the expression (and thus, potentially, activity) of the gluconeogenic enzymes: phosphoenolpyruvate carboxykinase (PEPCK) (encoded by *PCK1* gene) and glucose-6-phosphatase (G6Pase) [196]. In this study, we investigated the gene expression of the gluconeogenic enzymes to better understand the effect of $AMPK^{-/-}$ and nutritional status on gluconeogenesis in the liver. As expected, the expression of gluconeogenic genes were decreased (*PCK1* was 75% decreased, **P*<0.05) in re-fed livers (Fig. 3.7A and B), after a fasting period. There were no significant differences in the responses to

re-feeding between AMPK$^{-/-}$, when compared to WT, indicating that AMPK plays no effect in repressed gluconeogenesis upon re-feding.

Figure 3.7

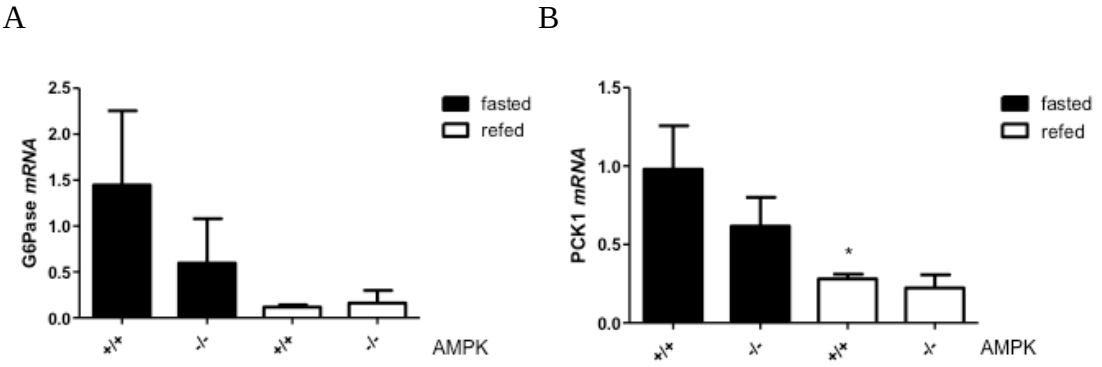


Figure 3.7: qRT-PCR showing reduced mRNA expression of gluconeogenic enzymes in livers of mice after a 4h period of re-feeding (re-fed), comparing to 24h fasted animals (fasted). Relative gene expression of G6Pase (A); PCK1 (PEPCK) (B) vs. 18S gene. Values are represented as means ± SEM (n=8). *$P$< 0.05 vs. fasted +/+. -/- = AMPK α1/2 knockout mice. +/+ = WT mice.

### 3.3.2.4 Acetylation levels of PGC-1α in AMPK $^{-/-}$ liver

AMPK and SIRT1 are metabolic sensors that can increase each other's activity [149]. AMPK increases SIRT1 activity, resulting in deacetylation and activation of the activity of one downstream SIRT1 target: PGC-1α [151]. In this study we aimed to understand the role of the SIRT1-PGC-1α axis in AMPK$^{-/-}$ liver, by immunoprecipitating PGC-1α, followed by a western blot to reveal the acetylated lysine protein residues in the purified PGC-1α proteins. PGC-1α had decreased mRNA expression in refed animals (Fig. 3.10A), a result that correlates with SIRT1 gene expression under the same conditions. Interestingly, PGC-1α was found to be less acetylated in lysine residues in livers of the AMPK deficient animals (~25%, *$P$<0.05, ±P<0.05) although, there is less acetylation in re-fed conditions than in fasting conditions for 24h (~20%, *$P$<0.05) (Fig.3.8A and 3.8B).

Figure 3.8

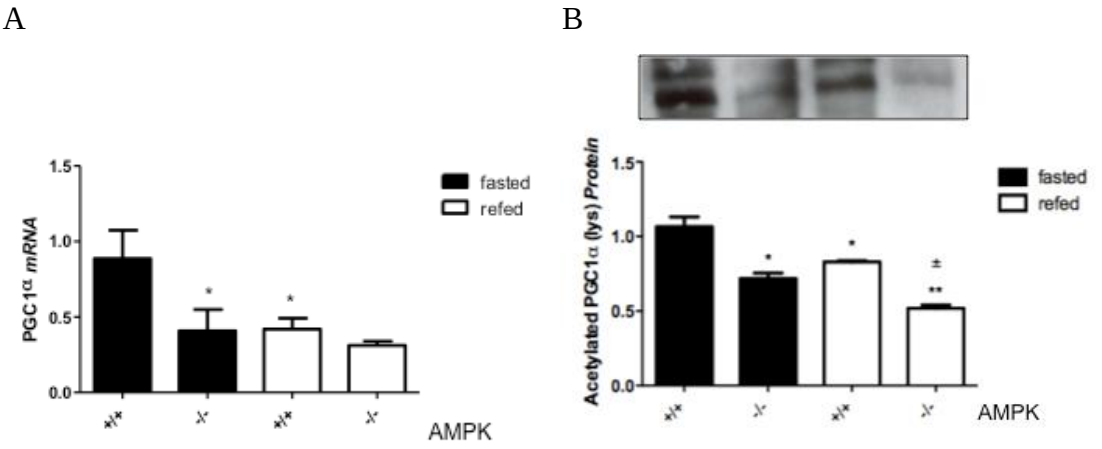


Figure 3.8: qRT-PCR showing PGC-1α gene expression vs. 18S gene (A); Western blot analysis showing acetylation levels on lysine residues of PGC-1α (B) in AMPK$^{-/-}$ and WT animals fasted for 24h (fasted) or refed for a 4h period (refed). Values are represented as means ± SEM (n=4). *$P$< 0.05 vs. fasted +/+; **$P$<0.01 vs. fasted; ±P<0.05 vs. +/+. -/- = AMPK α1/2 knockout mice. +/+ = WT mice.

### 3.3.3 Studies in hepatocyte cell culture: Effects of SIRT1 silencing

AMPK and SIRT1 are reported to exert similar effects on diverse processes such as cellular fuel metabolism, inflammation, and mitochondrial function [149]. Several lines of evidence suggest that these similarities occur because AMPK and SIRT1 both regulate each other and share many common target molecules [118]. Since we have previously studied the effects of AMPK knockout in the liver, we speculated that SIRT1 knockdown in liver cell line (H4IIEC3) could show that there is a possible feedback loop between SIRT1 and AMPK. In this context we studied the effects of SIRT1 knockdown in liver metabolism, *in vitro* using H4IIEC3 liver cell line.

#### 3.3.3.1 SIRT1 siRNA decreased SIRT1 gene expression in H4IIEC3 cells.

Cells were transfected with SIRT1 siRNA to knockdown SIRT1 protein and gene expression. Cells transfected with SIRT1 siRNA had lower expression of SIRT1 mRNA, although this result was not significant (Fig. 3.9A). However, the knockdown is similar in magnitude to that observed in AMPK$^{-/-}$ mice, so allows for a good

comparison with the *in vivo* situation. A significant reduction in PGC-1α (target of SIRT1) gene expression was observed (~98%, ****P*<0.005 vs. siRNA Scr) in cells transfected with SIRT1 siRNA comparing to the scrambled sequence siRNA (Fig. 3.9B).

Figure 3.9

A B

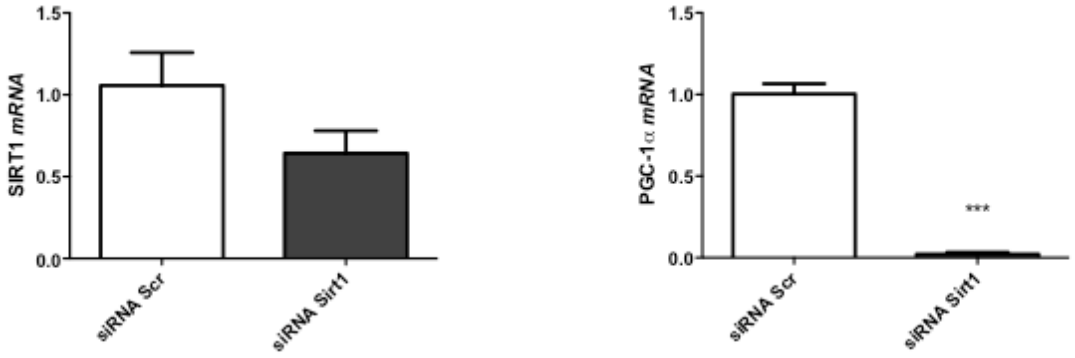


Figure 3.9: Relative gene expression of SIRT1 (A) and PGC-1α (B) vs. 18S gene. mRNA expression of SIRT1 and PGC-1α was analyzed by qRT-PCR. Values are represented as means ± SEM (n=4 repetitions). ****P*< 0.005 vs. Control. siRNA. Scr = Control or scrambled sequence; siRNA SIRT1 = SIRT1 knockdown cells for 72h.

### 3.3.3.2 SIRT1 silencing causes decreased AMPK activation

To better understand the possible feedback loop existing between SIRT1 and AMPK we investigated AMPK phosphorylation at $Thr^{172}$, when cells were subjected to SIRT1 knockdown. AMPK phosphorylation on $Thr^{172}$ was 10% decreased (***P*<0.005) in SIRT1 knockdown cells, when compared to the scrambled sequence (control) (Fig. 3.10).

Figure 3.10

A B

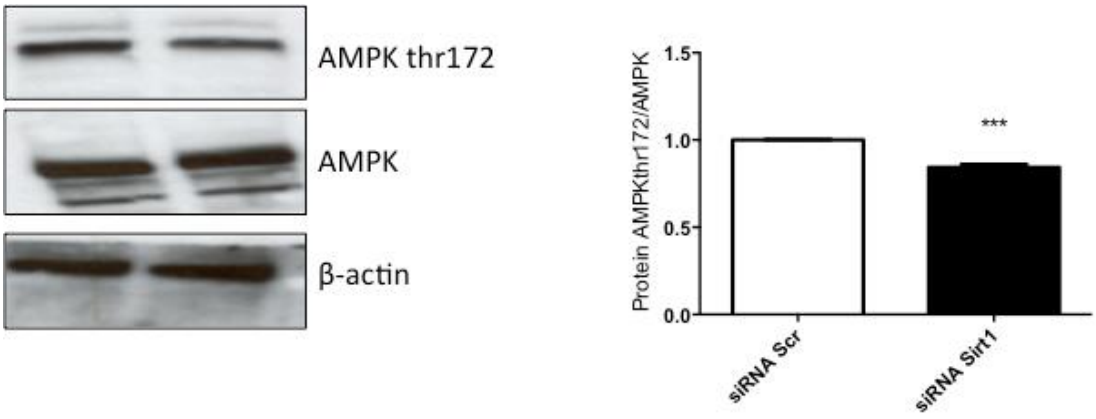


Figure 3.10: Western blot analysis showing that phospho-AMPK- thr$^{172}$ (MW: 63 kDa) protein is decreased as a consequence of SIRT1 knockdown, in H4IIEC3 cells. (A) Representative western blot. (B) Graph analysis of the representative western blot. Values are represented as means ± SEM (n=4 repetitions). ****P*< 0.005 vs. Control. siRNA Scr = Control or scrambled sequence; siRNA SIRT1 = SIRT1 knockdown cells for 72h.

### 3.3.3.3 Gluconeogenic genes differ in their responses to SIRT1 siRNA

As stated previously, SIRT1 deacetylates and activates PGC-1α, resulting in increased gluconeogenesis [129]. We speculated that SIRT1 knockdown could impair gene expression of the gluconeogenic enzymes (PEPCK, encoded by PCK1 gene, and G6Pase) [196]. PEPCK gene expression was 90% reduced (**P*<0.05) in response to SIRT1 knockdown (Fig.3.11A), whereas G6Pase gene expression tended to increase under the same conditions (Fig.3.11B).

Figure 3.11

A B

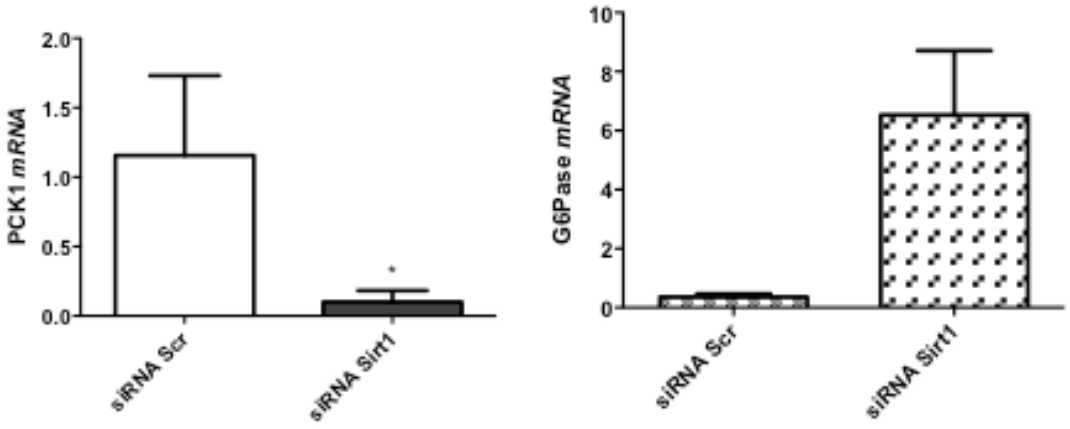


Figure 3.11: qRT-PCR analysis showing PCK1 (A) mRNA expression and G6Pase (B) mRNA expression in control cells compared to SIRT1 knockdown cells. Values are represented as means ± SEM (n= 2 to 4 repetitions). *$P$< 0.005 vs. Control. siRNA Scr = Control or scrambled sequence; siRNA SIRT1 = SIRT1 knockdown cells for 72h.

#### 3.3.3.4 SIRT6 is regulated by SIRT1

Like SIRT1, SIRT6 is a nuclear $NAD^+$ dependent deacetylase, known to prolong the lifespan of organisms and delay the aging process (and age related diseases such as T2DM), by repairing the DNA damage [197]. We studied the effect of SIRT1 knockdown in SIRT6 gene expression. SIRT6 protein and gene expression were decreased in SIRT1 knockdown H4IIEC3 cells. SIRT6 mRNA is 80% decreased when compared to the control group (*$P$<0.05, Fig. 3.12).

Figure 3.12

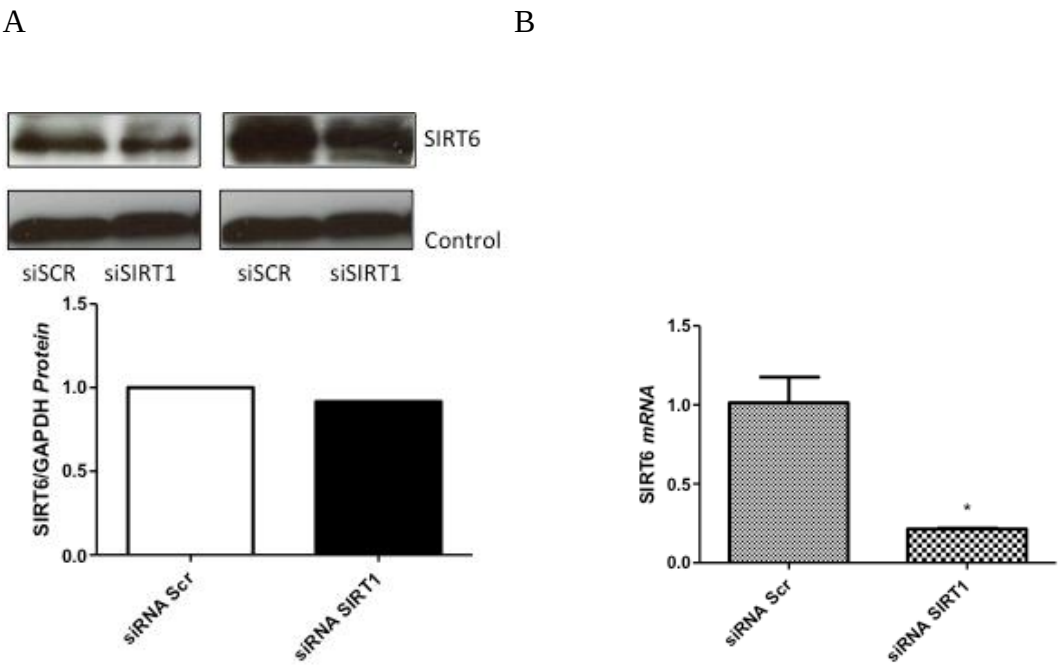


Figure 3.12: Decreased expression and activity of SIRT1 decreases SIRT6 protein and gene expression. Western Blot analysis showing decreased SIRT6 (MW: 37 kDa) protein expression in SIRT1 knockdown cells (A); qRT-PCR analysis showing a significant decrease of SIRT6 mRNA expression in SIRT1 knockdown cells (B). Values are represented as means ± SEM (n=4 repetitions). *$P$< 0.005 vs. Control. siRNA Scr = Control or scrambled sequence; siRNA SIRT1 = SIRT1 knockdown cells for 72h.

### 3.3.4 Effects of high-fat feeding and NMN treatment

We have previously seen that AMPK deficiency decreases the SIRT1 target gene (*PGC-1α*) expression and that this is related to decreased gluconeogenesis, upon fasting. Re-feeding (which suppresses gluconeogenesis) abrogates the effect of AMPK deficieny in liver. However, in H4IIEC3 cells, when SIRT1 is knockdown, there is a decreased protein and gene expression of AMPK. According with the studies developed in AMPK$^{-/-}$ liver and in H4IIEC3 cells, we speculate that there is a feedback loop between AMPK and SIRT1 in the liver and that this feedback loop regulates hepatic gluconeogenesis, depending of the nutritional status. To better understand how the nutritional status infuences SIRT1 target genes in regulating hepatic metabolism, we have also studied mice fed a high fat diet with or without NMN administration. NMN is the percurso of NAD$^{+}$ [179] and thereby (potentially)

increases SIRT1 activity by increasing $NAD^+$ availability [198], which could affect hepatic metabolism. High fat diet is very low in fat, when compared to other studies, because I am interested in the effects of a small increase in dietary fat, to better mimic what happens in human occidental diet.

Hepatocyte-specific deletion of SIRT1 alters fatty acid metabolism and results in hepatic steatosis and inflammation [133]. On the other hand, SIRT1 is significantly reduced in non-alcoholic fatty liver disease (NAFLD) induced by high-fat diet in rats [199]. The aim of this aspect of the project was to investigate the effects of high fat feeding on hepatic SIRT1 expression and determine how, by exposing tissues to the $NAD^+$ precursor NMN and thereby (potentially) increasing SIRT1 activity by increasing $NAD^+$ availability, could affect hepatic metabolism and hepatic insulin sensitivity.

#### 3.3.4.1 The effect of high fat feeding on body weights

Significant changes in body weight occurred during the high fat diet for 16 weeks (but not for 10 weeks) comparing to animals that were fed with a control diet for the same period (Table 3.1A). After intraperitoneal NMN administration (500 mg/kg body weight), 16h before sacrifice, mice tend to lose weight, although control + NMN mice gained weight (**$P$<0.05) (Table 3.1B).

Table 3.1

A

| | **10 weeks of diet** | | **16 weeks of diet** | |
|---|---|---|---|---|
| | Control | HF | Control | HF |
| **Initial weight (g)** | 24.0 ± 0.5 | 23.9 ± 1.2 | 24.1 ± 0.6 | 24.0 ± 1.4 |
| **Final weight (g)** | 28.5 ± 0.6 | 29.1 ± 2.0 | 31.4 ± 1.0 | 35.4 ± 3.0 |
| **Weight gained (g)** | 4.5 ± 0.7 | 5.2 ± 2.0 | 7.3 ± 1.3 | 11.4 ± 3.9** |

B

| Administration of NMN after 16 weeks of HF/Control diet | Control Vehicle | Control + NMN | HF Vehicle | HF + NMN |
|---|---|---|---|---|
| **Weight gained (g)** | -0.52± 0.43 | 0.46 ± 0.67 | -0.74 ± 0.45 | -0.26 ± 0.34 |

Table 3.1. A: Animal characteristics of *C57Bl/6* mice on control diet for 10 or 16 weeks (Control) or 11% saturated fat diet for 10 or 16 weeks (HF). Values are represented as means ± SEM (n= 5 or 10 mice per group). ***P* <0.005 vs. controls. The equality of variances was studied in Leven test (***P* <0.009). A t-test was used for independent samples. B: Weight gained on a control diet for 16 weeks after administration (or not) of 20 mg of NMN 24h prior sacrifice. Vehicles = not administrated with NMN. +NMN = intraperitoneal injection of 20 mg of NMN.

### 3.3.4.2 Glucose and insulin plasma levels upon high fat feeding

In addition to promoting glucose storage, insulin inhibits the production and release of glucose by the liver by blocking gluconeogenesis and glycogenolysis [5]. Inslin and glucose plasma levels were assessed in the liver of HF fed mice to understand how a moderate high fat diet affect the glucose homeostasis in the liver. Plasma glucose levels were significantly decreased in HF + NMN mice compared to HF mice (20%; **P*<0.05; Fig. 3.13A). Plasma insulin levels did not change significantly between HF and the control group (Fig. 3.13B).

Figure 3.13

A B

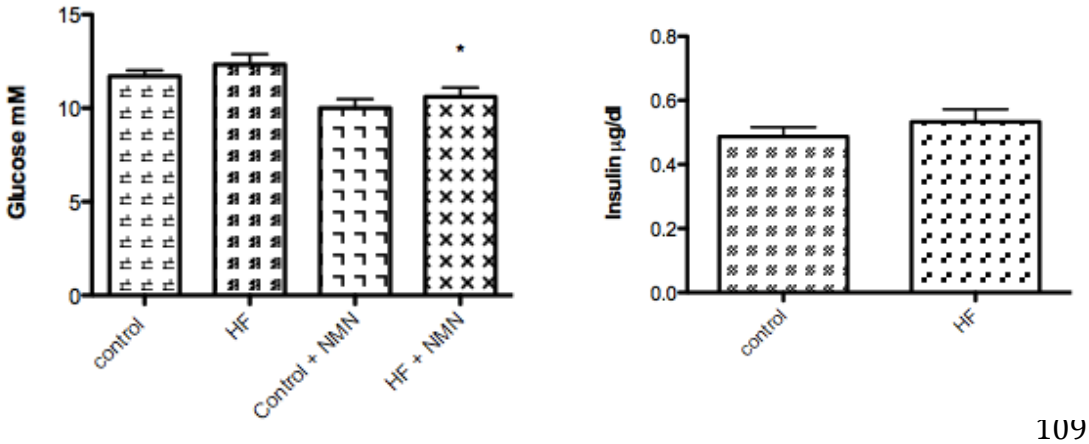

Figure 3.13: Plasma glucose (A) and insulin (B) concentrations in high fat fed mice or controls. HF = high fat diet for 16 weeks. NMN = intraperitoneal injection of 500 mg/kg body weight of NMN at 16 hours prior to tissue sampling. Results are expressed as means ± SEM. n = 5 mice in each group. Statistically significant effects of HF diet are indicated by $^{**}P<0.01$.

### 3.3.4.3 High fat feeding increases SIRT1 protein expression in liver

Previous studies have reported that high-fat feeding decreases SIRT1 gene expression in mice fed on high fat diet (60% energy from fat) [126]. In the present investigations, in which mice were maintained on a high-saturated fat diet (11% fat) for 16 weeks, high-fat feeding was associated with a modest increase in SIRT1 protein expression. A representative blot is shown in Fig. 3.14A. Quantification of the data (Fig. 3.14A) indicated that, although there was some variation between individual mice, SIRT1 protein expression increased in response to high-fat feeding relative to controls.

To assess the effects of modulating SIRT1 activity in HF mice, NMN (500 mg/kg body weight) was administered by intraperitoneal injection to control and high-fat fed mice 16 hours prior to tissue sampling. NMN administration had little effect on SIRT1 protein expression in livers of control mice maintained on standard diet (Fig. 3.14). In contrast, the administration of NMN to high-fat fed mice was associated with increased SIRT1 protein expression. The highest protein expression of SIRT1 was observed in high-fat-fed mice treated with NMN, approximately 6.0% higher levels of expression than seen in control mice that had not been treated with NMN. It can be concluded that high-fat feeding increases SIRT1 protein expression, an effect exaggerated by treatment with NMN (Fig. 3.14).

Figure 3.14

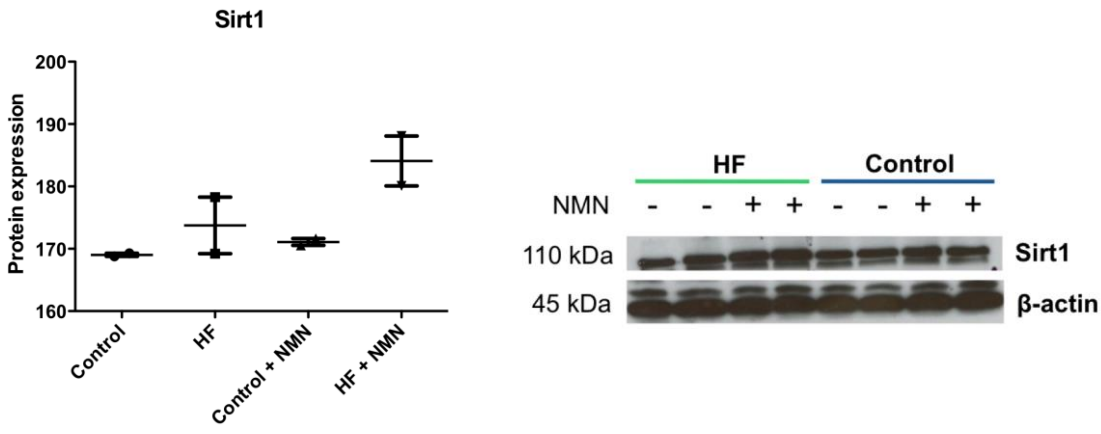

Figure 3.14: A representative Western blot of the protein SIRT1 (MW: 110 kDa) and the control β-actin (MW: 45 kDa) are displayed in control and high fat fed animals (HF), with or without NMN administration. HF = high fat diet for 16 weeks. NMN = intraperitoneal injection of 500 mg/kg body weight of NMN at 16 hours prior to tissue sampling. mRNA expression levels measured using qRT-PCR. n=3.

### 3.3.4.4 High fat feeding increases Akt activity in liver

PI3K/Akt pathway is considered to be the major effector of insulin action. Akt phosphorylation at Ser$^{473}$ is required for its activation [51, 200]. Protein levels of phosphor-(Ser$^{473}$)-Akt were increased in livers of high-fat fat mice compared with control mice on standard diet, suggesting increased Akt activity as protein expression of total (unphosphorylated and phosphorylated Akt) was unchanged (Fig. 3.15). Protein expression of phospho-Akt also increased with NMN treatment in control mice, but the effect of NMN treatment to increase phospho-Akt expression (i.e. Akt activity) did not appear to be additive with that of HF feeding (Fig. 3.15). This contrasts with effects of high-fat feeding and NMN to increase SIRT1 protein expression (Fig. 3.14).

Figure 3.15

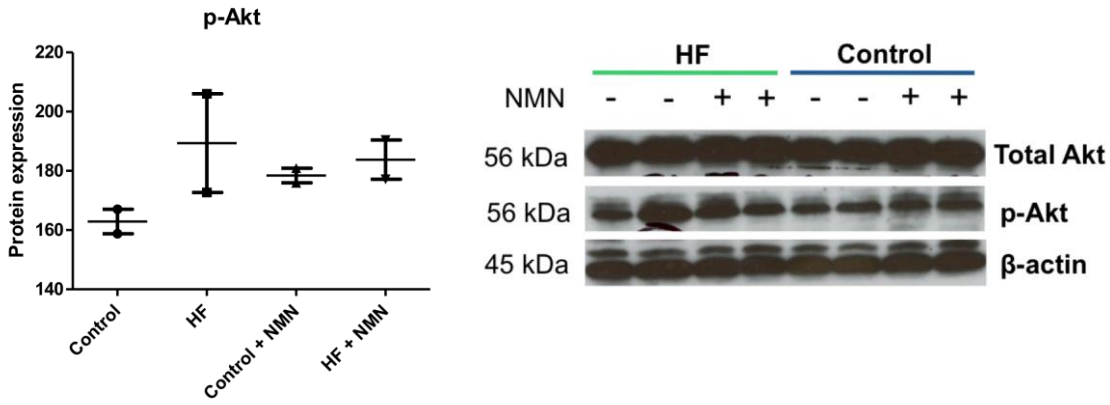


Figure 3.15: Western blot analysis of phospho-Akt-ser$^{473}$ (MW 56 kDa) in control and high fat fed animals (HF), with or without NMN (500 mg/kg body weight) administration as intraperitoneal injection, at 16 hours prior to tissue sampling; total Akt (MW 56 kDa) and the control protein: β -actin (MW 45 kDa) were also measured to compare changes in phospho-Aktser$^{473}$. As the density of the control and total-Akt bands are similar across the gel, changes witnessed in the levels of phospho-Akt-

ser$^{473}$ are due to its activation state. HF = high fat diet for 16 weeks. NMN = intraperitoneal injection of 20 mg of NMN.

#### 3.3.4.5 High fat feeding and NMN treatment have opposite effects on IRS-1 tyrosine phosphorylation in liver

Akt activation in livers of high-fat fed mice was unexpected (Fig. 3.15) as high-fat feeding is thought to cause tissue insulin resistance [201]. The intracellular actions of insulin are initiated by tyrosine phosphorylation of IRS-1 (Shulman 2000). Therefore, to confirm that Akt activation in response to high-fat feeding reflects increased insulin action, protein levels of tyrosine-phosphorylated IRS-1 were compared in livers of high fat fed and control mice, with or without NMN treatment. In contrast to Akt phosphorylation, tyrosine phosphorylation of IRS-1 was decreased by HF feeding (Fig. 3.16). This effect was reversed by NMN administration, with led to increased IRS-1 tyrosine phosphorylation in NMN treated HF fed mouse livers (Fig. 3.16). Levels of IRS-1 tyrosine phosphorylation were similar in NMN-treated control mice and NMN-treated high-fat-fed mice (Fig. 3.16).

Figure 3.16

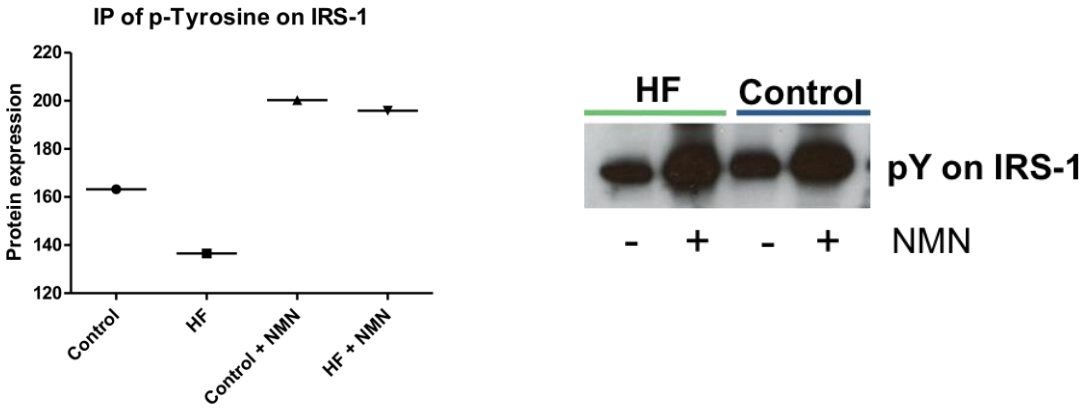


Figure 3.16: Western blot of the eluted phosphorylated tyrosine on IRS1 following an immunoprecipitation assay in control and high fat fed animals (HF), with or without NMN (500 mg/kg body weight) administration as intra-peritoneal injection, at 16 hours prior to tissue sampling. HF = high fat diet for 16 weeks. NMN = intra-peritoneal injection of 500 mg/kg body weight of NMN.

#### 3.3.4.6 Variations in PGC1α and PCK1 gene expression induced by high-fat feeding and NMN treatment

As indicated from decreased IRS-1 tyrosine phosphorylation, mice maintained on HF diet showed a modest decrease in insulin signalling; however, Akt activity was paradoxically increased. It was therefore investigated whether this dietary manipulation caused increases in gene expression of the gluconeogenic genes PCK1 and PGC1a, which would be consistent with decreased insulin sensitivity. Consistent with reduced insulin sensitivity, PGC-1α (Fig. 3.17A) and PCK1 (Fig. 3.17B; ~3-fold, **P*<0.05) mRNA levels were increased in HF fed mice compared to control.

NMN administration increased IRS-1 tyrosine phosphorylation in both control and high-fat fed mice, suggesting enhanced insulin sensitivity. Consistent with an NMN-mediated improvement in hepatic insulin sensitivity, NMN treatment decreased gene expression of PCK1 and PGC1α to control levels. NMN did not afect gene expression of either PGC-1α or PCK in control mice. The patterns of responses of SIRT1, PGC-1α and PEPCK to high-fat feeding and NMN-treatment are strikingly similar.

Figure 3.17

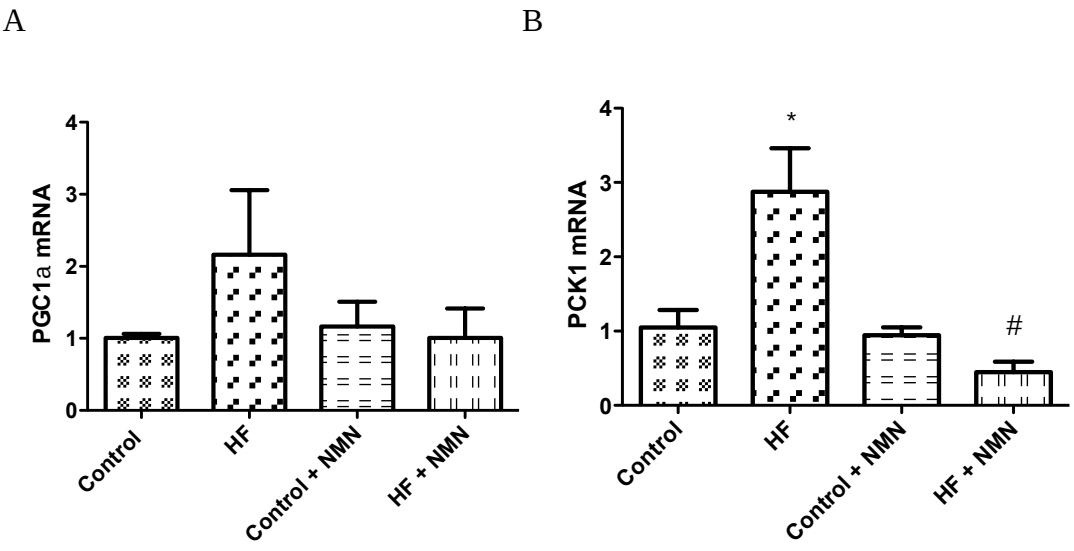


Figure 3.17: Relative expression of PGC-1α (A) and PCK1 (B) vs. 18S gene in control and high fat fed animals (HF), with or without NMN (500 mg/kg body weight) administration as intra-peritoneal injection, at 16 hours prior to tissue sampling. mRNA expression levels of PGC-1α and PCK1 measured using qRT-PCR. Data are means ± SEM, n=4. **P*<0.05 vs. control; #*P*<0.05 vs. control + NMN. HF = High fat diet.

### 3.3.4.7 Variations in phospho-AMPK and phospho-ACC protein expression induced by high-fat feeding and NMN treatment

AMPK and SIRT1 both respond to glucose scarcity with increased activity and both enzymes suppress FA synthesis whilst promoting FA oxidation. High-fat feeding caused concomitant increases in protein expression of phospho-AMPK and phospho-ACC (Fig. 3.18), indicative of increased AMPK activity. Although this is not very clear on the blot, the density analysis of the western blot shows a correlation between the two. NMN-treatment of control mice lowered phspho-AMPK-thr$^{172}$ protein expression (Fig. 3.18). Although this suggests lowered AMPK activity, protein expression of phosphoACC-ser$^{218}$ was too variable between samples to draw a firm conclusion (Fig. 3.18). NMN did not have a significant effect on either phospho-AMPK-thr$^{172}$ or phopsho-ACC-ser$^{218}$ protein expression in livers of HF fed mice.

Figure 3.18

A

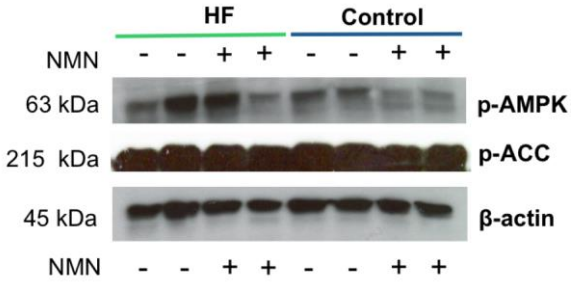


B

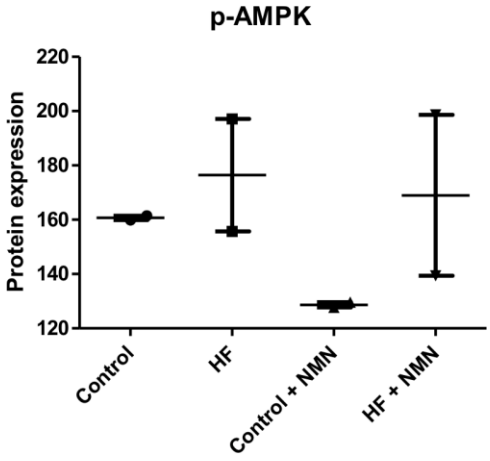


C

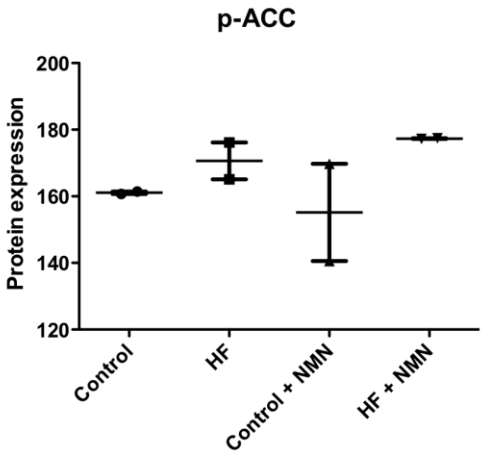

Figure 3.18: Western blot analysis of phospho-AMPK (MW 63 kDa) and phospho-ACC (MW 215 kDa) (A) in control and high fat fed animals (HF), with or without NMN (500 mg/kg body weight) administration as intraperitoneal injection, at 16 hours prior to tissue sampling. B-actin (MW: 45 kDa) was used to verify that the samples were equally loaded; Quantified data of the western blot for p-AMPK (B); Quantified data of the western blot for p-ACC (C). HF = high fat diet for 16 weeks. NMN = intraperitoneal injection of 500 mg/kg body weight of NMN.

## 3.4 Discussion

In the present study, liver specific AMPK$^{-/-}$ mice show decreased SIRT1 gene expression and SIRT1 knockdown cells have lower levels of PGC-1α gene expression and AMPK protein expression, suggesting a feedback loop between SIRT1 and AMPK, where SIRT1 deacetylates and activates AMPK through an upstream kinase of AMPK (perhaps LKB1), leading to AMPK activation; AMPK depletion, on the other hand, inhibits SIRT1 activity in the liver, under normal fed conditions. Gluconeogenesis gene expression could be regulated by the amount of glucose in the media (in addition to SIRT change). Since our H4IIEC3 cells were cultured in a media containing glucose, this could have affected the results about gluconeogenic gene expression. In the future, it would be interesting to study LKB1 acetylation levels together with SIRT1 activity, and NAMPT gene and protein expression in AMPK knockout livers of fasted mice, refed after a 24h period.

We investigated the expression of metabolically important genes encoding key regulators of lipid and glucose oxidation in liver, *in vivo* and *in vitro*. Fasting was employed as a metabolic challenge associated with an increased demand for supply of FA for oxidation. We found that in the liver, there was a fasting-induced reduction in the expression of lipogenic genes targeted by insulin (SREBP-1 and its target, SCD1). XBP-1 gene expression is, however, increased possibly due to decreased activity of SCD-1. Paton & Ntambi found that SCD-1 activity is required for efficient cholesterol esterification to monounsaturated fatty acid (MUFA) and that loss of its activity increases XBP-1-mediated free cholesterol synthesis [202]. XBP-1 induction may also be related to induction of endoplasmic reticulum stress and the activation of unfolded protein response (UPR), which can be induced by fasting [203], and involves XBP1 [204]. SIRT3 and PGC-1α gene expression were up-regulated in liver in response to fasting, which is important for increased fat oxidation under these conditions. The

increased PGC-1α gene expression might be a result of increased SIRT1 gene expression under the same conditions. Expression of SIRT3 in the liver is induced by PGC-1α through a mechanism involving estrogen-related receptor alpha (ERRα) [205]. SIRT3 dependent deacetylation of LCAD promotes β-oxidation [167]. SIRT1-PGC-1α-SIRT3 axis during fasting is important to prevent chronic mitochondrial protein hyperacetylation and reduced LCAD activity [167]. Decreased fatty acid oxidation due to decreased LCAD activity would eventually lead to obesity, insulin resistance and metabolic disorders [106, 206, 207].

Previous studies have shown that NAMPT-mediated $NAD^+$ biosynthesis is compromised by high fat diet and aging, contributing to the pathogenesis of T2DM. The same authors have also provided proof of the concept that promoting NAD+ biosynthesis by administering NMN, a key $NAD^+$ intermediate, can be an effective intervention to treat the pathophysiology of diet- and age-induced T2DM [208]. In our study, high fat diet tended to increase SIRT1 expression, bur the results were not statistically significant. Short term NMN administration did not have a significant effect of high fat feeding in SIRT1 gene expression, although, SIRT1 protein expression seems to be increased in HF fed plus NMN treated animals. Measuring SIRT1 activity with an enzymatic kit would be interesting to understand how SIRT1 activity is affected by diet. The mechansism by which NMN is transported into cells currently remains unknown; metabolic tissues and organs seem to utilize NMN and convert it to $NAD^+$ efficiently [208]. Therefore, an adequate and consistent supply of this key $NAD^+$ intermediate must be critical to maintain normal hepatic insulin sensitivity, in part through increased SIRT1 activity. Interestingly, HF mice, but not controls, lose weight after short term NMN administration. This can be explained either by possible increased lipolysis in HF mice, associated to NMN administration or by starvation as a result of NMN administration. It is possible that animals do not eat as much after the injection of NMN, possibly because NMN affects appetite mechanism for high fat diets. Further investigation is required to explain the loss of weight under these circumstances. To assess beneficial and possible adverse effects of NMN more comprehensively, it would be interesting to measure long-term NMN supplementation experiments in different dietary conditions (i.e. fasting, feeding, high fat feeding). It will be also of great interest to examine whether the effects of NMN

are synergistic with those of small chemical SIRT1 activators (e.g. AROS) [209], particularly in aged, diabetic individuals.

Studies performed *in vitro* have shown that resveratrol inhibited the phosphorylation of IRS1-Ser$^{307}$, which is a marker of insulin resistance [210], indicating that resveratrol (SIRT1 activator) improves insulin signalling [211]. In agreement with this, SIRT1 overexpression increased the phosphorylation of Akt, a downstream target of insulin signalling, in muscle cells and HEK293 cells, whereas the inhibition of SIRT1 induced the opposite response [211]. High fat feeding impairs tyrosine-phosphorylation of IRS-1, which indicates that high fat could impair insulin signalling. In contrast, in the liver, NMN treatment seems to increase IRS-1 tyrosine phosphorylation, perhaps ameliorating insulin-signalling pathway even in high fat fed animals. I suggest that NMN administration increases SIRT1 activity through increased $NAD^+$ and this, in turn, improves insulin signalling through phosphorylation of tyrosine residues in IRS1. This could increase Akt gene expression in response to IRS1 decrease as a compensatory effect, which could explain Akt activation in livers of high-fat fed mice.

AMPK is reported to activate SIRT1 in skeletal muscle by increased NAMPT concentrations or through increased β oxidation [150, 151]. A recent study has shown that a relative deficiency in carbohydrate intake or, albeit less likely, a relative excess of fat intake (in the absence of caloric deprivation) is sufficient to activate the AMPK-SIRT1-PGC1α energy-sensing cellular network in human skeletal muscle [212]. A similar mechanism could happen in the liver of high fat fed animals, where PGC-1α was increased in a significant way and AMPK and SIRT1 tended to be increased. In this chapter, the effect of fasting in increasing SIRT1-PGC1α axis is abrogated by the loss of AMPK. The acetylation levels of PGC-1α are significantly decreased in liver specific AMPK$^{-/-}$ mice, suggesting that AMPK has an effect in SIRT1 mediated PGC-1α acetylation and activation. PGC-1α's activation of gluconeogenic gene expression is dependent upon its acetylation state, which is controlled not only by the deacetylase SIRT1, but also by the acetyltransferase GCN5 [137, 138]. Nevertheless, whether other chromatin modifiers - particularly other sirtuins - can modulate PGC-1α acetylation is currently unknown.

Finally, it seems like SIRT6 is SIRT1 dependent. SIRT6 mRNA expression is decreased under SIRT1 knockdown conditions in H4IIEC3 cells. Since SIRT1 and SIRT6 are both nuclear, is possible that SIRT1 activates SIRT6 through deacetylation or that SIRT1 absence leads to SIRT6 inactivation. Dominy et al [107] have reported that SIRT6 strongly controls PGC-1α acetylation. Surprisingly, SIRT6 induces PGC-1α acetylation, through interaction and modification of GCN5, leading to GCN5 enhanced activity. Decreased acetylation levels of PGC-1α in $AMPK^{-/-}$ mice could be either because AMPK negatively regulates SIRT1 target genes, or because decreased activity of SIRT6 through decreased SIRT1 gene expression could impair PGC-1α acetylation status. Further studies with SIRT1 activity kit would be important to better understand this pathway.

In summary, fasted mice display an oxidative profile (enhanced expression of oxidative genes: PGC-1α, SIRT1 and SIRT3), with decreased plasma glucose and insulin levels, together with decreased expression of the lipogenic genes SREBP1 and SCD-1. High fat feeding impairs tyrosine-phosphorylation of IRS-1, possibly due to decreased SIRT1 activity, which could impair insulin signalling. Mice fed with a high fat diet had no significant changes in their weight gained, which possibly explains the difficulty of achieving statistically significant results to suggest an oxidative or lipogenic profile. It is possible that the diet was less apelative, and if so, HF mice have not had eaten as much as the controls. SIRT1 and AMPK seem to be involved in a reciprocal activation in liver, but further studies need to be done to better understand the link between these proteins.

**Chapter:**

*4. Studies on the roles of the SIRT1-AMPK regulatory axis in skeletal muscle in vivo and using L6 myoblasts*

**The studies described in this chapter have been published on *Life Sciences***: Silvestre MFP, Viollet B, Caton PW, Leclerc J, Sakakibara I, Foretz M, Holness MC, Sugden MC. (2014) The AMPK-SIRT signaling network regulates glucose tolerance under calorie restriction conditions. Life Sci 100(1)55-60.

## 4.1 Introduction

Chapter 3 has shown that, in the liver, AMPK deficiency decreases SIRT1 gene expression, and SIRT1 deficient H4IIEC3 cells have lower levels of PGC-1α gene expression and AMPK protein expression, suggesting a feedback loop between these two proteins (AMPK and SIRT1). In skeletal muscle this interaction remains unclear, but given the function of skeletal muscle as the major site of glucose uptake, this signalling network is potentially of great importance.

Calorie restriction (CR) has been shown to protect against onset age-related diseases [100, 213], in part through improvement of glucose tolerance and insulin signalling, and to reduce mortality linked to T2DM and cardiovascular diseases [214-218]. Of its target tissues, skeletal muscle is the major site of insulin-stimulated glucose disposal [219] and AMPK has important acute metabolic actions in this insulin-responsive tissue, such as LCFA oxidation (lipid-lowering effect), glucose uptake and glucose and glycogen breakdown (glucose-lowering effect) [19, 220, 221]. However, in marked contrast to the effects of AMPK, insulin suppresses fat oxidation and stimulates glycogen, lipid and protein synthesis and may often oppose the actions of AMPK [222, 223]. Interestingly, common actions of AMPK and insulin are also observed, in particular, stimulation of glucose uptake into skeletal muscle [38]. It has been recently established that AMPK acts as the prime initial sensor for fasting-induced adaptations in skeletal muscle and that SIRT1 downstream signalling is blunted in the absence of AMPK [166].

The research described in this chapter aims to understand the mechanisms by which AMPK and SIRT1 may interact to regulate glucose tolerance in skeletal muscle during CR. To clarify whether altered AMPK signalling could be associated with altered skeletal muscle metabolism, particularly with respect to SIRT1 expression or action, we analysed muscle-specific AMPKα1/2 knockout (AMPK $^{-/-}$) using CR and starvation as manipulations to modify glucose tolerance. In addition, L6 cells (skeletal

muscle myoblasts) were employed to determine regulatory interactions between AMPK and SIRT1.

## 4.2 Methods

Female skeletal muscle-specific AMPK$^{-/-}$ or WT mice were maintained on CR (CR-AMPK$^{-/-}$; WT-AMPK$^{-/-}$) or *ad libitum* (AL-AMPK$^{-/-}$; AL-AMPK$^{-/-}$) feeding regimes at Institute Cochin INSERM, Paris, France. Animal studies described in Chapter 2, Section 2.2.2.1 were reviewed and approved (agreement no. 75-886) by the Directeur Départemental des Services Vétérinaires of the Préfecture of Police of Paris. Mice were subjected to calorie restriction (30%) or ad libitum feeding (Chapter 2, section 2.2.2.5.1), and whole body glucose homeostasis and insulin sensitivity were assessed by an oral glucose tolerance test (oral gavage of glucose; 3 mg/kg/body weight) (Chapter 2, section 2.2.2.5.2) and insulin administration (5 minutes before sacrifice; 1 Unit of insulin/kg of body weight) (Chapter 2, section 2.2.2.5.3) respectively, as described in the general methods. Immunohistochemistry was performed as described in Chapter 2, section 2.2.2.5.4.

All the procedures carried on using these samples were performed in accordance with the principles and guidelines established by the European Convention for the Protection of Laboratory Animals.

Culture and treatment of the skeletal myoblast cell line, L6 was performed as described in Chapter 2, section 2.2.1.2. When cells had reached 70 – 80% confluency, they were either kept in the same medium (termed "fed cells") or incubated in either serum-free DMEM (without FCS) or Hank's Balanced Salt Solution (HBSS) with calcium and magnesium, (Appendix IV.) for 3.5 hours (termed "starved cells"). Fed and starved cells were incubated with 1 ml of media containing SIRT1 inhibitor Ex527 (10 □M; Tocris Bioscience, Bristol, UK). After 3 hours, cells were incubated for a further 30 minutes with insulin (100 nM) and/or recombinant mouse globular adiponectin (1 □g/ml; gAcrp30; BioVision, antibodies-online GmbH, Germany). Research has shown that gAcrp30 is more active than Acrp30 in mediating increased activity of AMPK and PPARα [224]. Negative controls consisted of 1ml of media containing an equal concentration of dimethyl sulphoxide (DMSO).

Western blotting (Chapter 2, 2.2.3.2), immunoprecipitation (Chapter 2, 2.2.3.3) and qRT-PCR (Chapter 2, 2.2.3.4) were conducted as described in the general methods section.

All data are expressed as mean ± SEM. Statistical comparisons were carried out using Graphpad Prism and StatView. Statistical differences were evaluated by unpaired t-test, two-way or one-way analysis of variance (ANOVA), followed by a Newman-Keuls, Bonferroni's or Fisher's post-test where appropriate. Statistical differences were accepted as $P<0.05$.

## 4.3 Results

***Studies of effects of AMPK deficiency in vivo using AMPK KO mice***

Here we investigated the role of AMPK in the insulin-sensitizing effect of calorie restriction and in the NAMPT-SIRT1 pathway, in skeletal mixed hindlimb muscle *in vivo*. We used skeletal muscle specific AMPK$^{-/-}$ under *ad libitum* fed (AL) conditions or after CR (30% of the food consumed by AL mice, for 10 weeks), with or without *in vivo* administration of insulin (1 Unit/kg of body weight).

### 4.3.1 Loss of AMPKα1 and -2 subunits decreases AMPK protein expression in skeletal muscle of AL and CR-fed mice

Skeletal muscle AMPK protein levels were undectable in AL- and CR-AMPK$^{-/-}$ mice (Fig. 4.1). Moreover, levels of AMPK activity, denoted by phosphorylation on Thr$^{172}$, were abolished in skeletal muscle of AL- and CR-AMPK$^{-/-}$ mice compared to AL-WT and CR-WT respectively (Fig. 4.1A).

Acetyl CoA Carboxylase (ACC) is a down stream target of AMPK, where by AMPK inhibits ACC activity through phosphorylation on Ser$^{218}$ [225]. Enhanced ACC phosphorylation at Ser$^{218}$ in skeletal muscle of CR-WT is clearly lost in AMPK$^{-/-}$ mice (Fig. 4.1A).

AL-AMPK$^{-/-}$ mice gained similar weight over 10 weeks compared to AL-WT mice and body weight reduction in CR-WT and CR-AMPK$^{-/-}$ was also comparable (Fig. 4.1B).

Taken together, these data demonstrate that these mice are suitable for study of the effects of reduced skeletal muscle AMPK signalling.

Figure 4.1

A

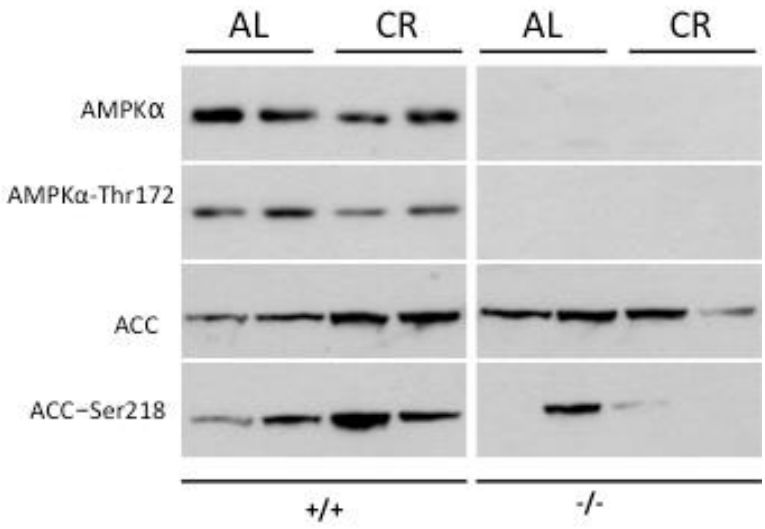


B

| | WT | | AMPK$^{-/-}$ | |
|---|---|---|---|---|
| | AL | CR | AL | CR |
| **Initial weight (g)** | 18.52 ± 2.4 | 21.0 ± 2.3 | 17.33 ± 1.4 | 21.16 ± 2.7 |
| **Final weight (g)** | 22.34 ± 2.9 | 20.25 ± 1.0 | 21.33 ± 1.2 | 20.44 ± 2.6 |
| **Weight gain (g)** | 3.82 ± 1.3 | -0.8 ± 2.3*** ### | 4.0 ± 2.3 | -0.72 ± 0.75*** ### |

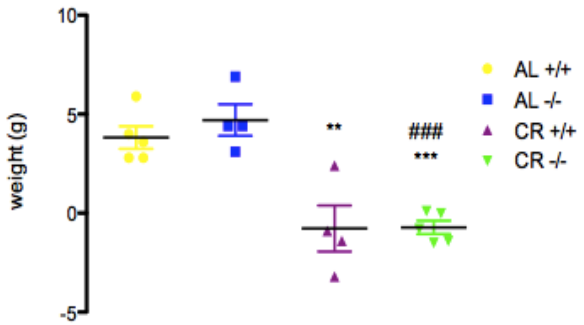

Figure 4.1: (A) Representative western blot of total AMPK and phospho-AMPK-thr172 protein (MW: 63 kDa) and of total ACC and phospho-ACC-ser218 protein (MW: 215 kDa). AL = mice fed ad libitum; CR = calorie restricted mice (30% caloric restriction); -/- = AMPK α1/2 knockout mice; +/+ = WT mice. (B) Weight gained after 10 weeks of AL vs. CR treatment. Data are presented as means ± SE. ***$P$<0.001 vs. AL +/+, ###$P$<0.001 vs. AL -/-, n= 4-5 per group.

### 4.3.2 AMPKα1/2 knockout impairs CR-mediated improvements in all body glucose tolerance

To assess the effects of the experimental diets and AMPK$^{-/-}$ on whole body glucose tolerance we utilized an oral glucose tolerance test (OGTT). There were no significant differences in basal fasting plasma glucose and insulin levels between the four groups (Fig. 4.2A and 4.2C). However, CR-WT mice displayed improved glucose tolerance, where blood glucose levels were significantly lower 20 – 40 minutes post-glucose injection, compared to AL-WT (*$P$<0.05) (Fig. 4.2A and 4.2B). Notably, this effect was lost in CR-AMPK$^{-/-}$ mice, demonstrating that skeletal muscle AMPK is required for mediating the beneficial effects of CR on glucose tolerance. Interestingly, glucose levels peaked at 40 minutes-post glucose injections in CR-AMPK$^{-/-}$, but at 20 minutes post-glucose in AL-AMPK$^{-/-}$ mice, perhaps indicating subtly different mechanisms of action. The early raised blood glucose levels were lost between 60 – 120 minutes, and blood glucose returned to basal levels after 120 minutes in all four groups (Fig. 4.2A). CR-WT mice did not display increased plasma insulin levels after 20 minutes compared to AL-WT and AL-AMPK$^{-/-}$, indicating that the improvements in glucose tolerance relative to these groups were likely mediated by increased peripheral insulin sensitivity, rather than elevated pancreatic insulin secretion (Fig. 4.2C). However, plasma insulin was slightly reduced in CR-AMPK$^{-/-}$ mice compared with the other three groups, suggesting that AMPK deficiency in CR may lead to lower insulin secretion (Fig. 4.2C).

In order to demonstrate that improved glucose tolerance following CR is not a result of a shift in fiber type, we have counted the number of myosin heavy chain I and myosin heavy chain IIA fibers in WT and AMPK$^{-/-}$ soleus and gastrocnemious muscle, under CR conditions. No changes were observed in the number of fibers in gastrocnemius and soleus muscle from CR-WT and CR-AMPK$^{-/-}$ mice. (Fig. 4.2D and 4.2E).

Figure 4.2

A

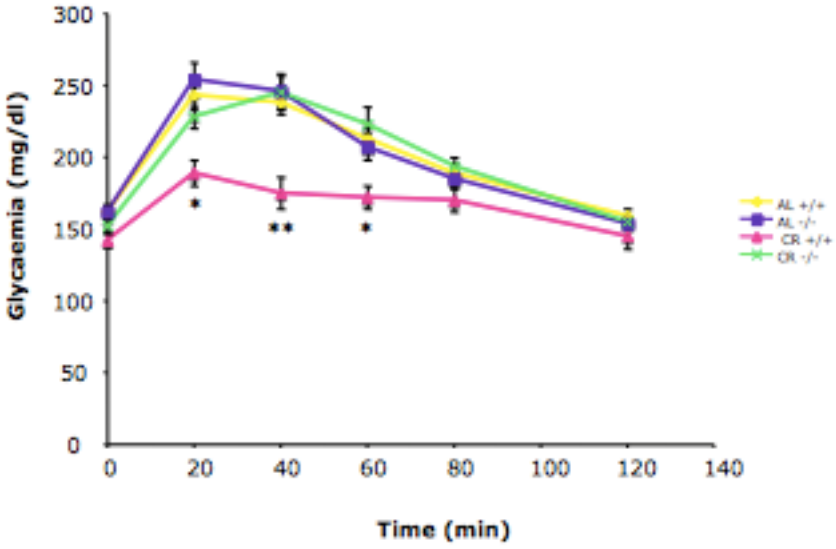


B

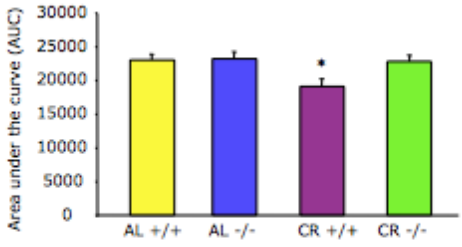


C

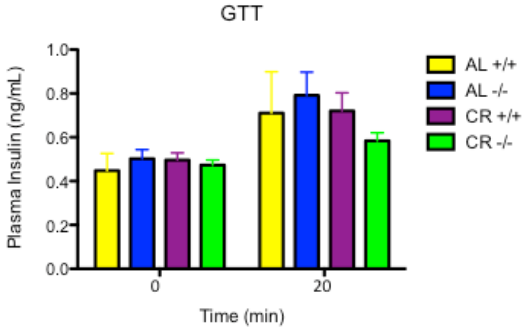


D

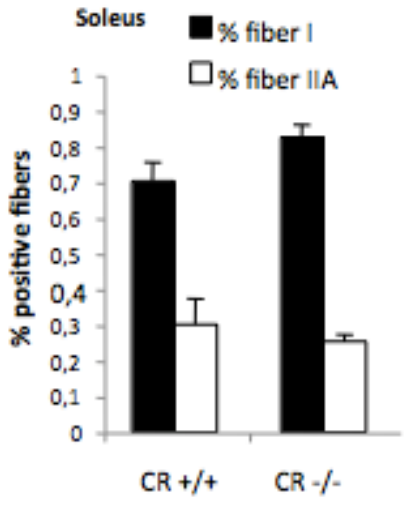


E

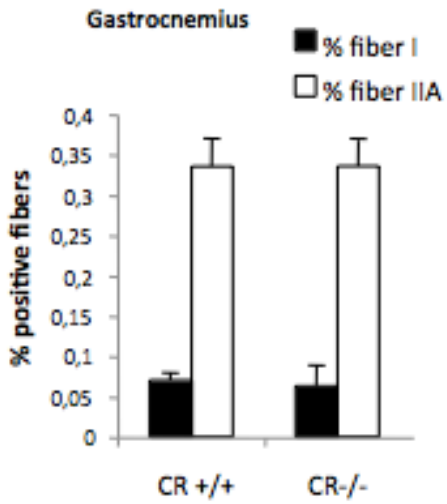

Figure 4.2: (A) Glycaemia after intra-peritoneal administration of glucose (3g/kg of body weight) (B); Area under the curve data (C); plasma glucose and insulin levels measured after 5-hours fasting and 20 min after oral gavage of glucose (3g/kg of body weight). Data are means ± SE (n=17-23); Quantification of immunostaining for MyHC I and MyHC IIA in gastrocnemius (C) and soleus (D) from CR-WT and CR-AMPK-/- mice. Results are presented as mean ± SEM (n = 3); *$P$< 0.05, **$P$<0.01 significantly different from AL-WT. AL = ad libitum fed mice; CR = calorie restricted mice (30% caloric restriction); -/- = AMPK α1/2 knockout mice. +/+ = WT mice.

### 4.3.3 NAMPT gene expression in skeletal muscle is suppressed by AMPK deletion in fed mice, an effect blunted by CR

Several studies have reported that NAMPT plays a protective role against various types of stresses [226]. These effects are thought to occur in part due to the $NAD^+$ biosynthetic activity of NAMPT, which results in activation of $NAD^+$-dependent sirtuin enzymes, particularly SIRT1 [227]. AMPK has been reported to induce NAMPT with consequent raised $NAD^+$ levels and increased SIRT1 activity [150]. We studied NAMPT gene expression in order to better understand the possible link AMPK-NAMPT-SIRT1 in CR. Loss of AMPKα1/2 subunits greatly decreased skeletal-muscle NAMPT mRNA expression in AL mice (~75% vs. AL AMPK $^{+/+}$, **$P$<0.01) (Fig. 4.3). CR also suppressed skeletal-muscle NAMPT gene expression in WT mice (~75% vs. AL AMPK $^{+/+}$, **$P$<0.01). Skeletal-muscle NAMPT gene expression levels were comparable in AL AMPK KO mice, CR WT mice and CR AMPK KO mice (~75% vs. AL AMPK $^{+/+}$, **$P$<0.01). This data shows that deficiency in AMPK and CR separately lower skeletal muscle NAMPT expression, but AMPK deficiency does not lead to further NAMPT mRNA decrease in CR mice (Fig. 4.3).

Figure 4.3

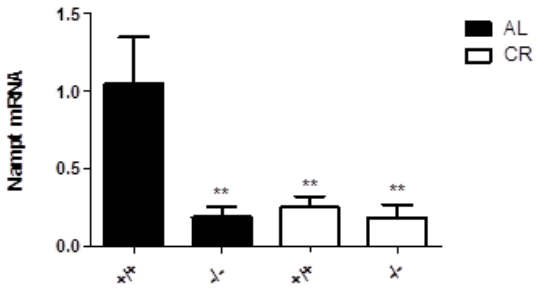

Figure 4.3: qRT-PCR showing NAMPT mRNA expression in CR and AL mice (AMPK$^{-/-}$ and WT) mice vs. 18S gene. Values are represented as mean ± SEM (n=4-6 per group). ***P*<0.01 vs. +/+ AL mice. AL = mice fed ad libitum; CR = calorie restricted mice (30% caloric restriction); -/- = AMPK α1/2 null mice. +/+ = WT mice.

### 4.3.4 SIRT1, SIRT6 and SIRT3 gene expression tend to be suppressed by AMPK deletion in skeletal muscles of AL fed mice

Previous studies have reported that SIRT1 activity is disrupted by AMPK inhibition [193]. To further examine these findings *in vivo*, with the aim of determining the mechanisms responsible for the altered glucose tolerance described above, SIRT1 gene expression was analyzed in skeletal muscle of WT and AMPK$^{-/-}$ mice, fed AL or CR. Loss of AMPK decreased SIRT1 mRNA expression in skeletal muscle of AL fed animals (Fig. 4.4A). However, in contrast, SIRT1 gene expression was unchanged in both CR-WT and CR-AMPK $^{-/-}$ mice (Fig. 4.4A).

A study has shown that in mice, absence of SIRT6 enhances insulin signalling and activation of Akt, leading to hypoglycemia and this is associated with increased membrane association of GLUT1 and GLUT4, which enhances glucose uptake [228]. In our previous studies in H4IIEC3 liver cell line (Chapter 3), we have shown that SIRT6 gene and protein expression is suppressed when SIRT1 is knockdown. In this chapter we measured SIRT6 gene expression to better understand if this dependence is tissue-specific and what are the consequences of this possible interaction to glucose homeostasis. Skeletal-muscle SIRT6 gene expression was moderately suppressed by AMPK deficiency, both in AL-fed mice and CR mice (c.f. SIRT1 gene expression, where the effect of CR is blocked by AMPK deficiency) (Fig. 4.4 B).

CR also induces the expression of SIRT3, particularly in brown adipose tissue (BAT) [113]. However, during CR in mice, cellular $NAD^+$ levels and the $NAD^+$/NADH ratio fluctuate significantly depending on tissue type, suggesting that sirtuins have tissue-specific responses to CR. Nevertheless, it appears that SIRT1 regulates energy metabolism and physical responses to CR, while SIRT3 is able to mediate CR-associated reduction of oxidative damage [109]. In muscle tissue we assessed SIRT3 mRNA. SIRT3 mRNA showed decreased gene expression in CR-AMPK$^{-/-}$ mice when

compared to CR-WT (~80%, ±±±$P$<0.001). AL mice did not exhibit differences in SIRT3 gene expression between WT and AMPK$^{-/-}$ mice (Fig 4.4C).

In summary, CR did not increase sirtuins' gene expression. In AL fed mice, AMPK deficiency caused a modest decrease in SIRT1 and SIRT6, but did not affect SIRT3. Under CR, all sirtuins have decreased gene expression when AMPK is deficient. SIRT6, and in a less extension, SIRT1 have modest decreases, while SIRT3 shows a significant marked decreased mRNA expression.

Figure 4.4

A

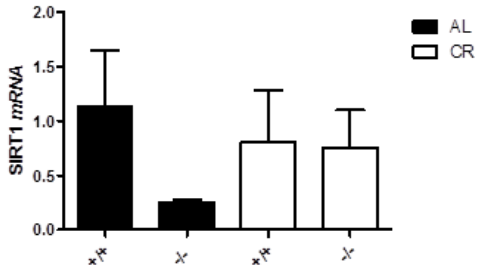


B

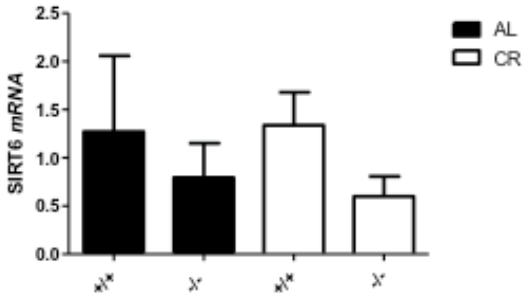


C

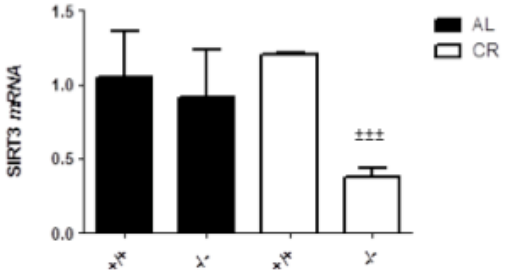


Figure 4.4: qRT-PCR showing A) SIRT1, B) SIRT6 and C) SIRT3 mRNA expression in AL and CR mice (AMPK$^{-/-}$ and WT) vs. 18S gene. Data are presented as mean ± SEM (n=4-6 per group), ±±±$P$<0.01 vs. +/+ CR; AL = mice fed ad libitum; CR = calorie restricted mice (30% caloric restriction); -/- = AMPK α1/2 knockout mice. +/+ = WT mice.

### 4.3.5 PGC- 1α gene and protein expression and acetylation status

In skeletal muscle, PGC-1α target genes for FA oxidation are induced by the deacetylase SIRT1, whilst GNC5 has been reported to acetylate and suppress PGC-1α

activity in skeletal muscle and in liver [139]. PGC-1α controls the transcription of *SIRT3* to activate thermogenesis in brown adipose tissue [229] and to suppress ROS production in the mitochondria [205]. SIRT6 has not been reported to interact with PGC-1α. According with these facts, and because SIRT6 changes were minimal in response to AMPK deficiency and CR, we speculated that PGC-1α gene and protein expression would occur in parallel with changes in SIRT1 and/or SIRT3 expression. Acetylation status was also assessed to verify whether SIRT1-dependent of PGC-1α was disturbed by changes in SIRT1 gene expression. Skeletal-muscle PGC-1α gene expression was similar in AL-WT mice and AL-AMPK$^{-/-}$ mice. It has been reported that gene and protein expression of PGC-1α in mouse skeletal muscle is enhanced by fasting [130] and, in the present experiments, PGC-1α gene expression was substantially increased in CR-WT mice compared with AL-AMPK$^{-/-}$ mice (~3-fold vs. AL-WT, $^{**}P<0.01$). The absence of AMPK led to ablation of CR-mediated increases in PGC-1α gene expression (<75% vs. CR-WT, $\pm\pm P<0.01$) (Fig. 4.5A). The marked increase in PGC-1α gene expression elicited by CR -WT mice was not, however, accompanied by any marked change in PGC-1α protein.

PGC-1α protein is deacetylated by SIRT1, and thus suppression of SIRT1 activity would be predicted to increase PGC-1α protein acetylation. When deacetylated, PGC-1α is activated and acts as a master regulator of mitochondrial biogenesis [151] PGC-1α protein was therefore immunoprecipitated and probed with anti–acetyl-lysine antibody to assess the acetylation level of PGC-1α (Fig. 4.5B). Skeletal-muscle PGC-1α acetylation was modestly (30%) but significantly ($^{*}P<0.05$) increased in AL-AMPK$^{-/-}$ mice compared with AL-WT mice, and substantially (0.5-fold, $^{*}P<0.05$) increased in CR-WT animals compared with AL-WT mice (>0.5-fold vs. AL AMPK $^{+/+}$, $^{*}P<0.05$). The absence of AMPK completely abrogated the CR-dependent increase in PGC-1α protein acetylation (~30% vs. CR –WT, $\pm P<0.05$).

Figure 4.5

A

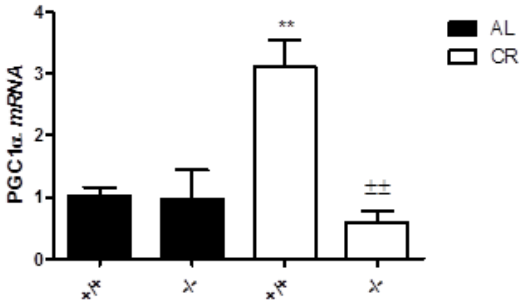


B

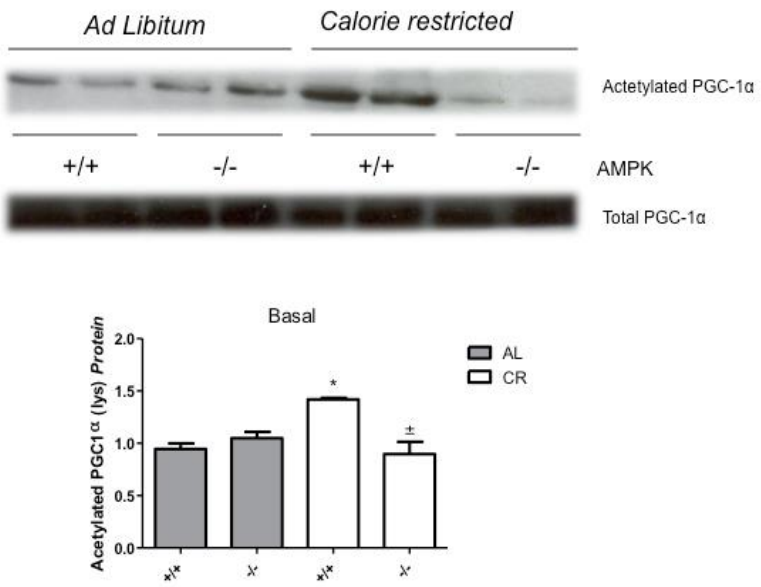


Figure 4.5: A: qRT-PCR analysis showing PGC-1α mRNA expression vs. 18S gene. B: Immunoprecipitation followed by western blotting analysis showing acetylation levels of PGC-1α in lysine residues (MW: 130 kDa), compared to total PGC-1α. Data are presented as mean ± SEM (n=4-6 per group), ***P*<0.01 vs. +/+ AL, ±±*P*<0.01 vs. +/+ CR, *P<0,05 vs. +/+ AL, ±*P*<0.05 vs. +/+ CR. AL = mice fed ad libitum; CR = calorie restricted mice (30% caloric restriction); -/- = AMPK α1/2 null mice.

### 4.3.6 Loss of AMPK α1/2 attenuates insulin-mediated activation of Akt

It has been reported that, in vascular smooth muscle cells, tyrosine (Tyr) phosphorylation of IRS-1 is negatively regulated by serine[794] phosphorylation of IRS-

1 by activated AMPK [230]. We therefore postulated that lack of AMPK might affect Tyr phosphorylation of IRS-1 in skeletal muscle. Thus, we analyzed the Tyr phosphorylation level of skeletal-muscle IRS-1 through immunoprecipitation (Fig. 4.6A). In WT mice, total IRS-1 protein expression in skeletal muscle of AL mice was increased by insulin stimulation, but decreased in CR mice. AMPK deficiency did not exert any major effect on total-IRS-1 protein expression. CR and acute insulin treatment did not exert additive effects on IRS-1 tyrosine phosphorylation (Fig. 4.6A).

AL- and CR-WT mice exhibited remarkable increases in skeletal-muscle Akt $Ser^{473}$ phosphorylation in response to insulin (~2-fold vs. basal, $*P<0.05$; $\pm P<0.05$) (Fig. 4.6B). This demonstrated increased Akt activation since total-Akt protein was unchanged. The response of Akt-$ser^{473}$ phosphorylation to insulin treatment was greatly attenuated in $AMPK^{-/-}$ mice (~63% vs. $AMPK^{+/+}$, $\#P<0.05$), (Fig 4.6B).

Figure 4.6

A

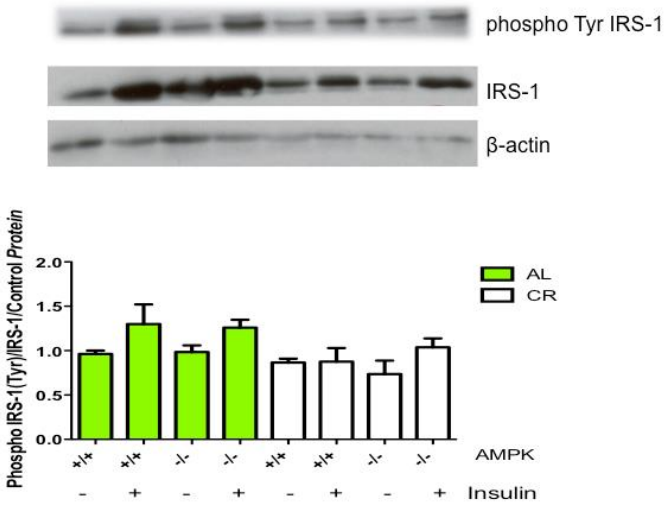

B

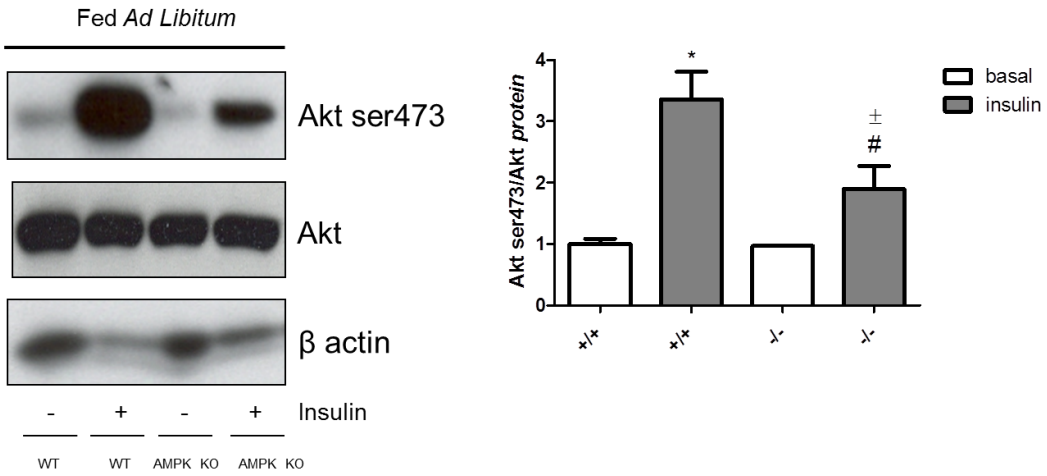


Figure 4.6: A: Immunoprecipitation followed by western blot analysis showing IRS tyrosine phosphosphorylation at tyrosine residues, compared to total IRS-1 protein expression (MW: 180 kDa). B: western blot analysis showing insulin-dependent Akt phosphorylation on ser$^{473}$ in AL animals. β-actin (MW: 45 kDa) was used to verify that the samples were equally loaded. Data shown are presented as mean ± SEM (n=4-6 per group), **P*<0.05 vs. +/+ AL mice, #*P*<0.05 vs. -/- AL mice, ±*P*<0.05 vs. +/+ CR mice. AL = mice fed ad libitum; CR = calorie restricted mice (30% caloric restriction); -/- = AMPK α1/2 null mice. +/+ = WT mice.

***Studies with L6 rat myoblasts***

Cultured L6 myoblasts were used to dissect out inter-relationships between AMPK and SIRT1 in more detail, since direct effects of activators and inhibitors on muscle cells could be identified. Adiponectin and insulin were used in these experiments as activators of AMPK and insulin signalling (including Akt phosphorylation), respectively. The SIRT1 inhibitor Ex527 was added to inhibit SIRT1 activity.

### 4.3.7 Serum starvation augments phospho-AMPK protein expression but suppresses Akt phosphorylation in L6 myoblasts

Preliminary experiments indicated that AMPK-Thr$^{172}$ phosphorylation status in L6 myoblasts was greatly influenced by the incubation medium selected. As shown in Fig. 4.7A, serum starvation, which mimics starvation/CR *in vivo* regarding AMPK activation, markedly increased phospho-AMPK-Thr$^{172}$ protein expression, without affecting total AMPK expression, indicative of AMPK activation.

In marked contrast, serum starvation greatly suppressed Akt-Ser$^{473}$ phosphorylation (Fig. 4.7A), an effect reversed by the addition of insulin (Fig 4.7B). Thus, AMPK activation by serum starvation correlates with decreased insulin signalling.

Figure 4.7

A

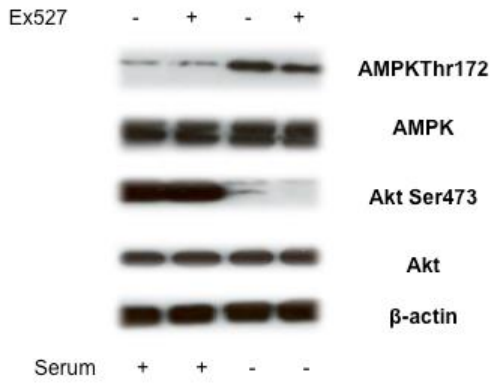


B

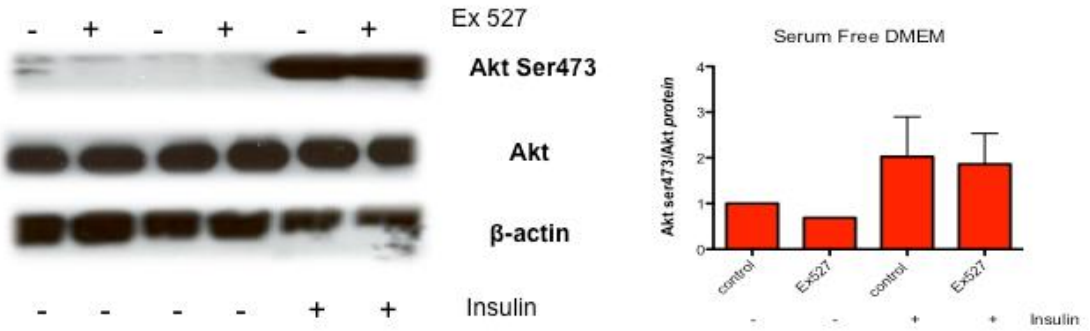


Figure 4.7: A: Western blot showing increased expression of total-AMPK and phospho-AMPK-Thr$^{172}$ (MW: 63 kDa), total Akt and phospho-Akt-ser$^{473}$ (MW: 56 kDa) in in serum starved (3.5 h) samples. β-actin (MW: 45 KDa) was used to verify that the samples were equally loaded. B: western blot analysis on serum starved L6 myoblasts, showing that insulin (100 nM) for 30 min markedly reverses the effect of serum starvation on Akt phosphorylation on Ser$^{473}$.

### 4.3.8 SIRT1 inhibition downregulates AMPK in starved L6 myoblasts

In Chapter 3, I have shown the suppressor effect of SIRT1 knockdown in AMPK protein expression in H4IIEC3 liver cell line. Ex527 is known to inhibit SIRT1 gene

expression in different cell types [231, 232]. qRT-PCR indicated significant mRNA expression of SIRT1 in starved L6 myoblasts, which was completely suppressed by the addition of the SIRT1 inhibitor Ex527 (~100% vs. control, ***P*<0.01; Fig.4.8A). The impact of SIRT1 inhibition on AMPK expression and activity was analyzed. Although AMPK total protein was unaffected by this manoevre, cells cultured in HBSS demonstrated significant down regulation of phosphor-AMPK-Thr$^{172}$ protein expression (~0.5-fold vs. control, **P*<0.05) suggesting that SIRT1 activity correlated positively with AMPK activation by phosphorylation, contrasting with the inverse relationship between AMPK activation and Akt activation (Fig. 4.8B). A similar result was obtained in serum-starved cells (Fig.4.8C) (Fig. 4.8B).

Figure 4.8

A

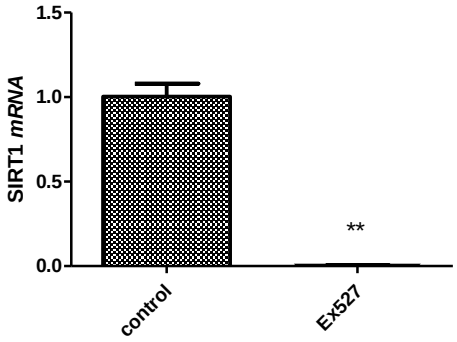

B C

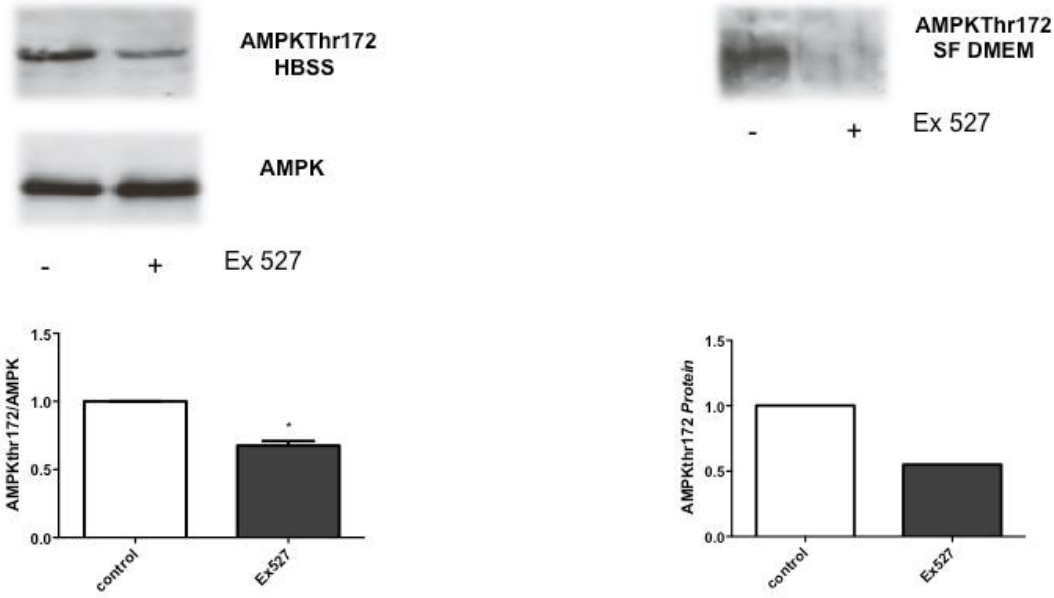


Figure 4.8: A: Changes in L6 SIRT1 mRNA level after culture with SIRT1 inhibitor, Ex527 (20 mg/ml of media), for 3.5 h. B and C: representative western blot of total AMPK and phospho-AMPK at Thr$^{172}$ (MW: 63 kDa) changes in cells cultured with Ex527 (20 mg/ml of media) for 3.5h comparing to control cells [cells cultured in HBSS (serum-free, 1mM glucose) for 3.5h] (B) or comparing to control cells [cultured in serum-free DMEM (serum-free, 25 mM glucose) for 3.5h (C). Total AMPK did not change between inhibit cells or control cells [cells cultured in HBSS (serum-free, 1mM glucose) for 3,5h (B). Blots were repeated 3 times with qualitatively similar results. β-actin (MW: 45 kDa) was used to verify that the samples were equally loaded. Data are means ± SE, **P*<0.05 vs. control.

### 4.3.9 Effect of adiponectin on phosphoAMPK-Thr$^{172}$ protein expression in serum-starved L6 myoblasts

It has been reported that adiponectin can activate AMPK [233, 234] and can regulate PGC-1α activity through AMPK/SIRT1 [152]. We therefore investigated whether adiponectin-dependent AMPK activation (indicated by phosphorylation of AMPK on Thr$^{172}$) is also affected by SIRT1 inhibition by Ex527. Adiponectin did not affect total AMPK protein expression but an effect of adiponectin to increase phosphorylation of AMPK at Thr$^{172}$ in L6 myoblasts was evident in the absence of serum. In the absence of adiponectin, the SIRT1 inhibitor Ex527 decreased AMPK at Thr$^{172}$ phosphorylation. In contrast, adiponectin-dependent phosphorylation of AMPK in serum- starved L6 myoblasts was little affected by SIRT1 inhibition by Ex527 (Fig.

4.9A). As discussed earlier, ACC is phosphorylated on Ser$^{218}$ by active AMPK [225] and so it was anticipated that increased phosphorylation of AMPK-Thr$^{172}$ would be accompanied by increased ACC2-Ser$^{218}$ phosphorylation. However, this was not found to be the case. Neither ACC-Ser$^{218}$ phosphorylation nor total-ACC protein expression was affected by adiponectin or Ex527, under conditions where AMPK-Thr$^{172}$ phosphorylation was marginally increased (Fig. 4.9B).

Figure 4.9

A

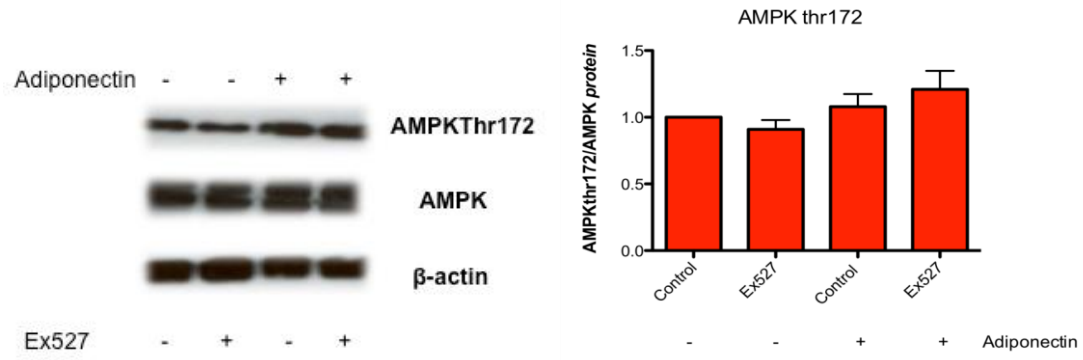


B

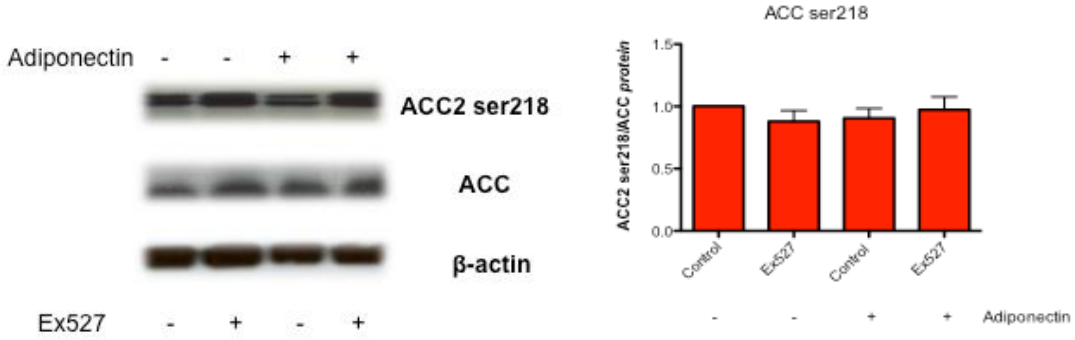


Figure 4.9: A) Representative western blot of the effect of adiponectin (1μg/μl for 30 min) and SIRT1 activator Ex527 (20mg/ml media for 3,5h) treatment under serum-free conditions in total AMPK and phospho-AMPK-thr172 (MW: 63 kDa); B) Western blot analysis showing the effect of SIRT1 inhibitor Ex527 (20 mg/ml of media for 3,5h) in ACC phosphorylation at ser$^{218}$ protein expression and total ACC protein expression (MW: 215 kDa) in serum starved cells for 3,5h treated or not with adiponectin (1μg/μl for 30 min). β-actin (MW: 45 KDa) was used to verify that the samples were equally loaded.

### 4.3.10 Effect of insulin and adiponectin combined treatment on AMPK thr$^{172}$ phosphorylation in L6 myoblasts

Insulin and AMPK have opposite effects on adipogenesis and adipocyte glucose uptake, although, effects of AMPK activation to suppress adipogenesis and adipocyte glucose uptake are beneficial in metabolic diseases (such as T2DM) associated with obesity since they attenuate expansion of the adipose tissue mass and the development of obesity [19]. A further series of studies, shown in Fig. 4.10A, investigated effects of adiponectin and insulin in combination on AMPK activity. Adiponectin and insulin added together tended to increase AMPK phosphorylation (Fig. 4.10).

Figure 4.10

A

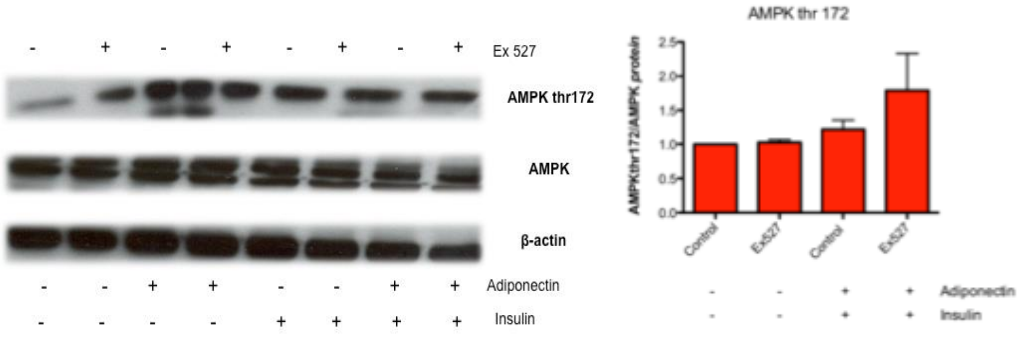


Figure 4.10: Western blot analysis showing the effect of insulin and adiponectin combined treatments on AMPK (MW: 63 kDa) phosphorylation at thr$^{172}$. Adiponectin = 1 μg/μl for 30 min in serum starved cells (3,5h of serum starvation); insulin = 100 nM treatment for 30 minutes in serum starved cells (3,5h of serum starvation). Ex527 treatment = 20 mg/ml of media for 3,5h. β-actin (MW: 45 kDa) was used to verify that the samples were equally loaded.

## 4.4 Discussion

CR-mediated improvement in whole body glucose tolerance is partly dependent on skeletal muscle AMPK activity. WT mice fed a CR diet displayed improved glucose tolerance, whilst this effect was ablated in the absence of skeletal muscle AMPK. These effects did not reflect differential effects in weight gain, since CR induced a significant body weight loss in WT and AMPK$^{-/-}$ mice.

The insulin sensitising effects of CR were reduced in AMPK$^{-/-}$ mice, suggesting that those effects are dependent in part on AMPK α1/2. AMPK phosphorylates and activates the insulin receptor, providing a direct link between AMPK and the insulin-signalling pathway. Moreover, given the known interaction between AMPK and mTORC-S6K1, these data suggest that a disrupted inactivation of mTORC-S6K1 signalling pathway contributes to the impaired insulin sensitizing effects of CR in AMPK$^{-/-}$ mice [235]. This pathway promotes energy conservation and survival of muscle exposed to severe glucose deprivation [236]. The ablation of CR-mediated insulin sensitization observed in AMPK$^{-/-}$ mice resulted in a consequent impairment in glucose tolerance. Studies have shown that acute inhibition of mTORC-S6K1 pathway, in cultured adipocytes, induces glucose uptake [237]. In our studies, is possible that AMPK$^{-/-}$-mediated activation of mTORC-S6K1 suppresses glucose uptake in CR muscle. AMPK-induced improvements in skeletal muscle insulin signalling result in increased blood glucose uptake into skeletal muscle [238, 239]. In addition, AMPK activity also promotes skeletal muscle glycogen synthesis capacity by increased glycogen synthase activity [221, 240], thus lowering blood glucose levels. Therefore, impaired glucose tolerance in CR-AMPK$^{-/-}$ mice likely occurs via both impaired glucose uptake and reduced glycogen storage in skeletal muscle, which are in turn mediated by impaired insulin signaling at the receptor level.

In addition to decreased skeletal muscle glucose tolerance, we also observed reduced serum insulin levels 20 minutes-post OGTT glucose infusion in CR-AMPK$^{-/-}$ mice. This suggests that first-phase glucose-stimulated insulin secretion (GSIS) from pancreatic β-cells is partially suppressed when AMPK is absent from skeletal muscle. Therefore, these data highlight the intriguing possibility for a mechanism by which crosstalk between insulin-sensitive tissues and pancreatic islets might occur. In particular myokines produced by an AMPK-dependent process may be important for regulation of β-cell insulin secretion in response to CR. This opens very interesting therapeutic perspectives. To date, only a few myokines, which are released from skeletal muscle and influence function of other tissues, have been identified [241]. Further studies on β-cells of muscle specific AMPK$^{-/-}$ mice must be done to better understand this pathway.

A key role for the enzyme NAMPT in protecting the body against age-induced T2D has been demonstrated [208]. NAMPT has also been reported as an important regulator of pancreatic insulin secretion and glucose homeostasis [130, 179]. In this study we demonstrated that the AMPK deficiency and inactivation in skeletal muscle is associated with changes in NAMPT expression and SIRT1 activity (as evidenced by PGC-1α deacetylation). Moreover, we also show that SIRT1 activity seems to be decreased when AMPK is lacking, which suggest that SIRT1 and AMPK may be linked, possibly through AMPK-mediated NAMPT expression. These findings are largely in agreement with other studies [150, 151], that have described links between skeletal muscle AMPK-SIRT1. Fulco et al. (2008) described a pathway where AMPK activates SIRT1 through increased NAMPT activity. They have used glucose restricted skeletal myoblasts with AMPK activation [150]. Canto et al (2009) also report a link between muscle AMPK and SIRT1, using the AMPK activator AICAR. However this study found no role for NAMPT in mediating this link [151]. According with this study, AMPK increases $NAD^+$/NADH ratio through increased mitochondrial β oxidation. In our studies, decreased AMPK activity in CR fed mice was also related to decreased PGC-1α and decreased SIRT3 gene expression, suggesting reduced mitochondrial β oxidation. According with this, both NAMPT and β oxidation could play a role in AMPK-depenent SIRT1 activation. The decrease of SIRT1 mRNA expression in skeletal muscle of AL-fed $AMPK^{-/-}$ mice was no longer observed when mice were subjected to CR, suggesting that caloric restriction plays an important role in protecting skeletal muscle from the effects of decreased SIRT1 expression (impaired insulin signalling and impaired glucose uptake), probably caused by a lack of AMPK [141]. The compromised SIRT1 activity in $AMPK^{-/-}$ mice abolished the SIRT1 dependent deacetylation of PGC-1α in AL fed mice. This down regulation of PGC-1α activity compromises its function on glucose and lipid metabolism [242]. Decreased PGC-1α gene expression possibly the reason by which AMPK deficiency decreases glucose uptake. The mechanism by which reduced PGC-1α leads to glucose uptake remains unknown. We suggest a mechanism based on a study from Michael et al. 2001, where PGC-1 mediates the increase in GLUT4 expression, in large part, by binding to and coactivating the muscle-selective transcription factor MEF2C [243]. According with this, decreased PGC-1α gene expression would lead to decreased GLUT4 expression and decreased glucose uptake. The fact that SIRT1 gene

expression did not change in CR conditions between WT and AMPK$^{-/-}$ is interesting, since previous studies have reported that CR leads to increased SIRT1 protein and gene expression [110]. However, our findings are consistent with some previous reports, where SIRT1 gene and protein expression have been reported to be unaffected by CR in skeletal muscle and adipose tissue [126].

Our study showed that a reduced activity of SIRT1 in AMPK$^{-/-}$ mice decreases SIRT6 protein and gene expression, suggesting that SIRT6 activity is positively regulated by SIRT1. Xiao et al. found that 60% of SIRT6$^{-/-}$ animals had very low levels of blood glucose and died shortly after weaning. Feeding the mice with glucose-containing water increased blood glucose and rescued 83% of mutant mice, suggesting that the hypoglycemia is a major cause for the lethality. They showed that SIRT6 deficiency results in more abundant membrane association of GLUT1 and GLUT4, which enhances glucose uptake. The authors further demonstrated that SIRT6 negatively regulates Akt phosphorylation at Ser$^{473}$ and Thr$^{308}$ through inhibition of multiple upstream molecules, including insulin receptor, IRS1, and IRS2. The absence of SIRT6, consequently, enhances insulin signalling and activation of Akt, leading to hypoglycemia. These data uncover an essential role of SIRT6 in modulating glucose metabolism through mediating insulin sensitivity [228]. Controversially, in our experiments, we found that reduced SIRT6 possibly due to reduced AMPK-mediated SIRT1 expression was associated with non-significant enhanced glucose plasma levels upon CR.

Changes in SIRT3 correlate with changes in PGC-1α. Expression of SIRT3 in the liver is induced by PGC-1α through a mechanism involving estrogen-related receptor alpha (ERRα) [205]. We have previously seen (Chapter 3) that SIRT1-PGC-1α-SIRT3 axis during fasting is important to prevent chronic mitochondrial protein hyperacetylation and reduced LCAD activity. Decreased fatty acid oxidation due to decreased LCAD activity would eventually lead to obesity, insulin resistance and metabolic disorders [106, 206, 207]. Is possible that a similar mechanism exists in skeletal muscle, where the SIRT1-PGC-1α-SIRT3 axis maintains mitochondrial β oxidation during CR to protect the body from metabolic disorders. Interestingly, SIRT3 and PGC-1α have also been reported to play an important role in aging. Joseph et al. (2012) have shown that levels of SIRT3 and PGC-1α were significantly reduced

(50%) in two groups of elderly participants (high- and low-functioning based on the Short Physical Performance Battery test) when compared to young [244]. Jing et al (2011) have shown decreased insulin-stimulated IRS-1 phosphorylation in SIRT3$^{-/-}$ mice, which was paralleled by a reduction in insulin-stimulated Akt and Erk phosphorylation. This impaired insulin signalling in skeletal muscle was reflected at the whole-body level through GTT, with significantly higher glucose levels in the SIRT3$^{-/-}$ mice at 60 min [169]. Taken together, these data indicate that SIRT3$^{-/-}$ mice display impaired insulin action and a lower rate of oxygen consumption with increased oxidative stress in skeletal muscle. Interestingly, in our studies, decreased SIRT3 expression correlates with higher glycaemia at 40 in CR-AMPK$^{-/-}$ mice, suggesting impaired insulin signalling under these circumstances.

*Investigation of the effects of AMPK activation by adiponectin in L6 myoblasts*

It is known already that AMPK responds to a requirement to increase cellular ATP production and/or to conserve available ATP [159], leading to an early cell cycle arrest [245]. It has been reported that the polyphenol resveratrol arrests cell cycling through AMPK activation and promotes apoptosis through inhibition of Akt signalling pathways [245]. According with the results obtained in L6 myoblasts, we speculate that starvation or depletion of essential proteins can cause a fast depletion of ATP and this effect is counter balanced by an increased phosphorylation of AMPK on Thr$^{172}$, in order to conserve the ATP available. In this context, Akt is modestly inhibited to reduce gene expression and proliferation and to promote cell arrest, protecting the cells against starvation. This effect is reversed by insulin, which is an anabolic protein.

SIRT1 inhibition down regulates AMPK activity in L6 myoblasts, which led us to hypothesise that a possible feedback loop might exist between these two proteins, where AMPK regulates SIRT1 activity through NAMPT concentrations and, on the other hand, SIRT1 regulates AMPK possibly through LKB1 deacetylation [66]. Further studies on LKB1 acetylation levels need to be done, to fully characterise this pathway.

Adiponectin is an anti-diabetic and anti-atherogenic adipokine and plasma adiponectin levels are decreased in obesity, insulin resistance and T2DM [246]. Adiponectin-dependent AMPK phosphorylation is not affected by the SIRT1 inhibitor Ex527. However, when adiponectin is not present, SIRT1 inhibition causes a modest reduction of AMPK phosphorylation on $thr^{172}$. It is possible that adiponectin abrogates the link between SIRT1 and AMPK, previously discussed in this chapter.

In summary, AMPK deficiency impairs the beneficial effects of CR on skeletal muscle glucose tolerance. This may occur through loss of direct AMPK effects on the insulin signaling machinery. Alternatively, downstream effects of AMPK deficiency are also likely to involved decreased activation and expression of NAMPT and the sirtuin enzymes, particularly SIRT1, but also SIRT3 and SIRT6 impairement, of which all lead to reduced insulin signalling, culminating in lower glucose uptake. In addition, decreased AMPK in skeletal muscle might lead to impaired glucose-induced insulin secretion (GIIS) signalling in pancreatic β-cells, reducing blood insulin content observed during GTT. This may occur through changes in AMPK-mediated myokine signalling, or as a result of increased glucolipotoxicity, occurring as a result of lower AMPK-mediated glucose uptake in skeletal muscle. AMPK and SIRT1 seem to be involved in a feedback loop that maintain fatty acid oxidation in a perfect level to protect muscle from the metabolic disorders during CR/fasting conditions. It is possible that adiponectin abrogates the link between SIRT1 and AMPK, activating AMPK ability to inhibit ACC and, as a consequence, allowing fatty acid oxidation and protecting the cells from the excessive anabolic signalling, caused by insulin, in fasting/CR conditions. Increased fatty oxidation would increase $NAD^+$/NADH, leading to increased SIRT1 gene expression. Further studies on LKB1 acetylation levels and $NAD^+$/NADH ratio must be done to better understand the feedback loop between SIRT1 and AMPK.

**Chapter:**

5. *A key role for interferon regulatory factors in mediating early life metabolic defects in male offspring of maternal protein restricted rats*

**The studies described in this chaper were accepted for publication on *Hormone and Metabolic Rsearch*:** Silvestre MFP, Kieswich J, Yaqoob MM, Holness MJ, Sugden MC, Caton PW. (2014) A key role for interferon regulatory factors in mediating early life metabolic defects in male offspring of maternal protein restricted rats (2014). Horm Metab Res 46(4):252-8.

## 5.1 Introduction

An adverse intra-uterine environment has also been implicated as a potential trigger for development of obesity in later life [247-249]. Examples of poor maternal nutrition include maternal consumption of diets high in saturated fat or a diet low in protein [247, 250]. Maternal consumption of a low protein (Maternal Low Protein; MLP) diet results in offspring with a low birth weight in humans and animal models [250]. Moreover, there exists a strong positive correlation between low birth-weight and the development in later life of obesity, insulin resistance and type 2 diabetes [251]. Epidemiological and experimental evidence suggests that an imbalance between prenatal (e.g. maternal protein restriction) and post-natal (e.g. excess dietary carbohydrate) nutrition can predispose to development of obesity [247]. In agreement, children exposed to growth-restricted conditions during development exhibit increased adiposity in childhood and later life [252], whilst the offspring of rats fed a low-protein diet display a greater predisposition to develop obesity and related metabolic disorders in response to high-fat feeding compared to controls [247, 251]. This phenomenon, termed the 'thrifty phenotype', suggests that fetal malnutrition may lead to physiological changes that programme the fetus for survival in what it predicts to be a poor nutritional environment. This evolutionary programming is less advantageous when food is abundant, potentially predisposing to obesity [251]. However, the underlying mechanisms responsible for this programming of obesity have yet to be described.

Recent studies have identified the immunoregulatory proteins, interferon regulatory factors 3 and 4 (IRF3 and IRF4) as key regulators of adipocyte function [253, 254]. IRF4 increases during adipocyte differentiation and functions to repress adipogenesis and lipogenesis and induce lipolysis in white adipose tissue. IRF4 expression is repressed by insulin, and consequently IRF4 levels are reduced in insulin resistant

mouse models, as well as being elevated during fasting and reduced during re-feeding. Adipocytes lacking IRF4 display increased expression of lipogenic genes including fatty acid synthase (FAS; gene code: *Fasn*) and sterol regulatory-element binding-protein 1 (SREBP1). Moreover, IRF4 knockout mice have larger adipocytes, are obese and develop T2DM. Less is known about the regulation of IRF3 [253, 254].

To further examine the early life mechanistic changes following exposure to an adverse intra-uterine environment responsible for onset of obesity and metabolic syndrome in later-life, we examined the role of IRF3 and IRF4 in the MLP model of fetal programming. Further to this, we investigated novel mechanisms involved in regulation of IRF3 and IRF4 in adipocytes and white adipose tissue.

## 5.2 Methods

We obtained visceral adipose tissue from the following *in vivo* models; (a) PPARα null mice, (b) offspring of rats fed a maternal-low protein diet (MLP rats), and (c) control mice administered metformin (these models are described in detail in the general methods; Chapter 2, sections 2.2.2.3, 2.2.2.4 and 2.2.2.2 respectively; metformin administration described in Chapter 2, section 2.2.2.5.9)

All the procedures carried on using these samples were performed in accordance with the principles and guidelines established by the European Convention for the Protection of Laboratory Animals (Scientific Procedures) Act 1986, published by HMSO, London.

Culture, treatment and transfection of the adipocyte cell line, 3T3-L1 (Chapter 2, section 2.2.1.3), western blotting (Chapter 2, section 2.2.3.2), qRT-PCR (Chapter 2, section 2.2.3.4) and plasma analysis (Chapter 2, section 2.2.2.8) were conducted as described in the general methods section.

Results are expressed as mean ± SEM. Statistical comparisons were obtained using GraphPad (GraphPad Software, CA, USA). Statistical differences were calculated using an unpaired t-test.

## 5.3 Results

### 5.3.1 Metabolic data for MLP offspring

Pregnant dams fed a low-protein diet did not exhibit any differences in food intake compared to controls (data not shown). Despite this MLP offspring weighed significantly less at 3 days of age than control litter mates (28%; $P<0.05$). After 8-weeks consumption of standard rodent diet, MLP offspring displayed no changes in fasting insulin (16.0 ± 3.2 □U/ml) compared to controls (14.4 ± 1.3 □U/ml). Additionally, no changes in fasting plasma glucose levels were found in MLP offspring (4.36 ± 0.13 mmol/l) compared to control (4.11 ± 0.21 mmol/l), whilst glucose area under the curve (AUC) analysis for glucose tolerance tests resulted in non significant increased AUC values for MLP (9.76 ± 1.29 mmol/L/min) compared to control (7.45 ± 0.79 mmol/L/min) (Fig. 5.1).

Figure 5.1

| | **CON** | **MLP** | ***P* value** |
|---|---|---|---|
| Fasting Glucose (mM) | 4.11 ± 0.13 | 4.36 ± 0.21 | 0.33 |
| Fasting Insulin (μU/ml) | 14.4 ± 1.3 | 16 ± 3.21 | 0.65 |
| Glucose – AUC (mmol/L/min) | 7.54 ± 0.79 | 9.76 ± 1.29 | 0.16 |

Figure 5.1: Table showing serum insulin and glucose changes between control and MLP rats fed a standard rodent diet during 8 weeks. Values are Mean ± SEM, n = 8.

### 5.3.2 MLP offspring display altered adipogenic and lipogenic gene expression

Whilst no significant changes in metabolic data were observed at this early stage in the MLP rats, it is possible that mechanistic changes may occur during this early-life period, which would predispose to later development of metabolic disease. Therefore, by focussing on altered lipogenesis and adipogenesis in white adipose tissue, we next attempted to identify early-life metabolic changes which would likely lead to onset of the established later-life metabolic defects induced by MLP. IRF3 and IRF4 are

recently identified repressors of adipogenesis and lipogenesis [253, 254]. Gene expression of IRF3 and IRF4 was markedly reduced in white adipose tissue of MLP rats compared to controls (Fig. 5.2A and 5.2B). These changes occurred in parallel with increased mRNA expression of SREBP1c, elevated mRNA and protein levels of FASN as well as increased ACC protein (Fig. 5.2C, 5.2D and 5.2E), consistent with a role for IRF4 in repressing transcription of these genes. This data implies that early life changes in IRF3 and IRF4 occur in MLP rats and may contribute to increased risk of development of obesity and metabolic syndrome in later life.

Figure 5.2

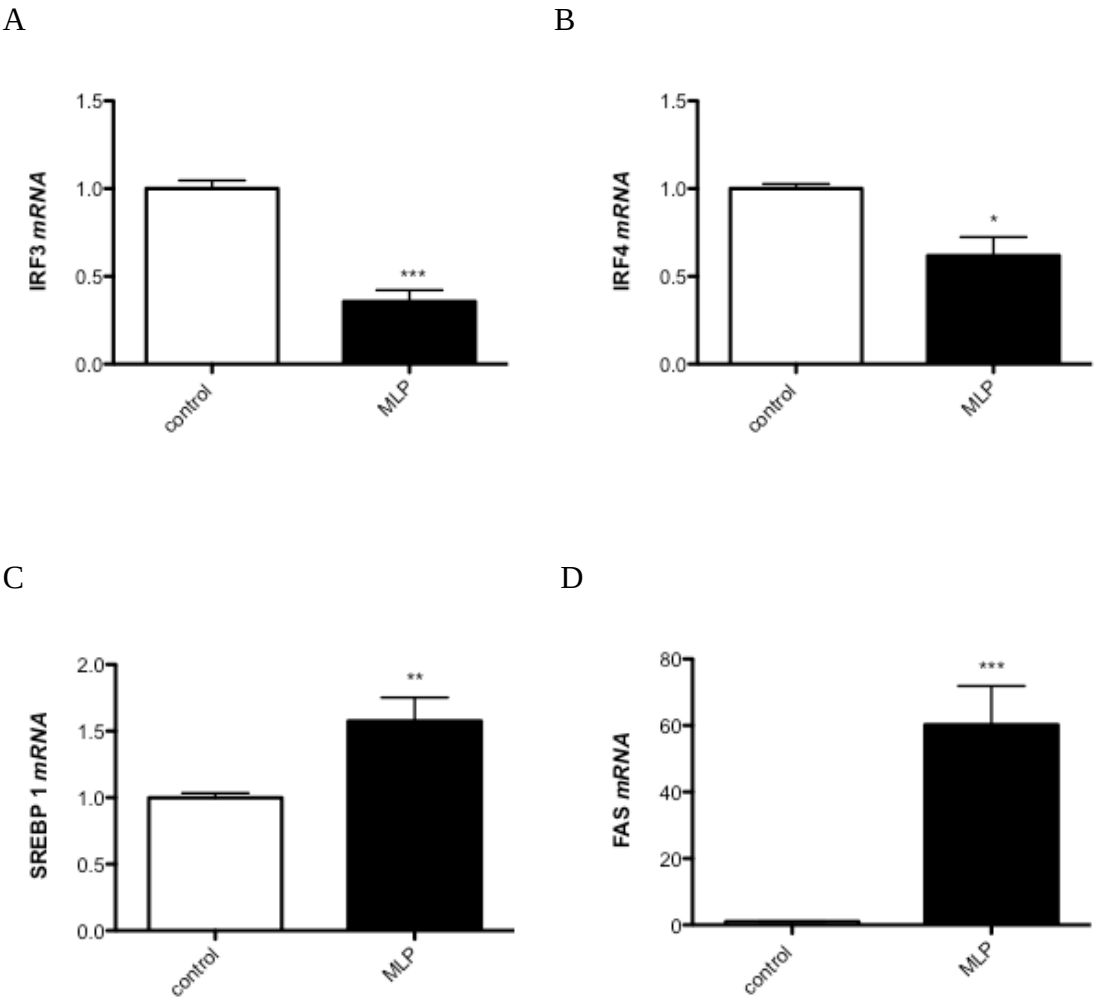

E

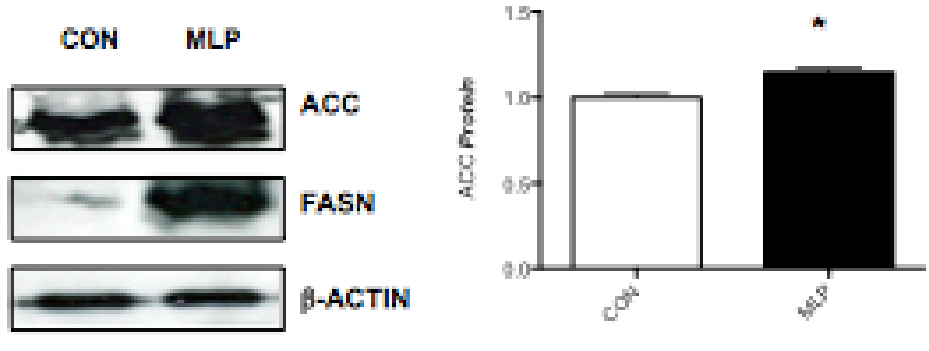


Figure 5.2: Reduced IRF levels in white adipose tissue of MLP offspring. Visceral WAT was isolated from 8-week old offspring of MLP and control Wistar rats (n = 6). Gene expression of (A) *Irf3*, (B) *Irf4*, (C) *Srebp1c* and (D) *Fasn*. (E) Protein levels of FASN and ACC. Western blots are representative. Data are expressed as mean ± SEM. * $P < 0.05$, ** $P < 0.01$, *** $P < 0.001$ vs. control. MLP = Maternal low protein diet (8% low-protein vs. 20% control diet during pregnancy and lactation); Offspring were maintained on standard diet after weaning (3 weeks) and then killed at 8 weeks.

### 5.3.3 IRF3 and IRF4 supression is associated with adiponectin signaling

Previous studies have demonstrated that insulin exerts regulatory control of IRF4, whilst less is known about IRF3 regulation in the context of obesity and metabolic syndrome. Insulin was reported to repress IRF4 expression *in vitro* in adipocytes and *in vivo* under fed conditions, and in obese, hyperinsulinaemic rodent models [253]. However, despite marked reductions in IRF3 and IRF4 expression, we did not observe significant changes in serum insulin levels in our models (Fig. 5.1A). This suggested the existence of an alternative regulatory mechanism controlling IRF4, and potentially IRF3, in white adipose tissue. Adipokines, such as adiponectin, are bioactive peptides secreted from adipose tissue, which exert metabolic control over a number of insulin sensitive tissues, including, in an autocrine manner, adipose tissue. We next investigated potential alterations in adiponectin signalling in MLP rats, with aim of determining alternative mechanisms of IRF3 and IRF4 regulation. Remarkably, we found that mRNA levels of adiponectin (ADIPOq; Fig. 5.3A) and adiponectin receptor 1 (AdipoR1) and receptor 2 (AdipoR2) were dramatically suppressed in MLP rats by ≈90% relative to control (Fig. 5.3B and 5.3C), suggesting that impaired adiponectin signalling may lead to decreased IRF3 and IRF4 expression. To investigate this further, we used the 3T3L1 adipocyte cell line. Consistent with

impaired adiponectin signalling and reduced IRF expression in the white adipose tissue of MLP rats, incubation of 3T3L1 adipocytes with adiponectin led to increased mRNA levels of IRF3 and IRF4 (Fig. 5.3D and 5.3E). This suggests that, in addition to insulin, adiponectin provides an additional level of regulatory control over IRF3 and IRF4 in white adipose tissue.

Figure 5.3

A

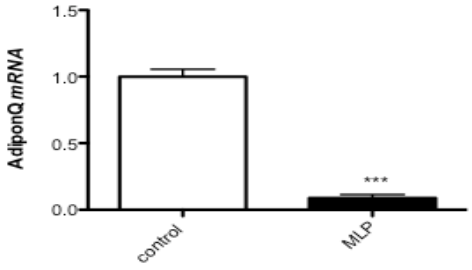


B

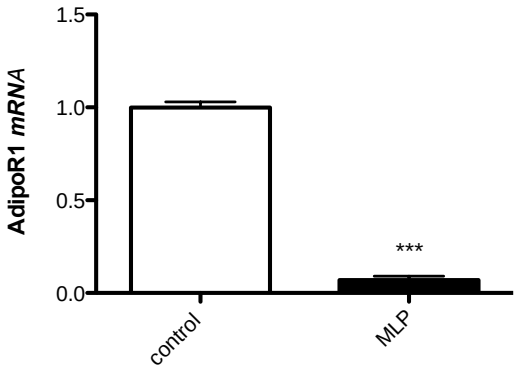


C

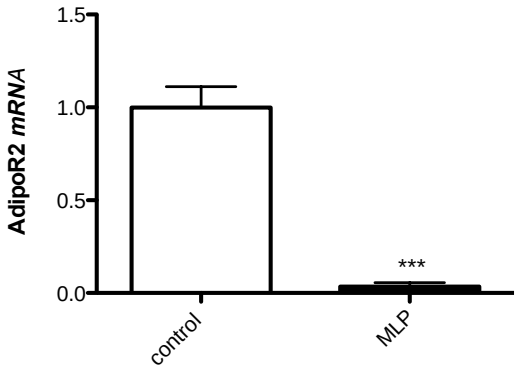

D

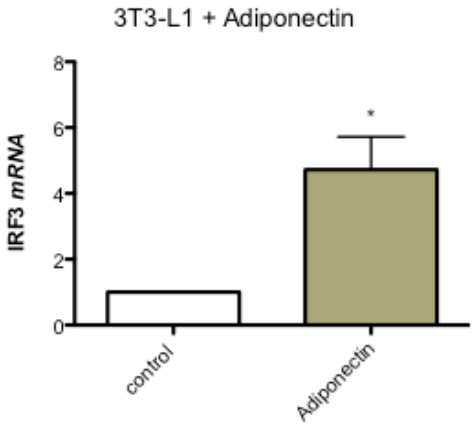


E

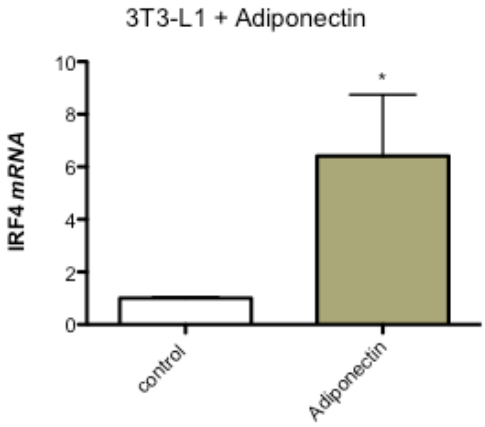


Figure 5.3: Impaired adiponectin signalling in white adipose tissue of MLP offspring leads to reduced IRF levels. Visceral WAT and serum were isolated from 8-week old offspring of MLP and control Wistar rats (n = 6); mRNA levels of (A) *AdipoQ*, (B) *AdipoR1*, and (C) *AdipoR2* in white adipose tissue. 3T3-L1 adipocytes were treated with adiponectin (30 □g/ml; 24 h) and mRNA levels of (D) *Irf3* and (E) *Irf4* were measured by qPCR. Data are expressed as mean ± SEM. * $P < 0.05$, *** $P < 0.001$ vs. control.

### 5.3.4 Adiponectin regulates IRF3 and IRF4 through AMPK and PPARα

Adiponectin, via signalling through adiponectin receptor 1 (AdipoR1) and receptor 2 (AdipoR2) has been reported to exert metabolic effects through activation of the energy sensing enzyme AMPK and the nuclear receptor PPARα [60]. Both AMPK and PPARα play important roles in regulating lipogenesis and fatty acid oxidation [133, 244, 255]. Consistent with observed reductions in adiponectin and AdipoR1 expression, MLP rats also displayed decreased protein levels of phospho($Thr^{172}$)-AMPK (Fig. 5.4A). Since phosphorylation at $Thr^{172}$ leads to AMPK activation, this observation suggests reduced AMPK activity in MLP rats. In addition, protein levels of phospho($Ser^{79}$)-ACC, a downstream target of AMPK, were also reduced in MLP offspring compared to control (Fig. 5.4A). Total protein levels of AMPK were unchanged, demonstrating that decreased AMPK activation did not occur because of MLP-induced reductions in total protein. In contrast, total-ACC protein levels were elevated in MLP mice, reflecting increased lipogenesis, changes that are consistent with increased lipogenic gene expression (Fig. 5.2E). Furthermore, reflecting decreased AdipoR2 expression, we also observed decreased mRNA levels of PPARα in MLP rats, compared to control (Fig. 5.4B). Transcriptional modulation by PPARα

requires the presence of the PGC1α. Consistent with this, PGC1α mRNA levels were also suppressed in MLP rat adipose tissue (Fig. 5.4C).

Figure 5.4

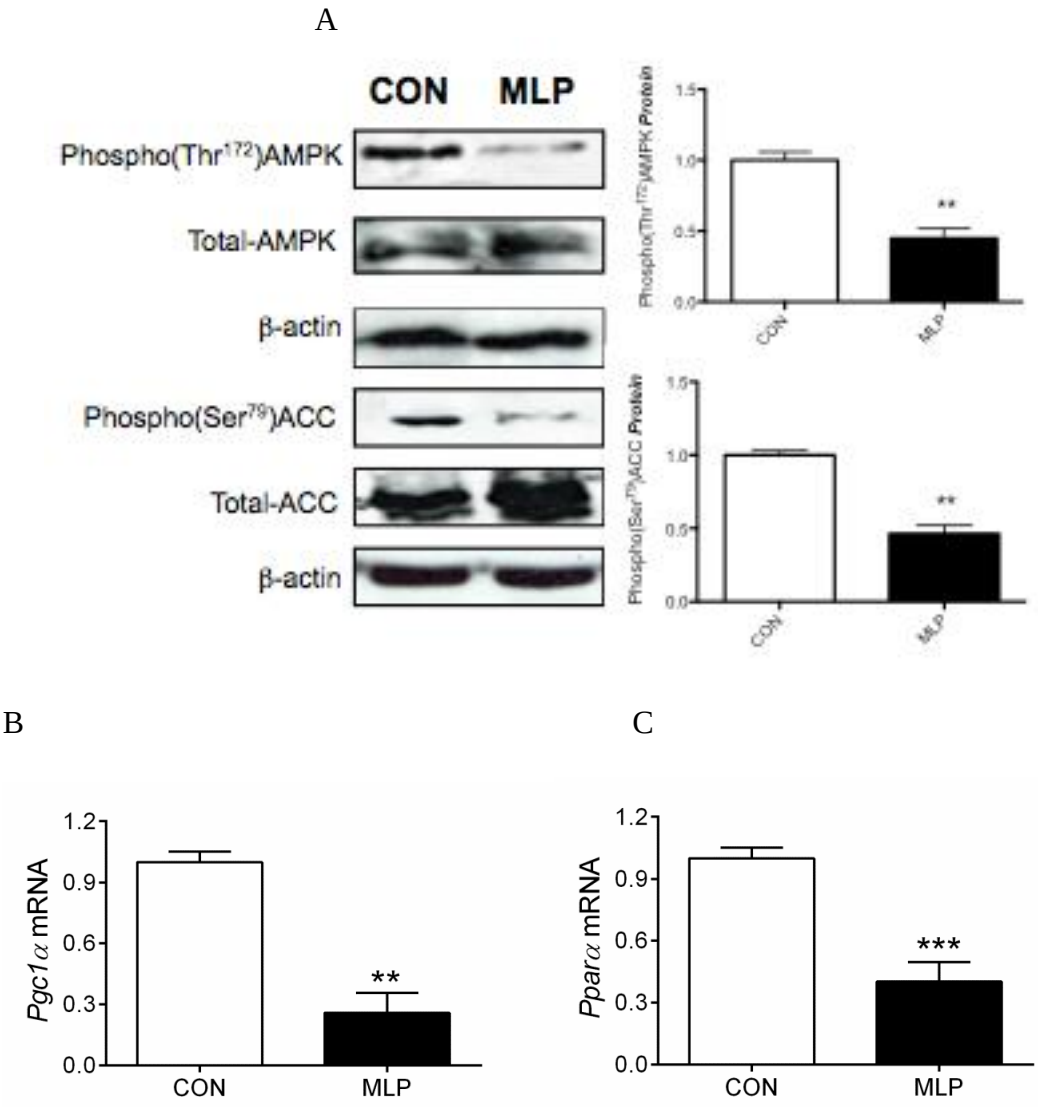


Figure 5.4: Reduced AMPK and PPARα signalling in white adipose tissue of MLP offspring. Visceral WAT was isolated from 8-week old offspring of MLP and control Wistar rats (n = 6); (A) protein levels of phospho(Thr$^{172}$)-AMPK, total-AMPK and phospho(Ser$^{79}$)-ACC; mRNA levels of (B) *Pparα* and (C) *Pgc1α*.Western blots are representative. Data are expressed as mean ± SEM. ** $p < 0.01$, *** $P < 0.001$ vs. control. MLP = Maternal low protein diet (8% low-protein vs. 20% control diet during pregnancy and lactation); Offspring were maintained on standard diet after weaning (3 weeks) and then killed at 8 weeks.

### 5.3.5 The potential role of Adiponectin-AMPK-PPAR signalling in regulating IRF3 and IRF4

To further analyse the potential role of adiponectin-AMPK-PPARα signalling in regulating IRF3 and IRF4 expression, we initially used 3T3L1 adipocytes. Use of 3T3L1 adipocytes allowed for specific examination of IRF4 regulation in a model lacking macrophages, which may influence results given the role of IRF4 in immune regulation [256]. Adipocyte differentiation was confirmed by measurement of mRNA levels of PPARγ (data not shown). Treatment of differentiated adipocytes with WY14643, a potent PPARα agonist, had no effect on IRF3 mRNA (Fig. 5.5A) but did induce expression of IRF4 (Fig. 5.5B). We further analysed these putative signalling mechanism using PPARα knockout mice, which displayed ≈90% reduction in PPARα mRNA levels in white adipose tissue, together with a marked reduction in PGC1α mRNA levels (Fig. 5.5C and 5.5D). Significantly, in PPARα knockout mice the normal IRF4 responses to fasting and feeding were disrupted (Fig. 5.5E). Consistent with previous reports [253], IRF4 levels were induced by fasting in WT mice. However, this effect was blunted in PPARα knockout mice, where IRF4 levels were reduced in fasted compared to fed mice. Similar to MLP rats, PPARα knockout mice also displayed reduced IRF4 levels (Fig. 5.5F), together with raised levels of ACC and SREBP1c (Fig. 5.5G-H), indicative of elevate lipogenesis and adipogenesis in white adipose tissue. Taken together, these results indicate that an adiponectin-PPARα signalling pathway induces IRF4 mRNA expression in white adipose tissue. Moreover, this pathway is dysregulated in response MLP, and this may in part mediate the metabolic defects associated with this MLP.

Figure 5.5

A B

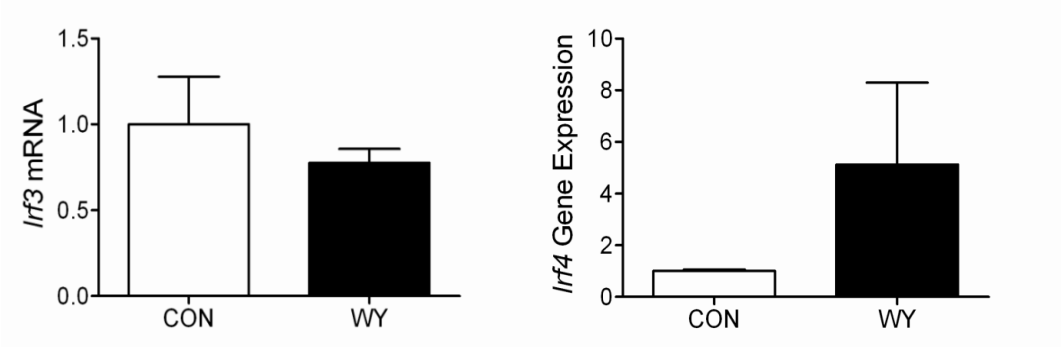

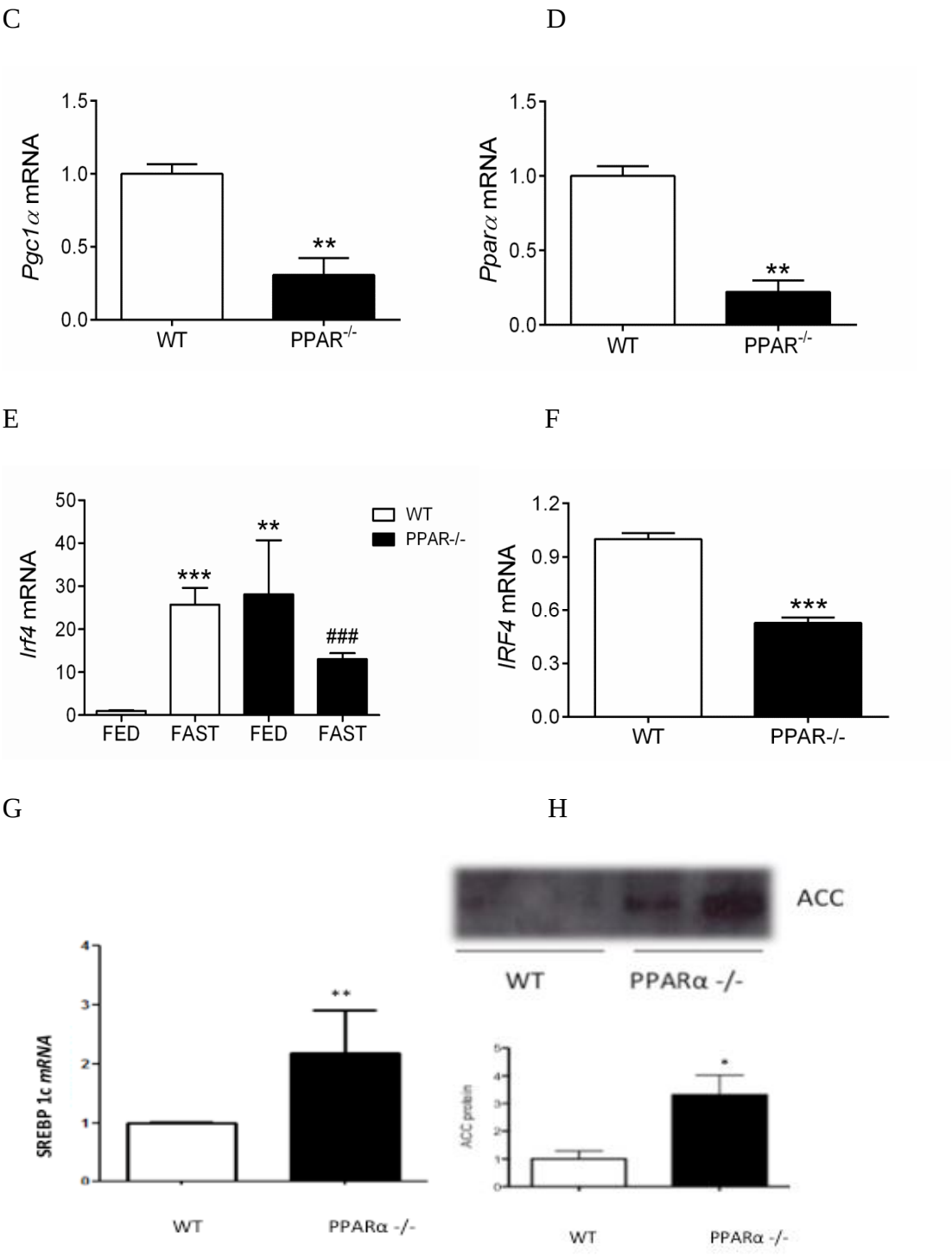


Figure 5.5: Adiponectin-PPARα signalling induces IRF4 expression in white adipose tissue. 3T3-L1 adipocytes were treated with WY14643 (WY) (10 □M; 24 h) and mRNA levels of (A) *Irf3* and (B) *Irf4* were measured by qPCR. Visceral WAT and serum were isolated from 8-week old PPARα knockout and control mice (n = 6); mRNA levels of (C) *Ppar*□ (D) *Pgc1*□, (E – F) *Irf4*, (G) *Srebp1c* were assessed by qPCR. (H) Protein levels of ACC. Western blots are representative. Data are expressed as mean ± SEM. * *P*< 0.05, ***P*<0.01, *** *P* < 0.001 vs. control (FED); ### *P*<0.001 v. control (FAST).

### 5.3.6 Adiponectin-AMPK signalling may regulate IRF3 in white adipose tissue

In contrast to IRF4, IRF3 was unaffected by PPARα agonist *in vitro*, indicating an alternative regulatory mechanism for IRF3 (Fig. 5.5A). Since adiponectin induced both IRF3 and IRF4, but PPARα regulated IRF4 only, we reasoned that AMPK, another target of adiponectin, may exert regulatory control over IRF3. To test this, we used metformin, as a known activator of AMPK [257], rather than for its actions as an anti-diabetic treatment. Administration of metformin to control mice led to significant induction of IRF3 (Fig. 5.6A) but had no effect on IRF4 mRNA levels (Fig. 5.6B), implying that adiponectin-AMPK signalling selectively induces IRF3 in white adipose tissue.

Figure 5.6

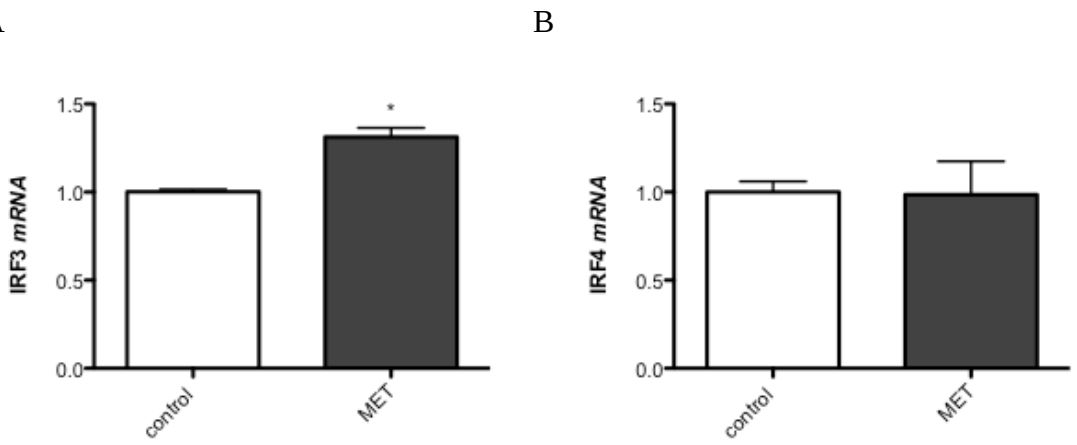


Figure 5.6: Adiponectin-AMPK signalling may regulate IRF3 expression in white adipose tissue. Visceral WAT was isolated from 8-week old C57Bl/6 mice administered metformin (250 mg/kg/day; 7 days) or saline equivalent (n = 6); mRNA levels of (A) *Irf3* and (B) *Irf4* were measured by qPCR. Data are expressed as mean ± SEM. * $P < 0.05$, vs. control.

## 5.4 Discussion

We report here that expression of IRF3 and IRF4, two key repressors of adipogenesis, are reduced in offspring of rats fed a protein-restricted diet during pregnancy and lactation, in parallel with no changes in fasting insulin and glucose levels. Human epidemiological studies have consistently reported that exposure to an adverse intrauterine environment, such as protein-restriction, leads to an increased risk of

development of obesity, T2DM and cardiovascular disease in later life [249, 251, 252]. Experimental model studies have reported that MLP offspring gain more weight, have increased susceptibility to development on metabolic syndrome and display impaired adipocyte function when placed a high fat diet [247, 258, 259]. However the underlying regulatory mechanisms driving these processes are yet to be fully elucidated. Our data provides evidence that a loss of ability to efficiently repress adipogenesis and lipogenesis, as a result of marked early-life reductions in IRF3 and IRF4, may contribute to impaired adipocyte function and increased risk of obesity in later life. Whilst metabolic changes observed in this model are mild, the early life mechanistic changes reported here would likely make a key contribution to the expected, and previously reported, metabolic deterioration likely observed in these animals in later life.

Previous studies have described that IRF4 expression and function is suppressed by insulin, and that as a result, IRF4 expression is lower in white adipose tissue depots obtained from rodent models characterised by insulin resistance; HFD, *ob/ob* and *db/db* mice [253]. Despite this well characterised role of insulin, our MLP model displayed a marked reduction in IRF3 and IRF4, without significant changes in serum insulin. Instead, our data point the involvement of the adiponectin-PPARα and adiponectin-AMPK signalling pathways in the regulation of IRF4 and IRF3 respectively. Adiponectin is a bioactive adipokine expressed at high levels and secreted from adipose tissue [260]. Adiponectin exerts metabolic regulatory effects via autocrine, paracrine and endocrine function, through the receptors adipoR1 and adipoR2, which in turn activate AMPK and PPARα [60, 260]. Conversely, PPARα agonists have been reported to upregulate adiponectin and AdipoR1 and AdipoR2, whilst adiponectin is suppressed in PPARα knockout mice [261]. PPARα is a transcription factor for genes involved in lipolysis and fatty acid oxidation and PPARα null mice maintained on a high-fat diet become more obese than WT [262]. Despite suppression of insulin levels and increases in FA supply, PPARα-deficient mice exhibit an impaired ability to adequately up-regulate hepatic FA oxidation in response to fasting [263]. Insulin resistance induced by excess of non-esterified FA and circulating TAG can be corrected by the administration of PPARα activators by actions to promote removal of intracellular lipid through tissue FA oxidation [93].

PPARα is activated under calorie restriction, increasing the expression of genes encoding mitochondrial FA oxidation enzymes, thereby increasing the capacity for FA oxidation and intracellular lipid clearance [163]. AMPK activation occurs in response to a rise in AMP associated with metabolic stresses that interfere with ATP production (e.g., hypoxia or calorie restriction/glucose deprivation) or accelerated ATP consumption (e.g., muscle contraction), so as to preserve or maintain tissue function [19]. Therefore, AMPK also plays an important role in regulating lipid homeostasis in adipose tissue, having been shown to inhibit lipogenesis and during the longer-term increase lipolysis [255]. The fact that PPARα levels and other oxidation genes (PGC-1α) and proteins (AMPK) are suppressed in MLP rats, while lipogenic genes are enhanced (SREBP-1c and FAS), suggest that these mice may develop a similar phenotype to PPARα-/- mice, and that the MLP phenotype may be a direct result of reduced PPARα levels, leading to increased IRF4 levels. Under both conditions, fatty acid oxidation is decreased and lipogenesis is enhanced, again potential involving an IRF-mediated mechanism. Several mechanisms for these actions of AMPK and PPARα have been described. Our data suggests a further mechanism of action, namely via induction of IRF3 and IRF4, and consequent repression of lipogenesis and induction of lipolysis in white adipose tissue. These changes were in turn regulated by adiponectin, and these signalling pathways were all impaired in MLP rats.

In addition to specific effects on lipolysis and lipogenesis, low levels of IRF4 may also reflect poorly differentiated adipocytes, since IRF4 is expressed only in fully differentiated adipocytes. Poorly differentiated adipocytes are often present in obesity and can lead to hypoxia, inflammation and an altered adipokine profile, including lower adiponectin levels [264]. Dysregulation of these processes are linked to onset of T2DM. Moreover, reduced adiponectin levels occurring as a result of poor differentiation, may represent an initial cause of the impaired adiponectin signalling observed in MLP mice. Alternatively, this mechanism of impaired adiponectin signalling may induce a feed-forward loop, with further reductions in adiponectin signalling and consequent worsening of the MLP phenotype. In addition, whilst adiponectin has been reported to induce PPARα, the reverse has also been documented, with adiponectin upregulated by PPARα agonists and suppressed in white adipose tissue of PPARα knockout mice [261]. Thus, suppressed PPARα levels

in MLP mice may contribute to further impairment of adiponectin signalling and consequent exacerbation of the MLP phenotype. Further studies are required to determine the exact mechanistic interactions by which PPARα regulates IRF4.

In addition to an established role in adipocytes, IRFs are present in macrophages and infiltrating lymphocytes. IRF4 is essential for the function and homeostasis of both mature B and mature T lymphocytes. IRF4-deficient mice exhibited a profound reduction in serum immunoglobulin concentrations and impaired T lymphocyte function [265]. The altered IRF levels could potentially represent reduced immune infiltrate into the white adipose tissue. Further research is needed to clarify this. However, given the increased inflammation and macrophage recruitment observed in response to reduced adiponectin levels in other studies [260], a reduced immune infiltrate seems unlikely, instead suggesting a specific role for adipocyte-IRF3 and IRF4 in this model.

In summary, we propose that in early life in response to protein restriction, adiponectin signalling is impaired leading to reduced activity of PPARα and AMPK, which in turn lead to decreased levels of IRF3 and IRF4. This would lead to an inability to repress adipogenesis and lipogenesis, and confer increased susceptibility to development of an obese phenotype in later-life.

**Chapter:**

*6. General Discussion*

## 6.1 Reciprocal interaction between SIRT1 and AMPK

SIRT1 expression was reduced in the liver and skeletal muscle of liver-specific and skeletal muscle-specific AMPK-/- mice, respectively. Moreover, SIRT1 knockdown or inhibition in cultured hepatocytes or skeletal myoblasts lowered AMPK levels and activity. This suggests that SIRT1 and AMPK may be linked, possibly by changes in NAD+/NADH ratio [151]. However, the decrease of SIRT1 in skeletal muscle of AL-fed AMPK-/- mice was no longer observed when mice were subjected to CR, suggesting that caloric restriction plays an important role in protecting skeletal muscle from the effects of decreased SIRT1 expression (which include impaired insulin signalling and impaired glucose uptake), probably caused by a lack of AMPK [141]. In WAT, decreased SIRT1 protein expression in MLP-offspring was also associated with decreased AMPK activity. AMPK activation by serum starvation correlates with a modestly decreased Akt phosphorylation, in L6 myoblasts (Chapter 4). Starvation or depletion of essential proteins can cause a fast depletion of ATP and this effect is counter balanced by an increased phosphorylation of AMPK on $thr^{172}$, in order to conserve the ATP available [266]. In this context, Akt is inhibited to reduce gene expression and proliferation and to promote cell arrest, protecting the cells against starvation. Insulin administration reverses this pathway, promoting anabolism [3].

Our results suggest a feedback loop between SIRT1 and AMPK, where, in skeletal muscle, AMPK activates SIRT1 through increased β oxidation. In fact, in our studies, decreased PGC-1α and SIRT3 gene expression levels (regulators of increased β oxidation) correlated with decreased SIRT1 in AMPK-/- muscle. Hirschey et al. have shown that mice lacking SIRT3 display an abnormal oxidizing capacity during fasting in liver, skeletal and cardiac muscle and brown adipose tissue, possibly due to hyperacetylation of the SIRT3 target, LCAD [167]. In parallel with these results, ATP levels were also lower in livers of mice lacking SIRT3 [167]. It is likely that the AMPK-SIRT1-PGC-1α-SIRT3 axis during fasting/CR is important to prevent chronic mitochondrial protein hyperacetylation and reduced LCAD activity. Decreased fatty acid oxidation due to decreased LCAD activity would eventually lead to obesity, insulin resistance and metabolic disorders [206, 207].

In the liver, SIRT1 has been reported to activate AMPK, possibly through deacetylation and activation of an upstream kinase of AMPK (perhaps LKB1); AMPK depletion, on the other hand, inhibits SIRT1 activity, under normal fed conditions. In the the present studies, SIRT1 knockdown H4IIEC3 cells revealed decreased levels of PGC-1α gene expression and AMPK protein expression, where liver specific AMPK deficient mice had lower expression of SIRT1 mRNA, decreased PGC-1α gene expression and impaired gluconeogenesis. Our results, in line with previous studies, reveal that there is a possible feedback loop between SIRT1 and AMPK. In the future, it would be interesting to study LKB1 acetylation levels together with SIRT1 activity in AMPK knockout livers of fasted mice, re-fed after a 24h period. Further studies will also focus on changes in $NAD^+$/NADH ratio together with SIRT1 activity in muscle specific $AMPK^{-/-}$. Identification of potential therapeutic targets through elucidation of novel mechanisms of metabolic regulation of AMPK complementing, for example, deacetylation catalyzed by the sirtuins, may prove to be important for the treatment of T2DM and other metabolic disorders associated with aging. Reduced mTORC1 activity, either as a consequence of dietary restriction or direct inhibition, extends lifespan in numerous lower and higher organisms [19]. Thus, exploration of the connections between AMPK, the SIRTs and mTORC1 presents a line of enquiry of huge potential relevance to T2DM and related metabolic disorders.

### 6.2 Adiponectin targeting obesity-related T2DM

In chapter 4, we have seen that adiponectin modestly increases AMPK phosphorylation on $thr^{172}$, which is related to stimulate fatty oxidation, through the adiponectin receptors, AdipoR1 and AdipoR2 [224, 267]. Adiponectin abrogates the link between SIRT1 and AMPK, activating AMPK ability to inhibit ACC and, as a consequence, allowing fatty acid oxidation and protecting the cells from the excessive anabolic signalling, caused by insulin, in fasting conditions. MLP-offspring display reduced expression of IRF3 and IRF4, in association with increased lipogenic gene expression in WAT (increased SREBP1 and FAS). IRF3 and IRF4 suppression may lead to obesity and T2D on MLP-offspring [253]. IRF3 and IRF4 are increased by adiponectin, through activation os AMPK and PPARα, respectively. This pathway

represses adipogenesis and lipogenesis, and confers protection against the development of an obese/diabetic phenotype.

### 6.3 Hepatic and muscular lipogenesis as a response to nutritional status

The decrease of SIRT1 mRNA expression in skeletal muscle of AL-fed AMPK$^{-/-}$ mice was no longer observed when mice were subjected to CR, suggesting that caloric restriction plays an important role in protecting skeletal muscle from the effects of decreased SIRT1 expression (impaired insulin signalling and impaired glucose uptake), probably caused by a lack of AMPK [141]. The fact that SIRT1 gene expression did not change in CR conditions between WT and AMPK$^{-/-}$ is interesting, since previous studies have reported that CR leads to increased SIRT1 protein and gene expression [110]. However, our findings are consistent with some previous reports, where SIRT1 gene and protein expression have been reported to be unaffected by CR in skeletal muscle and adipose tissue [126].

Chapter 3 described convincing evidence that fasted liver display an oxidative profile, even though, free cholesterol synthesis (mediated by XBP-1) is increased. The AMPK-SIRT1-PGC-1α-SIRT3 pathway has been suggested (in this thesis) to control fatty acid oxidation during fasting. Because the fatty acid oxidation pathway is a major contributor to the regulation of cellular energy balance, especially during fasting [268], the upregulation of this pathway and the increase in cellular NAD+ that both occur during the transition to fasting could work in synergy to maximally induce the deacetylation of LCAD, and subsequent increase its activity and fatty acid oxidation output.

### 6.4 AMPK-SIRT1 axis improves insulin-signaling pathway

Studies performed *in vitro* have shown that resveratrol inhibits the phosphorylation of IRS1-ser$^{307}$ and IRS2-thr$^{348}$, which are markers of insulin resistance [210], indicating that resveratrol (SIRT1 activator) improves insulin signalling [211]. In agreement with this, SIRT1 overexpression increases the phosphorylation of Akt, a downstream target of insulin signalling, in muscle cells and HEK293 cells, whereas the inhibition

of SIRT1 induced the opposite response [211]. In our studies performed in liver, Akt was modestly increased under high fat conditions, which was unexpected since high fat feeding is known to cause tissue insulin resistance [269]. Although, is important to verify that in our studies, high fat feeding was not associated to weight gain, possibly because mice did not eat as much as the controls. This is one of the possibly reasons why high fat diet did not cause insulin resistance. Our studies have also shown that NMN treatment seems to increase IRS-1 tyrosine phosphorylation, perhaps ameliorating insulin-signalling pathway even in high fat fed animals. It is possible that NMN administration increases $NAD^+$ availability to activate SIRT1 [270, 271], which in turn, improves insulin-signalling pathway. The mechanism through which SIRT1 improves insulin signalling remains unclear. However Wang et al. found that SIRT1 deficiency in the liver decreases phospho-Akt-ser$^{473}$ due to a reduced level of Rictor, a critical component of mTORC2, thereby underscoring an important role for SIRT1 in maintaining activity of mTORC2 complex and providing a mechanism how the hepatic insulin resistance caused by liver specific loss of SIRT1 eventually spread to other insulin-sensitive tissues/organs [272]. Changes in SIRT/AMPK (seen above, section 6.1) would likely induce lipogenesis and potential lipotoxicity mediated impaired insulin signalling. Increased fatty acid delivery through high fat diet and decreased fatty acid oxidation due to impaired SIRT1/AMPK signalling would led to lipid accumulation within hepatocytes, which inhibits tyrosine phosphorylation of IRS-1. Inhibition of tyrosine phosphorylation of IRS-1 follows serine phosphorylation of critical sites on IRS-1 and inhibits binding and activation of PI3K [273]. A number of different serine kinases could be responsible for serine phosphorylation of IRS-1. Candidates include members of the novel protein kinase C family, which may be activated by accumulation of lipid intermediates [273]. Further are required to fully carachterise the signalling mechanisms involved.

AMPK phosphorylates and activates the insulin receptor, providing a direct link between AMPK and the insulin-signalling pathway [236]. In our studies we have provided a primary evidence that insulin-dependent Akt phosphorylation on ser$^{473}$ is impaired on AMPK deficient muscle, suggesting that AMPK is crucial for insulin-dependent Akt phosphorylation on ser-$^{473}$ (Chapter 4). We already knew that in the liver SIRT1 stimulates insulin signalling through Akt (Chapter 3). It is possible that, in muscle, similarly to what happens in the liver, AMPK deficiency is impairing

NAMPT activity, which decreases SIRT1 activity due to a lack of $NAD^+$ and this, in turn, results in impaired acetylation of Rictor and impaired mTORC2/Akt signalling, known to promote hyperglycemia, oxidative damage and insulin resistance [272] (Fig. 6.1).

Figure 6.1

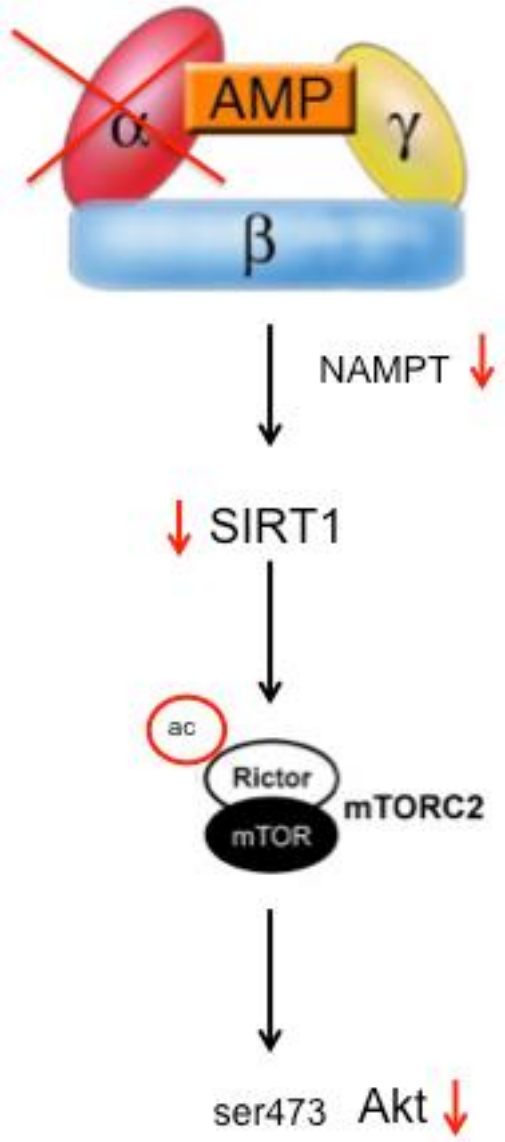


Figure 6.1: AMPK-mediated SIRT1 activity on insulin signaling pathway. Lack of AMPKα (catalytic subunit), but not AMPKβ or AMPKγ, results in decreased NAMPT activity, which culminates in decreased SIRT1 activity. Reduced activity of SIRT1 leads a higher acetylation of Ritctor (part of the complex mTORC2), which results in decreased Akt phosphorylation on ser473.

AMPK-induced increase in skeletal muscle and liver insulin signalling pathway results in higher blood glucose uptake [238, 239]. In addition, AMPK activity also improves skeletal muscle and liver glycogen synthesis capacity by increased glycogen synthase activity [220, 240], enhancing blood glucose disposal, allowing faster glycaemia reduction. Thus, decreased AMPK in skeletal muscle might account for impaired glucose-induced insulin secretion (GIIS) signaling in pancreatic β-cells, reducing blood insulin content observed during GTT. Therefore, these data provide some evidence for a mechanism by which the crosstalk between insulin-sensitive tissues and pancreatic islets might occur. Further studies on β-cells of muscle specific AMPK $^{-/-}$ mice must be done to better understand this pathway.

Decreased PGC-1α gene expression is possibly the reason by which AMPK deficiency decreases glucose uptake. We suggested a mechanism for this, based on a study from Michael et al. 2001, where PGC-1 mediates the increase in GLUT4 expression, in large part, by binding to and coactivating the muscle-selective transcription factor MEF2C [243]. According with this, decreased PGC-1α gene expression would lead to decreased GLUT4 expression and decreased glucose uptake. Another possibility is that decreased PGC-1α gene expression affects SIRT3 gene expression and this, in turn, would impair glucose uptake and insulin signaling. SIRT3$^{-/-}$ mice display impaired insulin action and a lower rate of oxygen consumption with increased oxidative stress in skeletal muscle [169]. In our studies, decreased SIRT3 expression correlates with higher glycaemia in CR-AMPK$^{-/-}$ mice, suggesting impaired insulin signalling under these circumstances.

### 6.5 SIRT3 and SIRT6

Research has yet to be undertaken to establish the intermediate steps with enzymes and transcriptional regulators involved in the activation of PPARα by SIRT3. Changes in SIRT3 correlate with changes in PGC-1α. Expression of SIRT3 in the liver is induced by PGC-1α through a mechanism involving estrogen-related receptor alpha (ERRα) [205]. We have seen that in liver and skeletal muscle SIRT1-PGC-1α-SIRT3 axis during fasting/CR is important to prevent chronic mitochondrial protein hyperacetylation and reduced LCAD activity. SIRT3 plays an important role in diabetes through regulation of mitochondrial oxidation, reactive oxygen species

production, and insulin resistance, in insulin sensitive tissues. It is another important therapeutic target for T2DM.

*SIRT6* is SIRT1 dependent. SIRT1 knockdown H4IIEC3 cells exibit decreased gene and protein expression of SIRT6. Since SIRT1 and SIRT6 are both nuclear, is possible that SIRT1 activates SIRT6 through deacetylation or that a lack of SIRT1 leads to SIRT6 inactivation. Dominey et al [107] have reported that SIRT6 strongly controls PGC-1α acetylation. Surprisingly, SIRT6 induces PGC-1α acetylation, through interaction and modification of GCN5, leading to GCN5 enhanced activity [107]. Decreased acetylation levels of PGC-1α in $AMPK^{-/-}$ livers could be either because AMPK negatively regulates SIRT1 target genes, or because decreased activity of SIRT6 through decreased SIRT1 gene expression could impair PGC-1α acetylation status. Further studies on SIRT1 activity would be important to better understand this pathway. Under conditions of normal glucose availability, SIRT6 represses expression of key enzymes, diverting pyruvate towards the mitochondrial citric acid cycle (TCA) for efficient ATP production [274]. According with this and based on our experiments, we can predict that SIRT6 can be involved in the pathway through which SIRT1 activates AMPK, with increased ATP production. Further studies involving SIRT6 acetylation levels and SIRT1 activity could help to understand better this mechanism.

## 6.6 Mechanism of IRF3 and IRF4 on the development of obesity-related T2DM in MLP-offspring

Previous studies have shown that MLP leads to telomere shortening and increased markers of cell senescence in rat islets [275]. MLP-offspring display reduced PGC-1α and reduced PPARα (both SIRT1 targets [133]) together with reduced SIRT1 protein expression. These observations suggest that maternal protein restriction can affect major metabolic pathways implicated in regulation of lifespan at a young age, which may explain the impact of maternal diet on longevity.

MLP mice are prone to development of obesity and insulin resistance [276]. MLP-offspring display reduced expression of adiponectin and adiponectin receptors

(Chapter 5). In agreement, phospho-AMPK protein expression and AMPK-dependent ACC phosphorylation were also reduced in our studies (Chapter 5), as well as *PPARα*. Our data supports the theory that MLP-offspring display impaired fatty oxidation and increased lipogenesis.

Adipose-specific IRF4 knockdown leads to increased lipogenesis and repressed lipolysis and, as a consequence, adipose-specific IRF4 downregulation leads to development of obesity and T2DM in mice [253]. IRF4 is required for lipolysis, at least in part due to direct effects on the expression of adipocyte triglyceride lipase and hormone-sensitive lipase. These studies establish a link between IRF4 and the disposition of calories in adipose tissue, with consequences for systemic metabolic homeostasis [253]. In Chapter 5, *IRF4* but not *IRF3* was enhanced in fasted adipose tissue. We can, therefore, conclude that IRF4 represses adipogenesis under fasting conditions. MLP-offspring display reduced expression of *IRF3* and *IRF4*, in association with increased lipogenic gene expression in WAT (Chapter 5). IRF3 and IRF4 suppression may lead to obesity on MLP-offspring. A study using Dams fed a low- (8%) protein diet during pregnancy and lactation to induce growth restriction in the offspring has shown that MLP-offspring undergo an age-dependent loss of glucose tolerance and insulin resistance resistance and by 17 mo of age have frank diabetes (reviewed in [277]). The level of protein restriction is a mild insult to the animals, because it results in only a modest reduction in birth weight and does not affect litter size. The offspring are weaned onto a standard diet containing 20% protein. These animals were compared to control offspring born to mothers fed a control diet containing 20% protein. The differences in protein expression occur prior to development of insulin resistance, suggesting that they are not consequences of hyperinsulinemia or hyperglycemia but play a role in determining future susceptibility to insulin resistance, cardiovascular disease, and T2DM. According to our studies, *IRF3* and *IRF4* suppression on MLP-offspring could be one of the mechanisms by which these rat model develop obesity-related insulin resistance, due to repression of fatty oxidation and enhanced lipogenesis. Further studies need to be done, using IRF3 and IRF4 agonists (perhaps AMPK and PPARα activators) to better understand if the overexpression of these genes could prevent the metabolic dysfunctions seen in MLP-offspring.

It is already established that the offspring of rats fed a low-protein diet display a greater predisposition to develop obesity and related metabolic disorders in response to high-fat feeding compared to controls [277, 278]. It is also known that PPARα$^{-/-}$ mice develop steatosis in liver and muscle on fasting because increased adipocyte lipolysis is not matched by augmented FA oxidation. On the other hand, insulin resistance induced by excess of non-esterified FA and circulating TAG can be corrected by the administration of PPARα activators by actions to promote removal of intracellular lipid through tissue FA oxidation [93]. So far, we found that MLP-offspring display a lipogenic profile, similar to the one observed in PPARα$^{-/-}$ mice (Chpter 5) and that *IRF4*, required for lipolysis, is under-expressed in MLP-offspring as well as in PPAR deficient mice. We also found that IRF4 is regulated by PPARα (Fig. 6.2). Given the importance of PPARα-dependent IRF4 activation in preventing obesity-related T2DM (through lipolysis) and the fact that MLP-offspring are predisposed to develop a diabetic phenotype in later life [279], we suggest that IRF4 can be a possible target for the prevention of obesity and obesity-related T2DM on MLP-offspring. There is significant interest in developing anti-inflammatory drugs as therapy for metabolic diseases such as T2DM and insulin resistance. Some 'inflammatory' proteins however, like IRF4 and IRF3, may play key roles in metabolic function, independent of their effect on immunity. These achievements will need to be fully explored before the potential of this therapeutic avenue can be fully realized.

Figure 6.2

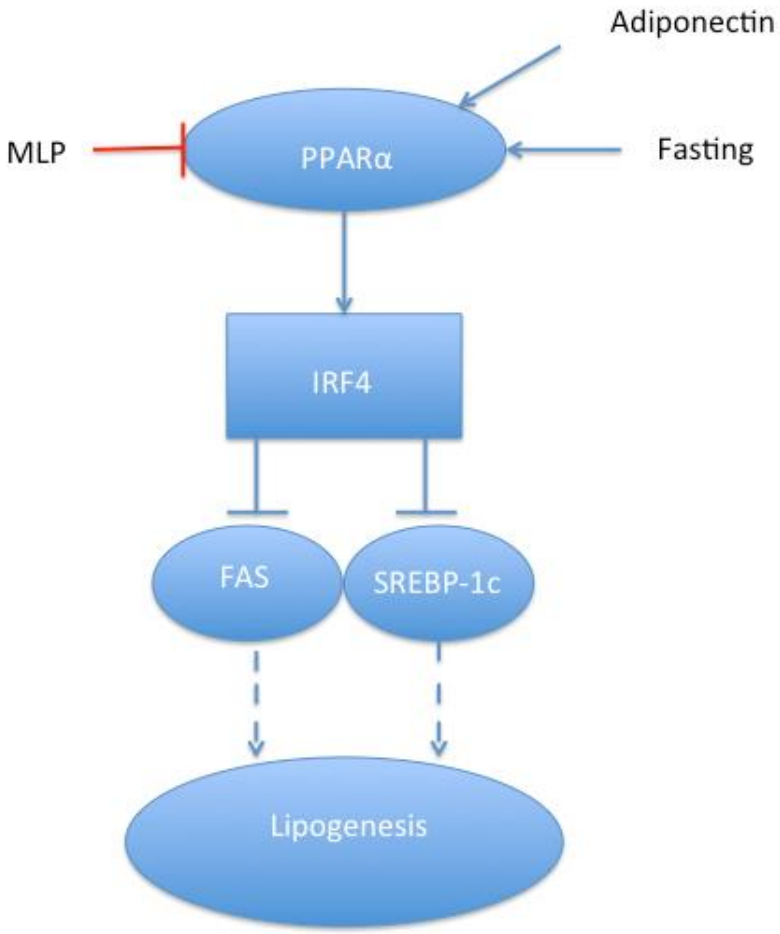


Figure 6.2: Activation of IRF4 through PPARα. Fasting and adiponectin activate PPARα activity, while MLP diet inhibits PPARα. When activated, PPARα regulates IRF4 activation, which inhbitis the lipogenic genes, FAS and SREBP-1c, reducing lipogenesis and stimulating lipolysis.

In our investigation, using WY14643 (a PPARα agonist) we developed primary evidence that PPARα regulates IRF4 but not IRF3 (Chapter 5). In contrast, AMPK may regulate IRF3 (but not IRF4). This is based on the fact that IRF3 and IRF4 are increased by adiponectin (Chapter 5), an adipokyne known to activate both AMPK and PPARα [224, 267]. Interestingly, metformin, known to activate AMPK but not PPARα [280], enhances IRF3, but not IRF4 in C57Bl6 mice (Chapter 5). Specific $AMPK^{-/-}$ adipose tissue and $AMPK^{-/-}$ adipocytes would be important to expand this work. Dr. Paul Caton, in my lab, is currently investigating these issues in AMPK deficient adipocytes.

## 6.7 Concluding remarks

In summary, there is a feedback loop between AMPK and SIRT1. AMPK activates SIRT1 through increased β oxidation (increased *PGC-1α* and increased *SIRT3*). In skeletal muscle AMPK deficiency impairs the beneficial effects of CR on glucose tolerance. This is linked to decreased SIRT1 gene expression, which could impair insulin signalling pathway, culminating in reduced glucose uptake.

It is likely that the AMPK-SIRT1-PGC-1α-SIRT3 axis during fasting/CR is important to prevent metabolic disorders. In liver, AMPK and SIRT1 activate each other to keep hepatic lipogenesis. Increased fatty acid delivery (through diet) and decreased fatty acid oxidation due to impaired SIRT1/AMPK signalling would led to lipid accumulation within hepatocytes, which inhibits tyrosine phosphorylation of IRS-1, decreasing insulin signalling. This can be reversed through NMN administration, suggesting that NMN is a potential therapeutic mechanism for T2DM.

IRF3 and IRF4 suppression may lead to obesity on MLT-offspring, due to repression of fatty oxidation and enhanced lipogenesis. Thus, targeting IRF3 and IRF4 in visceral fat through activation of AMPK and PPARα, respectively (perhaps using adiponectin) would be a novel approach for the treatment of T2DM

Identification of potential therapeutic targets through elucidation of novel mechanisms of metabolic regulation of AMPK and PPARα linked functions, complementing, for example, deacetylation catalyzed by the sirtuins, may prove to be important for the treatment of T2DM and other metabolic disorders associated with aging.

## References


1. Rutter, G.A., *Nutrient-secretion coupling in the pancreatic islet beta-cell: recent advances.* Mol Aspects Med, 2001. **22**(6): p. 247-84.
2. Roden, M. and E. Bernroider, *Hepatic glucose metabolism in humans--its role in health and disease.* Best Pract Res Clin Endocrinol Metab, 2003. **17**(3): p. 365-83.
3. Folli, F., et al., *Regulation of phosphatidylinositol 3-kinase activity in liver and muscle of animal models of insulin-resistant and insulin-deficient diabetes mellitus.* J Clin Invest, 1993. **92**(4): p. 1787-94.
4. White, M.F., et al., *A cascade of tyrosine autophosphorylation in the beta-subunit activates the phosphotransferase of the insulin receptor.* J Biol Chem, 1988. **263**(6): p. 2969-80.
5. Saltiel, A.R. and C.R. Kahn, *Insulin signalling and the regulation of glucose and lipid metabolism.* Nature, 2001. **414**(6865): p. 799-806.
6. Alessi, D.R. and P. Cohen, *Mechanism of activation and function of protein kinase B.* Curr Opin Genet Dev, 1998. **8**(1): p. 55-62.
7. Kotani, K., et al., *Requirement of atypical protein kinase clambda for insulin stimulation of glucose uptake but not for Akt activation in 3T3-L1 adipocytes.* Mol Cell Biol, 1998. **18**(12): p. 6971-82.
8. Fan, Y., K.G. Dickman, and W.X. Zong, *Akt and c-Myc differentially activate cellular metabolic programs and prime cells to bioenergetic inhibition.* J Biol Chem, 2010. **285**(10): p. 7324-33.
9. Cross, D.A., et al., *Inhibition of glycogen synthase kinase-3 by insulin mediated by protein kinase B.* Nature, 1995. **378**(6559): p. 785-9.
10. Leney, S.E. and J.M. Tavare, *The molecular basis of insulin-stimulated glucose uptake: signalling, trafficking and potential drug targets.* J Endocrinol, 2009. **203**(1): p. 1-18.
11. Kupriyanova, T.A. and K.V. Kandror, *Akt-2 binds to Glut4-containing vesicles and phosphorylates their component proteins in response to insulin.* J Biol Chem, 1999. **274**(3): p. 1458-64.
12. Lafontan, M. and D. Langin, *Lipolysis and lipid mobilization in human adipose tissue.* Prog Lipid Res, 2009. **48**(5): p. 275-97.
13. Assimacopoulos-Jeannet, F., et al., *In vivo effects of hyperinsulinemia on lipogenic enzymes and glucose transporter expression in rat liver and adipose tissues.* Metabolism, 1995. **44**(2): p. 228-33.
14. Holman, G.D. and I.V. Sandoval, *Moving the insulin-regulated glucose transporter GLUT4 into and out of storage.* Trends Cell Biol, 2001. **11**(4): p. 173-9.
15. Nishino, N., Y. Tamori, and M. Kasuga, *Insulin efficiently stores triglycerides in adipocytes by inhibiting lipolysis and repressing PGC-1alpha induction.* Kobe J Med Sci, 2007. **53**(3): p. 99-106.
16. Cho, H., et al., *Akt1/PKBalpha is required for normal growth but dispensable for maintenance of glucose homeostasis in mice.* J Biol Chem, 2001. **276**(42): p. 38349-52.

17. Cho, H., et al., *Insulin resistance and a diabetes mellitus-like syndrome in mice lacking the protein kinase Akt2 (PKB beta).* Science, 2001. **292**(5522): p. 1728-31.
18. George, S., et al., *A family with severe insulin resistance and diabetes due to a mutation in AKT2.* Science, 2004. **304**(5675): p. 1325-8.
19. Holness, M.J., et al., *Actions and interactions of AMPK with insulin, the peroxisomal-proliferator activated receptors and sirtuins.* Expert Rev Endocrinol Metab, 2012. **7**(2): p. 191-208.
20. Scully, T., *Diabetes in numbers.* Nature, 2012. **485**(7398): p. S2-3.
21. Lam, D.W. and D. LeRoith, *The worldwide diabetes epidemic.* Curr Opin Endocrinol Diabetes Obes, 2012. **19**(2): p. 93-6.
22. van Dieren, S., et al., *The global burden of diabetes and its complications: an emerging pandemic.* Eur J Cardiovasc Prev Rehabil, 2010. **17 Suppl 1**: p. S3-8.
23. Sardinha, L.B., et al., *Prevalence of overweight, obesity, and abdominal obesity in a representative sample of Portuguese adults.* PLoS One, 2012. **7**(10): p. e47883.
24. Cortez-Dias, N., et al., *Prevalence, management and control of diabetes mellitus and associated risk factors in primary health care in Portugal.* Rev Port Cardiol, 2010. **29**(4): p. 509-37.
25. *Executive summary: Standards of medical care in diabetes--2012.* Diabetes Care, 2012. **35 Suppl 1**: p. S4-s10.
26. Fonseca, V.A., *Defining and characterizing the progression of type 2 diabetes.* Diabetes Care, 2009. **32 Suppl 2**: p. S151-6.
27. Gerich, J.E., *The genetic basis of type 2 diabetes mellitus: impaired insulin secretion versus impaired insulin sensitivity.* Endocr Rev, 1998. **19**(4): p. 491-503.
28. Wang, E.J., et al., *Type 2 diabetes: identifying high risk Asian American subgroups in a clinical population.* Diabetes Res Clin Pract, 2011. **93**(2): p. 248-54.
29. Poulsen, P., et al., *Increased risk of type 2 diabetes in elderly twins.* Diabetes, 2009. **58**(6): p. 1350-5.
30. Iliadou, A., S. Cnattingius, and P. Lichtenstein, *Low birthweight and Type 2 diabetes: a study on 11 162 Swedish twins.* Int J Epidemiol, 2004. **33**(5): p. 948-53; discussion 953-4.
31. Lehtovirta, M., et al., *Evidence that BMI and type 2 diabetes share only a minor fraction of genetic variance: a follow-up study of 23,585 monozygotic and dizygotic twins from the Finnish Twin Cohort Study.* Diabetologia, 2010. **53**(7): p. 1314-21.
32. Wing, R.R., et al., *Behavioral science research in diabetes: lifestyle changes related to obesity, eating behavior, and physical activity.* Diabetes Care, 2001. **24**(1): p. 117-23.
33. van Tilburg, J., et al., *Defining the genetic contribution of type 2 diabetes mellitus.* J Med Genet, 2001. **38**(9): p. 569-78.
34. Hardy, O.T., M.P. Czech, and S. Corvera, *What causes the insulin resistance underlying obesity?* Curr Opin Endocrinol Diabetes Obes, 2012. **19**(2): p. 81-7.
35. Malandrucco, I., et al., *Very-low-calorie diet: a quick therapeutic tool to improve beta cell function in morbidly obese patients with type 2 diabetes.* Am J Clin Nutr, 2012. **95**(3): p. 609-13.

36. Viollet, B., et al., *Targeting the AMPK pathway for the treatment of Type 2 diabetes.* Front Biosci (Landmark Ed), 2009. **14**: p. 3380-400.
37. Samuel, V.T. and G.I. Shulman, *Mechanisms for insulin resistance: common threads and missing links.* Cell, 2012. **148**(5): p. 852-71.
38. Shulman, G.I., *Cellular mechanisms of insulin resistance.* J Clin Invest, 2000. **106**(2): p. 171-6.
39. Ciaraldi, T.P., et al., *Glucose transport in cultured human skeletal muscle cells. Regulation by insulin and glucose in nondiabetic and non-insulin-dependent diabetes mellitus subjects.* J Clin Invest, 1995. **96**(6): p. 2820-7.
40. Garvey, W.T., et al., *Evidence for defects in the trafficking and translocation of GLUT4 glucose transporters in skeletal muscle as a cause of human insulin resistance.* J Clin Invest, 1998. **101**(11): p. 2377-86.
41. Lillioja, S., et al., *Insulin resistance and insulin secretory dysfunction as precursors of non-insulin-dependent diabetes mellitus. Prospective studies of Pima Indians.* N Engl J Med, 1993. **329**(27): p. 1988-92.
42. Warram, J.H., et al., *Slow glucose removal rate and hyperinsulinemia precede the development of type II diabetes in the offspring of diabetic parents.* Ann Intern Med, 1990. **113**(12): p. 909-15.
43. Buchanan, T.A., et al., *Preservation of pancreatic beta-cell function and prevention of type 2 diabetes by pharmacological treatment of insulin resistance in high-risk hispanic women.* Diabetes, 2002. **51**(9): p. 2796-803.
44. Gerstein, H.C., et al., *Effect of rosiglitazone on the frequency of diabetes in patients with impaired glucose tolerance or impaired fasting glucose: a randomised controlled trial.* Lancet, 2006. **368**(9541): p. 1096-105.
45. DeFronzo, R.A., D. Simonson, and E. Ferrannini, *Hepatic and peripheral insulin resistance: a common feature of type 2 (non-insulin-dependent) and type 1 (insulin-dependent) diabetes mellitus.* Diabetologia, 1982. **23**(4): p. 313-9.
46. Randle, P.J., et al., *The glucose fatty-acid cycle. Its role in insulin sensitivity and the metabolic disturbances of diabetes mellitus.* Lancet, 1963. **1**(7285): p. 785-9.
47. Yki-Jarvinen, H., *Ectopic fat accumulation: an important cause of insulin resistance in humans.* J R Soc Med, 2002. **95 Suppl 42**: p. 39-45.
48. Karpe, F., J.R. Dickmann, and K.N. Frayn, *Fatty acids, obesity, and insulin resistance: time for a reevaluation.* Diabetes, 2011. **60**(10): p. 2441-9.
49. Samuel, V.T., K.F. Petersen, and G.I. Shulman, *Lipid-induced insulin resistance: unravelling the mechanism.* Lancet, 2010. **375**(9733): p. 2267-77.
50. Petersen, K.F., et al., *Impaired mitochondrial activity in the insulin-resistant offspring of patients with type 2 diabetes.* N Engl J Med, 2004. **350**(7): p. 664-71.
51. Savage, D.B., K.F. Petersen, and G.I. Shulman, *Disordered lipid metabolism and the pathogenesis of insulin resistance.* Physiol Rev, 2007. **87**(2): p. 507-20.
52. Saad, M.J., et al., *Modulation of insulin receptor, insulin receptor substrate-1, and phosphatidylinositol 3-kinase in liver and muscle of dexamethasone-treated rats.* J Clin Invest, 1993. **92**(4): p. 2065-72.
53. Asano, T., et al., *Role of phosphatidylinositol 3-kinase activation on insulin action and its alteration in diabetic conditions.* Biol Pharm Bull, 2007. **30**(9): p. 1610-6.

54. Danielsson, A., et al., *Short-term overeating induces insulin resistance in fat cells in lean human subjects.* Mol Med, 2009. **15**(7-8): p. 228-34.
55. Dresner, A., et al., *Effects of free fatty acids on glucose transport and IRS-1-associated phosphatidylinositol 3-kinase activity.* J Clin Invest, 1999. **103**(2): p. 253-9.
56. Wolfrum, C., et al., *Foxa2 regulates lipid metabolism and ketogenesis in the liver during fasting and in diabetes.* Nature, 2004. **432**(7020): p. 1027-32.
57. Gallwitz, B., *GLP-1 agonists and dipeptidyl-peptidase IV inhibitors.* Handb Exp Pharmacol, 2011(203): p. 53-74.
58. Zhang, Y., et al., *Metformin interacts with AMPK through binding to gamma subunit.* Mol Cell Biochem, 2012. **368**(1-2): p. 69-76.
59. LeBrasseur, N.K., et al., *Thiazolidinediones can rapidly activate AMP-activated protein kinase in mammalian tissues.* Am J Physiol Endocrinol Metab, 2006. **291**(1): p. E175-81.
60. Yoon, M.J., et al., *Adiponectin increases fatty acid oxidation in skeletal muscle cells by sequential activation of AMP-activated protein kinase, p38 mitogen-activated protein kinase, and peroxisome proliferator-activated receptor alpha.* Diabetes, 2006. **55**(9): p. 2562-70.
61. Oakhill, J.S., et al., *AMPK is a direct adenylate charge-regulated protein kinase.* Science, 2011. **332**(6036): p. 1433-5.
62. Viollet, B. and F. Andreelli, *AMP-activated protein kinase and metabolic control.* Handb Exp Pharmacol, 2011(203): p. 303-30.
63. Carling, D., et al., *AMP-activated protein kinase: nature's energy sensor.* Nat Chem Biol, 2011. **7**(8): p. 512-8.
64. Lizcano, J.M., et al., *LKB1 is a master kinase that activates 13 kinases of the AMPK subfamily, including MARK/PAR-1.* Embo j, 2004. **23**(4): p. 833-43.
65. Woods, A., et al., *LKB1 is the upstream kinase in the AMP-activated protein kinase cascade.* Curr Biol, 2003. **13**(22): p. 2004-8.
66. Lan, F., et al., *SIRT1 modulation of the acetylation status, cytosolic localization, and activity of LKB1. Possible role in AMP-activated protein kinase activation.* J Biol Chem, 2008. **283**(41): p. 27628-35.
67. Winder, W.W., et al., *Activation of AMP-activated protein kinase increases mitochondrial enzymes in skeletal muscle.* J Appl Physiol (1985), 2000. **88**(6): p. 2219-26.
68. Ruderman, N.B., et al., *AMPK as a metabolic switch in rat muscle, liver and adipose tissue after exercise.* Acta Physiol Scand, 2003. **178**(4): p. 435-42.
69. Rosen, E.D., et al., *Transcriptional regulation of adipogenesis.* Genes Dev, 2000. **14**(11): p. 1293-307.
70. Habinowski, S.A. and L.A. Witters, *The effects of AICAR on adipocyte differentiation of 3T3-L1 cells.* Biochem Biophys Res Commun, 2001. **286**(5): p. 852-6.
71. Dagon, Y., Y. Avraham, and E.M. Berry, *AMPK activation regulates apoptosis, adipogenesis, and lipolysis by eIF2alpha in adipocytes.* Biochem Biophys Res Commun, 2006. **340**(1): p. 43-7.
72. Kajita, K., et al., *Effect of fasting on PPARgamma and AMPK activity in adipocytes.* Diabetes Res Clin Pract, 2008. **81**(2): p. 144-9.
73. Laplante, M. and D.M. Sabatini, *mTOR signaling at a glance.* J Cell Sci, 2009. **122**(Pt 20): p. 3589-94.

74. Sengupta, S., T.R. Peterson, and D.M. Sabatini, *Regulation of the mTOR complex 1 pathway by nutrients, growth factors, and stress.* Mol Cell, 2010. **40**(2): p. 310-22.
75. Zoncu, R., A. Efeyan, and D.M. Sabatini, *mTOR: from growth signal integration to cancer, diabetes and ageing.* Nat Rev Mol Cell Biol, 2011. **12**(1): p. 21-35.
76. Laplante, M. and D.M. Sabatini, *An emerging role of mTOR in lipid biosynthesis.* Curr Biol, 2009. **19**(22): p. R1046-52.
77. Sengupta, S., et al., *mTORC1 controls fasting-induced ketogenesis and its modulation by ageing.* Nature, 2010. **468**(7327): p. 1100-4.
78. Mihaylova, M.M. and R.J. Shaw, *The AMPK signalling pathway coordinates cell growth, autophagy and metabolism.* Nat Cell Biol, 2011. **13**(9): p. 1016-23.
79. Sarbassov, D.D., et al., *Phosphorylation and regulation of Akt/PKB by the rictor-mTOR complex.* Science, 2005. **307**(5712): p. 1098-101.
80. Kumar, A., et al., *Fat cell-specific ablation of rictor in mice impairs insulin-regulated fat cell and whole-body glucose and lipid metabolism.* Diabetes, 2010. **59**(6): p. 1397-406.
81. Acosta-Jaquez, H.A., et al., *Site-specific mTOR phosphorylation promotes mTORC1-mediated signaling and cell growth.* Mol Cell Biol, 2009. **29**(15): p. 4308-24.
82. Cheng, S.W., et al., *Thr2446 is a novel mammalian target of rapamycin (mTOR) phosphorylation site regulated by nutrient status.* J Biol Chem, 2004. **279**(16): p. 15719-22.
83. Saha, A.K., et al., *Insulin resistance due to nutrient excess: is it a consequence of AMPK downregulation?* Cell Cycle, 2011. **10**(20): p. 3447-51.
84. Li, S., M.S. Brown, and J.L. Goldstein, *Bifurcation of insulin signaling pathway in rat liver: mTORC1 required for stimulation of lipogenesis, but not inhibition of gluconeogenesis.* Proc Natl Acad Sci U S A, 2010. **107**(8): p. 3441-6.
85. Yoon, M., *The role of PPARalpha in lipid metabolism and obesity: focusing on the effects of estrogen on PPARalpha actions.* Pharmacol Res, 2009. **60**(3): p. 151-9.
86. Sugden, M.C., M.G. Zariwala, and M.J. Holness, *PPARs and the orchestration of metabolic fuel selection.* Pharmacol Res, 2009. **60**(3): p. 141-50.
87. Duncan, J.G., *Peroxisome proliferator activated receptor-alpha (PPARalpha) and PPAR gamma coactivator-1alpha (PGC-1alpha) regulation of cardiac metabolism in diabetes.* Pediatr Cardiol, 2011. **32**(3): p. 323-8.
88. Sugden, M.C. and M.J. Holness, *Potential role of peroxisome proliferator-activated receptor-alpha in the modulation of glucose-stimulated insulin secretion.* Diabetes, 2004. **53 Suppl 1**: p. S71-81.
89. Tyagi, S., et al., *The peroxisome proliferator-activated receptor: A family of nuclear receptors role in various diseases.* J Adv Pharm Technol Res, 2011. **2**(4): p. 236-40.
90. Bouwens, M., L.A. Afman, and M. Muller, *Fasting induces changes in peripheral blood mononuclear cell gene expression profiles related to increases in fatty acid beta-oxidation: functional role of peroxisome proliferator activated receptor alpha in human peripheral blood mononuclear cells.* Am J Clin Nutr, 2007. **86**(5): p. 1515-23.

91. Leone, T.C., C.J. Weinheimer, and D.P. Kelly, *A critical role for the peroxisome proliferator-activated receptor alpha (PPARalpha) in the cellular fasting response: the PPARalpha-null mouse as a model of fatty acid oxidation disorders.* Proc Natl Acad Sci U S A, 1999. **96**(13): p. 7473-8.
92. Sugden, M.C., et al., *Peroxisome-proliferator-activated receptor-alpha (PPARalpha) deficiency leads to dysregulation of hepatic lipid and carbohydrate metabolism by fatty acids and insulin.* Biochem J, 2002. **364**(Pt 2): p. 361-8.
93. Ye, J.M., et al., *Peroxisome proliferator-activated receptor (PPAR)-alpha activation lowers muscle lipids and improves insulin sensitivity in high fat-fed rats: comparison with PPAR-gamma activation.* Diabetes, 2001. **50**(2): p. 411-7.
94. Tsuchida, A., et al., *Peroxisome proliferator-activated receptor (PPAR)alpha activation increases adiponectin receptors and reduces obesity-related inflammation in adipose tissue: comparison of activation of PPARalpha, PPARgamma, and their combination.* Diabetes, 2005. **54**(12): p. 3358-70.
95. Finck, B.N. and D.P. Kelly, *PGC-1 coactivators: inducible regulators of energy metabolism in health and disease.* J Clin Invest, 2006. **116**(3): p. 615-22.
96. Yoon, J.C., et al., *Control of hepatic gluconeogenesis through the transcriptional coactivator PGC-1.* Nature, 2001. **413**(6852): p. 131-8.
97. Leone, T.C., et al., *PGC-1alpha deficiency causes multi-system energy metabolic derangements: muscle dysfunction, abnormal weight control and hepatic steatosis.* PLoS Biol, 2005. **3**(4): p. e101.
98. Mattison, J.A., et al., *Impact of caloric restriction on health and survival in rhesus monkeys from the NIA study.* Nature, 2012. **489**(7415): p. 318-21.
99. McDonald, R.B. and J.J. Ramsey, *Honoring Clive McCay and 75 years of calorie restriction research.* J Nutr, 2010. **140**(7): p. 1205-10.
100. Colman, R.J., et al., *Caloric restriction delays disease onset and mortality in rhesus monkeys.* Science, 2009. **325**(5937): p. 201-4.
101. Berrington de Gonzalez, A., et al., *Body-mass index and mortality among 1.46 million white adults.* N Engl J Med, 2010. **363**(23): p. 2211-9.
102. Guarente, L., *Sirtuins as potential targets for metabolic syndrome.* Nature, 2006. **444**(7121): p. 868-74.
103. Ralser, M., S. Michel, and M. Breitenbach, *Sirtuins as regulators of the yeast metabolic network.* Front Pharmacol, 2012. **3**: p. 32.
104. Rine, J., et al., *A suppressor of mating-type locus mutations in Saccharomyces cerevisiae: evidence for and identification of cryptic mating-type loci.* Genetics, 1979. **93**(4): p. 877-901.
105. Michan, S. and D. Sinclair, *Sirtuins in mammals: insights into their biological function.* Biochem J, 2007. **404**(1): p. 1-13.
106. Hirschey, M.D., *Old enzymes, new tricks: sirtuins are NAD(+)-dependent de-acylases.* Cell Metab, 2011. **14**(6): p. 718-9.
107. Dominy, J.E., Jr., et al., *The deacetylase Sirt6 activates the acetyltransferase GCN5 and suppresses hepatic gluconeogenesis.* Mol Cell, 2012. **48**(6): p. 900-13.
108. Kim, W. and J.E. Kim, *SIRT7 an emerging sirtuin: deciphering newer roles.* J Physiol Pharmacol, 2013. **64**(5): p. 531-4.
109. Li, X. and N. Kazgan, *Mammalian sirtuins and energy metabolism.* Int J Biol Sci, 2011. **7**(5): p. 575-87.

110. Lin, S.J., et al., *Calorie restriction extends yeast life span by lowering the level of NADH.* Genes Dev, 2004. **18**(1): p. 12-6.
111. Picard, F., et al., *Sirt1 promotes fat mobilization in white adipocytes by repressing PPAR-gamma.* Nature, 2004. **429**(6993): p. 771-6.
112. Nisoli, E., et al., *Calorie restriction promotes mitochondrial biogenesis by inducing the expression of eNOS.* Science, 2005. **310**(5746): p. 314-7.
113. Shi, T., et al., *SIRT3, a mitochondrial sirtuin deacetylase, regulates mitochondrial function and thermogenesis in brown adipocytes.* J Biol Chem, 2005. **280**(14): p. 13560-7.
114. Tissenbaum, H.A. and L. Guarente, *Increased dosage of a sir-2 gene extends lifespan in Caenorhabditis elegans.* Nature, 2001. **410**(6825): p. 227-30.
115. Rogina, B. and S.L. Helfand, *Sir2 mediates longevity in the fly through a pathway related to calorie restriction.* Proc Natl Acad Sci U S A, 2004. **101**(45): p. 15998-6003.
116. Lin, S.J., P.A. Defossez, and L. Guarente, *Requirement of NAD and SIR2 for life-span extension by calorie restriction in Saccharomyces cerevisiae.* Science, 2000. **289**(5487): p. 2126-8.
117. Wang, Y. and H.A. Tissenbaum, *Overlapping and distinct functions for a Caenorhabditis elegans SIR2 and DAF-16/FOXO.* Mech Ageing Dev, 2006. **127**(1): p. 48-56.
118. Kaeberlein, M., et al., *Regulation of yeast replicative life span by TOR and Sch9 in response to nutrients.* Science, 2005. **310**(5751): p. 1193-6.
119. Kenyon, C.J., *The genetics of ageing.* Nature, 2010. **464**(7288): p. 504-12.
120. Burnett, C., et al., *Absence of effects of Sir2 overexpression on lifespan in C. elegans and Drosophila.* Nature, 2011. **477**(7365): p. 482-5.
121. Barzilai, N., et al., *The critical role of metabolic pathways in aging.* Diabetes, 2012. **61**(6): p. 1315-22.
122. Howitz, K.T., et al., *Small molecule activators of sirtuins extend Saccharomyces cerevisiae lifespan.* Nature, 2003. **425**(6954): p. 191-6.
123. Baur, J.A., et al., *Resveratrol improves health and survival of mice on a high-calorie diet.* Nature, 2006. **444**(7117): p. 337-42.
124. Minor, R.K., et al., *SRT1720 improves survival and healthspan of obese mice.* Sci Rep, 2011. **1**: p. 70.
125. Chen, D., et al., *Tissue-specific regulation of SIRT1 by calorie restriction.* Genes Dev, 2008. **22**(13): p. 1753-7.
126. Tauriainen, E., et al., *Distinct effects of calorie restriction and resveratrol on diet-induced obesity and Fatty liver formation.* J Nutr Metab, 2011. **2011**: p. 525094.
127. Yang, J., et al., *Activation of SIRT1 by resveratrol represses transcription of the gene for the cytosolic form of phosphoenolpyruvate carboxykinase (GTP) by deacetylating hepatic nuclear factor 4alpha.* J Biol Chem, 2009. **284**(40): p. 27042-53.
128. Liu, Y., et al., *A fasting inducible switch modulates gluconeogenesis via activator/coactivator exchange.* Nature, 2008. **456**(7219): p. 269-73.
129. Rodgers, J.T., et al., *Nutrient control of glucose homeostasis through a complex of PGC-1alpha and SIRT1.* Nature, 2005. **434**(7029): p. 113-8.
130. Caton, P.W., et al., *Nicotinamide mononucleotide protects against pro-inflammatory cytokine-mediated impairment of mouse islet function.* Diabetologia, 2011. **54**(12): p. 3083-92.

131. Rodgers, J.T. and P. Puigserver, *Fasting-dependent glucose and lipid metabolic response through hepatic sirtuin 1.* Proc Natl Acad Sci U S A, 2007. **104**(31): p. 12861-6.
132. Erion, D.M., et al., *SirT1 knockdown in liver decreases basal hepatic glucose production and increases hepatic insulin responsiveness in diabetic rats.* Proc Natl Acad Sci U S A, 2009. **106**(27): p. 11288-93.
133. Purushotham, A., et al., *Hepatocyte-specific deletion of SIRT1 alters fatty acid metabolism and results in hepatic steatosis and inflammation.* Cell Metab, 2009. **9**(4): p. 327-38.
134. Li, X., et al., *SIRT1 deacetylates and positively regulates the nuclear receptor LXR.* Mol Cell, 2007. **28**(1): p. 91-106.
135. Wang, R.H., C. Li, and C.X. Deng, *Liver steatosis and increased ChREBP expression in mice carrying a liver specific SIRT1 null mutation under a normal feeding condition.* Int J Biol Sci, 2010. **6**(7): p. 682-90.
136. Li, Y., et al., *Hepatic overexpression of SIRT1 in mice attenuates endoplasmic reticulum stress and insulin resistance in the liver.* Faseb j, 2011. **25**(5): p. 1664-79.
137. Lerin, C., et al., *GCN5 acetyltransferase complex controls glucose metabolism through transcriptional repression of PGC-1alpha.* Cell Metab, 2006. **3**(6): p. 429-38.
138. Gerhart-Hines, Z., et al., *Metabolic control of muscle mitochondrial function and fatty acid oxidation through SIRT1/PGC-1alpha.* Embo j, 2007. **26**(7): p. 1913-23.
139. Dominy, J.E., Jr., et al., *Nutrient-dependent regulation of PGC-1alpha's acetylation state and metabolic function through the enzymatic activities of Sirt1/GCN5.* Biochim Biophys Acta, 2010. **1804**(8): p. 1676-83.
140. Nemoto, S., M.M. Fergusson, and T. Finkel, *SIRT1 functionally interacts with the metabolic regulator and transcriptional coactivator PGC-1{alpha}.* J Biol Chem, 2005. **280**(16): p. 16456-60.
141. Schenk, S., et al., *Sirt1 enhances skeletal muscle insulin sensitivity in mice during caloric restriction.* J Clin Invest, 2011. **121**(11): p. 4281-8.
142. Odegaard, J.I. and A. Chawla, *Mechanisms of macrophage activation in obesity-induced insulin resistance.* Nat Clin Pract Endocrinol Metab, 2008. **4**(11): p. 619-26.
143. Konner, A.C. and J.C. Bruning, *Selective insulin and leptin resistance in metabolic disorders.* Cell Metab, 2012. **16**(2): p. 144-52.
144. Tajtakova, M., et al., *Serum levels of leptin, adiponectin, retinol binding protein 4 and leptin/adiponectin molar ratio as another possible marker of insulin resistance in obese.* Bratisl Lek Listy, 2010. **111**(4): p. 212-5.
145. Qiao, L. and J. Shao, *SIRT1 regulates adiponectin gene expression through Foxo1-C/enhancer-binding protein alpha transcriptional complex.* J Biol Chem, 2006. **281**(52): p. 39915-24.
146. Suchankova, G., et al., *Concurrent regulation of AMP-activated protein kinase and SIRT1 in mammalian cells.* Biochem Biophys Res Commun, 2009. **378**(4): p. 836-41.
147. Zang, M., et al., *AMP-activated protein kinase is required for the lipid-lowering effect of metformin in insulin-resistant human HepG2 cells.* J Biol Chem, 2004. **279**(46): p. 47898-905.

148. Hou, X., et al., *SIRT1 regulates hepatocyte lipid metabolism through activating AMP-activated protein kinase.* J Biol Chem, 2008. **283**(29): p. 20015-26.
149. Ruderman, N.B., et al., *AMPK and SIRT1: a long-standing partnership?* Am J Physiol Endocrinol Metab, 2010. **298**(4): p. E751-60.
150. Fulco, M., et al., *Glucose restriction inhibits skeletal myoblast differentiation by activating SIRT1 through AMPK-mediated regulation of Nampt.* Dev Cell, 2008. **14**(5): p. 661-73.
151. Canto, C., et al., *AMPK regulates energy expenditure by modulating NAD+ metabolism and SIRT1 activity.* Nature, 2009. **458**(7241): p. 1056-60.
152. Iwabu, M., et al., *Adiponectin and AdipoR1 regulate PGC-1alpha and mitochondria by Ca(2+) and AMPK/SIRT1.* Nature, 2010. **464**(7293): p. 1313-9.
153. Lombard, D.B., et al., *Mammalian Sir2 homolog SIRT3 regulates global mitochondrial lysine acetylation.* Mol Cell Biol, 2007. **27**(24): p. 8807-14.
154. Nogueiras, R., et al., *Sirtuin 1 and sirtuin 3: physiological modulators of metabolism.* Physiol Rev, 2012. **92**(3): p. 1479-514.
155. Mailloux, R.J., et al., *The tricarboxylic acid cycle, an ancient metabolic network with a novel twist.* PLoS One, 2007. **2**(8): p. e690.
156. Kawamura, Y., et al., *Sirt3 protects in vitro-fertilized mouse preimplantation embryos against oxidative stress-induced p53-mediated developmental arrest.* J Clin Invest, 2010. **120**(8): p. 2817-28.
157. Qiu, X., et al., *Calorie restriction reduces oxidative stress by SIRT3-mediated SOD2 activation.* Cell Metab, 2010. **12**(6): p. 662-7.
158. Someya, S., et al., *Sirt3 mediates reduction of oxidative damage and prevention of age-related hearing loss under caloric restriction.* Cell, 2010. **143**(5): p. 802-12.
159. Ahn, B.H., et al., *A role for the mitochondrial deacetylase Sirt3 in regulating energy homeostasis.* Proc Natl Acad Sci U S A, 2008. **105**(38): p. 14447-52.
160. Shimazu, T., et al., *SIRT3 deacetylates mitochondrial 3-hydroxy-3-methylglutaryl CoA synthase 2 and regulates ketone body production.* Cell Metab, 2010. **12**(6): p. 654-61.
161. Jing, E., et al., *Sirt3 regulates metabolic flexibility of skeletal muscle through reversible enzymatic deacetylation.* Diabetes, 2013. **62**(10): p. 3404-17.
162. Kendrick, A.A., et al., *Fatty liver is associated with reduced SIRT3 activity and mitochondrial protein hyperacetylation.* Biochem J, 2011. **433**(3): p. 505-14.
163. Barroso, E., et al., *The PPARbeta/delta activator GW501516 prevents the down-regulation of AMPK caused by a high-fat diet in liver and amplifies the PGC-1alpha-Lipin 1-PPARalpha pathway leading to increased fatty acid oxidation.* Endocrinology, 2011. **152**(5): p. 1848-59.
164. Lee, W.J., et al., *AMPK activation increases fatty acid oxidation in skeletal muscle by activating PPARalpha and PGC-1.* Biochem Biophys Res Commun, 2006. **340**(1): p. 291-5.
165. Canto, C. and J. Auwerx, *Calorie restriction: is AMPK a key sensor and effector?* Physiology (Bethesda), 2011. **26**(4): p. 214-24.
166. Canto, C., et al., *Interdependence of AMPK and SIRT1 for metabolic adaptation to fasting and exercise in skeletal muscle.* Cell Metab, 2010. **11**(3): p. 213-9.

167. Hirschey, M.D., et al., *SIRT3 regulates mitochondrial fatty-acid oxidation by reversible enzyme deacetylation.* Nature, 2010. **464**(7285): p. 121-5.
168. Kersten, S., et al., *Peroxisome proliferator-activated receptor alpha mediates the adaptive response to fasting.* J Clin Invest, 1999. **103**(11): p. 1489-98.
169. Jing, E., et al., *Sirtuin-3 (Sirt3) regulates skeletal muscle metabolism and insulin signaling via altered mitochondrial oxidation and reactive oxygen species production.* Proc Natl Acad Sci U S A, 2011. **108**(35): p. 14608-13.
170. Hu, X., et al., *AMP activated protein kinase-alpha2 regulates expression of estrogen-related receptor-alpha, a metabolic transcription factor related to heart failure development.* Hypertension, 2011. **58**(4): p. 696-703.
171. Weinstein, I.B., et al., *Type C virus from cell cultures of chemically induced rat hepatomas.* Science, 1972. **178**(4065): p. 1098-100.
172. Yaffe, D., *Retention of differentiation potentialities during prolonged cultivation of myogenic cells.* Proc Natl Acad Sci U S A, 1968. **61**(2): p. 477-83.
173. Shi, H., et al., *Sexually dimorphic responses to fat loss after caloric restriction or surgical lipectomy.* Am J Physiol Endocrinol Metab, 2007. **293**(1): p. E316-26.
174. Miniou, P., et al., *Gene targeting restricted to mouse striated muscle lineage.* Nucleic Acids Res, 1999. **27**(19): p. e27.
175. Viollet, B., et al., *The AMP-activated protein kinase alpha2 catalytic subunit controls whole-body insulin sensitivity.* J Clin Invest, 2003. **111**(1): p. 91-8.
176. Jorgensen, S.B., et al., *Knockout of the alpha2 but not alpha1 5'-AMP-activated protein kinase isoform abolishes 5-aminoimidazole-4-carboxamide-1-beta-4-ribofuranosidebut not contraction-induced glucose uptake in skeletal muscle.* J Biol Chem, 2004. **279**(2): p. 1070-9.
177. Islam, K.K., et al., *Deficiency of PPARalpha disturbs the response of lipogenic flux and of lipogenic and cholesterogenic gene expression to dietary cholesterol in mouse white adipose tissue.* Biochim Biophys Acta, 2005. **1734**(3): p. 259-68.
178. Gonzalez, F.J., *Recent update on the PPAR alpha-null mouse.* Biochimie, 1997. **79**(2-3): p. 139-44.
179. Revollo, J.R., et al., *Nampt/PBEF/Visfatin regulates insulin secretion in beta cells as a systemic NAD biosynthetic enzyme.* Cell Metab, 2007. **6**(5): p. 363-75.
180. Trinder, P., *Determination of blood glucose using an oxidase-peroxidase system with a non-carcinogenic chromogen.* J Clin Pathol, 1969. **22**(2): p. 158-61.
181. Lowry, O.H., et al., *Protein measurement with the Folin phenol reagent.* J Biol Chem, 1951. **193**(1): p. 265-75.
182. Laemmli, U.K., *Cleavage of structural proteins during the assembly of the head of bacteriophage T4.* Nature, 1970. **227**(5259): p. 680-5.
183. Livak, K.J. and T.D. Schmittgen, *Analysis of relative gene expression data using real-time quantitative PCR and the 2(-Delta Delta C(T)) Method.* Methods, 2001. **25**(4): p. 402-8.
184. Braissant, O., et al., *Differential expression of peroxisome proliferator-activated receptors (PPARs): tissue distribution of PPAR-alpha, -beta, and -gamma in the adult rat.* Endocrinology, 1996. **137**(1): p. 354-66.

185. Sugden, M.C. and M.J. Holness, *Mechanisms underlying regulation of the expression and activities of the mammalian pyruvate dehydrogenase kinases.* Arch Physiol Biochem, 2006. **112**(3): p. 139-49.
186. Frescas, D., L. Valenti, and D. Accili, *Nuclear trapping of the forkhead transcription factor FoxO1 via Sirt-dependent deacetylation promotes expression of glucogenetic genes.* J Biol Chem, 2005. **280**(21): p. 20589-95.
187. van den Berghe, G., *The role of the liver in metabolic homeostasis: implications for inborn errors of metabolism.* J Inherit Metab Dis, 1991. **14**(4): p. 407-20.
188. Browning, J.D. and J.D. Horton, *Molecular mediators of hepatic steatosis and liver injury.* J Clin Invest, 2004. **114**(2): p. 147-52.
189. Samuel, V.T., et al., *Mechanism of hepatic insulin resistance in non-alcoholic fatty liver disease.* J Biol Chem, 2004. **279**(31): p. 32345-53.
190. Lee, A.H., et al., *Regulation of hepatic lipogenesis by the transcription factor XBP1.* Science, 2008. **320**(5882): p. 1492-6.
191. Guan, K.L. and Y. Xiong, *Regulation of intermediary metabolism by protein acetylation.* Trends Biochem Sci, 2011. **36**(2): p. 108-16.
192. Lee, C.W., et al., *AMPK promotes p53 acetylation via phosphorylation and inactivation of SIRT1 in liver cancer cells.* Cancer Res, 2012. **72**(17): p. 4394-404.
193. Wang, S., P. Song, and M.H. Zou, *Inhibition of AMP-activated protein kinase alpha (AMPKalpha) by doxorubicin accentuates genotoxic stress and cell death in mouse embryonic fibroblasts and cardiomyocytes: role of p53 and SIRT1.* J Biol Chem, 2012. **287**(11): p. 8001-12.
194. Finley, L.W., et al., *SIRT3 opposes reprogramming of cancer cell metabolism through HIF1alpha destabilization.* Cancer Cell, 2011. **19**(3): p. 416-28.
195. Bao, J., et al., *SIRT3 is regulated by nutrient excess and modulates hepatic susceptibility to lipotoxicity.* Free Radic Biol Med, 2010. **49**(7): p. 1230-7.
196. Yabaluri, N. and M.D. Bashyam, *Hormonal regulation of gluconeogenic gene transcription in the liver.* J Biosci, 2010. **35**(3): p. 473-84.
197. Lombard, D.B., et al., *SIRT6 in DNA repair, metabolism and ageing.* J Intern Med, 2008. **263**(2): p. 128-41.
198. Guarente, L., *Sir2 links chromatin silencing, metabolism, and aging.* Genes Dev, 2000. **14**(9): p. 1021-6.
199. Deng, X.Q., L.L. Chen, and N.X. Li, *The expression of SIRT1 in nonalcoholic fatty liver disease induced by high-fat diet in rats.* Liver Int, 2007. **27**(5): p. 708-15.
200. Taniguchi, C.M., et al., *Divergent regulation of hepatic glucose and lipid metabolism by phosphoinositide 3-kinase via Akt and PKClambda/zeta.* Cell Metab, 2006. **3**(5): p. 343-53.
201. Oakes, N.D., et al., *Development and initial evaluation of a novel method for assessing tissue-specific plasma free fatty acid utilization in vivo using (R)-2-bromopalmitate tracer.* J Lipid Res, 1999. **40**(6): p. 1155-69.
202. Paton, C.M. and J.M. Ntambi, *Loss of stearoyl-CoA desaturase activity leads to free cholesterol synthesis through increased Xbp-1 splicing.* Am J Physiol Endocrinol Metab, 2010. **299**(6): p. E1066-75.
203. Wang, L., et al., *Mammalian target of rapamycin complex 1 (mTORC1) activity is associated with phosphorylation of raptor by mTOR.* J Biol Chem, 2009. **284**(22): p. 14693-7.

204. Sage, A.T., et al., *Metabolic syndrome and acute hyperglycemia are associated with endoplasmic reticulum stress in human mononuclear cells.* Obesity (Silver Spring), 2012. **20**(4): p. 748-55.
205. Kong, X., et al., *Sirtuin 3, a new target of PGC-1alpha, plays an important role in the suppression of ROS and mitochondrial biogenesis.* PLoS One, 2010. **5**(7): p. e11707.
206. Han, D.H., et al., *Deficiency of the mitochondrial electron transport chain in muscle does not cause insulin resistance.* PLoS One, 2011. **6**(5): p. e19739.
207. Zhang, D., et al., *Mitochondrial dysfunction due to long-chain Acyl-CoA dehydrogenase deficiency causes hepatic steatosis and hepatic insulin resistance.* Proc Natl Acad Sci U S A, 2007. **104**(43): p. 17075-80.
208. Yoshino, J., et al., *Nicotinamide mononucleotide, a key NAD(+) intermediate, treats the pathophysiology of diet- and age-induced diabetes in mice.* Cell Metab, 2011. **14**(4): p. 528-36.
209. Haigis, M.C. and D.A. Sinclair, *Mammalian sirtuins: biological insights and disease relevance.* Annu Rev Pathol, 2010. **5**: p. 253-95.
210. Draznin, B., *Molecular mechanisms of insulin resistance: serine phosphorylation of insulin receptor substrate-1 and increased expression of p85alpha: the two sides of a coin.* Diabetes, 2006. **55**(8): p. 2392-7.
211. Frojdo, S., et al., *Phosphoinositide 3-kinase as a novel functional target for the regulation of the insulin signaling pathway by SIRT1.* Mol Cell Endocrinol, 2011. **335**(2): p. 166-76.
212. Draznin, B., et al., *Effect of dietary macronutrient composition on AMPK and SIRT1 expression and activity in human skeletal muscle.* Horm Metab Res, 2012. **44**(9): p. 650-5.
213. Smith, D.L., Jr., T.R. Nagy, and D.B. Allison, *Calorie restriction: what recent results suggest for the future of ageing research.* Eur J Clin Invest, 2010. **40**(5): p. 440-50.
214. Hammer, S., et al., *Prolonged caloric restriction in obese patients with type 2 diabetes mellitus decreases myocardial triglyceride content and improves myocardial function.* J Am Coll Cardiol, 2008. **52**(12): p. 1006-12.
215. Jazet, I.M., et al., *Loss of 50% of excess weight using a very low energy diet improves insulin-stimulated glucose disposal and skeletal muscle insulin signalling in obese insulin-treated type 2 diabetic patients.* Diabetologia, 2008. **51**(2): p. 309-19.
216. Larson-Meyer, D.E., et al., *Effect of calorie restriction with or without exercise on insulin sensitivity, beta-cell function, fat cell size, and ectopic lipid in overweight subjects.* Diabetes Care, 2006. **29**(6): p. 1337-44.
217. Weiss, E.P., et al., *Improvements in glucose tolerance and insulin action induced by increasing energy expenditure or decreasing energy intake: a randomized controlled trial.* Am J Clin Nutr, 2006. **84**(5): p. 1033-42.
218. Marchal, J., et al., *Effects of chronic calorie restriction or dietary resveratrol supplementation on insulin sensitivity markers in a primate, Microcebus murinus.* PLoS One, 2012. **7**(3): p. e34289.
219. Shulman, G.I., et al., *Quantitation of muscle glycogen synthesis in normal subjects and subjects with non-insulin-dependent diabetes by 13C nuclear magnetic resonance spectroscopy.* N Engl J Med, 1990. **322**(4): p. 223-8.
220. O'Neill, H.M., *AMPK and Exercise: Glucose Uptake and Insulin Sensitivity.* Diabetes Metab J, 2013. **37**(1): p. 1-21.

221. O'Neill, H.M., G.P. Holloway, and G.R. Steinberg, *AMPK regulation of fatty acid metabolism and mitochondrial biogenesis: implications for obesity.* Mol Cell Endocrinol, 2013. **366**(2): p. 135-51.
222. Pessin, J.E. and A.R. Saltiel, *Signaling pathways in insulin action: molecular targets of insulin resistance.* J Clin Invest, 2000. **106**(2): p. 165-9.
223. Rennie, M.J., *Exercise- and nutrient-controlled mechanisms involved in maintenance of the musculoskeletal mass.* Biochem Soc Trans, 2007. **35**(Pt 5): p. 1302-5.
224. Yamauchi, T., et al., *Cloning of adiponectin receptors that mediate antidiabetic metabolic effects.* Nature, 2003. **423**(6941): p. 762-9.
225. Hutchinson, D.S. and T. Bengtsson, *AMP-activated protein kinase activation by adrenoceptors in L6 skeletal muscle cells: mediation by alpha1-adrenoceptors causing glucose uptake.* Diabetes, 2006. **55**(3): p. 682-90.
226. Yang, H., et al., *Nutrient-sensitive mitochondrial NAD+ levels dictate cell survival.* Cell, 2007. **130**(6): p. 1095-107.
227. Zhang, T., et al., *Enzymes in the NAD+ salvage pathway regulate SIRT1 activity at target gene promoters.* J Biol Chem, 2009. **284**(30): p. 20408-17.
228. Xiao, C., et al., *SIRT6 deficiency results in severe hypoglycemia by enhancing both basal and insulin-stimulated glucose uptake in mice.* J Biol Chem, 2010. **285**(47): p. 36776-84.
229. Giralt, A., et al., *Peroxisome proliferator-activated receptor-gamma coactivator-1alpha controls transcription of the Sirt3 gene, an essential component of the thermogenic brown adipocyte phenotype.* J Biol Chem, 2011. **286**(19): p. 16958-66.
230. Ning, J. and D.R. Clemmons, *AMP-activated protein kinase inhibits IGF-I signaling and protein synthesis in vascular smooth muscle cells via stimulation of insulin receptor substrate 1 S794 and tuberous sclerosis 2 S1345 phosphorylation.* Mol Endocrinol, 2010. **24**(6): p. 1218-29.
231. Wu, L., et al., *Activation of SIRT1 protects pancreatic beta-cells against palmitate-induced dysfunction.* Biochim Biophys Acta, 2012. **1822**(11): p. 1815-25.
232. Simic, P., et al., *SIRT1 regulates differentiation of mesenchymal stem cells by deacetylating beta-catenin.* EMBO Mol Med, 2013. **5**(3): p. 430-40.
233. Yamauchi, T., et al., *Adiponectin stimulates glucose utilization and fatty-acid oxidation by activating AMP-activated protein kinase.* Nat Med, 2002. **8**(11): p. 1288-95.
234. Kubota, N., et al., *Adiponectin stimulates AMP-activated protein kinase in the hypothalamus and increases food intake.* Cell Metab, 2007. **6**(1): p. 55-68.
235. Wang, P., et al., *Loss of AMP-activated protein kinase-alpha2 impairs the insulin-sensitizing effect of calorie restriction in skeletal muscle.* Diabetes, 2012. **61**(5): p. 1051-61.
236. Chopra, I., et al., *Phosphorylation of the insulin receptor by AMP-activated protein kinase (AMPK) promotes ligand-independent activation of the insulin signalling pathway in rodent muscle.* Diabetologia, 2012. **55**(3): p. 783-94.
237. Tremblay, F., et al., *Activation of the mammalian target of rapamycin pathway acutely inhibits insulin signaling to Akt and glucose transport in 3T3-L1 and human adipocytes.* Endocrinology, 2005. **146**(3): p. 1328-37.
238. Lee, J.O., et al., *Metformin induces Rab4 through AMPK and modulates GLUT4 translocation in skeletal muscle cells.* J Cell Physiol, 2011. **226**(4): p. 974-81.

239. Burcelin, R., et al., *GLUT4, AMP kinase, but not the insulin receptor, are required for hepatoportal glucose sensor-stimulated muscle glucose utilization.* J Clin Invest, 2003. **111**(10): p. 1555-62.
240. Moore, M.C., et al., *Regulation of hepatic glucose uptake and storage in vivo.* Adv Nutr, 2012. **3**(3): p. 286-94.
241. Plomgaard, P., P.A. Halban, and K. Bouzakri, *Bimodal impact of skeletal muscle on pancreatic beta-cell function in health and disease.* Diabetes Obes Metab, 2012. **14 Suppl 3**: p. 78-84.
242. Benton, C.R., et al., *Increased levels of peroxisome proliferator-activated receptor gamma, coactivator 1 alpha (PGC-1alpha) improve lipid utilisation, insulin signalling and glucose transport in skeletal muscle of lean and insulin-resistant obese Zucker rats.* Diabetologia, 2010. **53**(9): p. 2008-19.
243. Michael, L.F., et al., *Restoration of insulin-sensitive glucose transporter (GLUT4) gene expression in muscle cells by the transcriptional coactivator PGC-1.* Proc Natl Acad Sci U S A, 2001. **98**(7): p. 3820-5.
244. Joseph, A.M., et al., *The impact of aging on mitochondrial function and biogenesis pathways in skeletal muscle of sedentary high- and low-functioning elderly individuals.* Aging Cell, 2012. **11**(5): p. 801-9.
245. Rashid, A., et al., *Resveratrol enhances prostate cancer cell response to ionizing radiation. Modulation of the AMPK, Akt and mTOR pathways.* Radiat Oncol, 2011. **6**: p. 144.
246. Hotta, K., et al., *Plasma concentrations of a novel, adipose-specific protein, adiponectin, in type 2 diabetic patients.* Arterioscler Thromb Vasc Biol, 2000. **20**(6): p. 1595-9.
247. Cottrell, E.C. and S.E. Ozanne, *Early life programming of obesity and metabolic disease.* Physiol Behav, 2008. **94**(1): p. 17-28.
248. Fernandez-Twin, D.S., et al., *Maternal low-protein diet programs cardiac beta-adrenergic response and signaling in 3-mo-old male offspring.* American journal of physiology Regulatory, integrative and comparative physiology, 2006. **291**: p. R429-436.
249. Barker, D.J., *Obesity and early life.* Obes Rev, 2007. **8 Suppl 1**: p. 45-9.
250. Holness, M.J., M.L. Langdown, and M.C. Sugden, *Early-life programming of susceptibility to dysregulation of glucose metabolism and the development of Type 2 diabetes mellitus.* Biochem J, 2000. **349 Pt 3**: p. 657-65.
251. Hales, C.N. and D.J. Barker, *Type 2 (non-insulin-dependent) diabetes mellitus: the thrifty phenotype hypothesis.* Diabetologia 1992. **35**: p. 595-601.
252. Forsen, T., et al., *The fetal and childhood growth of persons who develop type 2 diabetes.* Ann Intern Med, 2000. **133**(3): p. 176-82.
253. Eguchi, J., et al., *Transcriptional control of adipose lipid handling by IRF4.* Cell Metab, 2011. **13**(3): p. 249-59.
254. Eguchi, J., et al., *Interferon regulatory factors are transcriptional regulators of adipogenesis.* Cell Metab, 2008. **7**(1): p. 86-94.
255. Bijland, S., S.J. Mancini, and I.P. Salt, *Role of AMP-activated protein kinase in adipose tissue metabolism and inflammation.* Clin Sci (Lond), 2013. **124**(8): p. 491-507.
256. Eguchi, J., et al., *Interferon regulatory factor 4 regulates obesity-induced inflammation through regulation of adipose tissue macrophage polarization.* Diabetes, 2013. **62**: p. 3394-3403.
257. Zhou, G., et al., *Role of AMP-activated protein kinase in mechanism of metformin action.* J Clin Invest, 2001. **108**(8): p. 1167-74.

258. Zhang, T., et al., *Maternal protein restriction permanently programs adipocyte growth and development in adult male rat offspring.* J Cell Biochem, 2007. **101**(2): p. 381-8.
259. Bol, V.V., B.M. Reusens, and C.A. Remacle, *Postnatal catch-up growth after fetal protein restriction programs proliferation of rat preadipocytes.* Obesity (Silver Spring), 2008. **16**(12): p. 2760-3.
260. Turer, A.T. and P.E. Scherer, *Adiponectin: mechanistic insights and clinical implications.* Diabetologia, 2012. **55**(9): p. 2319-26.
261. Qiao, L., et al., *Energy intake and adiponectin gene expression.* Am J Physiol Endocrinol Metab, 2011. **300**(5): p. E809-16.
262. Guerre-Millo, M., et al., *PPAR-alpha-null mice are protected from high-fat diet-induced insulin resistance.* Diabetes, 2001. **50**(12): p. 2809-14.
263. Leone, T.C., C.J. Weinheimer, and D.P. Kelly, *A critical role for the peroxisome proliferator-activated receptor alpha (PPARalpha) in the cellular fasting response: the PPARalpha-null mouse as a model of fatty acid oxidation disorders.* Proc Natl Acad Sci U S A 1999. **96**: p. 7473 –7478.
264. Sun, K., C.M. Kusminski, and P.E. Scherer, *Adipose tissue remodeling and obesity.* J Clin Invest, 2011. **121**(6): p. 2094-101.
265. Mittrucker, H.W., et al., *Requirement for the transcription factor LSIRF/IRF4 for mature B and T lymphocyte function.* Science, 1997. **275**(5299): p. 540-3.
266. Oakhill, J.S., et al., *beta-Subunit myristoylation is the gatekeeper for initiating metabolic stress sensing by AMP-activated protein kinase (AMPK).* Proc Natl Acad Sci U S A, 2010. **107**(45): p. 19237-41.
267. Akingbemi, B.T., *Adiponectin receptors in energy homeostasis and obesity pathogenesis.* Prog Mol Biol Transl Sci, 2013. **114**: p. 317-42.
268. McGarry, J.D. and D.W. Foster, *Regulation of hepatic fatty acid oxidation and ketone body production.* Annu Rev Biochem, 1980. **49**: p. 395-420.
269. Oakes, N.D., et al., *Mechanisms of liver and muscle insulin resistance induced by chronic high-fat feeding.* Diabetes, 1997. **46**(11): p. 1768-74.
270. Dietrich, L.S., et al., *Nicotinamide mononucleotide pyrophosphorylase activity in animal tissues.* J Biol Chem, 1966. **241**(1): p. 188-91.
271. Jayaram, H.N., P. Kusumanchi, and J.A. Yalowitz, *NMNAT expression and its relation to NAD metabolism.* Curr Med Chem, 2011. **18**(13): p. 1962-72.
272. Wang, R.H., et al., *Hepatic Sirt1 deficiency in mice impairs mTorc2/Akt signaling and results in hyperglycemia, oxidative damage, and insulin resistance.* J Clin Invest, 2011. **121**(11): p. 4477-90.
273. Savage, D.B., K.F. Petersen, and G.I. Shulman, *Mechanisms of insulin resistance in humans and possible links with inflammation.* Hypertension, 2005. **45**(5): p. 828-33.
274. Zhong, L., et al., *The histone deacetylase Sirt6 regulates glucose homeostasis via Hif1alpha.* Cell, 2010. **140**(2): p. 280-93.
275. Tarry-Adkins, J.L., et al., *Maternal diet influences DNA damage, aortic telomere length, oxidative stress, and antioxidant defense capacity in rats.* Faseb j, 2008. **22**(6): p. 2037-44.
276. Martin-Gronert, M.S. and S.E. Ozanne, *Mechanisms linking suboptimal early nutrition and increased risk of type 2 diabetes and obesity.* J Nutr, 2010. **140**(3): p. 662-6.
277. Martin-Gronert, M.S. and S.E. Ozanne, *Experimental IUGR and later diabetes.* J Intern Med, 2007. **261**(5): p. 437-52.

278. Ravelli, A.C., et al., *Glucose tolerance in adults after prenatal exposure to famine.* Lancet, 1998. **351**(9097): p. 173-7.
279. Vickers, M.H., *Developmental programming of the metabolic syndrome - critical windows for intervention.* World J Diabetes, 2011. **2**(9): p. 137-48.
280. Boyle, J.G., et al., *AMP-activated protein kinase is activated in adipose tissue of individuals with type 2 diabetes treated with metformin: a randomised glycaemia-controlled crossover study.* Diabetologia, 2011. **54**(7): p. 1799-809.

## Appendices

Appendix I: Dulbecco's Modified Eagle's Medium (DMEM)

Appendix II: Foetal Calf Serum (FCS)

Appendix III: Dulbecco's Phosphate Buffered Saline (DPBS)

Appendix IV: Hanks Balanced Salt Solution (HBSS)

Appendix V: Protocol QIAGEN Total RNA isolation from animal cells (RNeasy mini kit)

Appendix VI: Protocol QIAGEN Total RNA isolation kit for animal tissues (RNeasy midi kit)

Appendix VII: Protocol QIAGEN Total RNA isolation kit for animal fibrous tissues (RNeasy mini kit)

Appendix VIII: Protocol QIAGEN Total RNA isolation kit for adipose tissue (RNeasy midi kit)

Appendix IX: Protocol glucose assay kit

Appendix X: Protocol insulin assay kit

Appendix XI: Protocol RC DC-BioRad protein assay

Appendix XII: Antibodies' dilutions

Appendix XIII: Primer sequences

Appendix I

Dulbecco's Modified Eagle's Medium (DMEM):

| **Component** | **g/L** |
|---|---|
| **Ionic salts** | |
| $CaCl_2$ | 0.2 |
| $Fe(NO_3)_3.9H_2O$ | 0.0001 |
| MgSO4 | 0.09767 |
| KCl | 0.4 |
| $NaHCO_3$ | 3.7 |
| NaCl | 6.4 |
| $NaH_2PO_4$ | 0.109 |
| **Amino Acids** | |
| L-Alanyl-L-Glutamine | - |
| L-Arginine.HCl | 0.084 |
| L-Cysteine.2HCl | 0.0626 |
| L-Glutamine | - |
| Glycine | 0.03 |
| L-Histidine.HCl. $H_2O$ | 0.042 |
| L-Isoleucine | 0.105 |
| L-Leucine | 0.105 |
| L-Lysine.HCl | 0.146 |
| L-Methionine | 0.03 |
| L-Phenylalanine | 0.066 |
| L-Serine | 0.042 |
| L-Threonine | 0.095 |
| L-Tryptophan | 0.016 |
| L-Tyrosine.2Na.$2H_2O$ | 0.10379 |
| L-Valine | 0.094 |
| **Vitamins** | |
| Choline Chloride | 0.004 |
| Folic Acid | 0.004 |

| | |
|---|---|
| *myo*-Inositol | 0.0072 |
| Niacinamide | 0.004 |
| D-Pantothenic Acid.1/2Ca | 0.004 |
| Pyridoxal.HCl | - |
| Pyridoxine.HCl | 0.004 |
| Riboflavin | 0.0004 |
| Thiamine.HCl | 0.004 |
| **Other** | |
| D-Glucose | 4.5 |
| HEPES | - |
| Phenol Red.Na | 0.0159 |
| Pyruvic Acid.Na | - |
| **ADD** | |
| Glucose | - |
| L-Glutamine | 0.584 |
| $NaHCO_3$ | - |

Appendix II

Foetal Calf Serum (FCS):

| | |
|---|---|
| pH@RT | 7.5 |
| Osmolarity | 7.25 mOsm/Kg |
| Sterility | Sterile |
| Endotoxin | 0.2 EU/ml |
| Haemoglobin | 12.72 mg % |
| Total Protein | 3.74 g % |
| **Biochemical Profile** | |
| Sodium | 136 mM/L |
| Potassium | 11 mM/L |
| Chloride | 100 mMol/L |
| Uric Acid | 2.2 mg% |
| Calcium | 14.1 mg% |
| Phosphorous | 10.8 mg% |
| Alkaline Phosphatase | 396 IU/L |
| LDH | 518 IU/L |
| SGOT | 38 IU/L |
| SGPT | <6 IU/L |
| Gamma GT | 7 IU/L |
| Cholesterol | 34 mg% |
| Bilirubin | 0.16 mg% |
| Glucose | 60 mg% |
| Urea | 39 mg% |
| Creatinine | 3.1 mg% |
| Total Triglycerides | 55 mg% |
| Albumin | 1.69 g% |
| Alpha Globulins | 1.300 g% |
| Beta Globulins | 0.690 g% |
| Gamma Globulins | 0.070 g% |
| Iron | 173 μg% |

Appendix III

Dulbecco's Phosphate Buffered Saline (DPBS):

| **Component** | **g/L** |
|---|---|
| **Inorganic salts** | |
| $CaCl_2.2H_2O$ | - |
| $MgCl_2.6H_2O$ | - |
| KCl | 0.2 |
| $KH_2PO_4$ (anhydrous) | 0.2 |
| NaCl | 8.0 |
| $Na_2HPO_4$ (anhydrous) | 1.15 |

Appendix IV

Hanks Balanced Salt Solution (HBSS):

| **Component** | **g/L** |
|---|---|
| **Inorganic Salts** | |
| $CaCl_2.2H_2O$ | 0.185 |
| $MgSO_4$ (anhydrous) | 0.09767 |
| KCl | 0.4 |
| $KH_2PO_4$ (anhydrous) | 0.06 |
| $NaHCO_3$ | 0.35 |
| NaCl | 8.0 |
| $Na_2HPO_4$ (anhydrous) | 0.04788 |
| **Other** | |
| D-Glucose | 1.0 |
| Phenol Red.Na | 0.011 |
| **ADD** | |
| $NaHCO_3$ | - |

Apendix V

Protocol QIAGEN Total RNA isolation from animal cells (RNeasy mini kit)

It is essential to begin with the correct number of cells in order to obtain optimal RNA yield and purity with RNeasy mini columns. The maximum amount of starting material is 1.0 x $10^7$ cells and the maximum binding capacity of the RNeasy spin column is 100 µg RNA. For our cell types, QIAGEN recommends starting with no more than 3–4 x $10^6$ cells.

All steps of the RNeasy protocol should be performed at room temperature. All centrifugation steps are performed at 20-25°C in a standard laboratory microcentrifuge. Always wear gloves and use RNAse free equipment!

Procedure:

1. Add 10 µl β-ME per 1 ml Buffer RLT. Dispense in a fume hood and wear appropriate protective clothing. Buffer RLT containing β-ME can be stored at room temperature for up to 1 month.
2. Buffer RPE is supplied as a concentrate. Before using for the first time, add 4 volumes of ethanol (96–100%) as indicated on the bottle to obtain a working solution.
3. Determine the number of cells (no more than 1.0 x $10^7$). Completely aspirate the cell-culture medium and wash the cells with PBS.
   Note: Incomplete removal of cell-culture medium will inhibit lysis and dilute the lysate, affecting the conditions for binding of RNA to the RNeasy membrane. Both effects may reduce RNA yield.
4. Add 350 µl of RLT buffer (when using 3 x x $10^6$ cells) containing β-mercaptoethanol (β-ME) (10 µl/ ml). Collect the lysate with a rubber policeman. Pipet the lysate into a microcentrifuge tube. Vortex or pipet to mix, and ensure that no cell clumps are visible before proceeding to step 5.
5. Vortex the lysate for 30 seconds to disrupt and homogenize the cell lysate.
6. Add 1 volume of 70% ethanol to the homogenized lysate, and mix well by pipetting. Do not centrifuge.

Note: When purifying RNA from certain cell lines, precipitates may be visible after addition of ethanol. This does not affect the procedure.

7. Transfer the sample, including any precipitate that may have formed, to an RNeasy spin column placed in a 2 ml collection tube (supplied by QIAGEN). Close the lid gently, and centrifuge for 15 s at 8000 x g (10,000 rpm). Discard the flow-through. Reuse the collection tube in step 8.
8. Add 700 µl Buffer RW1 to the RNeasy spin column. Close the lid gently, and centrifuge for 15 s at 8000 x g (10,000 rpm) to wash the spin column membrane. Discard the flow-through. Reuse the collection tube in step 9.

   Note: After centrifugation, carefully remove the RNeasy spin column from the collection tube so that the column does not contact the flow-through. Be sure to empty the collection tube completely.
9. Add 500 µl Buffer RPE to the RNeasy spin column. Close the lid gently, and centrifuge for 15 s at 8000 x g (10,000 rpm) to wash the spin column membrane. Discard the flow-through. Reuse the collection tube in step 10.

   Note: Buffer RPE is supplied as a concentrate. Ensure that ethanol is added to Buffer RPE before use.
10. Add 500 µl Buffer RPE to the RNeasy spin column. Close the lid gently, and centrifuge for 2 min at 8000 x g (10,000 rpm) to wash the spin column membrane.

    The long centrifugation dries the spin column membrane, ensuring that no ethanol is carried over during RNA elution. Residual ethanol may interfere with downstream reactions.

    Note: After centrifugation, carefully remove the RNeasy spin column from the collection tube so that the column does not contact the flow-through. Otherwise, carryover of ethanol will occur.
11. Optional: Place the RNeasy spin column in a new 2 ml collection tube (supplied by QIAGEN), and discard the old collection tube with the flow-through. Close the lid gently, and centrifuge at full speed for 1 min. Perform this step to eliminate any possible carryover of Buffer RPE, or if residual flow-through remains on the outside of the RNeasy spin column after step 10.
12. Place the RNeasy spin column in a new 1.5 ml collection tube (supplied). Add 30–50 µl RNase-free water directly to the spin column membrane. Close the lid gently, and centrifuge for 1 min at 8000 x g (10,000 rpm) to elute the RNA.

13. Repeat step 10 using another 30–50 µl RNasefree water, or using the eluate from step 10 (if high RNA concentration is required). Reuse the collection tube from step 12.

    If using the eluate from step 10, the RNA yield will be 15–30% less than that obtained using a second volume of RNase-free water, but the final RNA concentration will be higher.

Appendix VI

Protocol QIAGEN Total RNA isolation kit for animal tissues (RNeasy midi kit)

It is essential to begin with the correct amount of tissue in order to obtain optimal RNA yield and purity with RNeasy columns. A minimum amount of 20 mg and a maximum of 250 mg of tissue can generally be processed with RNeasy midi columns. 1 mg of RNA is the maximum binding capacity of the RNeasy midi column.

To process, do not allow tissue to thaw during handling prior to disruption in Buffer RLT. All steps of the RNeasy protocol should be performed at room temperature. All centrifugation steps are performed at 20-25°C in a standard laboratory centrifuge. Always wear gloves and use RNAse free equipment!

Procedure:

1. Add, before use, 10 µl β-Mercaptoethanol (β-ME) per 1 ml of Buffer RLT (dispense in a fume hood and wear appropriate protective clothing). Use a 15 ml tube.
2. Buffer RPE is supplied as a concentrate. Before using for the first time, add 4 volumes of ethanol (96–100%) as indicated on the bottle to obtain a working solution.
3. Add a piece of tissue sample (not more than 250 mg) to 4 ml of Buffer RLT and homogenize the sample with tissue homogenizer at full speed, until complete homogenization. Frozen tissues should not be allowed to thaw during handling. The relevant procedures should be carried out as quickly as possible.
4. Centrifuge the tissue lysate for 10 min at 3000–5000 x g. Carefully transfer the supernatant to a new 15 ml tube (not supplied) by pipetting. Use only this supernatant (lysate) in subsequent steps. In most preparations a small pellet will form, sometimes accompanied by a fatty upper layer. Transferring the pellet or the fatty layer may reduce the amount of RNA that binds to the membrane and cause the spin column to clog.

Note: To avoid transferring contaminants, hold the pipet tip underneath the fatty upper layer, and do not disturb the pellet.

5. Add 1 volume (4.0 ml) of 70% ethanol to the homogenized lysate, and mix immediately by shaking vigorously. Ensure that any precipitates are resuspended. Do not centrifuge. Continue without delay with step 6.

   If some lysate is lost during steps 3 and 4, adjust volume of ethanol accordingly.

6. Apply the sample to an RNeasy midi column placed in a 15 ml centrifuge tube (supplied by QIAGEN), and close the tube gently. Maximum loading volume is 4.0 ml. Centrifuge for 5 min at 3000–5000 x g. Discard the flow-through. Reuse the centrifuge tube in step 7.

   If the maximum amount of starting material is used, it may be necessary to increase centrifugation time to 10 min in order to allow the lysate to completely pass through the column.

   If the volume exceeds 4.0 ml, load aliquots successively onto the RNeasy column, and centrifuge as above. Discard the flow-through after each centrifugation step.

7. Add 4.0 ml Buffer RW1 to the RNeasy column. Close the centrifuge tube gently, and centrifuge for 5 min at 3000–5000 x g to wash the column. Discard the flow-through. Reuse the centrifuge tube in step 8.

8. Add 2.5 ml Buffer RPE to the RNeasy column. Close the centrifuge tube gently, and centrifuge for 2 min at 3000–5000 x g to wash the column. Discard the flow-through. Reuse the centrifuge tube in step 9.

   Note: Buffer RPE is supplied as a concentrate. Ensure that ethanol is added to Buffer RPE before use.

9. Add another 2.5 ml Buffer RPE to the RNeasy column. Close the centrifuge tube gently, and centrifuge for 5 min at 3000–5000 x g to dry the RNeasy silica-gel membrane. It is important to dry the RNeasy membrane since residual ethanol may interfere with downstream reactions. This centrifugation ensures that no ethanol is carried over during elution.

   Note: Following the centrifugation, remove the RNeasy column from the centrifuge tube carefully so the column does not contact the flow-through as this will result in carryover of ethanol.

10. To elute, transfer the RNeasy column to a new 15 ml collection tube (supplied by QIAGEN). Pipet the appropriate volume of RNase-free water (250 µl for 250 mg of tissue) directly onto the RNeasy silica-gel membrane. Close the tube gently. Let it stand for 1 min, and then centrifuge for 3 min at 3000–5000 x g.
11. Repeat the elution step (step 10) as described with a second volume of RNase-free water.

    To obtain a higher total RNA concentration, this second elution step may be performed using the first eluate (from step 10). The yield will be 15–30% less than the yield obtained using a second volume of RNase-free water, but the final concentration will be higher.

Appendix VII

Protocol QIAGEN Total RNA isolation kit for animal fibrous tissues (RNeasy mini kit)

It is essential to begin with the correct amount of tissue in order to obtain optimal RNA yield and purity with RNeasy columns. The maximum amount of starting material is 30 mg of tissue sample and the maximum binding capacity of the RNeasy spin column is 100 μg RNA.

To process, do not allow tissue to thaw during handling prior to disruption in Buffer RLT. All steps of the RNeasy protocol should be performed at room temperature. All centrifugation steps are performed in a standard laboratory centrifuge. Always wear gloves and use RNAse free equipment!

Procedure:

1. Add 10 μl β-ME per 1 ml Buffer RLT. Dispense in a fume hood and wear appropriate protective clothing. Buffer RLT containing β-ME can be stored at room temperature for up to 1 month.
2. Buffer RPE is supplied as a concentrate. Before using for the first time, add 4 volumes of ethanol (96–100%) as indicated on the bottle to obtain a working solution.
3. Heat a water bath or heating block to 55°C for proteinase K digestion in step 8.
4. Remove the tissue sample from storage. Determine the amount of tissue. Do not use more than 30 mg. Proceed immediately to step 5. Frozen tissues should not be allowed to thaw during handling. The relevant procedures should be carried out as quickly as possible.
5. Add the determined amount of tissue (30 mg) to 300 μl of buffer RLT and homogenize the sample at full speed with tissue homogenizer until complete homogenization (usually between 20-90 seconds).
6. Add 590 μl RNase-free water to the lysate. Then add 10 μl proteinase K solution, and mix thoroughly by pipetting.

7. Incubate at 55°C for 10 min.
8. Centrifuge at 20–25°C for 3 min at 10,000 x g. A small pellet of tissue debris will form, sometimes accompanied by a thin layer or film on top of the supernatant.
9. Pipet the supernatant (approximately 900 µl) into a new 1.5 ml or 2 ml microcentrifuge tube (not supplied). Avoid transferring any of the pellet. If this is unavoidable, a small amount of pelleted debris may be carried over without affecting the RNeasy procedure. Hold the pipet tip under the thin layer or film on top of the supernatant, if present. This layer will usually adhere to the outside of the pipet tip and should not be transferred.
10. Add 0.5 volumes (usually 450 µl) of ethanol (96–100%) to the cleared lysate. Mix well by pipetting. Do not centrifuge. Precipitates may be visible after addition of ethanol. This does not affect the procedure.
11. Transfer 700 µl of the sample, including any precipitate that may have formed, to an RNeasy Mini spin column placed in a 2 ml collection tube. Close the lid gently, and centrifuge at 20–25°C for 15 s at 8000 x g (10,000 rpm). Discard the flow-through. Reuse the collection tube in step 12.
12. Repeat step 11 using the remainder of the sample. Discard the flow-through. Reuse the collection tube in step 13.
13. Add 350 µl Buffer RW1 to the RNeasy spin column. Close the lid gently, and centrifuge at 20–25°C for 15 s at 8000 x g (10,000 rpm) to wash the membrane. Discard the flow-through. Reuse the collection tube in step 16.
14. Add 10 µl DNase I stock solution to 70 µl Buffer RDD. Mix by gently inverting the tube, and centrifuge briefly to collect residual liquid from the sides of the tube.

    Note: DNase I is especially sensitive to physical denaturation. Mixing should only be carried out by gently inverting the tube. Do not vortex.
15. Add the DNase I incubation mix (80 µl) directly to the RNeasy spin column membrane, and place on the benchtop (20–30°C) for 15 min.

    Note: Be sure to add the DNase I incubation mix directly to the RNeasy spin column membrane. DNase digestion will be incomplete if part of the mix sticks to the walls or the O-ring of the spin column.

16. Add 350 µl Buffer RW1 to the RNeasy spin column. Close the lid gently, and centrifuge for 15 s at 8000 x g (10,000 rpm) at 20–25°C. Discard the flow-through. Reuse the collection tube in step 17.
17. Add 500 µl Buffer RPE to the RNeasy spin column. Close the lid gently, and centrifuge at 20–25°C for 15 s at 8000 x g (10,000 rpm) to wash the membrane. Discard the flow-through. Reuse the collection tube in step 18.

    Note: Buffer RPE is supplied as a concentrate. Ensure that ethanol is added to Buffer RPE before use.
18. Add 500 µl Buffer RPE to the RNeasy spin column. Close the lid gently, and centrifuge at 20–25°C for 2 min at 8000 x g (10,000 rpm) to wash the membrane. The long centrifugation dries the spin column membrane, ensuring that no ethanol is carried over during RNA elution. Residual ethanol may interfere with downstream reactions.

    Note: After centrifugation, carefully remove the RNeasy spin column from the collection tube so that the column does not contact the flow-through. Otherwise, carryover of ethanol will occur.
19. Optional: Place the RNeasy spin column in a new 2 ml collection tube (supplied), and discard the old collection tube with the flow-through. Close the lid gently, and centrifuge at full speed for 1 min.

    Perform this step to eliminate any possible carryover of Buffer RPE, or if residual flow-through remains on the outside of the RNeasy spin column after step 18.
20. Place the RNeasy spin column in a new 1.5 ml collection tube (supplied by QIAGEN). Add 30–50 µl RNase-free water directly to the RNeasy spin column membrane. Close the lid gently. To elute the RNA, centrifuge for 1 min at 8000 x g (10,000 rpm) at 20–25°C.
21. Repeat step 20 using using another 30-50 µl of RNase-free water or using the eluate from step 20. Reuse the collection tube from step 20. If the expected RNA yield is >30 µg, there is no need to repeat step 20. Using the eluate from step 20, the RNA yield will be 15–30% less than that obtained using a second volume of RNase-free water, but the final RNA concentration will be higher.

Appendix VIII

Protocol QIAGEN Total RNA isolation kit for adipose tissue (RNeasy midi kit)

It is essential to begin with the correct amount of tissue in order to obtain optimal RNA yield and purity with RNeasy columns. A maximum of 500 mg of tissue can generally be processed with RNeasy midi columns. 1 mg of RNA is the maximum binding capacity of the RNeasy midi column.

To process, do not allow tissue to thaw during handling prior to disruption in Buffer RLT. All steps of the RNeasy protocol should be performed at room temperature. All centrifugation steps are performed at 20-25°C in a standard laboratory centrifuge. Always wear gloves and use RNAse free equipment!

Procedure:

1. Add 10 µl β-ME per 1 ml Buffer RLT. Dispense in a fume hood and wear appropriate protective clothing. Buffer RLT containing β-ME can be stored at room temperature for up to 1 month.
2. Buffer RPE is supplied as a concentrate. Before using for the first time, add 4 volumes of ethanol (96–100%) as indicated on the bottle to obtain a working solution.
3. Remove the tissue sample from storage. Determine the amount of tissue. Do not use more than 500 mg. Proceed immediately to step 4.
4. Place the tissue in a suitably sized vessel containing 5 ml QIAzol Lysis Reagent.
5. Note: Use a suitably sized vessel with sufficient extra headspace to accommodate foaming, which may occur during homogenization. Generally, round-bottomed tubes allow more efficient disruption and homogenization than conical-bottomed tubes.
6. Place the tip of the tissue homogenizer disposable probe into the vessel and operate the tissue homogenizer at full speed until the lysate is uniformly homogeneous (usually 30–60 s).

Note: To avoid damage to the tissue homogenizer and disposable probe during operation, make sure the tip of the probe remains submerged in the buffer.

Note: Incomplete homogenization leads to significantly reduced RNA yields and can cause clogging of the RNeasy spin column.

Foaming may occur during homogenization, especially of brain tissue. If this occurs, let the homogenate stand at room temperature for 2–3 min until the foam subsides before continuing with the procedure.

7. Place the tube containing the homogenate on the benchtop at room temperature (15–25°C) for 5 min.

   This step promotes dissociation of nucleoprotein complexes.

8. Add 1 ml chloroform. Securely cap the tube containing the homogenate, and shake it vigorously for 15 s. Thorough mixing is important for subsequent phase separation.

9. Place the tube containing the homogenate on the benchtop at room temperature for 2–3 min.

10. Centrifuge at 5000 x g for 15 min at 4°C. After centrifugation, heat the centrifuge to room temperature (15–25°C) if the same centrifuge will be used in the later steps of this procedure. After centrifugation, the sample separates into 3 phases: an upper, colorless aqueous phase containing RNA; a white interphase; and a lower, red, organic phase. For tissues with an especially high fat content, an additional, clear phase may be visible below the red, organic phase. The volume of the aqueous phase should be approximately 3 ml.

11. Transfer the upper, aqueous phase to a new tube (not supplied). Add 1 volume (usually 3 ml) of 70% ethanol, and mix thoroughly by vortexing. Do not centrifuge. Proceed immediately to step 12.

    Note: The volume of lysate may be less than 3 ml due to loss during homogenization and centrifugation. Precipitates may be visible after addition of ethanol. Resuspend precipitates completely by vigorous shaking, and proceed immediately to step 12.

12. Transfer up to 4 ml of the sample to an RNeasy Midi spin column placed in a 15 ml collection tube (supplied by QIAGEN). Close the lid gently, and centrifuge for 5 min at 3000–5000 x g at room temperature (15–25°C). Discard the flow-through. Reuse the collection tube in step 13.

13. Repeat step 12 using the remainder of the sample (up to 4 ml). Discard the flowthrough. Reuse the collection tube in step 14.
14. Add 4 ml Buffer RW1 to the RNeasy spin column. Close the lid gently, and centrifuge for 5 min at 3000–5000 x g to wash the membrane. Discard the flowthrough. Reuse the collection tube in step 15.
15. Add 2.5 ml Buffer RPE to the RNeasy spin column. Close the lid gently, and centrifuge for 2 min at 3000–5000 x g to wash the membrane. Discard the flowthrough. Reuse the collection tube in step 16.

    Note: Buffer RPE is supplied as a concentrate. Ensure that ethanol is added to Buffer RPE before use.
16. Add 2.5 ml Buffer RPE to the RNeasy spin column. Close the lid gently, and centrifuge for 5 min at 3000–5000 x g to wash the membrane.

    The long centrifugation dries the spin column membrane, ensuring that no ethanol is carried over during RNA elution. Residual ethanol may interfere with downstream reactions.

    Note: After centrifugation, carefully remove the RNeasy spin column from the collection tube so that the column does not contact the flow-through. Otherwise, carryover of ethanol will occur.
17. Place the RNeasy spin column in a new 15 ml collection tube (supplied by QIAGEN). Add the appropriate volume of RNase-free water (150 -250 µl) directly to the spin column membrane. Close the lid gently. To elute the RNA, wait for 1 min and then centrifuge for 3 min at 3000–5000 x g.
18. Repeat step 17 using another volume of RNase-free water, or using the eluate from step 17 (if high RNA concentration is required). Reuse the collection tube from step 17. If using the eluate from step 17, the RNA yield will be 15–30% less than that obtained using a second volume of RNase-free water, but the final RNA concentration will be higher.

Appendix IX

Protocol Glucose Assay Kit

1. This assay can be used on serum and plasma samples.
2. Prepare glucose standards by labeling 9 clean test tubes from 0-8.
3. Add 250 µl of ultrapure water to tubes 1-8. Add 500 µl of ultrapure water to tube 0.
4. Add 250 µl of glucose standard to tube 1 and mix thoroughly.
5. Serially dilute the glucose standard* by removing 250 µl from tube 1 and adding it to tube 2; mix thoroughly. Next, remove 250 µl from tube 2 and place it into tube 3; mix thoroughly. Repeat this process for tubes 4-8. Tube 0 only has ultrapure water and is used as the blank.

Table 6.

| Tube | Glucose concentration (mg/dl) | Glucose concentration (mM) |
|---|---|---|
| 1 | 720.72 | 40 |
| 2 | 360.36 | 20 |
| 3 | 180.18 | 10 |
| 4 | 90.09 | 5 |
| 5 | 45.05 | 2.5 |
| 6 | 22.52 | 1.25 |
| 7 | 11.26 | 0.625 |
| 8 | 5.63 | 0.3125 |
| 0 | 0 | 0 |

* Glucose standard is 1.441 g/dL

6. Load 2 µl of sample or standard (in duplicate) to a well.
7. Add 300 µl of the reagent to each well and mix thoroughly.
8. Incubate for 20 minutes at room temperature and read the absorbance at 490 nm.

9. Calculate the values of glucose samples using the equation obtained from the linear regression of the standard curve by substituting the corrected absorbance values for each sample into the equation.

Figure 6

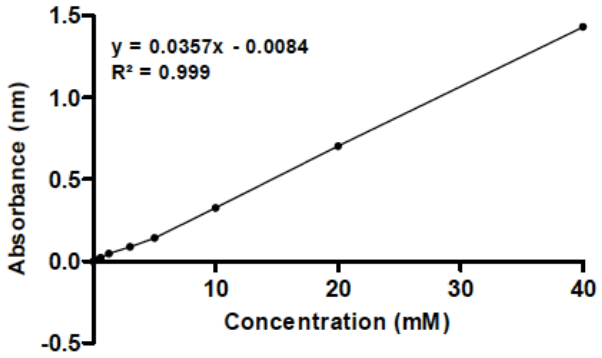


Figure 6: Illustration of glucose assay standard curve.

Appendix X

Protocol Insulin ELISA

1. This assay can be used on serum and plasma samples.
2. All reagents and samples must be brought to room temperature before use.
3. Prepare the needed volume of Enzyme Conjugate by mixing 5 µl Enzyme Conjugate 11x with 50 µl Enzyme Conjugate Buffer (1+10) for each sample.
4. Prepare the needed volume of Wash Buffer by diluting 100 µl Wash Buffer 21x in 2000 µl redistilled water (1+20) for each sample.
5. Prepare a calibration curve for each assay run.
6. Add 10 µl of calibrator or sample to an anti-insulin well and add 50 µl Enzyme Conjugate. Perform each determination in duplicate for calibrators and samples.
7. Incubate on a shaker for 2 hours at room temperature (18-25°C).
8. Wash 10 times by adding 200 µl Wash Buffer to each well. Aspirate completely. After the final wash, invert and tap the plate firmly against absorbent paper.
9. Add 200 µl TMB substrate to each well.
10. Incubate for 15 minutes at room temperate.
11. Add 50 µl Stop Solution to each well. Put the plate on a shaker for approximately 5 seconds to ensure mixing of substrate and Stop Solution.
12. Measure the absorbance at 450 nm and evaluate.

Figure 7

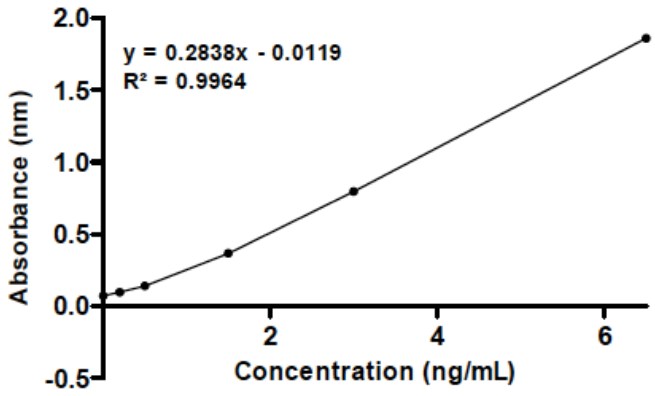


Figure 7: Illustration of Insulin ELISA standard curve

Appendix XI

Protocol RC DC-BioRad protein assay

1. Prepare protein standards by labeling 9 clean test tubes from 0 – 8.
2. Add 500 µl of water to tubes 0 and 2-8.
3. In tube 1, add 1mg of BSA to 1 ml of ultrapure water and mix by vortexing until the solution is homogenized.
4. Pipette 500 µl from tube 1 to tube 2 and vortex it. Then, pipette 500 µl from tube 2 to tube 3 and vortex it.
5. Repeat the dilution step to the next tubes (4, 5, 6, 7 and 8) to make the standard curve.
6. Tube 0 will has only ultrapure water and is used as blank.

Table 8.

| Tube | BSA concentration mg/ml |
|---|---|
| 1 | 1 |
| 2 | 0.5 |
| 3 | 0.25 |
| 4 | 0.125 |
| 5 | 0.0625 |
| 6 | 0.03125 |
| 7 | 0.015625 |
| 8 | 0.0078125 |
| 0 | 0 |

Table 8: Table showing BSA consecutive dilutions

7. Add 5 µl extracted sample to 25 µl reagent A (20 µl surfactant solution to 1 mL alkaline copper tartrate solution).
8. Add 200 µl Folin reagent.

9. Incubate at room temperature for 30 min.
10. Measure absorbance (650 nm) on an optical plate reader.
11. Use the dilutions of bovine serum albumin (BSA; 3.9·10-3 – 2 mg/mL) previously made and calculate the concentration of the sample, using the equation obtained from the linear regression of the standard curve by substituting the corrected absorbance values for each sample into the equation.

Figure 8

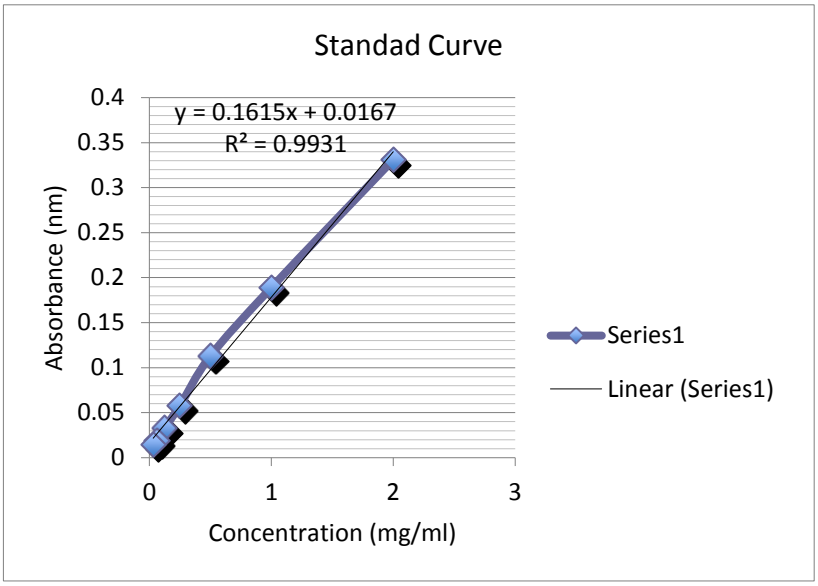


Figure 8: Illustrates a standard curve for protein assay

Appendix XII

Antibodies' dilutions:

| Antibody | Dilution factor |
|---|---|
| mouse anti-p53 | 1: 1000 |
| rabbit anti-acetylated lysine | 1: 1000 |
| rabbit anti-ACC | 1:10 000 |
| rabbit anti-phospho-ACC-ser218 | 1: 1000 |
| polyclonal rabbit anti-AMPK | 1: 1000 |
| polyclonal rabbit anti-phospho-AMPK-thr172 | 1: 1000 |
| polyclonal rabbit anti-Akt | 1: 10 000 |
| polyclonal rabbit anti-phospho-Akt-ser473 | 1: 1000 |
| rabbit anti-β-actin | 1: 5000 |
| mouse anti-SIRT1 | 1: 1000 |
| rabbit anti-SIRT6 | 1: 1000 |
| goat anti-PGC-1α | 1: 1000 |
| mouse anti-IRS-1 | 1: 1000 |
| mouse anti-phospho-tyrosine | 1: 1000 |
| mouse anti-GAPDH | 1: 10 000 |
| goat anti rabbit (secondary) | 1: 10 000 |
| rabbit anti-mouse (secondary) | 1: 10 000 |

Appendix XIII

Primer sequences:

| Gene | Forward Primer | Reverse Primer |
|---|---|---|
| ACC mouse | TCCTGCGTGTGTGTTCGG | AGTCTGCTTCAGCAATAAATTCAG |
| FAS mouse | CACTGCATTGACGGCCGGGT | GGACAAGCCCAGGCTGCGAG |
| G6Pase mouse | AGGGTAAAAGAAAAGAGCGTT G | GTAGACATGGCTTGCATATGGT |
| GCN-5 mouse | AATGAGCAGGTCAAGGGCTATG | TACTCCTTTAGGTGGTTCATCAGGT |
| NAMPT mouse | GCGAGCGAGCGGTGACT | CTGCGAGCAAGGAGAAAAATG |
| PCK1 mouse | TGCTGCAGAACACAAGGGC | GGTCGCATGGCAAAGGG |
| PDHK4 mouse | AGGCAAGACATCGGGTGG | CCTGGGTGAAGGGTTGACACT |
| PGC-1α mouse | CATTTGATGCACTGACAGATGGA | CCGTCAGGCATGGAGGAA |
| PGC-1β mouse | GGCCTTGTGTCAAGGTGGAT | GGTGCTTATGCAGTTCCGTAC |
| PPARα mouse | AGCCATGTACGTAGCCATCCA | TCTCCGGAGTCCATCACAAT |
| SCD-1 mouse | CGCCCAAGCTGGAGTACGTC | GGGCCCATTCGTACACGTCA |
| SIRT1 mouse | CAGGTTGCAGGAATCCAAACAAATCAGGCAAGATGCTGT | CAGTGTCATGGTTCCTTTGCCACCGAGGAACTACCTGAT |
| SIRT3 mouse | TGCTACTCATCTTGGGACCT | CACCAGCCTTTCCACACC |
| SIRT6 mouse | CCGTCACGGGACAGAGCAGTCG | GGTCTCCAGAGGGTCAGAGGGGT |

| | | |
|---|---|---|
| SREBP-1α mouse | GGAGCCATGGATTGCACAT T | GCTTCCAGAGAGGAGGCCA G |
| SREBP-1c mouse | GCAGACCCTGGTGAGTGG | GTCGGTGGATGGGCAGTTT |
| TNFα mouse | CGGAGTCCGGGCAGGT | GCTGGGTAGAGAATGGATG AACA |
| XBP-1 mouse | AAGAACACGCTTGGGAATG G | CTGCACCTGCTGCGGAC |
| AdipoR1 rat | CTTCTACTGCTCCCCACAGC | TCCCAGGAACACTCCTGCTC |
| AdipoR2 rat | CCACACAACACAAGAATCC G | CCCTTCTTCTTGGGAGAATG G |
| Adipo R1 mouse | ACGTTGGAGAGTCATCCCG TAT | CTCTGTGTGGATGCGGAAG AT |
| AdipoR2 mouse | TCCCAGGAAGATGAAGGGT TTAT | TTCCATTCGTTCGATAGCAT GA |
| AdipoQ | AATCCTGCCCAGTCATGAA G | CATCTCCTGGGTCACCCTTA |
| IRF3 mouse/rat | GGCTTGTGATGGTCAAGGT | CATGTCCTCCACCAAGTCCT |
| IRF4 mouse | GGAGGCCAGAGCATCAAGC | AATCCCCGGAGAGTTTGCA |
| IRF4 rat | TTGACTTTTCCTTCTCTTCCC TCA | CTTGCCTTTAAATAGTGCCC AAG |

Life Sciences 100 (2014) 55–60

Contents lists available at ScienceDirect

Life Sciences

journal homepage: www.elsevier.com/locate/lifescie

# The AMPK-SIRT signaling network regulates glucose tolerance under calorie restriction conditions

M.F.P. Silvestre [a,b,*], B. Viollet [c,d,e], P.W. Caton [a], J. Leclerc [c,d,e], I. Sakakibara [c,d,e], M. Foretz [c,d,e], M.C. Holness [a], M.C. Sugden [a]

[a] Barts and the London, School of Medicine and Dentistry, Queen Mary University of London, London, UK
[b] Faculdade de Medicina da Universidade de Lisboa, Lisboa, Portugal
[c] INSERM, U1016, Institut Cochin, Paris, France
[d] CNRS, UMR8104, Paris, France
[e] Université Paris Descartes, Sorbonne Paris Cité, Paris, France

ARTICLE INFO

*Article history:*
Received 29 August 2013
Accepted 27 January 2014
Available online 13 February 2014

*Keywords:*
AMP protein kinase (AMPK)
Calorie restriction
Glucose
Insulin
SIRT1
PGC-1α

ABSTRACT

*Aims:* SIRT1 and AMP-activated protein kinase (AMPK) share common activators, actions and target molecules. Previous studies have suggested that a putative SIRT1-AMPK regulatory network could act as the prime initial sensor for calorie restriction-induced adaptations in skeletal muscle—the major site of insulin-stimulated glucose disposal. Our study aimed to investigate whether a feedback loop exists between AMPK and SIRT1 in skeletal muscle and how this may be involved glucose tolerance.
*Main methods:* To investigate this, we used skeletal muscle-specific AMPKα1/2 knockout mice (AMPKα1/2$^{-/-}$) fed *ad libitum* (AL) or a 30% calorie restricted (CR) diet and L6 rat myoblasts incubated with SIRT1 inhibitor (EX527).
*Key findings:* CR-AMPKα1/2$^{-/-}$ displayed impaired glucose tolerance ($^{*}p < 0.05$), in association with down-regulated SIRT1 and PGC-1α expression (<300% vs. CR-WT, $^{\pm\pm}p < 0.01$). Moreover, AMPK activity was decreased following SIRT1 inhibition in L6 cells (~0.5-fold vs. control, $^{*}p < 0.05$).
*Significance:* This study demonstrates that skeletal muscle-specific AMPK deficiency impairs the beneficial effects of CR on glucose tolerance and that these effects may be dependent on reduced SIRT1 levels.


## Introduction

The downregulation of AMPK activity in response to high glucose, with a parallel decrease in SIRT1 activity, was observed in cultured HepG2 cells (Suchankova et al., 2009; Zang et al., 2004). This was associated with increased lactate release, suggesting a decrease in the $NAD^+$/NADH ratio, which likely contributed to the decrease in SIRT1 activity. These findings together with the demonstration that SIRT1 and AMPK share common activators, actions and target molecules (Ruderman et al., 2010) led us to an examination of a possible link between the SIRT1 and the AMPK in skeletal muscle. The precise interactions between SIRT1 and AMPK in skeletal muscle remain unclear, but given the function of skeletal muscle as the major site of glucose uptake and the known metabolic regulatory roles of SIRT1-AMPK, this signaling network is potentially of great importance. For example, AMPK has important acute metabolic actions in skeletal muscle, such as the promotion of long chain fatty acids (LCFA), oxidation (lipid-lowering effect), glucose uptake and glucose and glycogen breakdown (glucose-lowering effect) (Holness et al., 2012; O'Neill, 2013a; O'Neill, 2013b). SIRT1 has been shown to play an important role in controlling glucose metabolism, insulin action, fat storage and nutrient sensing (Guarente, 2006; Barzilai et al., 2012).

However, in marked contrast to the effects of AMPK, insulin suppresses fat oxidation and stimulates glycogen, lipid and protein synthesis and may often oppose the actions of AMPK (Pessin and Saltiel, 2000; Rennie, 2007). Interestingly, common actions of AMPK and insulin are also observed, in particular, the stimulation of glucose uptake into skeletal muscle (Shulman, 2000). It has been recently established that AMPK acts as the prime initial sensor for fasting-induced adaptations in skeletal muscle and that SIRT1 downstream signaling is blunted in the absence of AMPK (Cantó et al., 2010).

Caloric restriction (CR) has been shown to protect against onset age-related diseases (Colman et al., 2009; Smith et al., 2010) and to reduce mortality linked to T2DM and cardiovascular diseases (Hammer et al., 2008; Marchal et al., 2012). The effects of CR have been linked to changes in activity of AMPK and SIRT1.

The research here described aims to understand the mechanisms by which AMPK and SIRT1 may interact to regulate glucose tolerance in

* Corresponding author at: Centre for Diabetes, Blizard Institute, Bart's and the London School of Medicine and Dentistry, Queen Mary University of London, 4 Newark Street E1 2AT London, UK.
*E-mail addresses:* m.silvestre@qmul.ac.uk, m.silvestre@auckland.ac.nz (M.F.P. Silvestre).

http://dx.doi.org/10.1016/j.lfs.2014.01.080
0024-3205/

skeletal muscle during CR. To understand these signalling pathways, we utilized skeletal muscle-specific AMPK α1/2 double knockout mice subjected to CR as manipulations to modify glucose tolerance. In addition, L6 skeletal muscle myoblasts were used to determine regulatory interactions between AMPK and SIRT1.

## Materials and methods

### *Experimental animals*

Female skeletal muscle-specific AMPKα1/2-knockout ($AMPK^{-/-}$) or wild-type control (WT) mice were maintained on CR (CR-$AMPK^{-/-}$; WT-$AMPK^{-/-}$) or *ad libitum* (AL-$AMPK^{-/-}$; AL-$AMPK^{-/-}$) feeding regimes at Institut Cochin, INSERM, Paris, France. CR was conducted between 2.5 and 4 months of age and lasted for 10 weeks. Food was adjusted on a daily basis to ensure that CR mice consumed 70% of the calories consumed by AL-fed mice (calculated on the average of food intake during the last week before starting the caloric restriction protocol). Mice were sacrificed in the immediate post-absorptive state or after 5 h of fasting (all groups).

All mice were maintained on a 12:12-h light–dark cycle (light from 7 am to 7 pm), with controlled temperature (22 °C ± 2 °C) and air conditioned environment, and received standard high-carbohydrate rodent chow.

Mouse studies were reviewed and approved (agreement no. 75-886) by the Directeur Départemental des Services Vétérinaires of the Préfecture of Police of Paris and were performed in accordance with the principles and guidelines established by the European Convention for the Protection of Laboratory Animals.

### Oral glucose tolerance test (OGTT)

To examine whole-body glucose homeostasis, mice (17/group) were fasted overnight, followed by oral gavage of glucose (3 g/kg of body weight). Blood samples for glucose analysis were collected from the tail vein at 0, 20, 40, 60, 80 and 120 min after glucose gavage. Blood glucose concentration was measured in whole blood with an automatic glucose monitor (Glucotrend II; Roche Diagnostics). Serum insulin levels were measured in the blood samples collected during OGTT at time 0 and at time 20 min, using a specific ELISA (Linco, St Charles, MO).

### *Cell culture*

Cells were cultured at 37 °C and 5% $CO_2$, in DMEM containing 25 mM of glucose, non-essential amino acids and supplemented with 10% (v/v) foetal calf serum (FCS), 2 mM glutamate, 500 IU/ml penicillin and 100 μM streptomycin. For treatments, myoblasts were either maintained in DMEM (with FCS), as described above (termed 'fed cells') or in serum-free DMEM (without FCS; termed 'starved cells'). Fed and starved cells were incubated with SIRT1 inhibitor Ex527 (10 M; 3.5 h; Tocris Bioscoence). Negative controls consisted of 1 ml of media containing an equal concentration of DMSO.

### *Immunoblotting*

Immunoblotting was conducted as previously described (Laemmli, 1970), using the primary antibodies (anti ACC, anti-phospho-ACC-$ser^{218}$, anti-AMPK, anti-AMPK-$thr^{172}$, anti-PGC-1α and anti-acetyl lysine) and secondary antibodies anti-rabbit and anti-mouse (Cell Signaling Technologies, MA, USA). Reference protein measurements were made with mouse monoclonal anti-β-actin (clone AC-15; Sigma, Poole, UK) primary antibody.

### *Quantitative RT-PCR*

All gene expression was measured by qRT-PCR, as previously described (Higuchi et al., 1992) using Taqman or Sybr green methodology. The following primers were used: NAMPT, 5′-GCGAGCGAGCGGTGACT-3′ and 5′-CTGCGAGCAAGGAGAAAAATG-3′; PGC-1α, 5′-CATTTGATGC ACTGACAGATGGA-3′ and 5′-CCGTCAGGCATGGAGGAA-3′; SIRT1, 5′-CAGGTTGCAGGAATCCAAACAAATCAGGCAAGATGCTGT-3′ and 5′-CAGT GTCATGGTTCCTTTGCCACCGAGGAACTACCTGAT-3′; SIRT3, 5′-TGCTAC TCATCTTGGGACCT-3′ and 5′-CACCAGCCTTTCCACACC-3′; SIRT6, 5′-CCGTCACGGGACAGAGCAGTCG-3′ and 5′-GGTCTCCAGAGGGTCAGAGG GGT-3′. Gene expression was determined by $\Delta\Delta C_T$ normalized against 18S control ribosomal RNA.

### *Immunohistochemistry*

Soleus and gastrocnemius muscles were embedded in cryomatrix and quickly frozen in isopentane cooled with liquid nitrogen. Cryostat sections (10 μm) were washed in PBS, permeabilized with 0.1% Triton X-100 and left for 1 h in blocking solution (1× PBS, 1.5% goat serum, 0.1% Triton X-100). Rabbit poly-clonal antibodies directed against Laminin (Z0097, Dako) (1/100 dilution) and monoclonal antibodies against MyHCI (NOQ7.5.4D, Sigma) and MyHCIIA (SC-71, Santa Cruz biotechnology) were applied overnight at 4 °C to the treated sections. The next day, after three washes with 1× PBS containing 0.05% Tween-20, cryosections were incubated for 1 h with appropriate fluorescent secondary antibodies (Alexa Fluor 488 goat anti-rabbit IgG 1/1000 dilution, Alexa Fluor 594 goat anti-mouse IgG 1/1000 dilution; Invitrogen). After three washes with 1× PBS containing 0.05% Tween 20, samples were mounted in Vectashield mounting medium.

### *Statistical analysis*

Results are expressed as mean ± SEM. Statistical comparisons were obtained using GraphPad (GraphPad Software, CA, USA). Statistical differences were calculated using a paired *t*-test or a two-way ANOVA followed by Bonferroni's post-test, where appropriate.

## Results

### *Loss of AMPKα1 and AMPKα2 subunits decreases AMPK protein expression in the skeletal muscle of AL- and CR-fed mice*

Skeletal muscle AMPK protein levels were undetectable in AL- and CR-$AMPK^{-/-}$ mice (Fig. 1). Moreover, levels of AMPK activity, denoted by phosphorylation on $Thr^{172}$, were abolished in the skeletal muscle of AL- and CR-$AMPK^{-/-}$ mice compared to AL-WT and CR-WT, respectively (Fig. 1A).

Acetyl CoA carboxylase (ACC) is a down stream target of AMPK, whereby AMPK inhibits ACC activity through phosphorylation on $Ser^{218}$ (Hutchinson and Bengtsson, 2006). Enhanced ACC phosphorylation at $Ser^{218}$ in the skeletal muscle of CR-WT is clearly lost in $AMPK^{-/-}$ mice (Fig. 1). ACC phosphorylation at $Ser^{218}$ was increased in the skeletal muscle of CR-WT mice but was clearly lost in CR-$AMPK^{-/-}$ mice (Fig. 1A).

AL-$AMPK^{-/-}$ mice gained similar weight over 10 weeks compared to AL-WT mice, and body weight reduction in CR-WT and CR-$AMPK^{-/-}$ was also comparable (Fig. 1B).

Taken together, these data demonstrate that these mice are suitable for study of the effects of reduced skeletal muscle AMPK signalling.

### *AMPKα1/2 knockout impairs CR-mediated improvements in whole-body glucose tolerance*

To assess the effects of the experimental diets and $AMPK^{-/-}$ on whole body glucose tolerance and insulin secretion, we utilized an

A

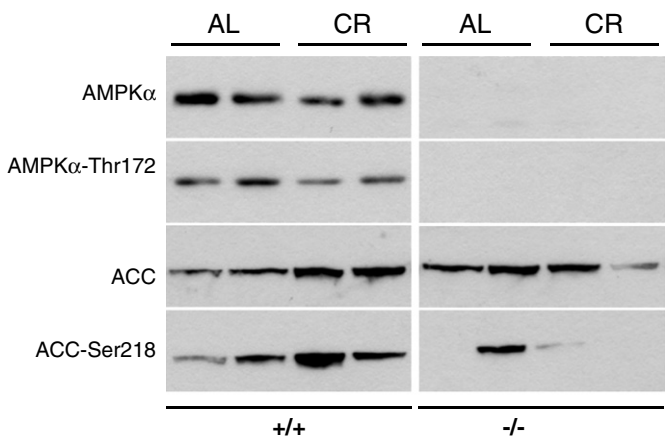


B

| | WT | | AMPK$^{-/-}$ | |
|---|---|---|---|---|
| | AL | CR | AL | CR |
| **Initial weight (g)** | 18.52 ± 2.4 | 21.0 ± 2.3 | 17.33 ± 1.4 | 21.16 ± 2.7 |
| **Final weight (g)** | 22.34 ± 2.9 | 20.25 ± 1.0 | 21.33 ± 1.2 | 20.44 ± 2.6 |
| **Weight gain (g)** | 3.82 ± 1.3 | -0.8 ± 2.3*** ### | 4.0 ± 2.3 | -0.72 ± 0.75*** ### |

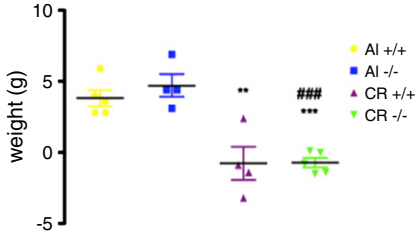


**Fig. 1.** (A) Representative western blot of total AMPK and phospho-AMPK-thr$^{172}$ protein (MW: 63 kDa) and of total ACC and phospho-ACC-ser$^{218}$ protein (MW: 215 kDa). AL = mice fed ad libitum; CR = calorie restricted mice (30% caloric restriction); −/− = AMPK α1/2 knockout mice; +/+ = WT mice. (B) Weight gained after 10 weeks of AL vs. CR treatment. Data are presented as mean ± SE. ***$p < 0.001$ vs. AL +/+, ###$p < 0.001$ vs. AL$^{-/-}$, $n = 4$–5 per group. −/− = AMPK α1/2 knockout mice.

oral glucose tolerance test (OGTT). There were no significant differences in basal fasting plasma glucose and insulin levels between the four groups (Figs. 2A and C). However, CR-WT mice displayed improved glucose tolerance, where blood glucose levels were significantly lower 20–40 min post-glucose injection compared to AL-WT (*$p < 0.05$) (Figs. 2A and B). Notably, this effect was lost in CR-AMPK$^{-/-}$ mice, demonstrating that skeletal muscle AMPK is required for mediating the beneficial effects of CR on glucose tolerance. Interestingly, glucose levels peaked at 40 min post-glucose injections in CR-AMPK$^{-/-}$, but at 20 min post-glucose in AL-AMPK$^{-/-}$ mice, perhaps indicating subtly different mechanisms of action. The early raised blood glucose levels were lost between 60 and 120 min, and blood glucose returned to basal levels after 120 min in all four groups (Fig. 2A). CR-WT mice did not display increased plasma insulin levels after 20 min compared to AL-WT and AL-AMPK$^{-/-}$, indicating that the improvements in glucose tolerance relative to these groups were likely mediated by increased peripheral insulin sensitivity rather than elevated pancreatic insulin secretion (Fig. 2C). However, plasma insulin was slightly reduced in CR-AMPK$^{-/-}$ mice compared with the other three groups, suggesting that AMPK deficiency in CR may lead to lower insulin secretion (Fig. 2C).

In order to demonstrate that improved glucose tolerance following CR is not a result of a shift in fiber type, we have counted the number of myosin heavy chain I and myosin heavy chain IIA fibers in WT and KO soleus and gastrocnemius muscle, under CR conditions. No changes were observed in the number of fibers in gastrocnemius and soleus muscle from CR-WT and CR-KO mice (Figs. 2D and E).

*SIRT1, SIRT6 and SIRT3 gene expressions are suppressed by AMPK deletion in the skeletal muscle of AL-fed mice*

NAD$^+$ biosynthetic activity of NAMPT results in activation of NAD$^+$-dependent sirtuin enzymes, particularly SIRT1 (Yang et al., 2007). AMPK has been reported to induce NAMPT with consequent raised NAD$^+$ levels and increased SIRT1 activity (Fulco et al., 2008). We studied NAMPT gene expression in order to better understand the possible link AMPK-NAMPT-SIRT1 in CR. Loss of AMPKα1/2 subunits led to a marked decrease in skeletal muscle NAMPT mRNA expression in AL mice (<75% vs. AL-AMPK $^{+/+}$, **$p < 0.01$) (Fig. 3A). CR also suppressed skeletal muscle NAMPT gene expression in WT mice (<75% vs. AL-AMPK $^{+/+}$, **$p < 0.01$). Skeletal muscle NAMPT gene expression levels were comparable in AL-AMPK$^{-/-}$ mice, CR WT mice and CR-AMPK$^{-/-}$ mice (<75% vs. AL-AMPK $^{+/+}$, **$p < 0.01$). This data shows that deficiency in AMPK and CR separately lower skeletal muscle NAMPT expression, but AMPK deficiency does not lead to further NAMPT mRNA decrease in CR mice (Fig. 3.1A).

We next undertook to determine the relevance of the observed NAMPT/AMPK changes to sirtuin levels and function. SIRT1 has been reported to improve glucose uptake in skeletal muscle (Guarente, 2006). Loss of AMPK decreased SIRT1 mRNA expression in the skeletal muscle of AL-fed animals (Fig. 3.1B). However, in contrast, SIRT1 gene expression was unchanged in both CR-WT and CR-AMPK$^{-/-}$ mice (Fig. 3.1B).

SIRT6, another nuclear sirtuin, reportedly enhances skeletal muscle insulin signaling and activation of Akt in mice, leading to hypoglycemia and associated increases in membrane association of GLUT1 and GLUT4,

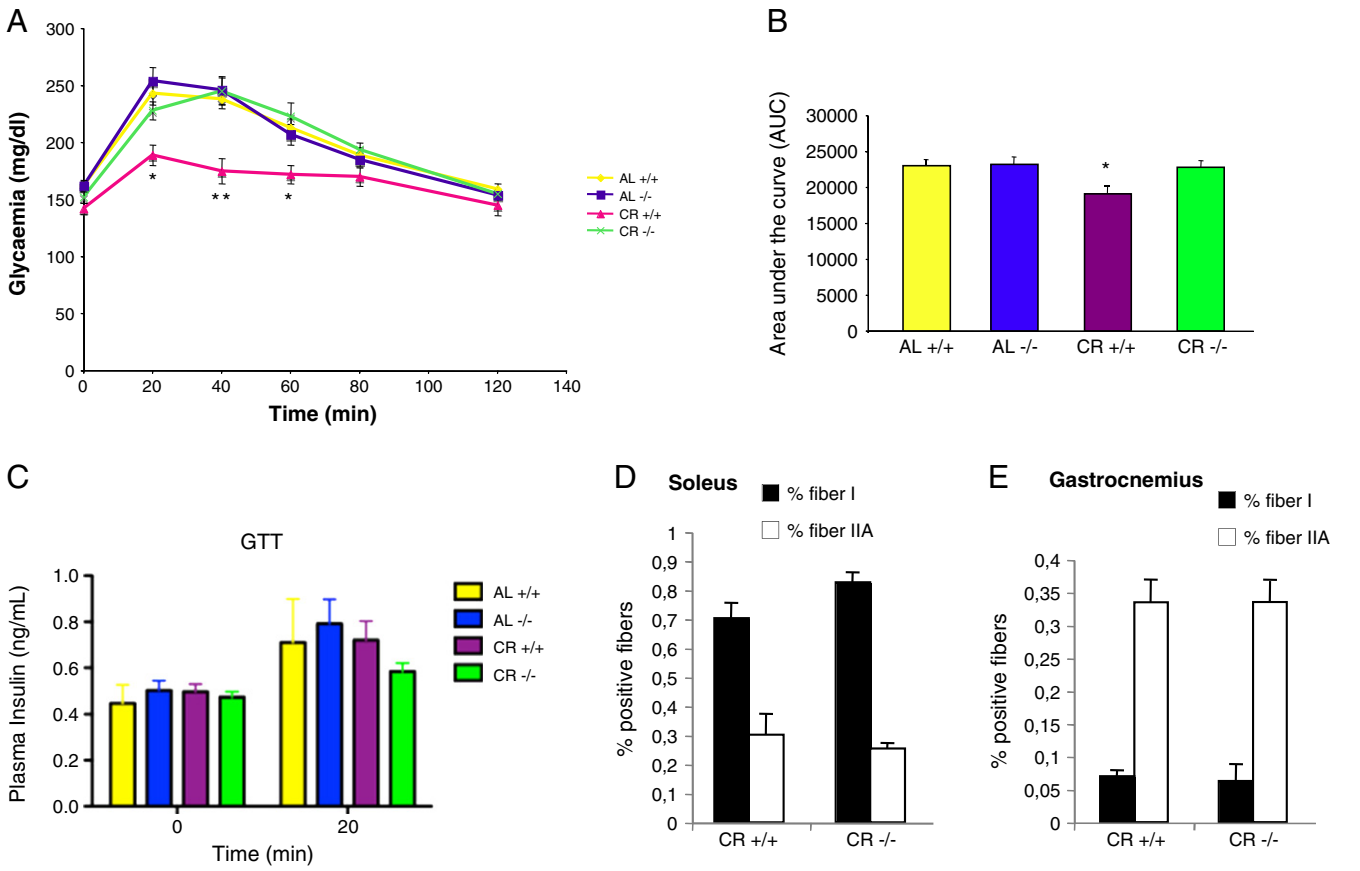


**Fig. 2.** (A) Glycemia after intra-peritoneal administration of glucose (3 g/kg of body weight) (B); area under the curve data (C); plasma glucose and insulin levels measured after 5-h fasting and 20 min after oral gavage of glucose (3 g/kg of body weight). Data are presented as mean ± SE ($n$ = 17–23). Quantification of immunostaining for MyHC I and MyHC IIA in gastrocnemius (C) and soleus (D) from CR-WT and CR-AMPK$^{-/-}$ mice. Results are presented as mean ± SEM ($n$ = 3); $^{*}p < 0.05$, $^{**}p < 0.01$ significantly different from AL-WT. AL = mice fed ad libitum; CR = calorie restricted mice (30% caloric restriction); −/− = AMPK α1/2 knockout mice. +/+ = WT mice.

which enhances glucose uptake (Xiao et al., 2010). Skeletal muscle SIRT6 gene expression was moderately suppressed by AMPK deficiency, both in AL-fed mice and CR mice (cf. SIRT1 gene expression, where the effect of CR is blocked by AMPK deficiency) (Fig. 3.1C).

The mitochondrial sirtuin, SIRT3, has been reported to mediate CR-associated reduction of oxidative damage (Li and Kazgan, 2011) as well as to promote fatty acid oxidation and insulin sensitivity in skeletal muscle. SIRT3 mRNA showed decreased gene expression in CR-AMPK$^{-/-}$ mice when compared to CR-WT (<80%, $^{\pm\pm\pm}p < 0.001$). In contrast, there were no observed differences in SIRT3 mRNA levels between AL-WT and AL-AMPK$^{-/-}$ mice (Fig. 3.1D).

In summary, CR did not increase gene expression of SIRT1, SIRT3 or SIRT6. In AL-fed mice, AMPK deficiency caused a modest decrease in SIRT1 and SIRT6 but did not affect SIRT3. Under CR, all sirtuins have decreased gene expression when AMPK is deficient. SIRT6, and to a lesser extent, SIRT1, are modestly decreased, while SIRT3 shows a significant marked decreased mRNA expression.

*PGC-1α gene and protein expression and acetylation status*

In skeletal muscle, PGC-1α target genes for FA oxidation are induced by the deacetylase SIRT1 (Dominy et al., 2010). PGC-1α controls the transcription of *SIRT3* to activate thermogenesis in brown adipose tissue (Giralt et al., 2011) and to suppress the production of reactive oxygen species (ROS) in the mitochondria (Kong et al., 2010). SIRT6 has not been reported to interact with PGC-1α. Accordingly, and because SIRT6 changes were minimal in response to AMPK deficiency and CR, we speculated that PGC-1α gene and protein expression would be altered in parallel with changes in SIRT1 and/or SIRT3 expression. Acetylation status was also assessed to verify whether SIRT1 activity altered in association with changes in SIRT1 gene expression. Skeletal muscle PGC-1α gene expression was similar in AL-WT mice and AL-AMPK$^{-/-}$ mice. It has been reported that gene and protein expression of PGC-1α in mouse skeletal muscle is enhanced by fasting (Caton et al., 2011), and in the present experiments, PGC-1α gene expression was substantially increased in CR-WT mice compared with AL-AMPK$^{-/-}$ mice (>3-fold vs. AL-WT, $^{**}p < 0.01$). The absence of AMPK led to ablation of CR-mediated increases in PGC-1α gene expression (<300% vs. CR-WT, $^{\pm\pm}p < 0.01$) (Fig. 3.2A). The marked increase in PGC-1α gene expression elicited by CR-WT mice was not, however, accompanied by any marked change in PGC-1α protein.

PGC-1α protein is deacetylated by SIRT1, and thus suppression of SIRT1 activity would be predicted to increase PGC-1α protein acetylation. When deacetylated, PGC-1α is activated and acts as a master regulator of mitochondrial biogenesis (Cantó et al., 2009). PGC-1α protein was therefore immunoprecipitated and probed with anti-acetyl-lysine antibody to assess the acetylation level of PGC-1α. Skeletal muscle PGC-1α acetylation was modestly (30%) but significantly ($^{*}p < 0.05$) increased in AL-AMPK$^{-/-}$ mice compared with AL-WT mice and substantially (0.5-fold, $^{*}p < 0.05$) increased in CR-WT animals compared with AL-WT mice (>0.5-fold vs. AL-AMPK$^{+/+}$, $^{*}p < 0.05$). The absence of AMPK completely abrogated the CR-dependent increase in PGC-1α protein acetylation (<30% vs. CR –WT, $\pm\, p < 0.05$).

*SIRT1 inhibition downregulates AMPK in starved L6 myoblasts*

Ex527 is known to inhibit SIRT1 gene expression in different cell types (Cantó et al., 2009; Wu et al., 2012). In agreement, we show

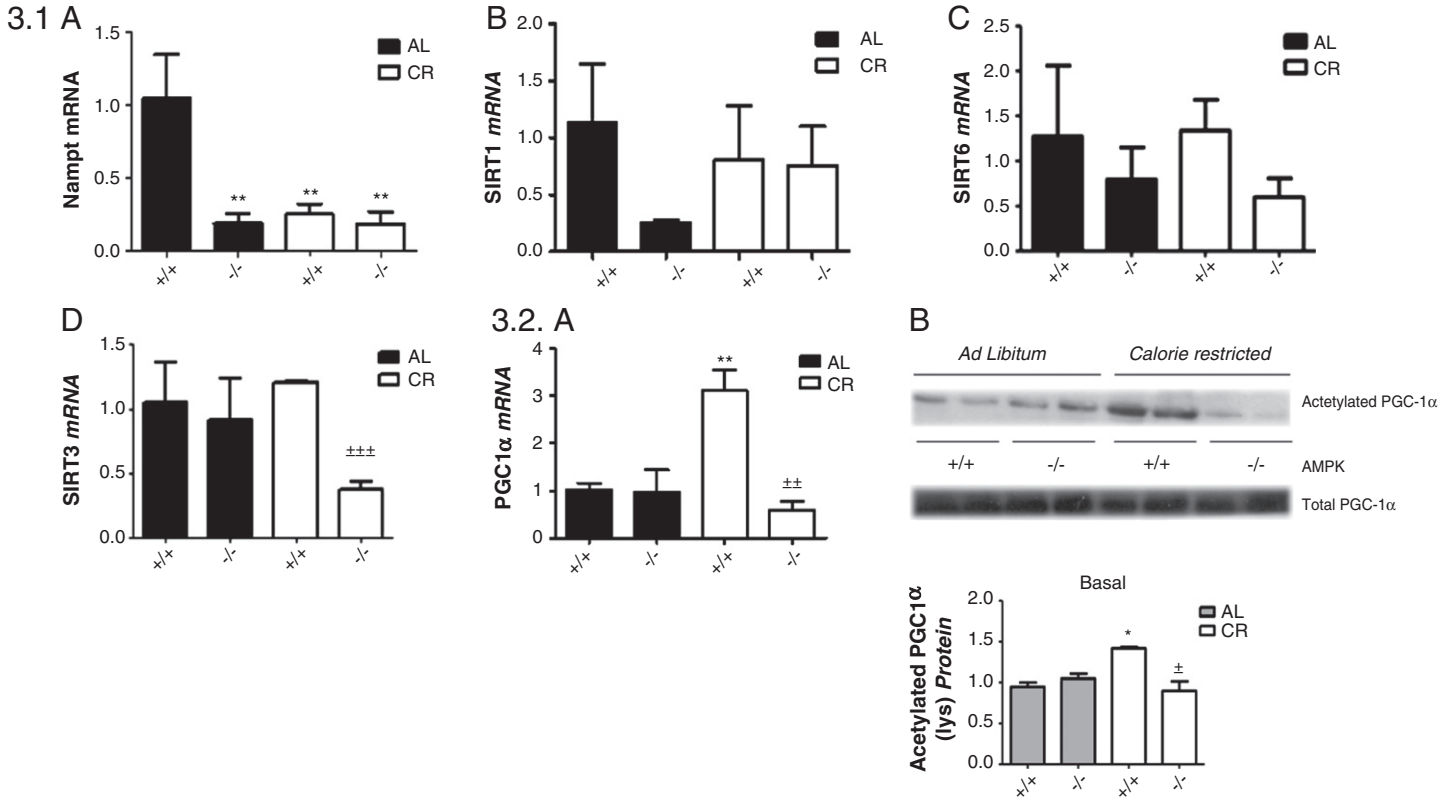


**Fig. 3.** (3.1) qRT-PCR showing NAMPT (A), SIRT1 (B) SIRT6 (C) and SIRT3 (D) mRNA expression in CR and AL mice (AMPK$^{-/-}$ and WT) vs. 18S gene. Values are presented as mean ± SEM ($n$ = 4–6 per group). $^{**}p < 0.01$ vs. +/+ AL mice; $^{\pm\pm\pm}p < 0.01$ vs. +/+ CR. AL = mice fed ad libitum; CR = calorie restricted mice (30% caloric restriction); −/− = AMPK α1/2 null mice; +/+ = WT mice. (3.2) (A) qRT-PCR analysis showing PGC-1α mRNA expression vs. 18S gene. (B) Immunoprecipitation followed by western blotting analysis showing acetylation levels of PGC-1α in lysine residues (MW: 130 kDa), compared to total PGC-1α. Data are presented as mean ± SE ($n$ = 4–6 per group), $^{**}p < 0.01$ vs. +/+ AL, $^{\pm\pm}p < 0.01$ vs. +/+ CR, $^{*}p < 0.05$ vs. +/+ AL, $^{\pm}p < 0.05$ vs. +/+ CR. AL = mice fed ad libitum; CR = calorie restricted mice (30% caloric restriction); −/− = AMPK α1/2 null mice.

here that SIRT1 mRNA levels were suppressed in starved L6 myoblasts, incubated with Ex527 (~100% vs. control, $^{**}p < 0.01$; Fig. 4A). The impact of SIRT1 inhibition on AMPK expression and activity was analyzed in fed and starved cells. Although total AMPK protein was unaffected by SIRT1 inhibition, a significant down regulation of phosphoAMPK-Thr$^{172}$ protein expression (~0.5-fold vs. control, $^{*}p < 0.05$) was observed in fed cells, suggesting that SIRT1 activity correlated positively with AMPK activity, contrasting with the inverse relationship between AMPK activation and Akt activation (Fig. 4B). In addition, similar findings were observed in serum-starved cells (Figs. 4C and B).

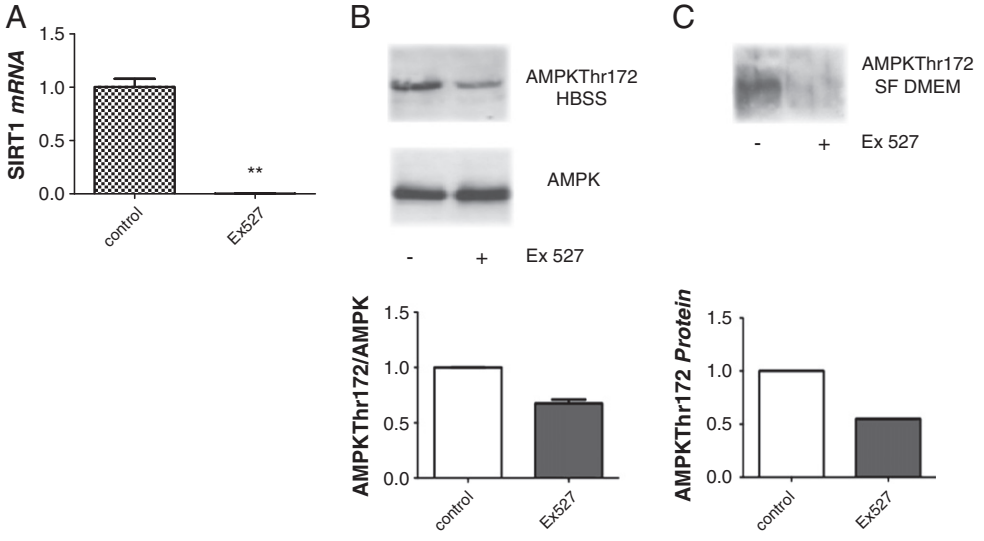


**Fig. 4.** (A) Changes in L6 SIRT1 mRNA level after culture with SIRT1 inhibitor, Ex527 (20 mg/ml of media), for 3.5 h. (B and C) Representative western blot of total AMPK and phospho-AMPK at Thr$^{172}$ (MW: 63 kDa) changes in cells cultured with Ex527 (20 mg/ml of media) for 3.5 h comparing to control cells [cells cultured in HBSS (serum-free, 1 mM glucose) for 3.5 h] (B) or comparing to control cells [cultured in serum-free DMEM (serum-free, 25 mM glucose) for 3.5 h (C). Total AMPK did not change between inhibit cells or control cells [cells cultured in HBSS (serum-free, 1 mM glucose) for 3.5 h (B). Blots were repeated 3 times with qualitatively similar results. β-Actin (MW: 45 kDa) was used to verify that the samples were equally loaded. Data are presented as mean ± SE, $^{*}p < 0.05$ vs. control.

## Discussion

We report here that CR-mediated improvement in whole body glucose tolerance is partly dependent on skeletal muscle AMPK activity. WT mice fed a CR diet displayed improved glucose tolerance, while this effect was ablated in the absence of skeletal muscle AMPK. These effects did not reflect differential effects in weight gain since CR induced a significant body weight loss in WT and AMPK$^{-/-}$ mice.

AMPK phosphorylates and activates the insulin receptor, providing a direct link between AMPK and the insulin signaling pathway; this pathway promotes energy conservation and survival of muscle exposed to severe glucose deprivation (Chopra et al., 2012). AMPK-induced increase in skeletal muscle and liver insulin signaling pathway results in increased blood glucose uptake (Lin et al., 2004; Burcelin et al., 2003). In addition, AMPK activity also improves skeletal muscle and liver glycogen synthesis capacity by increased glycogen synthase activity (O'Neill, 2013a, 2013b; Moore et al., 2012), enhancing blood glucose disposal, allowing faster glycemia reduction.

In addition to decreased skeletal muscle glucose tolerance, we also observed reduced serum insulin levels 20 min post-OGTT glucose infusion in CR-AMPK$^{-/-}$ mice. This suggests that first-phase glucose-stimulated insulin secretion (GSIS) from pancreatic β-cells is partially suppressed when AMPK is absent from skeletal muscle. Therefore, these data highlight the intriguing possibility for a mechanism by which a crosstalk between insulin-sensitive tissues and pancreatic islets might occur. In particular, myokines produced by an AMPK-dependent process may be important for the regulation of β-cell insulin secretion in response to CR. This opens very interesting therapeutic perspectives. Further studies on β-cells of muscle-specific AMPK$^{-/-}$ mice must be done to better understand this pathway.

The importance of NAMPT in protecting the body against age-induced T2D has been reported (Yoshino et al., 2011). This occurs in part through improved insulin secretion and glucose homeostasis (Revollo et al., 2007), via increases in $NAD^+$ levels and consequent SIRT1 activation. In this study, we demonstrated that the AMPK inactivation in skeletal muscle is associated with changes in NAMPT expression and SIRT1 activity. Previous studies have shown that (Caton et al., 2011; Fulco et al., 2008) SIRT1 activity seems to be decreased when AMPK is lacking, as a result of decreased AMPK-mediated NAMPT expression, which suggest that SIRT1 and AMPK may be linked (Fulco et al., 2008). However, the decrease of SIRT1 mRNA expression in the skeletal muscle of AL-fed AMPK$^{-/-}$ mice was no longer observed when mice were subjected to CR, suggesting that caloric restriction plays an important role in protecting skeletal muscle from the effects of decreased SIRT1 expression when AMPK is absent. The compromised SIRT1 activity in AMPK$^{-/-}$ mice abolished the SIRT1 dependent deacetylation of PGC-1α in AL-fed mice. This down regulation of PGC-1α activity compromises its function on glucose and lipid metabolism (Benton et al., 2010). The decreased PGC-1α gene expression is a possible mechanism by which AMPK deficiency decreases insulin secretion and glucose uptake. While some studies have reported increased SIRT1 mRNA and protein in response to CR (Schenk et al., 2011), our study is consistent with previous reports that have shown SIRT1 gene and protein expression to be unaffected by CR in skeletal muscle and adipose tissue (Tauriainen et al., 2011). Interestingly, SIRT1 inhibition down regulates AMPK activity in L6 myoblasts, which suggests a possible feedback loop that might exist between these two proteins, where AMPK regulates SIRT1 activity through NAMPT concentrations and, on the other hand, SIRT1 regulates AMPK possibly through LKB1 deacetylation (Lan et al., 2008). Xiao et al. found that 60% of SIRT6($^{-/-}$) animals had very low levels of blood glucose and died shortly after weaning (Xiao et al., 2010). Feeding the mice with glucose-containing water increased blood glucose and rescued 83% of mutant mice, suggesting that the hypoglycemia is a major cause for the lethality. They showed that SIRT6 deficiency results in more abundant membrane association of GLUT1 and GLUT4, which enhances glucose uptake. The authors further demonstrated that SIRT6 negatively regulates Akt phosphorylation at $Ser^{473}$ and $Thr^{308}$ through the inhibition of multiple upstream molecules, including insulin receptor, IRS1 and IRS2. The absence of SIRT6, consequently, enhances insulin signaling and activation of Akt, leading to hypoglycemia. These data uncover an essential role of SIRT6 in modulating glucose metabolism through mediating insulin sensitivity (Xiao et al., 2010). Controversially, in our experiments, we found that reduced SIRT6 possibly due to reduced AMPK-mediated SIRT1 expression was associated with non-significant enhanced glucose plasma levels upon CR.

In summary, AMPK deficiency impairs the beneficial effects of CR on glucose tolerance, possibly because it is linked to decreased SIRT1 gene expression, which could impair insulin signaling pathway, culminating in reduced glucose uptake.

### Conflict of interest statement

The authors of this article certify that they have no affiliations with or involvement in any organization or entity with any financial interest, or non-financial interest in the subject matter or materials discussed in this manuscript.

## References


Barzilai N, Huffman DM, Muzumdar RH, Bartke A. Diabetes 2012;61(6):1315–22.
Benton CR, Holloway GP, Han XX, Yoshida Y, Snook LA, Lally J, et al. Diabetologia 2010;53(9):2008–19.
Burcelin R, Crivelli V, Perrin C, Da Costa A, Mu J, Kahn BB, et al. J Clin Invest 2003;111(10). 1555–156.
Cantó C, Gerhart-Hines Z, Feige JN, Lagouge M, Noriega L, Milne JC, et al. Nature 2009;458(7241):1056–60.
Cantó C, Jiang LQ, Deshmukh AS, Mataki C, Coste A, Lagouge M, et al. Cell Metab 2010;11(3):213–9.
Caton PW, Kieswich J, Yaqoob MM, Holness MJ, Sugden MC. Diabetes Obes Metab 2011;13(12):1097–104.
Chopra I, Li HF, Wang H, Webster KA. Diabetologia 2012;55(3):783–94.
Colman RJ, Anderson RM, Johnson SC, Kastman EK, Kosmatka KJ, Beasley TM, et al. Science 2009;325(5937):201–4.
Dominy Jr JE, Lee Y, Gerhart-Hines Z, Puigserver P. Biochim Biophys Acta 2010;1804(8): 1676–83.
Fulco M, Cen Y, Zhao P, Hoffman EP, McBurney MW, Sauve AA, et al. Dev Cell 2008;14(5): 661–73.
Giralt A, Hondares E, Villena JA, Ribas F, Díaz-Delfín J, Giralt M, et al. J Biol Chem 2011;286(19):16958–66.
Guarente L. Nature 2006;444:868–74.
Hammer S, Snel M, Lamb HJ, Jazet IM, van der Meer RW, Pijl H, et al. J Am Coll Cardiol 2008;52(12):1006–12.
Higuchi R, Dollinger G, Walsh PS, Griffith R. Biotechnol (NY) 1992;10(4):413–7.
Holness MJ, Sugden PH, Silvestre MFP, Sugden MC. Expert Rev Endocrinol Metab 2012;7(2):191–208.
Hutchinson DS, Bengtsson T. Diabetes 2006;55(3):682–90.
Kong X, Wang R, Xue Y, Liu X, Zhang H, Chen Y, et al. PLoS One 2010;5(7):e11707.
Laemmli UK. Nature 1970;227(5259):680–5.
Lan F, Cacicedo JM, Ruderman N, Ido Y. J Biol Chem 2008;283(41):27628–35.
Li X, Kazgan N. Int J Biol Sci 2011;7(5):575–87.
Lin SJ, Ford E, Haigis M, Liszt G, Guarente L. Genes Dev 2004;18(1):12–6.
Marchal J, Blanc S, Epelbaum J, Aujard F, Pifferi F. PLoS One 2012;7(3):e34289.
Moore MC, Coate KC, Winnick JJ, An Z, Cherrington AD. Adv Nutr 2012;3(3):286–94.
O'Neill. Diabetes Metab J 2013a;37(1):1–21.
O'Neill. Mol Cell Endocrinol 2013b;366(2):135–51. [25].
Pessin JE, Saltiel AR. J Clin Invest 2000;106(2):165–9.
Rennie MJ. Biochem Soc Trans 2007;35(5):1302–5.
Revollo JR, Körner A, Mills KF, Satoh A, Wang T, Garten A, et al. Cell Metab 2007;6(5):363–75.
Ruderman NB, Xu XJ, Nelson L, Cacicedo JM, Saha AK, Lan F, et al. Am J Physiol Endocrinol Metab 2010;298(4):E751–60.
Schenk S, McCurdy CE, Philp A, Chen MZ, Holliday MJ, Bandyopadhyay GK, et al. J Clin Invest 2011;11:4281–8.
Shulman GI. J Clin Invest 2000;106:171–6.
Smith Jr DL, Nagy TR, Allison DB. Eur J Clin Invest 2010;40(5):440–50.
Suchankova G, Nelson LE, Gerhart-Hines Z, Kelly M, Gauthier MS, Saha AK, et al. Biochem Biophys Res Commun 2009;378(4):836–41.
Tauriainen E, Luostarinen M, Martonen E, et al. J Nutr Metab 2011;2011:525094.
Wu L, Zhou L, Lu Y, et al. Biochim Biophys Acta 2012;1822(11):1815–25.
Xiao C, Kim HS, Lahusen T, et al. J Biol Chem 2010;285(47):36776–84.
Yang H, Yang T, Baur JA, et al. Cell 2007;130(6):1095–107.
Yoshino J, Mills KF, Yoon MJ, Imai S. Cell Metab 2011;14(4):528–36. [5].
Zang M, Zuccollo A, Hou X, et alJ Biol Chem 2004;279(46):47898–905.

# A Key Role for Interferon Regulatory Factors in Mediating Early-Life Metabolic Defects in Male Offspring of Maternal Protein Restricted Rats

Authors
M. F. P. Silvestre[1], J. Kieswich[2], M. M. Yaqoob[2], M. J. Holness[1], M. C. Sugden[1], P. W. Caton[1]

Affiliations
[1] Centre for Diabetes, Bart's and the London School of Medicine and Dentistry, Queen Mary University of London, London, UK
[2] Department of Translational Medicine and Therapeutic, William Harvey Research Institute, Charterhouse Square, London, UK

Key words
- interferon regulatory factor
- maternal low protein
- adiponectin

## Abstract

An adverse intra-uterine environment, induced by maternal consumption of diets high in saturated fat or low in protein have been implicated as a potential trigger for development of metabolic disease in later life. However, the underlying mechanisms responsible for this programming of obesity have yet to be described. Recent studies have demonstrated that interferon regulatory factors 3 (IRF3) and 4 (IRF4) function to repress adipogenesis. We investigated whether impaired IRF3 and IRF4 function may predispose to development of metabolic disease in a model of programmed obesity. Changes in IRF3 and IRF4 levels, adipogenic gene expression, and adiponectin signalling were measured in white adipose tissue from programmed male offspring of rat dams fed a low-protein diet (MLP), which are predisposed to obesity. 3T3L1 adipocytes were used to determine novel regulatory mechanisms governing IRF expression. IRF3 and IRF4 levels were suppressed in MLP rats, together with raised lipogenic and adipogenic gene expression. Adiponectin and adiponectin receptor 1 and 2 mRNA levels were reduced in MLP rats, along with levels of PPARα and activity of AMP-activated protein kinase (AMPK), 2 downstream targets of adiponectin. Further studies determined that both IRF3 and IRF4 are induced by adiponectin, with adiponectin-AMPK and adiponectin-PPARα signalling regulating IRF3 and IRF4, respectively. We have demonstrated that impaired ability to repress adipogenesis and lipogenesis, through dysregulated adiponectin-PPARα-AMPK-IRF signalling, may play a causal role in predisposing MLP offspring to development of obesity and metabolic disease in later life.

**Supporting Information** for this article is available online at http://www.thieme-connect.de/ejournals/toc/hmr

received 30.10.2013
accepted 10.02.2014

Bibliography
DOI http://dx.doi.org/10.1055/s-0034-1370933
Published online: March 13, 2014
Horm Metab Res 2014; 46: 252–258

ISSN 0018-5043

Correspondence
***M. F. P. Silvestre***
Centre for Diabetes
Blizard Institute
Queen Mary University of London
4 Newark Street
London E1 2AT
UK
Tel.: +44/208/7882 2364
Fax: +44/208/7882 2186
m.silvestre@qmul.ac.uk

## Introduction

An adverse intra-uterine environment has also been implicated as a potential trigger for development of obesity in later life [1–3]. Examples of poor maternal nutrition include maternal consumption of diets high in saturated fat or a diet low in protein diet [1,4]. Maternal consumption of a low protein (Maternal Low Protein; MLP) diet results in offspring with a low birth weight in humans and animal models [4]. Moreover, there exists a strong positive correlation between low birth-weight and the development in later life of obesity, insulin resistance, and type 2 diabetes [5]. Epidemiological and experimental evidence suggests that an imbalance between prenatal (e.g., maternal protein restriction) and post-natal (e.g., excess dietary carbohydrate) nutrition can predispose to development of obesity [1]. In agreement, children exposed to growth-restricted conditions during development exhibit increased adiposity in childhood and later life [6], whilst the offspring of rats fed a low-protein diet display a greater predisposition to develop obesity and related metabolic disorders in response to high-fat feeding compared to controls [1,5]. This phenomenon, termed the 'thrifty phenotype', suggests that foetal malnutrition may lead to physiological changes that programme the foetus for survival in what it predicts to be a poor nutritional environment. This evolutionary programming is less advantageous when food is abundant, potentially predisposing to obesity [5]. However, the underlying mechanisms responsible for this programming of obesity have yet to be described.

Recent studies have identified the immunoregulatory proteins, interferon regulatory factors 3 and 4 (IRF3 and IRF4) as key regulators of adipocyte function [7,8]. IRF4 increases during adi-

pocyte differentiation and functions to repress adipogenesis and lipogenesis and induce lipolysis in white adipose tissue. IRF4 expression is repressed by insulin, and consequently IRF4 levels are reduced in insulin resistant mouse models, as well as being elevated during fasting and reduced during re-feeding. Adipocytes lacking IRF4 display increased expression of lipogenic genes including fatty acid synthase (FAS; gene code: *Fasn*) and sterol regulatory-element binding-protein 1 (SREBP1). Moreover, IRF4 knockout mice have larger adipocytes, are obese, and develop T2DM. Less is known about the regulation of IRF3 [7, 8]. To further examine the early life mechanistic changes following exposure to an adverse intra-uterine environment responsible for onset of obesity and metabolic syndrome in later-life, we examined the role of IRF3 and IRF4 in the MLP model of foetal programming. Further to this, we investigated novel mechanisms involved in regulation of IRF3 and IRF4 in adipocytes and white adipose tissue.

## Materials and Methods

### Experimental animals

Studies were conducted in adherence to the regulations of the UK Animal Scientific Procedures Act (1986), under project license PPL 70/7276. All animals were maintained on a 12-h light/dark cycle (light from 07:00 AM). All experiments were conducted in the fed state, unless stated otherwise. Animals were sacrificed under $CO_2$ asphyxiation.

### Maternal low protein model

Pregnant female Wistar rats (250–300 g; Charles River, Kent, UK) were randomly assigned to either control (CON; 20% protein) or an isocaloric maternal low protein (MLP; 8%) diets (Hope Farms BV, Woerden, Netherlands) and maintained on the respective diet throughout pregnancy and lactation (12 rats/group). Pregnant dams fed the low-protein diet did not exhibit any differences in caloric intake compared to controls. Despite this, MLP offspring weighed significantly less at 3 days of age than CON offspring (28%; $p < 0.05$). Male offspring were weaned at 24 days and maintained on standard rodent diet thereafter. CON and MLP offspring were killed at 8 weeks and visceral WAT depots were snap-frozen for analysis, whilst blood was collected for measurement of glucose and insulin.

### PPARα–/– mice

Male PPARα–/– mice, bred onto a SV/129 genetic background, were provided by Drs. J. Peters and F. J. Gonzalez (National Institutes of Health, Bethesda, MD). Wild-type SV/129 mice (from Charles River, UK) were used as controls.

### Metformin treatment

Eight-week-old male C57Bl/6 mice (Charles River, Kent, UK) maintained on standard rodent diet were administered metformin (250 mg/kg/day) or an equal volume of water daily for 7 days by oral gavage.

### 3T3L1 Culture and differentiation

3T3-L1 preadipocytes were cultured (37 °C; 5% $CO_2$) in Dulbecco's Modified Eagle Media (DMEM; 25 mM glucose) supplemented with 10% bovine calf serum (BCS), (both Sigma Aldrich, Poole, UK) until confluent. Two days post-confluence (differentiation day 0), to induce differentiation media was changed and replaced with DMEM/10% foetal calf serum (FCS) supplemented with insulin (1 µg/ml), dexamethasone (0.25 mM), and isobutyl-1-methylxanthine IBMX (0.5 mM). After 2 days (differentiation day 2), media was replaced with DMEM/10% FCS supplemented with insulin (1 µg/ml). After 4 days (differentiation day 4) media was replaced with DMEM/10% FCS. All media contained 100 U/ml penicillin and 100 µg/ml streptomycin (both Sigma Aldrich, Poole, UK). Differentiation of pre-adipocytes to adipocytes was confirmed by measurement of PPARγ gene expression. Treatments, carried out on differentiation day 8, were as follows; adiponectin (30 µg/ml), WY-14643 (10 µM) for 24 h. All treatments were carried out in DMEM containing 10% FCS.

### Immunoblotting

Solubilised protein samples [10 µg; measured and equalised in each fraction using an RC-DC BioRad system (BioRad, UK)] were separated by SDS-PAGE and transferred onto PDVF membrane (GE Healthcare, Amersham, UK). Blots were blocked with 5% (w/v) bovine serum albumin (BSA) or 5% milk in Tris-buffered saline/0.1% Tween-20 (TBS/T) solution and then incubated overnight in primary antibody. Antibodies used in this study are anti-phospho($Thr^{172}$)-AMP-activated protein kinase (AMPK), anti-AMPK, anti-phospho($Ser^{171}$)-acetyl CoA carboxylase (ACC) and anti-ACC (Cell Signalling Technologies, MA, USA). Detection of bands was achieved by using the chemiluminescence substrate SuperSignal West Pico (Pierce, Rockford, IL, USA). Reference protein measurements were made with mouse monoclonal anti-β-actin (clone AC-15; Sigma, Poole, UK) primary antibody in a 3% (w/v) milk-TBS/T solution, at 4 °C.

### Quantitative RT-PCR

Gene expression was measured by qRT-PCR, using Taqman® or Sybr green® methodology. Gene expression was determined by ΔΔCt methodology, normalised against 18S ribosomal RNA (Applied Biosystems, UK). Changes in gene expression are represented as fold change relative to one, where control equals one. All primer and probes are from Eurogentec, UK. A list of primers can be found in supplemental **Table 1S** (Supporting Information).

### Serum insulin and glucose

Insulin was analysed by ELISA (Mercodia, Uppsala, Sweden) using rat insulin as standard. Plasma glucose was measured by a glucose oxidase/peroxidase method (Roche Diagnostics, Lewes, UK).

### Statistical analysis

Results are expressed as mean ± SEM. Statistical comparisons were obtained using GraphPad (GraphPad Software, CA, USA). Statistical differences were calculated using an unpaired *t*-test.

## Results

### Metabolic data for MLP offspring

Pregnant dams fed a low-protein diet did not exhibit any differences in food intake compared to controls (data not shown). Despite this MLP offspring weighed significantly less at 3 days of age than control litter mates (28%; $p < 0.05$). After 8-weeks consumption of standard rodent diet, MLP offspring displayed no changes in fasting insulin (16.0 ± 3.2 µU/ml) compared to controls (14.4 ± 1.3 µU/ml) ($p = 0.65$). Additionally, no changes in

fasting plasma glucose levels were found in MLP offspring (4.36 ± 0.13 mmol/l) compared to control (4.11 ± 0.21 mmol/l) (p = 0.33), whilst glucose area under the curve (AUC) analysis for glucose tolerance tests resulted in a nonsignificant increased AUC values for MLP (9.76 ± 1.29 mmol/l/min) compared to control (7.45 ± 0.79 mmol/l/min) (p = 0.16) (**Table 1**).

## MLP offspring display altered adipogenic and lipogenic gene expression

Whilst no significant changes in metabolic data were observed at this early stage in the MLP rats, it is possible that mechanistic changes may occur during this early-life period, which would predispose to later development of metabolic disease. Therefore, by focussing on altered lipogenesis and adipogenesis in white adipose tissue, we next attempted to identify early-life metabolic changes, which would likely lead to onset of the established later-life metabolic defects induced by MLP. IRF3 and IRF4 are recently identified as repressors of adipogenesis and lipogenesis [7, 8]. Gene expression of IRF3 and IRF4 was markedly reduced in white adipose tissue of MLP rats as compared to controls (**Fig. 1a, b**). These changes occurred in parallel with increased mRNA expression of SREBP1c, elevated mRNA and protein levels of FASN as well as increased ACC protein (**Fig. 1c–e**), consistent with a role for IRF4 in repressing transcription of these genes. This data implies that early life changes in IRF3 and IRF4 occur in MLP rats and may contribute to increased risk of development of obesity and metabolic syndrome in later life.

**Table 1** Serum insulin and glucose changes between control and MLP rats.

| | CON | MLP | p-Value |
|---|---|---|---|
| Fasting glucose (mM) | 4.11 ± 0.13 | 4.36 ± 0.21 | 0.33 |
| Fasting insulin (μU/ml) | 14.4 ± 1.3 | 16 ± 3.21 | 0.65 |
| Glucose – AUC (mmol/l/min) | 7.54 ± 0.79 | 9.76 ± 1.29 | 0.16 |

## IRF3 and IRF4 suppression is associated with impaired adiponectin signalling

Previous studies have demonstrated that insulin exerts regulatory control of IRF4, whilst less is known about IRF3 regulation in the context of obesity and metabolic syndrome. Insulin was reported to repress IRF4 expression in vitro in adipocytes and in vivo under fed conditions, and in obese, hyperinsulinaemic rodent models [7]. However, despite marked reductions in IRF3 and IRF4 expression, we did not observe significant changes in serum insulin levels in our models (**Table 1**). This suggested the existence of an alternative regulatory mechanism controlling IRF4, and potentially IRF3, in white adipose tissue. Adipokines, such as adiponectin, are bioactive peptides secreted from adipose tissue, which exert metabolic control over a number of insulin sensitive tissue, including, in an autocrine manner, adipose tissue. We next investigated potential alterations in adiponectin signalling in MLP rats, with the aim of determining alternative mechanisms of IRF3 and IRF4 regulation. Remarkably, we found that mRNA levels of adiponectin (AdipoQ;

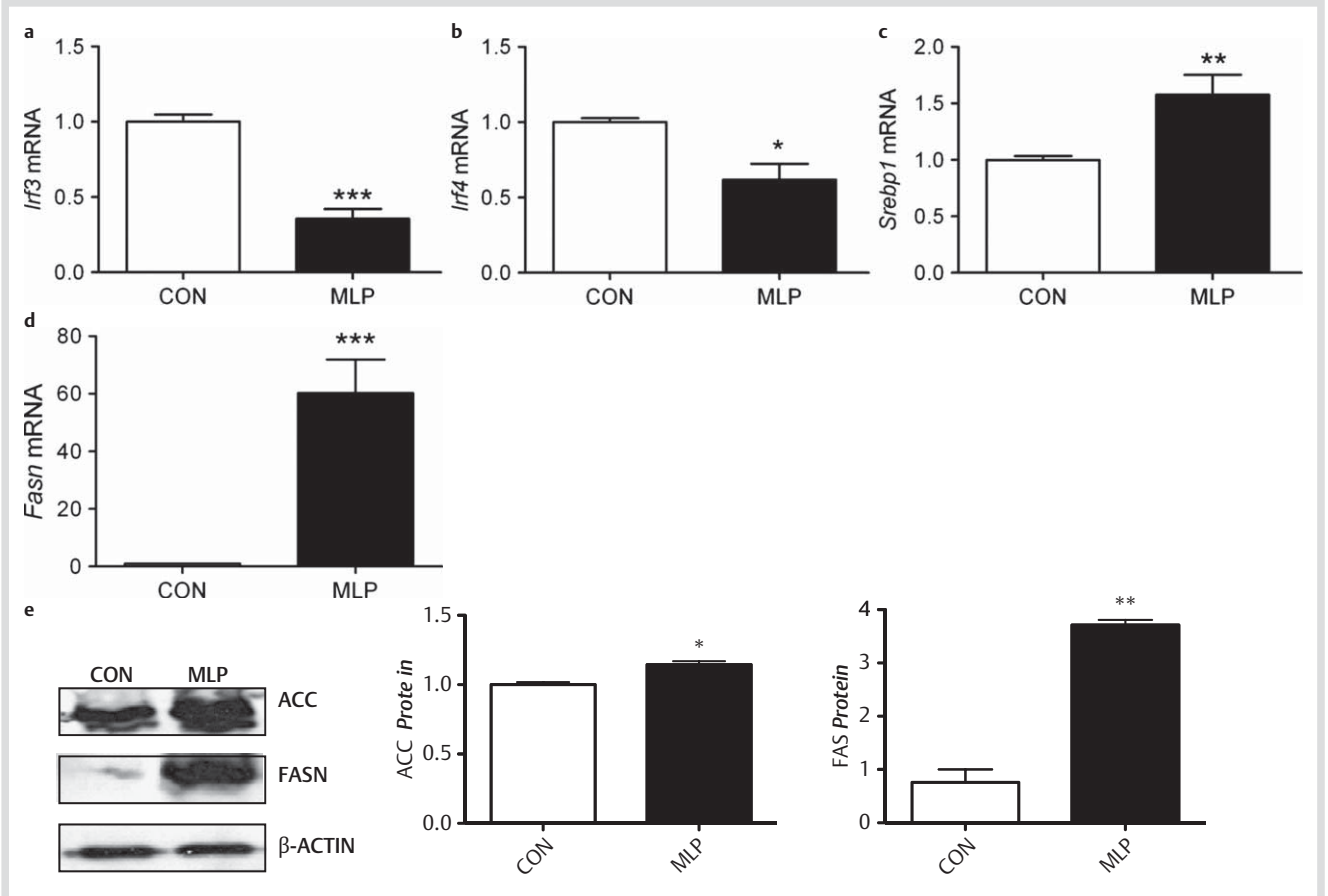


**Fig. 1** Reduced IRF levels in white adipose tissue of MLP offspring. Visceral WAT was isolated from 8-week-old offspring of MLP and control Wistar rats (n = 6); Gene expression of **a** *Irf3*, **b** *Irf4*, **c** *Srebp1c*, and **d** *Fasn*. **e** Protein levels of FASN and ACC. Western blots are representative. Data are expressed as mean ± SEM. *p < 0.05, **p < 0.01, ***p < 0.001 vs. control.

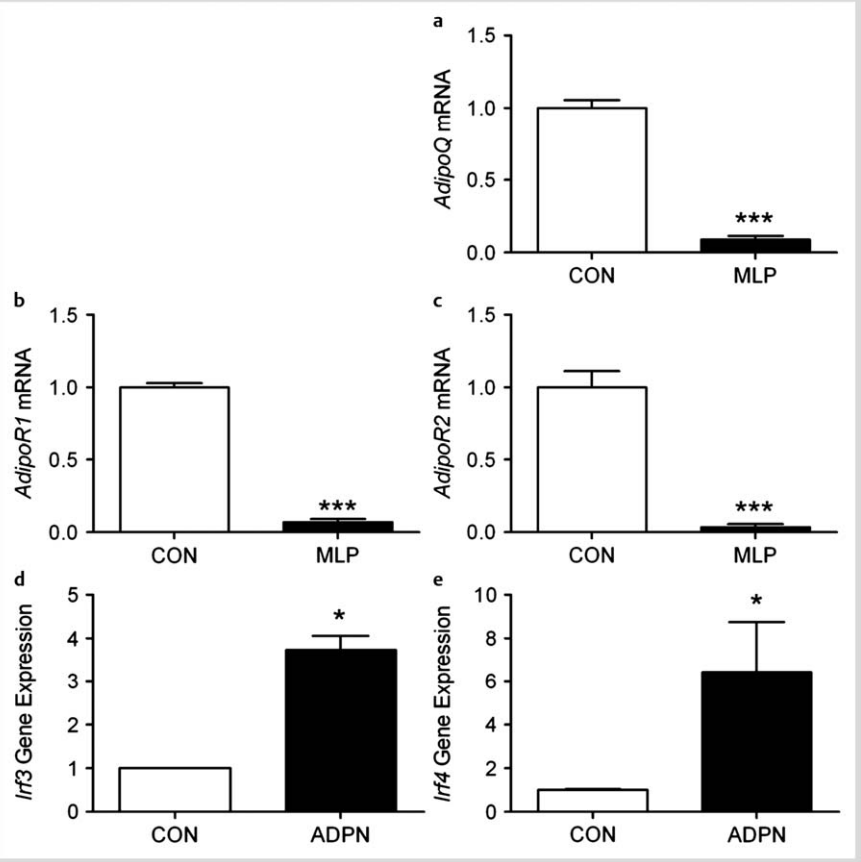


**Fig. 2** Impaired adiponectin signalling in white adipose tissue of MLP offspring leads to reduced IRF levels. Visceral WAT and serum were isolated from 8-week-old offspring of MLP and control Wistar rats (n = 6); **a** serum insulin levels; mRNA levels of **b** *AdipoQ*, **c** *AdipoR1*, and **d** *AdipoR2* in white adipose tissue. 3T3-L1 adipocytes were treated with adiponectin (30 µg/ml; 24 h) and mRNA levels of **e** *Irf3* and **f** *Irf4* were measured by qPCR. Data are expressed as mean ± SEM. $^{*}p < 0.05$, $^{***}p < 0.001$ vs. control.

**Fig. 2a**) and adiponectin receptor 1 (AdipoR1) and receptor 2 (AdipoR2) were dramatically suppressed in MLP rats by ≈90% relative to control (**Fig. 2b, c**), suggesting that impaired adiponectin signalling may lead to decreased IRF3 and IRF4 expression. To investigate this further, we used the 3T3L1 adipocyte cell line. Consistent with impaired adiponectin signalling and reduced IRF expression in the white adipose tissue of MLP rats, incubation of 3T3L1 adipocytes with adiponectin led to increased mRNA levels of IRF3 and IRF4 (**Fig. 2d, e**). This suggests that, in addition to insulin, adiponectin provides an additional level of regulatory control over IRF3 and IRF4 in white adipose tissue.

## Adiponectin regulates IRF3 and IRF4 through AMPK and PPARα

Adiponectin, via signalling through AdipoR1 and AdipoR2 has been reported to exert metabolic effects through activation of the energy sensing enzyme AMP-activated protein kinase (AMPK) and the nuclear receptor peroxisome-proliferator activated receptor α (PPARα) [9]. Both AMPK and PPARα play important roles in regulating lipogenesis and fatty acid oxidation [9–11]. Consistent with observed reductions in adiponectin and AdipoR1 expression, MLP rats also displayed decreased protein levels of phospho($Thr^{172}$)-AMPK (**Fig. 3a**). Since phosphorylation at $Thr^{172}$ leads to AMPK activation, this observation suggests reduced AMPK activity in MLP rats. In addition, protein levels of phospho($Ser^{79}$)-ACC, a downstream target of AMPK, were also reduced in MLP offspring compared to control (**Fig. 3a**). Total protein levels of AMPK were unchanged, demonstrating that decreased AMPK activation did not occur because of MLP-induced reductions in total protein. In contrast, total-ACC protein levels were elevated in MLP mice, reflecting increased lipogenesis, changes that are consistent with increased lipogenic gene expression (**Fig. 1e**). Furthermore, reflecting decreased AdipoR2 expression, we also observed decreased mRNA levels of PPARα in MLP rats, compared to control (**Fig. 3b**). Transcriptional modulation by PPARα requires the presence of the co-activator PPARγ co-activator 1α (PGC1α). Consistent with this, PGC1α mRNA levels were also suppressed in MLP rat adipose tissue (**Fig. 3c**).

To further analyse the potential role of adiponectin-AMPK-PPARα signalling in regulating IRF3 and IRF4 expression, we initially used 3T3L1 adipocytes. Use of 3T3L1 adipocytes allowed for specific examination of IRF4 regulation in a model lacking macrophages, which may influence results given the role of IRF4 in immune regulation [12]. Adipocyte differentiation was confirmed by measurement of mRNA levels of PPARγ (data not shown). Treatment of differentiated adipocytes with WY14643, a potent PPARα agonist, had no effect on IRF3 mRNA (**Fig. 4a**) but did induce expression of IRF4 (**Fig. 4b**). We further analysed these putative signalling mechanism using PPARα knockout mice, which displayed ≈90% reduction in PPARα mRNA levels in white adipose tissue, together with a marked reduction in PGC1α mRNA levels (**Fig. 4c, d**). Significantly, in PPARα knockout mice the normal IRF4 responses to fasting and feeding were disrupted (**Fig. 4e**). Consistent with previous reports [7] IRF4 levels were induced by fasting in wild-type mice. However, this effect was blunted in PPARα knockout mice, where IRF4 levels were reduced in fasted compared to fed mice. Similar to MLP rats, PPARα knockout mice also displayed reduced IRF4 levels (**Fig. 4f**), together with raised levels of ACC and SREBP1c (**Fig. 4g, h**), indicative of elevate lipogenesis and adipogenesis in white adipose tissue. Taken together, these results indicate that an adiponectin-PPARα signalling pathway induces IRF4 mRNA expression in white adipose tissue. Moreover, this path-

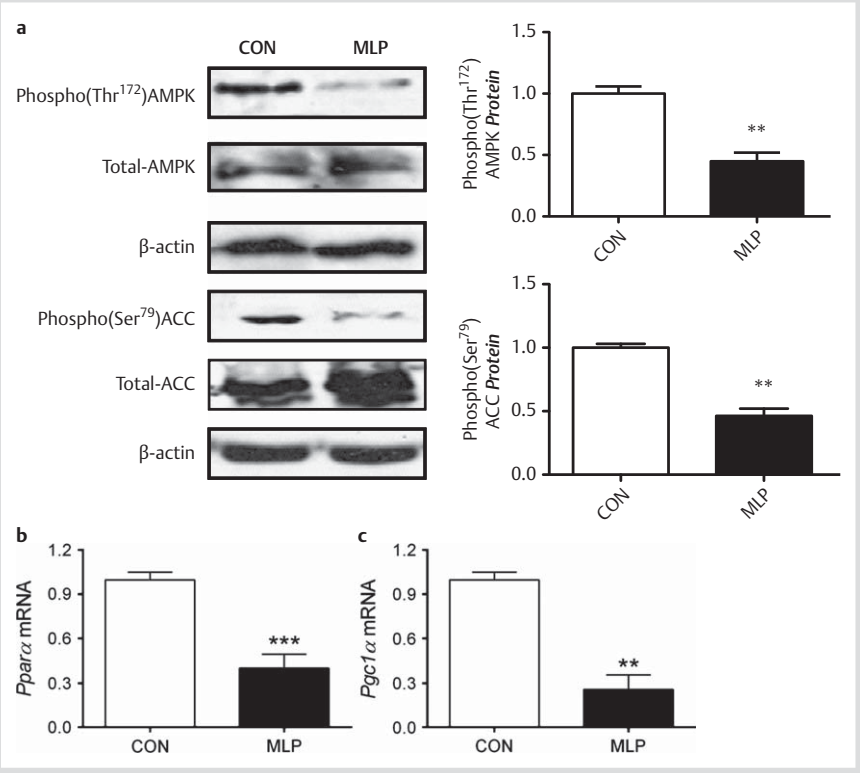


**Fig. 3** Reduced AMPK and PPARα signalling in white adipose tissue of MLP offspring. Visceral WAT was isolated from 8-week-old offspring of MLP and control Wistar rats (n = 6); **a** protein levels of phospho(Thr$^{172}$)-AMPK, total-AMPK and phospho(Ser$^{79}$)-ACC; mRNA levels of **b** *Pparα* and **c** *Pgc1α*.Western blots are representative. Data are expressed as mean ± SEM. $^{**}p<0.01$, $^{***}p<0.001$ vs. control.

way is dysregulated in response MLP, and this may in part mediate the metabolic defects associated with this MLP.

### Adiponectin-AMPK signalling may regulate IRF3

In contrast to IRF4, IRF3 was unaffected by PPARα agonist in vitro, indicating an alternative regulatory mechanism for IRF3 (**Fig. 4a**). Since adiponectin induced both IRF3 and IRF4, but PPARα regulated IRF4 only, we reasoned that AMPK, another target of adiponectin, may exert regulatory control over IRF3. To test this, we used metformin, as a known activator of AMPK [13], rather than for its actions as an anti-diabetic treatment. Administration of metformin to control mice led to significant induction of IRF3 (**Fig. 5a**) but had no effect on IRF4 mRNA levels (**Fig. 5b**), implying that adiponectin-AMPK signalling selectively induces IRF3 in white adipose tissue.

## Discussion

We report here that expression of IRF3 and IRF4, 2 key repressors of adipogenesis, are reduced in offspring of rats fed a protein-restricted diet during pregnancy and lactation, in parallel with no changes in fasting insulin and glucose. Human epidemiological studies have consistently reported that exposure to an adverse intrauterine environment, such as protein-restriction, leads to an increased risk of development of obesity, T2DM, and cardiovascular disease in later life [3,5,6]. Experimental model studies have reported that MLP offspring gain more weight, have increased susceptibility to development on metabolic syndrome and display impaired adipocyte function when placed a high fat diet [1,14,15]. However, the underlying regulatory mechanisms driving these processes are yet to be fully elucidated. Our data provides evidence that a loss of ability to efficiently repress adipogenesis and lipogenesis, as a result of marked early-life reductions in IRF3 and IRF4, may contribute to impaired adipocyte function and increased risk of obesity in later life. Whilst metabolic changes observed in this model are mild, the early life mechanistic changes reported here would likely make a key contribution to the expected, and previously reported, metabolic deterioration likely observed in these animals in later life.

Previous studies have described that IRF4 expression and function is suppressed by insulin, and that as a result, IRF4 expression is lower in white adipose tissue depots obtained from rodent models characterised by insulin resistance; HFD, *ob*/*ob* and *db*/*db* mice [7]. Despite this well characterised role of insulin, our MLP model displayed a marked reduction in IRF3 and IRF4, without significant changes in serum insulin. Instead, our data point the involvement of the adiponectin-PPARα and adiponectin-AMPK signalling pathways in the regulation of IRF4 and IRF3 respectively. Adiponectin is a bioactive adipokine expressed at high levels and secreted from adipose tissue [16]. Adiponectin exerts metabolic regulatory effects via autocrine, paracrine, and endocrine function, through the receptors adipoR1 and adipoR2, which in turn activate AMPK and PPARα [9,16]. Conversely, PPARα agonists have been reported to upregulate adiponectin and AdipoR1 and AdipoR2, whilst adiponectin is suppressed in PPARα knockout mice [17]. PPARα is a transcription factor for genes involved in lipolysis and fatty acid oxidation and PPARα null mice maintained on a high-fat diet become more obese than wild type [18]. Despite suppression of insulin levels and increases in FA supply, PPARα-deficient mice exhibit an impaired ability to adequately upregulate hepatic FA oxidation in response to fasting [19]. Insulin resistance induced by excess of nonesterified FA and circulating TAG can be corrected by the administration of PPARα activators by actions to promote removal of intracellular lipid through tissue FA oxidation [20]. PPARα is activated under calorie restriction, increasing the expression of genes encoding mitochondrial FA oxidation enzymes, thereby increasing the capacity for FA oxidation and

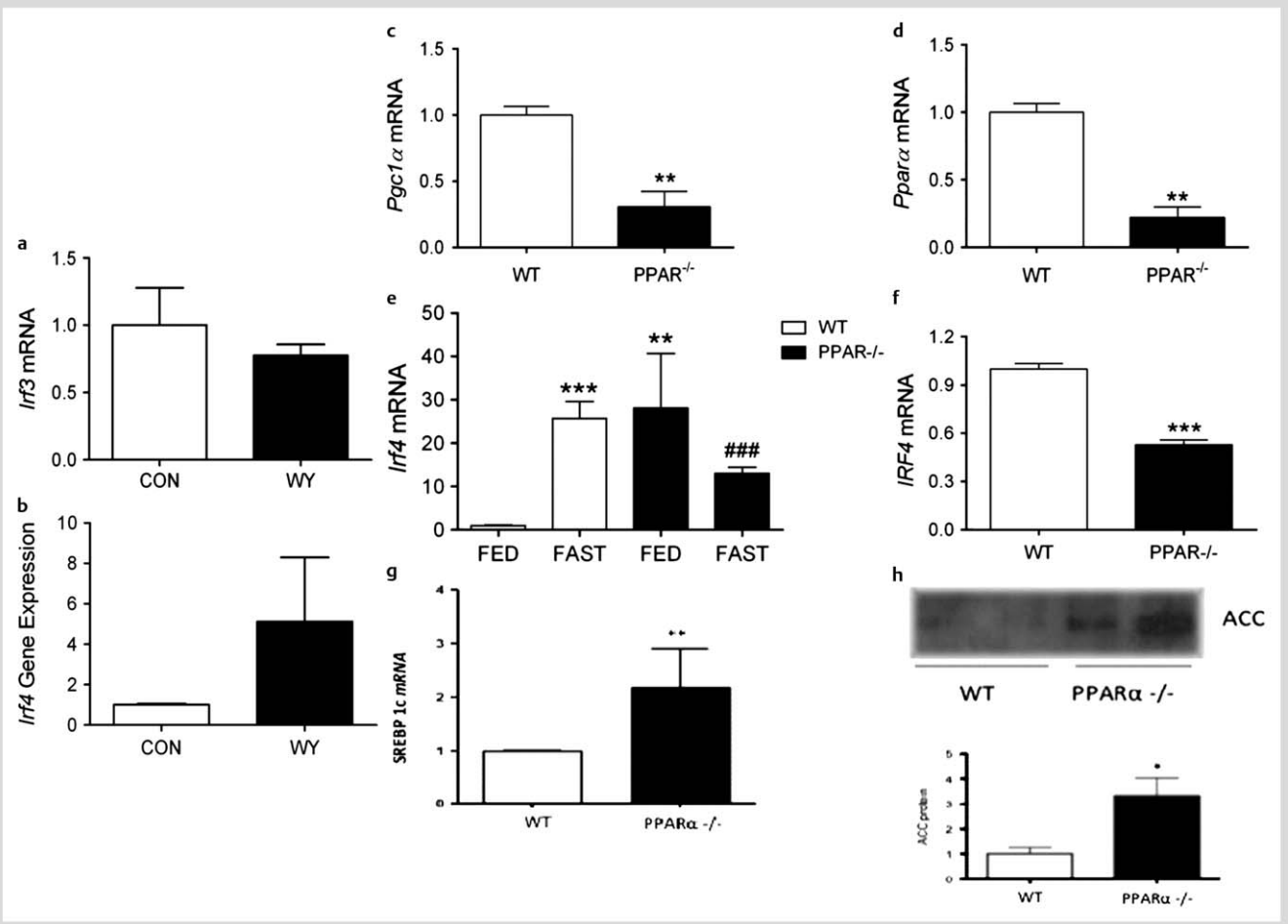


**Fig. 4** Adiponectin-PPARα signalling induces IRF4 expression in white adipose tissue. 3T3-L1 adipocytes were treated with WY14643 (10 µM; 24 h) and mRNA levels of **a** *Irf3* and **b** *Irf4* were measured by qPCR. Visceral WAT and serum were isolated from 8-week-old PPARα knockout and control mice (n = 6); mRNA levels of **c** *Pparα* **d** *Pgc1α*, **e**, **f** *Irf4*, **g** *Srebp1c* were assessed by qPCR. **h** Protein levels of ACC. Western blots are representative. Data are expressed as mean ± SEM. $^{*}p<0.05$, $^{**}p<0.01$, $^{***}p<0.001$ vs. control (FED); $^{\#\#\#}p<0.001$ vs. control (FAST).

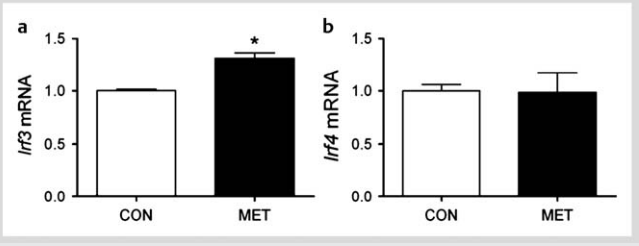


**Fig. 5** Adiponectin-AMPK signalling may regulate IRF3 expression in white adipose tissue. Visceral WAT was isolated from 8-week-old C57Bl/6 mice administered metformin (250 mg/kg/day; 7 days) or saline equivalent (n = 6); mRNA levels of **a** *Irf3* and **b** *Irf4* were measured by qPCR. Data are expressed as mean ± SEM. $^{*}p<0.05$ vs. control.

intracellular lipid clearance [21]. AMPK activation occurs in response to a rise in AMP associated with metabolic stresses that interfere with ATP production (e.g., hypoxia or calorie restriction/glucose deprivation) or accelerated ATP consumption (e.g., muscle contraction), so as to preserve or maintain tissue function [22]. Therefore, AMPK also plays an important role in regulating lipid homeostasis in adipose tissue, having been shown to inhibit lipogenesis and during the longer-term increase lipolysis [10]. The fact that PPARα levels and other oxidation genes (PGC-1α) and proteins (AMPK) are suppressed in MLP rats, while lipogenic genes are enhanced (SREBP-1c and FAS), suggest that these mice may develop a similar phenotype to PPARα –/– mice, and that the MLP phenotype may be a direct result of reduced PPARα levels, leading to increased IRF4 levels. Under both conditions, fatty acid oxidation is decreased and lipogenesis is enhanced, again potential involving an IRF-mediated mechanism. Several mechanisms for these actions of AMPK and PPARα have been described. Our data suggests a further mechanism of action, namely via induction of IRF3 and IRF4, and consequent repression of lipogenesis and induction of lipolysis in white adipose tissue. These changes were in turn regulated by adiponectin, and these signalling pathways were all impaired in MLP rats. In addition to specific effects on lipolysis and lipogenesis, low levels of IRF4 may also reflect poorly differentiated adipocytes, since IRF4 is expressed only in fully differentiated adipocytes. Poorly differentiated adipocytes are often present in obesity and can lead to hypoxia, inflammation, and an altered adipokine profile, including lower adiponectin levels [23]. Dysregulation of these processes are linked to onset of T2DM. Moreover, reduced adiponectin levels occurring as a result of poor differentiation, may represent an initial cause of the impaired adiponectin signalling observed in MLP mice. Alternatively, this mechanism of impaired adiponectin signalling may induce a feed-forward loop, with further reductions in adiponectin signalling and consequent worsening of the MLP phenotype. In addition, whilst

adiponectin has been reported to induce PPARα, the reverse has also been documented, with adiponectin upregulated by PPARα agonists and suppressed in white adipose tissue of PPARα knockout mice [17]. Thus, suppressed PPARα levels in MLP mice may contribute to further impairment of adiponectin signalling and consequent exacerbation of the MLP phenotype. Further studies are required to determine the exact mechanistic interactions by which PPARα regulates IRF4.

In addition to an established role in adipocytes, IRFs are present in macrophages and infiltrating lymphocytes. IRF4 is essential for the function and homeostasis of both mature B and mature T lymphocytes. IRF4-deficient mice exhibited a profound reduction in serum immunoglobulin concentrations and impaired T lymphocyte function [24]. The altered IRF levels could potentially represent reduced immune infiltrate into the white adipose tissue. Further research is needed to clarify this. However, given the increased inflammation and macrophage recruitment observed in response to reduced adiponectin levels in other studies [16], a reduced immune infiltrate seems unlikely, instead suggesting a specific role for adipocyte-IRF3 and IRF4 in this model.

In summary, we propose that in early life in response to protein restriction adiponectin signalling is impaired leading to reduced activity of PPARα and AMPK, which in turn lead to decreased levels of IRF3 and IRF4. This would lead to an inability to repress adipogenesis and lipogenesis, and confer increased susceptibility to development of an obese phenotype in later-life.

## Acknowledgements

This research was supported by Diabetes UK grants BDA:RD08/0003665, BDA:RD06/0003424, BDA:RD03/0002725. PWC is the recipient of an EFSD/Lilly Research Fellowship. MFPS was funded by Fundacao Para a Ciencia e Tecnologia, Ministerio da Educacao e Ciencia, Portugal. We thank Dr. C. Walker for tissue sampling and adipocyte preparation, Dr S. Greenwald for help with the MLP modelling, and Dr. Peter King for provision of 3T3L1 adipocytes.

## Conflict of Interest

The authors declare that they have no conflict of interest that could be perceived as prejudicing the impartiality of the research reported.

## References

1 *Cottrell EC*, *Ozanne SE*. Early life programming of obesity and metabolic disease. Physiol Behav 2008; 94: 17–28
2 *Fernandez-Twinn DS*, *Ekizoglou S*, *Wayman A*, *Petry CJ*, *Ozanne SE*. Maternal low-protein diet programs cardiac beta-adrenergic response and signaling in 3-mo-old male offspring. Am J Physiol Regul Integr Comp Physiol 2006; 291: R429–R436
3 *Barker DJ*. Obesity and early life. Obes Rev 2007; 8 (Suppl 1): 45–49
4 *Holness MJ*, *Langdown ML*, *Sugden MC*. Early-life programming of susceptibility to dysregulation of glucose metabolism and the development of Type 2 diabetes mellitus. Biochem J 2000; 349: 657–665
5 *Hales CN*, *Barker DJ*. Type 2 (non-insulin-dependent) diabetes mellitus: the thrifty phenotype hypothesis. Diabetologia 1992; 35: 595–601
6 *Forsen T*, *Eriksson J*, *Tuomilehto J*, *Reunanen A*, *Osmond C*, *Barker D*. The fetal and childhood growth of persons who develop type 2 diabetes. Ann Intern Med 2000; 133: 176–182
7 *Eguchi J*, *Wang X*, *Yu S*, *Kershaw EE*, *Chiu PC*, *Dushay J*, *Estall JL*, *Klein U*, *Maratos-Flier E*, *Rosen ED*. Transcriptional control of adipose lipid handling by IRF4. Cell Metab 2011; 13: 249–259
8 *Eguchi J*, *Yan QW*, *Schones DE*, *Kamal M*, *Hsu CH*, *Zhang MQ*, *Crawford GE*, *Rosen ED*. Interferon regulatory factors are transcriptional regulators of adipogenesis. Cell Metab 2008; 7: 86–94
9 *Yoon MJ*, *Lee GY*, *Chung JJ*, *Ahn YH*, *Hong SH*, *Kim JB*. Adiponectin increases fatty acid oxidation in skeletal muscle cells by sequential activation of AMP-activated protein kinase, p38 mitogen-activated protein kinase, and peroxisome proliferator-activated receptor alpha. Diabetes 2006; 55: 2562–2570
10 *Bijland S*, *Mancini SJ*, *Salt IP*. Role of AMP-activated protein kinase in adipose tissue metabolism and inflammation. Clin Sci (Lond) 2013; 124: 491–507
11 *Purushotham A*, *Schug TT*, *Xu Q*, *Surapureddi S*, *Guo X*, *Li X*. Hepatocyte-specific deletion of SIRT1 alters fatty acid metabolism and results in hepatic steatosis and inflammation. Cell Metab 2009; 9: 327–338
12 *Eguchi J*, *Kong X*, *Tenta M*, *Wang X*, *Kang S*, *Rosen ED*. Interferon regulatory factor 4 regulates obesity-induced inflammation through regulation of adipose tissue macrophage polarization. Diabetes 2013; 62: 3394–3403
13 *Zhou G*, *Myers R*, *Li Y*, *Chen Y*, *Shen X*, *Fenyk-Melody J*, *Wu M*, *Ventre J*, *Doebber T*, *Fujii N*, *Musi N*, *Hirschman MF*, *Goodyear LJ*, *Moller DE*. Role of AMP-activated protein kinase in mechanism of metformin action. J Clin Invest 2001; 108: 1167–1174
14 *Zhang T*, *Guan H*, *Arany E*, *Hill DJ*, *Yang K*. Maternal protein restriction permanently programs adipocyte growth and development in adult male rat offspring. J Cell Biochem 2007; 101: 381–388
15 *Bol VV*, *Reusens BM*, *Remacle CA*. Postnatal catch-up growth after fetal protein restriction programs proliferation of rat preadipocytes. Obesity (Silver Spring) 2008; 16: 2760–2763
16 *Turer AT*, *Scherer PE*. Adiponectin: mechanistic insights and clinical implications. Diabetologia 2012; 55: 2319–2326
17 *Qiao L*, *Lee B*, *Kinney B*, *Yoo HS*, *Shao J*. Energy intake and adiponectin gene expression. Am J Physiol Endocrinol Metab 2011; 300: E809–E816
18 *Guerre-Millo M*, *Rouault C*, *Poulain P*, *Andre J*, *Poitout V*, *Peters JM*, *Gonzalez FJ*, *Fruchart JC*, *Reach G*, *Staels B*. PPAR-alpha-null mice are protected from high-fat diet-induced insulin resistance. Diabetes 2001; 50: 2809–2814
19 *Leone TC*, *Weinheimer CJ*, *Kelly DP*. A critical role for the peroxisome proliferator-activated receptor alpha (PPARalpha) in the cellular fasting response: the PPARalpha-null mouse as a model of fatty acid oxidation disorders. Proc Natl Acad Sci USA 1999; 96: 7473–7478
20 *Ye JM*, *Doyle PJ*, *Iglesias MA*, *Watson DG*, *Cooney GJ*, *Kraegen EW*. Peroxisome proliferator-activated receptor (PPAR)-alpha activation lowers muscle lipids and improves insulin sensitivity in high fat-fed rats: comparison with PPAR-gamma activation. Diabetes 2001; 50: 411–417
21 *Barroso E*, *Rodríguez-Calvo R*, *Serrano-Marco L*, *Astudillo AM*, *Balsinde J*, *Palomer X*, *Vázquez-Carrera M*. The PPARb/d activator GW501516 prevents the down-regulation of AMPK caused by a high-fat diet in liver and amplifies the PGC-1a-Lipin 1-PPARa pathway leading to increased fatty acid oxidation. Endocrinology 2011; 152: 1848–1859
22 *Holness MJ*, *Sugden PH*, *Silvestre MFP*, *Sugden MC*. Actions and interactions of AMPK with insulin, the peroxisomal-proliferator activated receptors and sirtuins. Expert Rev Endocrinol Metab 2012; 7: 191–208
23 *Sun K*, *Kusminski CM*, *Scherer PE*. Adipose tissue remodeling and obesity. J Clin Invest 2011; 121: 2094–2101
24 *Mittrücker HW*, *Matsuyama T*, *Grossman A*, *Kündig TM*, *Potter J*, *Shahinian A*, *Wakeham A*, *Patterson B*, *Ohashi PS*, *Mak TW*. Requirement for the transcription factor LSIRF/IRF4 for mature B and T lymphocyte function. Science 1997; 275: 540–543